THE FORMATION KINETICS, MECHANISMS, AND THERMODYNAMICS OF S(IV)–ALDEHYDE ADDITION COMPOUNDS

Thesis by

Terese Marie Olson

In Partial Fulfillment of the Requirements

for the Degree of

Doctor of Philosophy

California Institute of Technology

Pasadena, California

1988

(Submitted 25 February 1988)

ACKNOWLEDGEMENTS

For all his great technical advice, support, and the faith he was willing to invest in allowing a civil engineer to undertake this project, I am deeply grateful to my advisor, Michael Hoffmann. I also would like to thank Jim Morgan, Glen Cass, John Seinfeld, and Harry Gray for serving on my examining committee. The financial support of the Electric Power Research Institute, the Environmental Protection Agency, and the Public Health Service was especially appreciated.

A deep debt is owed to Eric Betterton, Bill Munger, and Scott Boyce. Their corollary research interests and their advice have aided tremendously the progress and eased the interpretation of this work.

Special thanks go to my friends Lori Torry, Alicia Gonzalez, Martha Conklin, Ken Leung, my office–mate Liyuan Liang, and Bob Arnold, who tried his best to remedy my gross ignorance of microbiology and baseball scorecards.

To my mother and father: nothing could ever repay the love, encouragement, and advice you have always given me.

Finally, I dedicate this work to my husband, Steve, who talked me into coming here in the first place and then helped me to persevere through it. His support and unlimited sacrifices have made all this possible.

ABSTRACT

The reaction kinetics and thermodynamics of the reversible addition of S(IV) and several aldehydes were studied at low pH in order to determine which carbonyl–bisulfite adducts are potential S(IV) reservoirs in atmospheric water droplets. Benzaldehyde, glyoxal, glyoxylic acid, and hydroxyacetaldehyde were chosen as aldehyde substrates.

Spectrophotometric methods were employed to study the reaction kinetics. Between pH 1 – 3, the two rate–determining steps for adduct formation were the addition of HSO_3^- and SO_3^{2-} to the carbonyl carbon atom. The sulfite ion was a much more effective nucleophile than bisulfite; rate constants for sulfite addition are four to five orders of magnitude higher than for bisulfite. Below pH 1, some specific acid catalysis was also observed.

Adduct stability constants were determined by spectrophotometry and from microscopic reversibility relationships. Linear–free–energy relationships between carbonyl–bisulfite adduct stabilities and the Taft σ^* parameter were found to hold for a limited set of aldehyde substrates. A relatively high correlation exists between bisulfite adduct stability constants and carbonyl hydration constants.

Criteria were formulated, which can be used to predict the potential effectiveness of a carbonyl to significantly stabilize S(IV) in droplets. Modeling calculations for an open atmosphere show that adduct formation rates are much slower than mass transfer and S(IV) oxidation rates under most fog– and cloud–water conditions. Formation rates of hydroxyacetaldehyde–, glyoxal–, and glyoxylic acid – bisulfite addition compounds are comparable to, or faster than, formation rates of hydroxymethanesulfonate, which has been identified in droplets. Equilibrium calculations suggest that these three addition compounds can also stabilize a significant excess of SO_2 in the liquid phase.

TABLE OF CONTENTS

LIST OF FIGURES

LIST OF FIGURES (*continued*)

LIST OF FIGURES (*continued*)

LIST OF FIGURES (*continued*)

LIST OF FIGURES (*continued*)

LIST OF TABLES

LIST OF TABLES *(continued)*

LIST OF TABLES *(continued)*

LIST OF REFERENCES

OVERVIEW

This project was undertaken to determine whether other carbonyl–bisulfite addition compounds, besides α–hydroxymethanesulfonate (HMS), represent significant reservoirs for S(IV) in atmospheric water droplets. The approach taken involved studying the reaction kinetics and thermodynamics for a selected set of aldehyde substrates. This selected set includes benzaldehyde, glyoxal (CHOCHO), glyoxylic acid ($CHOCO_2H$) and hydroxyacetaldehyde. These aldehydes were chosen because they have been either detected or predicted to form in the atmosphere.

Hydroxyalkylsulfonate formation at low pH ($\leq$ 3) can be described by the following three–term generalized rate expression:

$$\frac{d[RCH(OH)SO_3^-]}{dt} = (k_0[RCHOH^+] + k_1[RCHO])[HSO_3^-] + k_2[RCHO][SO_3^{2-}] .$$

The k_0 term corresponds to the proton–catalyzed addition of bisulfite. The k_1 and k_2 terms correspond to the addition of bisulfite and sulfite, respectively, to the carbonyl carbon. Sulfite is by far the most effective nucleophile; ratios of k_2/k_1 ranged from 3×10^4 to 10^5. Only the sulfite addition pathway is rapid enough to result in significant macroscopic adduct formation rates over fog– and cloud–water time scales. The activation entropies associated with the k_1 step are substantially more negative than those for the k_2 step. To explain these differences, it is postulated that bisulfite addition requires a more ordered, cyclic transition state, whereas sulfite addition does not. The rate constants k_1 and k_2 did not correlate closely with the Taft σ^* parameter and hence steric and solvent bonding effects are thought to be as important as electric field effects for some addition compounds. A

better correlation was found between k_1 and k_2.

Stability constants of the aldehyde–bisulfite adducts were determined by spectrophotometrically measuring the concentrations of free S(IV) or aldehyde in equilibrated solutions. For the glyoxal and glyoxylic acid adducts, these direct determinations were checked by calculating the equilibrium constant as $K = k_{formation}/ k_{dissociation}$. Intrinsic stabilities, defined as

$$K_{intr} = \frac{[R_1R_2C(OH)SO_3^-]}{[R_1COR_2]\ [HSO_3^-]},$$

for addition compounds with the same number of α–hydrogen atoms adjacent to the carbonyl carbon atom were found to correlate reasonably well with the Taft σ^* parameter. The presence of an α–phenyl substituent or an α–carboxylate group, however, leads to substantially smaller and larger values of K_{intr} than the Taft correlation would predict. An LFER of high correlation was found to exist between carbonyl–bisulfite adduct stabilities and carbonyl hydration constants. These correlations could be used to predict yet unknown adduct stabilities.

Apparent formation constants, defined in terms of the total concentration of hydrated and unhydrated aldehyde, are relatively invariant ($2 \times 10^4 - 3.6 \times 10^6$ M^{-1}) for predominantly hydrated aldehydes. This result implies that the aldehydes that are the most effective in stabilizing SO_2 are those with the greatest solubilities and abundance in the atmosphere.

Modeling calculations were performed to compare hydroxyalkylsulfonate formation rates in a foggy, polluted atmosphere with mass transfer and S(IV) oxidation rates. Except in the near neutral pH range or in the case of unusually large droplets, hydroxyalkylsulfonates form much more slowly than the time scales of either of these two processes. Calculated macroscopic removal rates of SO_2 from the gas phase because of adduct formation were significant only above pH 5 and

when an excess of aldehyde was present in the atmosphere. Assuming equal gas–phase concentrations of aldehyde in an open atmosphere, formation rates of the glyoxal– and glyoxylic acid – bisulfite addition compounds were comparable to HMS rates. Under this same assumption, hydroxyacetaldehyde–bisulfite adducts form *faster* than HMS.

Since kinetic limitations appeared to be absent, the potential of hydroxyalkylsulfonates to serve as S(IV) reservoirs was examined thermodynamically. While HMS was found to be the most effective reservoir, glyoxal, glyoxylic acid and hydroxyacetaldehyde were all predicted to lead to significant S(IV) enrichment. This result is due primarily to the high solubilities of these compounds.

CHAPTER 1

Introduction

Many developments have led up to and motivated this work, but perhaps the key point of understanding has come with the recognition that fog– and cloudwater droplets play an important role in removing pollutants from the atmosphere. Because they are relatively small in size (with diameters ranging from 1 to 100 μm), these droplets are effective scavengers of soluble gas–phase pollutants; they are typically much more concentrated with respect to solutes than rainwater droplets. Furthermore, the longer atmospheric residence times of these small droplets (hours to days), enables some chemical reactions to take place that are otherwise too slow to proceed over rain droplet time scales. Once intensive efforts were made to collect and analyze fogwater (Waldman *et al.*, 1982; Jacob and Hoffmann, 1983; Munger *et al.*, 1983; Jacob *et al.*, 1984a,b), investigators quickly discovered that Henry's law solubility relationships alone could not account for the high concentrations of S(IV) and formaldehyde that were observed (Munger *et al.*, 1984). Others also reported that dissolved SO_2 and oxidants, such as H_2O_2 and O_3, were often present simultaneously (Richards *et al.*, 1983; Kok *et al.*, 1986; Hoigne *et al.*, 1985). Based on these observations, Munger *et al.* (1986) proposed that the elevated concentrations of S(IV) were due to the formation of the formaldehyde–bisulfite addition compound (α–hydroxymethanesulfonate, abbreviated HMS in this work) and successfully identified it in fogwater at concentrations exceeding 200 μM. Later, Ang *et al.* (1987) identified HMS in rainwater, but at much lower levels.

In urban atmospheres, especially photochemically polluted ones, a variety of carbonyls are present. The National Research Council's Committee on Aldehydes (1981) estimated that of the 10 – 50 ppb hourly average concentration range of total aldehyde present in urban environments, 30 – 75% consists of formaldehyde.

Attempts have been made to identify the composition of the remaining carbonyl fraction (Grosjean, 1982; Snider and Dawson, 1985); acetaldehyde, propanal, butanal, 2–butanone, benzaldehyde, and 2,3–butadione are among those that have been detected. Other evidence suggests that this list is far from complete. Glyoxal (CHOCHO), methylglyoxal (CH_3COCHO) (Steinberg and Kaplan, 1984; Igawa *et al.*, 1988), glyoxylic acid ($CHOCO_2H$), and pyruvic acid (CH_3COCO_2H) (Steinberg *et al.*, 1985) have been detected in precipitation and fog samples. Theoretical calculations (Calvert and Madronich, 1987) and experimental studies (Tuazon *et al.*, 1984, 1986) indicate that α–dicarbonyl and unsaturated γ–dicarbonyl compounds are major gas–phase oxidation products of aromatic hydrocarbon mixtures. Calvert and Madronich have also shown by calculation that γ–hydroxy–aldehydes and α–hydroxy–carbonyls are significant oxidation products of alkane and alkene mixtures, respectively. Knowing that formaldehyde serves as a reservoir for S(IV) in atmospheric water droplets and that a wide variety of other aldehydes are present, the obvious question became: *How important are other carbonyls in stabilizing S(IV)?*

Although the overall addition of S(IV) species with carbonyl compounds,

$$R_1COR_2 + HSO_3^- \rightleftharpoons R_1R_2CH(OH)SO_3^- , \qquad (1)$$

is a familiar reaction to organic chemists and a useful tool in organic synthesis, surprisingly few detailed studies of the reaction were available. Formaldehyde–S(IV) addition, also known as the "formaldehyde clock reaction" (Jones and Oldham, 1963), was studied as early as 1929 by Wagner, then later by Skrabal and Skrabal (1936) and Sørensen and Andersen (1970), and most recently by Boyce and Hoffmann (1984); Deister *et al.* (1986); Kok *et al.* (1986); and Dong and Dasgupta (1986). The only other detailed studies of S(IV) addition with

carbonyls had been conducted with benzaldehyde (Stewart and Donnally, 1932a,b) and isobutryaldehyde (Green and Hine, 1974). In order to answer the above question, it was clear that more research was needed.

Objectives. Several objectives were identified at the outset of this work. For the following set of aldehyde substrates: benzaldehyde (Chap. 3), glyoxal (Chap. 4), glyoxylic acid (Chap. 5), and hydroxyacetaldehyde (Chap. 6), thermodynamic and mechanistic details of the bisulfite addition reaction were sought. In conjunction with these studies, Betterton and Hoffmann (1987) also examined the kinetics and thermodynamics of methylglyoxal–bisulfite adduct formation. The information gained in these endeavors was to be used to develop criteria for predicting which hydroxyalkylsulfonates are important reservoirs for S(IV). Finally, we planned to use the results to compare adduct formation rates with mass transfer rates and S(IV) oxidation rates under ambient atmospheric conditions. Chapter 2 contains the results of these modeling calculations and summarizes the implications of this study.

REFERENCES

Ang, C.C., Lipari, F., and Swarin, S.J. (1987) *Environ. Sci. Technol.* **21**, 102–105.

Betterton, E.A. and Hoffmann, M.R. (1987) *J. Phys. Chem.* **91**, 3011–3020.

Boyce, S.D. and Hoffmann, M.R. (1984) *J. Phys. Chem.* **88**, 4740–4746.

Calvert, J.G. and Madronich, S. (1987) *J. Geophys. Res.* **92**, 2211–2220.

Deister, U. Neeb, R., Helas G., and Warneck, P. (1986) *J. Phys. Chem.* **90**, 3213–3217.

Dong, S. and Dasgupta, P.K. (1986) *Atmos. Environ.* **20**, 1635–1637.

Green, L.R. and Hine, J. (1974) *J. Org. Chem.* **39**, 3896–3901.

Grosjean, D. (1982) *Environ. Sci. Technol.* **16**, 254–262.

Hoigne, J., Bader, H., Haag, W.R., and Staehelin, J. (1985) *Water Res.* **19**, 993–1004.

Igawa, M., Munger, J.W., and Hoffmann, M.R. (1988) *Anal. Chem.* (in review).

Jacob, D.J. and Hoffmann, M.R. (1983) *J. Geophys. Res.* **88C**, 6611–6621.

Jacob, D.J., Wang, R–F.T., and Flagan, R.C. (1984a) *Environ. Sci. Technol.* **18**, 827–833.

Jones, P. and Oldham, K.B. (1963) *J. Chem. Ed.* **40**, 366–367.

Kok, G.L., Gitlin, S.N., and Lazrus, A.L. (1986) *J. Geophys. Res.* **91**, 2801–2804.

Munger, J.W., Jacob, D.J., Waldman, J.M., and Hoffmann, M.R. (1983) *J. Geophys. Res.* **88**, 5109–5121.

Munger, J.W., Jacob, D.J., and Hoffmann, M.R. (1984) *J. Atmos. Chem.* **1**, 335–350.

Munger, J.W., Tiller, C., and Hoffmann, M.R. (1986) *Science* **231**, 247–249.

National Research Council (1981) *Formaldehyde and Other Aldehydes*, National Academy Press, Washington, D.C.

Richards, L.W., Anderson, J.A., Blumenthal, D.L., McDonald, J.A., Kok, G.L., and Lazrus, A.L. (1983) *Atmos. Environ.* **17**, 911–914.

Skrabal, A. and Skrabal, R. (1936) *Sitzungsber Akad. Wiss. Wien, Math Naturwissen Kl. Abt. 2B* **145**, 617–647.

Snider, J.R. and Dawson, G.A. (1985) *J. Geophys. Res.*, **90 D2**, 3797–3805.

Sørensen, P.E. and Andersen, V.S. (1970) *Acta Chem. Scand.* **24**, 1301–1306.

Steinberg, S. and Kaplan, I.R. (1984) *Intern. J. Environ. Anal. Chem.* **18**, 253–266.

Steinberg, S., Kawamura, K., and Kaplan, I.R. (1985) *Intern. J. Environ. Anal. Chem.* **19**, 251–260.

Stewart, T.D. and Donnally, L.H. (1932a) *J. Am. Chem. Soc.* **54**, 2333–2340.

Stewart, T.D. and Donnally, L.H. (1932b) *Ibid.* **54**, 3555–3569.

Tuazon, E.C., Atkinson, R., MacLeod, H., Biermann, H.W., Winer, A.M. Carter, W.P.L., and Pitts, J.N. Jr. (1984) *Environ. Sci. Technol.* **18**, 981–984.

Tuazon, E.C., MacLeod, H., Atkinson, R., and Carter, W.P.L. (1986) *Environ. Sci. Technol.* **20**, 383–387.

Wagner, C. (1929) *Ber. Dtsch. Chem. Ges. B* **62**, 2873–2877.

Waldman, J.M., Munger, J.W., Jacob, D.J., Flagan, R.C., Morgan, J.J., and Hoffmann, M.R. (1982) *Science*, **218**, 677–680.

CHAPTER 2

Hydroxyalkylsulfonate Formation: Its Role as a S(IV) Reservoir in Atmospheric Water Droplets

by

Terese M. Olson and Michael R. Hoffmann

Submitted to: *Atmospheric Environment*, January 1988

Abstract

Kinetic and thermodynamic data obtained for the addition of S(IV) species with several aldehydes, including benzaldehyde, glyoxal, methylglyoxal, acetaldehyde, hydroxyacetaldehyde, and glyoxylic acid, were used to predict their effectiveness as reservoirs for S(IV) in atmospheric water droplets. A linear–free–energy relationship between hydroxyalkylsulfonate stabilities and carbonyl hydration constants is presented, which can be used to estimate the stability constants of other unknown carbonyl–bisulfite adducts. Formation rates of at least four of the adducts studied were greater than or comparable to the formation rate of α–hydroxymethanesulfonate (HMS). Under most fog– and cloudwater conditions, we have shown that these rates are slower than gas transfer processes. Equilibrium calculations in an open atmosphere indicate that hydroxyacetaldehyde, glyoxal, glyoxylic acid, and to a smaller extent, methylglyoxal, lead to potentially significant enrichment of S(IV) in the liquid phase, although HMS is an even better reservoir for S(IV). Scavenging of SO_2 from the gas phase that is due to hydroxyalkylsulfonate formation becomes important at high liquid water contents, pH $\geq$ 5, and when an excess partial pressure of the aldehyde is present. The overall dissolution of RCHO and SO_2 into a droplet and the subsequent formation of the hydroxyalkylsulfonate also result in a net increase in acidity which, in a weakly buffered solution, can be more than a unit drop in pH.

NOMENCLATURE

ν	Reaction rate (M s^{-1})
K	Equilibrium constant, subscripts and superscripts denote the following reactions: *a* Acid dissociation (M) *h* Hydration *d* Dehydration *1* Hydroxyalkylsulfonate formation (M^{-1}) *app* Apparent adduct formation constant (M^{-1})
k	Rate constant, subscripts refer to: *0* proton catalyzed addition of HSO_3^- and RCHO (M^{-1} s^{-1}) *1* RCHO + HSO_3^- (M^{-1} s^{-1}) *2* RCHO + SO_3^{2-} (M^{-1} s^{-1}) *d* spontaneous dehydration (s^{-1}) *H* proton catalyzed dehydration (M^{-1} s^{-1}) *OH* hydroxide catalyzed dehydration (M^{-1} s^{-1})
α	Ionization fraction of S(IV) species
β	Distribution fraction of RCHO species
$\{H^+\}$	Hydrogen ion activity (M)
pH	– Log ($\{H^+\}$)
P	Gas–phase partial pressure (atm)
H	Intrinsic Henry's Law constant (M atm^{-1})
H^*	Effective Henry's Law constant (M atm^{-1})
R	Universal gas constant (l atm^{-1} M^{-1})
T	Temperature (°K)
$\mathscr{D}_{aq}$	Aqueous diffusion coefficient (cm^2 s^{-1})
$\mathscr{D}_g$	Gas–phase diffusion coefficient (cm^2 s^{-1})
$\bar{v}$	Average molecular speed (cm s^{-1})
ξ	Dimensionless sticking coefficient
a	Droplet radius (cm)

τ Characteristic times (s), subscripts refer to the following processes:
- *d.a.* aqueous diffusion
- *d.g.* gas–phase diffusion
- *r.a* chemical reaction based on aqueous reagent concentration
- *r.g.* chemical reaction based on gas–phase reagent concentration
- *phase* interfacial phase equilibrium

L Liquid water content (volume fraction)

ρ Fraction of aqueous and gas–phase S(IV) bound as hydroxyalkylsulfonates

$\frac{d\rho}{dt}$ Macroscopic removal rate of SO_2 (%/hr)

f_e S(IV) enrichment factor in aqueous phase

Introduction

The addition reaction of carbonyl compounds with dissolved S(IV) species ($H_2O \cdot SO_2$, HSO_3^-, and SO_3^{2-}) to form α–hydroxyalkylsulfonates has been implicated as a pathway for the stabilization of S(IV) in the aqueous phase. Before the specific identification of these compounds, their presence was suspected on the basis of the large measured excesses of S(IV) and aldehydes, over the amounts expected from Henry's law calculations (Munger *et al.*, 1984; Klippel and Warneck, 1980; Grosjean, 1982). In addition, the coexistence of dissolved SO_2 and oxidants, such as H_2O_2 and O_3, were reported (Richards *et al.*, 1983; Kok *et al.*, 1986; Hoigne *et al.*, 1985). Analytical techniques to specifically identify the formaldehyde–bisulfite adduct, hydroxymethanesulfonate (HMS) were later developed by Munger *et al.* (1986) and Ang *et al.* (1987). They reported HMS concentrations in fog– and rainwater samples that periodically exceeded 100 μM.

The effectiveness of formaldehyde as a reservoir for S(IV) can be attributed to four important properties. First, formaldehyde is highly soluble because of its extensive hydration to form methylene glycol ($CH_2(OH)_2$) in water. HMS, which has a formation constant, $K_{HMS} = [CH_2(OH)SO_3^-]/([HSO_3^-][HCHO])$, of 6.6×10^9 M^{-1}, is favored thermodynamically (Deister *et al.*, 1986). A third factor, the rapid kinetics of HMS formation in slightly acidic solution, allows this reaction to proceed at time scales shorter than or comparable to the lifetime of fogs and clouds. Finally, formaldehyde is often an abundant pollutant in urban atmospheres. According to the National Research Council's Committee on Aldehydes (1981), hourly average concentrations of total aldehyde range from 10 – 50 ppb in polluted urban environments with 30 – 75% consisting of formaldehyde.

Other carbonyls may represent significant adduct reservoirs for S(IV). In the

gas phase, acetaldehyde, propanal, butanal, 2–butanone, benzaldehyde (Grosjean, 1982), and 2,3–butadione (Snider and Dawson, 1985) have been detected. Carbonyls such as acetaldehyde, propanal, acetone, acrolein, n–butanal, 2–butanone, n–pentanal, n–hexanal, benzaldehyde (Grosjean and Wright, 1983; Kawamura and Kaplan, 1983); glyoxal, methylglyoxal (Steinberg and Kaplan, 1984; Igawa *et al.*, 1988); glyoxylic acid and pyruvic acid (Steinberg *et al.*, 1985), have also been identified in the droplet phase. Theoretical calculations have shown that the major gas–phase oxidation products of alkanes in a NO_x–rich atmosphere are γ–hydroxy–aldehydes and γ–hydroxy–ketones (Calvert and Madronich, 1987). The oxidation of aromatic hydrocarbon mixtures have been shown experimentally to yield α–dicarbonyls and unsaturated γ–dicarbonyls (Tuazon *et al.*, 1984, 1986). Aldehydes that are known to have large apparent Henry's law constants include glyoxal, methylglyoxal, and hydroxyacetaldehyde (Betterton and Hoffmann, 1988). Glyoxylic acid is also expected to be highly soluble since it is extensively hydrated in solution. While the hydration properties of a wide variety of carbonyls have been studied, relatively few studies of the bisulfite addition compounds were available. This led us to select a series of potentially important aldehydes (benzaldehyde, glyoxal, methylglyoxal, acetaldehyde, hydroxyacetaldehyde, and glyoxylic acid) and to determine the stabilities and formation rates of their respective bisulfite adducts. Structures, names, and abbreviations used throughout this paper for each of the addition compounds are listed in Table 1. The mechanisms of each of these reactions have been discussed in detail elsewhere (Olson *et al.*, 1986, 1988; Betterton and Hoffmann, 1987; Betterton *et al.*, 1988; Olson and Hoffmann, 1988a,b).

In this paper we have used the results of these studies to develop linear–free–energy correlations that can be used to predict yet unknown rate and stability

constants. Comparisons of the rates of aldehyde–bisulfite formation rates under atmospheric conditions, and of the characteristic reaction time scales with mass transport and S(IV) oxidation rates are also presented. Equilibrium calculations were made to predict which hydroxyalkylsulfonates lead to potential enrichment of S(IV) and to determine under what atmospheric conditions adduct formation leads to the partitioning of SO_2 from the gas phase to the droplet phase.

Experimental Procedures

The procedures used to study the reaction kinetics involved following either the disappearance of free aldehyde or S(IV) spectrophotometrically under pseudo–first–order conditions. Stability constants were determined either by measuring the unbound concentration of S(IV) or aldehyde in equilibrated solutions, or by calculating them from measured forward and reverse rate constants as $K_{eq} = k_f/k_r$. The details of all procedures have been described elsewhere (Olson *et al.*, 1986, 1988; Betterton and Hoffmann, 1987; Betterton *et al.*, 1988; Olson and Hoffmann, 1988a,b).

Results and Discussion

Below pH ~3, the rate of adduct formation is governed by the nucleophilic attack of bisulfite or sulfite on the carbonyl carbon of the electrophile. As with the addition of other strong nucleophiles to the carbonyl group (Jencks, 1964), sulfite addition is not strongly catalyzed by general acids or bases. Specific acid catalysis is observable at pH $\leq$ 1. The mechanism for the formation of hydroxyalkyl–sulfonates in the simplest case is given by Equations 1–8.

$$RCH(OH)_2 \overset{K_d}{\rightleftharpoons} RCHO + H_2O \quad \text{(fast)} \quad (1)$$

$$H_2O \cdot SO_2 \overset{K_{a1}}{\rightleftharpoons} HSO_3^- + H^+ \quad \text{(fast)} \quad (2)$$

$$HSO_3^{2-} \overset{K_{a2}}{\rightleftharpoons} SO_3^{2-} + H^+ \quad \text{(fast)} \quad (3)$$

$$RCHO + HSO_3^- \underset{k_{-1}}{\overset{k_1}{\rightleftharpoons}} RCH(OH)SO_3^- \quad \text{(slow)} \quad (4)$$

$$RCHO + SO_3^{2-} \underset{k_{-2}}{\overset{k_2}{\rightleftharpoons}} RCH(O^-)SO_3^- \quad \text{(slow)} \quad (5)$$

$$RCHO + H^+ \overset{1/K_{a0}}{\rightleftharpoons} RCHOH^+ \quad \text{(fast)} \quad (6)$$

$$RCHOH^+ + HSO_3^- \underset{k_{-0}}{\overset{k_0}{\rightleftharpoons}} RCH(OH)SO_3^- + H^+ \quad \text{(slow)} \quad (7)$$

$$RCH(OH)SO_3^- \overset{K_{a4}}{\rightleftharpoons} RCH(O^-)SO_3^- + H^+ \quad \text{(fast)} \quad (8)$$

Among the aldehydes studied, this mechanism is appropriate for formaldehyde, benzaldehyde, methylglyoxal, and hydroxyacetaldehyde, and the corresponding three–term rate expression is

$$\nu_1 = \frac{d[RCH(OH)SO_3^-]}{dt} = \left(\frac{k_0\{H^+\}\alpha_1}{K_{a0}} + k_1\alpha_1 + k_2\alpha_2\right)\left(\frac{K_d}{1 + K_d}\right)[S(IV)][RCHO]_t, \quad (9)$$

where

$$[S(IV)] = [H_2O \cdot SO_2] + [HSO_3^-] + [SO_3^{2-}] \quad (10)$$

$$\alpha_1 = \frac{[HSO_3^-]}{[S(IV)]} = \frac{K_{a1}\{H^+\}}{\{H^+\}^2 + K_{a1}\{H^+\} + K_{a1}K_{a2}} \quad (11)$$

$$\alpha_2 = \frac{[SO_3^{2-}]}{[S(IV)]} = \frac{K_{a1}K_{a2}}{\{H^+\}^2 + K_{a1}\{H^+\} + K_{a1}K_{a2}}. \quad (12)$$

The acid dissociation constants, K_{a1} and K_{a2}, are defined by Equations 2 and 3, and $\{H^+\}$ refers to the hydrogen ion activity.

The mechanism for glyoxal (CHOCHO), while analogous to the one above, is slightly more complicated, since glyoxal exists predominantly as the dihydrated *gem*–diol ($CH(OH)_2CH(OH)_2$) and since it can react to form mono– and di–bisulfite addition compounds. In our experiments, an excess of glyoxal over S(IV) was maintained so that only GMBS (see Table 1) was favored. A mechanism was proposed in which Equations 1, 4, and 5 were replaced by:

$$(CH(OH)_2)_2 \overset{K_{d1}}{\rightleftharpoons} CH(OH)_2CHO + H_2O \qquad \text{(fast)} \quad (1a)$$

$$CH(OH)_2CHO \overset{K_{d2}}{\rightleftharpoons} CHOCHO + H_2O \qquad \text{(fast)} \quad (1b)$$

$$CH(OH)_2CHO + HSO_3^- \underset{k_{-1}'}{\overset{k_1'}{\rightleftharpoons}} CH(OH)_2CH(OH)SO_3^- \qquad \text{(slow)} \quad (4a)$$

$$CHOCHO + HSO_3^- \underset{k_{-1}''}{\overset{k_1''}{\rightleftharpoons}} CHOCH(OH)SO_3^- \qquad \text{(slow)} \quad (4b)$$

$$CH(OH)_2CHO + SO_3^{2-} \underset{k_{-2}'}{\overset{k_2'}{\rightleftharpoons}} CH(OH)_2CH(O^-)SO_3^- \qquad \text{(slow)} \quad (5a)$$

$$CHOCHO + SO_3^{2-} \underset{k_{-2}''}{\overset{k_2''}{\rightleftharpoons}} CHOCH(O^-)SO_3^- \,. \qquad \text{(slow)} \quad (5b)$$

Specific acid catalysis was not observed, so consequently the rate expression for the formation of GMBS is

$$\nu_2 = \frac{d[GMBS]}{dt} = (k_{1,app}\,\alpha_1 + k_{2,app}\,\alpha_2)\,[S(IV)]\,[CHOCHO]_t, \qquad (13)$$

where

$$k_{1,app} = k_1'\beta_1 + k_1''\beta_2 \qquad (14)$$

$$k_{2,app} = k_2'\beta_1 + k_2''\beta_2 \tag{15}$$

$$\beta_1 = \frac{[CH(OH)_2CHO]}{[CHOCHO]_t} = \frac{K_{d1}}{1 + K_{d1} + K_{d1}K_{d2}} \tag{16}$$

$$\beta_2 = \frac{[CHOCHO]}{[CHOCHO]_t} = \frac{K_{d1}K_{d2}}{1 + K_{d1} + K_{d1}K_{d2}}. \tag{17}$$

The mechanism for α–keto acids such as glyoxylic acid ($CHOCO_2H$) is also similar to Equations 1 – 8; however, since the unhydrated and hydrated forms of glyoxylic acid have pK_a's of 2.0 (Sørensen *et al.*, 1974) and 3.3 (Kuta, 1959) respectively, additional dehydration and acid–base equilibria must be included. Below pH 2.9, the mechanism we proposed is obtained by deleting the specific acid catalysis step (Equation 7) and replacing Equations 1, 6, and 8 with the following:

$$CH(OH)_2CO_2H \overset{K_{d1}}{\rightleftharpoons} CHOCO_2H + H_2O \quad \text{(fast)} \quad \text{(1c)}$$

$$CH(OH)_2CO_2^- \overset{K_{d2}}{\rightleftharpoons} CHOCO_2^- + H_2O \quad \text{(fast)} \quad \text{(1d)}$$

$$CHOCO_2H \overset{K_{a3}}{\rightleftharpoons} CHOCO_2^- + H^+ \quad \text{(fast)} \quad \text{(6a)}$$

$$CH(OH)_2CO_2H \overset{K_{a4}}{\rightleftharpoons} CH(OH)_2CO_2^- + H^+ \quad \text{(fast)} \quad \text{(6b)}$$

$$CH(OH)SO_3^-CO_2H \overset{K_{a5}}{\rightleftharpoons} CH(OH)SO_3^-CO_2^- + H^+ \quad \text{(fast)} \quad \text{(8a)}$$

$$CH(OH)SO_3^-CO_2^- \overset{K_{a6}}{\rightleftharpoons} CH(O^-)SO_3^-CO_2^-. \quad \text{(fast)} \quad \text{(8b)}$$

The reactive carbonyl species in steps 4 and 5 is $CHOCO_2H$; the addition of $CHOCO_2^-$ and HSO_3^- is too slow to compete with proton transfer rates, and the addition step of $CHOCO_2^-$ and SO_3^{2-} would be inconsistent with the

pH–dependence we observed (pH $\leq$ 2.9). The rate expression describing the disappearance of S(IV) in the presence of glyoxylic acid is therefore:

$$\nu_3 = (k_1\alpha_1\beta_1 + k_2\alpha_2\beta_1)\,[CHOCO_2H]_t\,[S(IV)]\,, \tag{18}$$

where

$$\beta_1 = \frac{[CHOCO_2H]}{[CHOCO_2H]_t} = \frac{K_{d1}K_{d2}\{H^+\}}{K_{d2}(1+K_{d1})\{H^+\} + K_{a3}K_{d1}(1+K_{d2})} \tag{19}$$

$$[CHOCO_2H]_t = [CHOCO_2H] + [CHOCO_2^-] + [CH(OH)_2CO_2H] + [CH(OH)_2CO_2^-]\,. \tag{20}$$

The rate constants in Equations 9, 13, and 18, for each of the substrates we have studied, are presented in Table 2. In comparing those rate constants that are intrinsic with Taft's σ^* parameters for the corresponding substituent R, there is an overall increase in the rate constants with increasing σ^*. Taft's σ^* parameter is a measure of the polarizing strength of the substitutent group with respect to a reference group. Typically, this reference substituent is taken as the methyl group ($\sigma^*_{CH_3} = 0$). Compilations of σ^* values are available (Perrin *et al.*, 1981). Plots of log k_1 and log k_2 vs σ^*, as shown in Fig. 1, however, do not yield linear correlations using the data in Table 2 alone. Consequently, the Taft parameter cannot be used to estimate accurately k_1 or k_2 for other carbonyls. A better correlation exists between k_1 and k_2 as Fig. 2 demonstrates. With this correlation, one of the rate constants could be estimated if the other constant was known.

Although the rate–determining steps for adduct formation under the pH conditions of our experiments were the nucleophilic addition steps of Equations 4, 5, and 7, it is possible to show that Equation 1 (dehydration) becomes rate–limiting at sufficiently high pH. The rate of dehydration is catalyzed by H^+

and OH^-, and in the absence of other catalysts, the rate expression is

$$\nu_4 = (k_d + k_H\{H^+\} + k_{OH}\{OH^-\})[RCH(OH)_2] , \quad (21)$$

where k_d is the spontaneous first–order rate constant, and k_H and k_{OH} are catalytic second–order constants. Dehydration is also catalyzed by HSO_3^- and SO_3^{2-}; however, for most liquid–phase concentrations of S(IV) present in the atmosphere, this catalysis is weak compared to the other terms in Equation 21. As we have previously shown for HMS, Equation 21 becomes slower than Equation 9 under neutral pH conditions and in the presence of sufficient S(IV) (Olson and Hoffmann, 1986).

The α–hydroxyalkylsulfonates with the highest intrinsic stabilities, K_1, where

$$K_1 = \frac{[R_1R_2C(OH)SO_3^-]}{[R_1COR_2]\ \ [HSO_3^-]} , \quad (22)$$

are HMS, HAMS, GMBS and HSEA. Thermodynamic constants for carbonyl–bisulfite adducts are listed in Table 3 according to the magnitudes of the Taft $\Sigma\sigma^*$ parameter ($\Sigma\sigma^* = \sigma^*_{R_1} + \sigma^*_{R_2}$). Previously, we have shown that linear–free–energy correlations of log K_1 with $\Sigma\sigma^*$ resemble the LFER for log K_h vs $\Sigma\sigma^*$ (Olson and Hoffmann, 1988b). From the more extensive data base of hydration constants, it is clear that carbonyl substrates with the same number of α–hydrogens correlate well with the Taft parameter, except when R_1 or R_2 is a phenyl ring or carboxylate group. The similarities between these correlations suggests that a linear–free–energy relationship also exists between log K_1 and log K_h. This relationship is demonstrated in Fig. 3 and the linearity of the plot suggests that it could be used to estimate unknown stabilities of bisulfite–addition compounds if the corresponding hydration constant is available.

In order to compare the relative effectiveness of the carbonyls listed in Table 3 as reservoirs of S(IV) in droplets, it is necessary to examine the apparent adduct stabilities, ${}^{app}K_1$, where

$$ {}^{app}K_1 = \frac{[R_1R_2C(OH)SO_3^-]}{([R_1COR_2] + [R_1R_2C(OH)_2])\,[HSO_3^-]} . \tag{23} $$

Droplet concentrations of hydroxyalkylsulfonates at equilibrium in an open atmosphere are related to ${}^{app}K_1$, the reagent partial pressures, P, and apparent Henry's law constants, H*, by the expression:

$$ [R_1R_2C(OH)SO_3^-] = {}^{app}K_1\, P_{RCHO} H^*_{RCHO} P_{SO_2} H^*_{SO_2} \alpha_1 . \tag{24} $$

When $K_h \gg 1$, ${}^{app}K_1 \cong K_1/K_h$ and since log K_1 is linearly related to log K_h with slope ~ 1 (see Fig. 3), *predominantly* hydrated carbonyls should have nearly equal apparent stability constants. For glyoxylic acid, methylglyoxal, and hydroxyacetaldehyde, ${}^{app}K_1$ ranged from $2 \times 10^5 - 4 \times 10^5$ M^{-1} (see Table 3). For other hydrated aldehydes, such as glyoxal and formaldehyde, ${}^{app}K_1$ was an order of magnitude below and above this range, respectively. This result has important implications regarding the expected abundance of bisulfite addition compounds in the atmosphere. Since the apparent stabilities of adducts derived from predominantly hydrated aldehydes are of approximately the same magnitude, the most effective reservoirs for S(IV) will be the most soluble aldehydes that also have significant sources in the environment.

Atmospheric Implications

It is now possible with the kinetic data we obtained to compare the formation rates of other carbonyl–bisulfite addition compounds with the rate of HMS formation in a polluted open atmosphere. Four potentially important adducts were selected for these calculations: HAMS, GMBS, DHES, and HSEA. Assuming equal gas–phase concentrations of aldehyde and SO_2 (10 ppbv), and using Equations 9, 13, 18, and 21, the resulting pH dependence of Fig. 4 was obtained. Values of the kinetic constants in Equation 21 for hydroxyacetaldehyde, methylglyoxal and glyoxylic acid have been determined by Sørensen (1972), Wasa and Musha (1970), and Sørensen *et al.* (1974), and are given in Table 4. Those for glyoxal, however, are not known so we could calculate only GMBS formation rates at low pH. For each of the adducts considered in Fig. 4, formation rates become pH–independent when dehydration becomes the rate–limiting step. The onset of this change in the mechanism occurs at much lower pH for HSEA than for DHES, HAMS, or HMS.

Figure 4 also illustrates that the formation rates of HAMS, GMBS, and DHES are faster than HMS formation rates. At low pH, HSEA also forms faster than HMS, but it forms slightly slower than HMS above pH 5. Since reaction rates of the four selected adducts are faster than or comparable to that of HMS, which is known to form in droplets, it is unlikely that kinetic limitations would prevent their formation either.

In the above calculations, it was assumed that mass transport limitations do not exist. This condition is typically met, for example, in the case of S(IV) oxidation by H_2O_2 at pH < 7 or O_3 at pH > 7 (Freiberg and Schwartz, 1981). In order to demonstrate that gas transfer to fog– or cloudwater is rapid with respect to the chemical reaction of hydroxyalkylsulfonate formation, we used the approach

first developed by Schwartz and Freiberg (1981). This approach involves comparing the characteristic times of diffusion and interfacial phase equilibrium with the characteristic reaction times. The characteristic time corresponding to the establishment of phase equilibrium at the interface has been derived as:

$$\tau_{phase} = \mathscr{D}_{aq} \left[\frac{4H^*RT}{\bar{v}\ \xi} \right]^2, \tag{25}$$

where $\mathscr{D}_{aq}$ is the aqueous diffusion coefficient of the reagent, H* is the effective Henry's Law constant, R is the universal gas constant, $\bar{v}$ is the average molecular speed, and ξ is a dimensionless sticking coefficient that is commonly set equal to one (Schwartz and Freiberg, 1981). Aqueous– and gas–phase diffusion occurs over characteristic times given, respectively, by:

$$\tau_{d\cdot a\cdot} = \frac{a^2}{\pi^2 \mathscr{D}_{aq}} \tag{26}$$

$$\tau_{d\cdot g\cdot} = \frac{a^2}{\pi^2 \mathscr{D}_{g}} \tag{27}$$

for a droplet of radius, a. The characteristic reaction times, $\tau_{r\cdot a\cdot}$ and $\tau_{r\cdot g\cdot}$, for the disappearance of S(IV) relative to the aqueous and gas–phase concentrations are:

$$\tau_{r\cdot a\cdot} = \frac{[S(IV)]_{aq}}{-\frac{d[S(IV)]}{dt}} \tag{28}$$

$$\tau_{r\cdot g\cdot} = \frac{[SO_2]_g}{-\frac{d[S(IV)]}{dt}}. \tag{29}$$

Using the example of DHES formation, we have compared these time scales as a function of pH for a 20 μm diameter droplet in a moderately polluted

atmosphere (P_{SO_2} = 10 ppbv, $P_{CH_2(OH)CHO}$ = 10 ppbv). The expressions for $\tau_{r\cdot a\cdot}$ and $\tau_{r\cdot g\cdot}$ were obtained by setting the slowest of ν_1 or ν_4 equal to –d[S(IV)]/dt. By this approach one can show that if $\nu_1 < \nu_4$, then

$$\tau_{r\cdot a\cdot} = \left[\frac{1 + K_d}{K_d}\right]\left[\frac{1}{(k_1\alpha_1 + k_2\alpha_2)\, P_{CH_2(OH)CHO} H^*_{CH_2(OH)CHO}}\right] \tag{30}$$

or if ($\nu_4 < \nu_1$), then

$$\tau_{r\cdot a\cdot} = \frac{\frac{P_{SO_2} H_{SO_2}}{\alpha_0}}{(k_d + k_H\{H^+\} + k_{OH}\{OH^-\})\, P_{CH_2(OH)CHO} H^*_{CH_2(OH)CHO}}, \tag{31}$$

and that

$$\tau_{r\cdot g\cdot} = \frac{\tau_{r\cdot a\cdot,\,max}}{\frac{H_{SO_2} RT}{\alpha_0}}. \tag{32}$$

Many of the constants required in these calculations were obtained from the literature or were estimated. These values are given in Table 4. Results of the calculations shown in Fig. 5, demonstrate that $\tau_{r\cdot a\cdot}$ is much larger than either $\tau_{d\cdot a\cdot}$ or τ_{phase}, and that $\tau_{r\cdot g\cdot} \gg \tau_{d\cdot g\cdot}$ over the entire pH range. Based on the previous comparison of adduct formation rates (Fig. 4), we do not expect that mass transfer limitations would exist under these conditions if DHES were replaced by any of the other slower forming aldehyde–bisulfite addition compounds we have studied.

To define the domains in which steady–state saturation can be assumed we adopted the following criteria recommended by Schwartz (1984):

$$\tau_{phase} < 0.1\, \tau_{r\cdot a\cdot}$$

$$\tau_{d\cdot a\cdot} < 0.1\, \tau_{r\cdot a\cdot}$$

$$\tau_{d\cdot g\cdot} < 0.1\, \tau_{r\cdot g\cdot}\ .$$

For DHES and HMS formation, the gas–phase concentrations of aldehyde which satisfy these three criteria can be calculated as a function of pH. The resulting boundary lines for two droplet sizes are shown in Figs. 6a and b for HMS and Figs. 6c and d for DHES. Below these lines, chemical reaction rates are much slower than mass transport rates. In the case of HMS, very little of the area denoting conditions observed in fog or clouds lies above these lines. Steady–state saturation assumptions, therefore, are legitimate for HMS except for very large droplets ($a \geq 100\ \mu m$) with pH ≥ 5, in an atmosphere containing high gas–phase concentrations of aldehyde. This situation might occur, for example, if an ammonia–laden cloud were to intercept a source plume containing SO_2 and aldehydes. Since DHES forms more rapidly than HMS, the onset of mass transport limitations for DHES occurs at smaller aldehyde concentrations and lower pH. Under most fog– and cloudwater conditions, however, Figs. 6c and d show that DHES formation is still limited by chemical reaction rates.

Steady–state saturation assumptions are also inappropriate if the liquid water content, L (volume fraction), is sufficient to scavenge most of the gas–phase SO_2 or aldehyde. To illustrate the conditions under which this happens, macroscopic SO_2 removal rates due to the formation of HMS, defined as

$$\frac{d\rho}{dt} = \left[\frac{\frac{-d[S(IV)]}{dt} \cdot L}{\left[\frac{P_{SO_2} H_{SO_2} L}{\alpha_0}\right] + \frac{P_{SO_2}}{RT}} \right] \times 100 \qquad (\%/hr) \qquad (33)$$

were calculated for a polluted atmosphere at high and low liquid water contents. The solid lines in Fig. 7 imply that within the typical liquid water content range of fogs and clouds, significant scavenging of SO_2 can occur above pH 5. Removal rates below pH 4, however, are quite slow, and significant scavenging of SO_2 from

the gas phase would not be expected over the duration of most fog events.

It is important to point out that although hydroxyalkylsulfonates are not directly oxidizable by such oxidants as H_2O_2 and O_3, they cannot form if H_2O_2 or O_3 is present. This is because the oxidation of S(IV) species is more rapid than the formation rates of aldehyde–bisulfite addition compounds. A gas–phase concentration of 1 ppbv H_2O_2, for example, results in the SO_2 removal rates shown by the dashed lines in Fig. 7. These oxidation rates were calculated using the rate law recommended by Hoffmann and Calvert (1985):

$$-\frac{d[S(IV)]}{dt} = \frac{k_{1,app}\{H^+\}\alpha_1[H_2O_2][S(IV)]}{1 + k_{2,app}\{H^+\}}, \tag{34}$$

where $k_{1,app} = 7.45 \times 10^7\ M^{-1}s^{-1}$ and $k_{2,app} = 13\ M^{-1}$ at 25° C. Below pH 5, any SO_2 dissolving into a droplet would be oxidized by H_2O_2 rather than bind with HCHO.

The adducts we considered in Fig. 4 have formation rates greater than or comparable to HMS; it is therefore necessary to examine whether or not these adducts are thermodynamically favorable reservoirs for S(IV). Thermodynamic calculations of the total concentration of S(IV), which would be present at equilibrium because of the formation of HAMS, GMBS, HSEA, DHES or HMS in an open atmosphere, were made to determine the resultant maximum enrichment of S(IV), which could occur. Enrichment factors, f_e, defined as:

$$f_e = \frac{[RCH(OH)SO_3^-] + [S(IV)]}{[S(IV)]} \tag{35}$$

were calculated and plotted in Fig. 8 using the indicated gas–phase concentrations of aldehydes and SO_2. Other addition compounds were considered, such as HES and HPMS but were not included in Fig. 8 since their values of f_e are ≈ 1 at all

pH. The solubility of most aldehydes, such as HCHO, $CH_2(OH)CHO$, and CH_3COCHO, is pH–independent, and the degree of S(IV) enrichment resulting when they react with dissolved SO_2 is constant and is a maximum between pH 3 to 5. One exception to this trend is glyoxal. Because it is able to also form GDBS, the equation describing S(IV) enrichment in this case is more complicated, *viz.*,

$$f_e = \frac{[GMBS] + 2[GDBS] + [S(IV)]}{[S(IV)]} . \qquad (36)$$

The [GDBS] term in Equation 36 becomes significant when SO_2 is sufficiently soluble, since the concentration of GDBS is proportional to $[S(IV)]^2$. This explains the increase in excess S(IV) above pH 5 shown for the conditions in Fig. 8. α–Keto acids, such as glyoxylic acid, are increasingly soluble at pH greater than the pK_a of the carboxylic acid group. The increase in f_e above pH 4 that is due to the formation of HSEA (see Fig. 8) is therefore primarily the result of the pH–dependent solubility of glyoxylic acid. (The apparent stabilities of $CH(OH)SO_3^-CO_2H$ and $CH(OH)SO_3^-CO_2^-$ are similar, as discussed above.) Hydroxyacetaldehyde is an unusually effective reservoir for S(IV) because of its large intrinsic Henry's law constant (H). For most aldehydes, H ranges between 1 – 10 M atm^{-1}; for hydroxyacetaldehyde, H = 4100 M atm^{-1} (Betterton and Hoffmann, 1988).

The curves in Fig. 8 indicate that three of the compounds we have studied, GMBS, DHES, and HSEA, are potentially important reservoirs for S(IV) by comparison with HMS. Enrichment factors that are due to HAMS formation are greater than one, but are substantially less than the values of f_e that are due to HMS formation. These comparisons assume equal gas–phase concentrations of the aldehydes, although formaldehyde is thought to be more abundant. At present, the ambient gas–phase concentrations of glyoxal, hydroxacetaldehyde, and

glyoxylic acid, and thus their abundance relative to formaldehyde, are unknown. Based on the high fogwater concentrations of glyoxylic acid reported by Steinberg *et al.* (1985), however, gas–phase concentrations comparable to those of formaldehyde would be required if the source of $CHOCO_2H$ is indeed from the gas phase.

Enrichment calculations based on fixed gas–phase concentrations of SO_2 and aldehydes are not realistic when adduct formation results in the depletion of either reagent from the atmosphere. This occurs with high liquid water contents and at pH values where SO_2 is sufficiently soluble. To demonstrate the conditions in which scavenging is expected for SO_2, we calculated the fraction of total S(IV) bound as hydroxyalkylsulfonates, assuming fixed gas–phase concentrations of the reagents. This fraction, ρ, can be expressed as

$$\rho = \frac{\dfrac{f_e H_{SO_2} L}{\alpha_0}}{\dfrac{f_e H_{SO_2} L}{\alpha_0} + \dfrac{1}{RT}}. \qquad (37)$$

For moderate liquid water contents ($\sim 10^{-2}$ g/m^3), and equal gas–phase concentrations of SO_2 and RCHO, the results in Fig. 9a indicate that SO_2 is not significantly scavenged from the gas phase below pH 5.5 for any of the adducts shown. If the liquid water content is increased to 10^{-1}, SO_2 scavenging that is due to adduct formation becomes appreciable above pH ~5, as shown in Fig. 9b. Optimal conditions for the depletion of SO_2 occur in dense fogs when the gas–phase concentration of aldehyde is in excess (see Fig. 9c). The curves in Figs. 9a,b,c consider each adduct separately; a greater change in the distribution of S(IV) would occur if more than one highly stable adduct formed simultaneously. Our calculations demonstrate that for most fogwater conditions, hydroxyalkylsulfonate

formation does not lead to a large change in the distribution of S(IV). Greater scavenging of SO_2 is expected in clouds, which can be supersaturated and have higher liquid water contents.

The preceding thermodynamic calculations are simplistic because they are based on a fixed equilibrium pH. However, unless the pH–buffering capacity within the droplet is sufficient, hydroxyalkylsulfonate formation will lead to a net drop in pH. The effect of the dissolution of one equivalent of SO_2 and RCHO from the gas phase results in the formation of one equivalent of the addition compound and the liberation of a proton, as given by the overall equilibrium:

$$SO_{2(g)} + RCHO_{(g)} \overset{H_2O}{\rightleftharpoons} RCH(OH)SO_3^- + H^+ . \qquad (38)$$

To illustrate the effect of HMS formation on pH as an example, we calculated the equilibrium droplet pH in an open atmosphere, buffered only by the ambient gas–phase concentration of CO_2 ($P_{CO_2} = 3.2 \times 10^{-4}$ atm) for different concentrations of HCHO and SO_2. The results are presented in Fig. 10. By comparing the calculated pH for atmospheres containing more than 10 ppb HCHO with the y–intercepts of Fig. 9, it is apparent that HMS formation can often lead to at least a unit drop in pH.

Conclusions

Kinetic studies of the formation of several aldehyde–bisulfite addition compounds at low pH have allowed us to propose a general mechanism whereby the addition steps of the carbonyl with either HSO_3^- or SO_3^{2-} are rate–limiting. By calculation, it is possible to show that dehydration of the *gem*–diol can become rate–limiting at sufficiently high pH. Rate constants corresponding to the addition of HSO_3^- and SO_3^{2-} at the carbonyl carbon center increase in general as the

α–substituents to the carbonyl group become more electron–withdrawing. They do not, however, correlate closely with the Taft σ^* parameter.

Calculated formation rates of HAMS, GMBS, HSEA and DHES in an open atmosphere were greater than or comparable to HMS formation rates when the concentrations of aldehydes in the gas phase were equal. Adduct formation rates are also much slower than mass–transfer rates, except under extreme conditions (i.e., large droplets, high pH, and high partial pressures of SO_2 and aldehydes). Furthermore, if effective S(IV) oxidants such as H_2O_2 are present, hydroxyalkylsulfonates will not form, since S(IV) oxidation rates are orders of magnitude faster than adduct formation rates.

The intrinsic stability of carbonyl–bisulfite addition compounds having a single hydrogen adjacent to the carbon center, $R_1R_2C(OH)SO_3^-$, were found to correlate reasonably well with the Taft σ^* parameter. A better correlation is obtained by plotting log K_1 vs log K_h. From this LFER, unknown carbonyl–bisulfite adduct stabilities can be predicted when hydration constants are available.

Of those bisulfite addition compounds other than HMS, which have been studied, GMBS, DHES, and HSEA were determined to be the greatest potential reservoirs for S(IV). Sulfur(IV) enrichment comparisons, however, were based on equal gas–phase concentrations of formaldehyde, hydroxyacetaldehyde, glyoxal, and glyoxylic acid, and so their importance as reservoirs for S(IV) will depend on their relative abundance in the atmosphere. The high solubilities of hydroxyacetaldehyde, glyoxal and glyoxylate were shown to contribute substantially to their effectiveness as reservoirs for S(IV). Other aldehydes that have not yet been studied, but which are also expected to have high solubilities, are β–hydroxyaldehydes (e.g., $CH_2(OH)CH_2CHO$), β–keto acids (e.g.,

$CHOCH_2CO_2H$), and β–dicarbonyls (e.g., $CHOCH_2CHO$).

Significant scavenging of SO_2 from the gas phase which is due to adduct formation, is not generally expected except in the presence of high liquid water contents, above pH 5, and when there is a large excess of aldehyde in the gas phase. Hydroxyalkylsulfonate formation can have an appreciable effect on droplet pH. Equilibrium calculations indicate that HMS formation can easily account for a unit drop in pH when formaldehyde concentrations exceed 10 ppb.

A number of questions remain, especially regarding the fates of these addition compounds, once they form in droplets. Since the dissociation rates of these compounds are quite slow, it is likely that the sulfonate salts are left behind as part of the haze aerosol (as NaHMS, $Ca(HMS)_2$, or NH_4HMS, etc.) after the fog evaporates. They might then either be removed through deposition processes or serve as condensation nuclei for the next fog event. Preliminary evidence obtained in this laboratory also suggests that $OH^{\cdot}$ readily oxidizes HMS. The mechanism and importance of this reaction are not known, but further study is warranted.

Acknowledgements. We gratefully acknowledge the Electric Power Research Institute (RP1630–47), the Environmental Protection Agency (R811496–01–1), and the Public Health Service (ES04635–01) for their financial support.

REFERENCES

Andrew S.P.S. (1955) A simple method of measuring gaseous diffusion coefficients. *Chem. Engng. Sci.* **4**, 269–272.

Ang C.C., Lipari F., and Swarin S.J. (1987) Determination of hydroxymethane–sulfonate in wet deposition samples. *Environ. Sci. Technol.* **21**, 102–105.

Bell R.P. (1966) The reversible hydration of carbonyl compounds. *Adv. Phys. Org. Chem.* **4**, 1–29.

Bell R.P and Evans P.G. (1966) Kinetics of the dehydration of methylene glycol in aqueous solution. *Proc. R. Soc. Lond. Ser. A* **291**, 297–323.

Betterton E.A. and Hoffmann M.R. (1987) Kinetics, mechanism, and thermodynamics of the reversible reaction of methylglyoxal with S(IV). *J. Phys. Chem.* **91**, 3011–3020.

Betterton E.A and Hoffmann M.R. (1988) Henry's law constants of some environmentally important aldehydes. *Environ. Sci. Technol.* (in review).

Betterton E.A., Erel Y., and Hoffmann M.R. (1988) Aldehyde–bisulfite adducts: Prediction of some of their thermodynamic and kinetic properties. *Environ. Sci. Technol.* **22**, 92–99.

Boyce S.D. and Hoffmann M.R. (1984) Kinetics and mechanism of the formation of hydroxymethanesulfonic acid at low pH. *J. Phys. Chem.* **88**, 4740–4746.

Burroughs L.F. and Sparks A.H. (1973) Sulfite–binding power of wines and ciders. I. Equilibrium constants for the dissociation of carbonyl bisulfite compounds. *J. Sci. Food Agric.* **24**, 187–198.

Calvert J.G. and Madronich S. (1987) Theoretical study of the initial products of the atmospheric oxidation of hydrocarbons. *J. Geophys. Res.* **92**, 2211–2220.

Deister U., Neeb R., Helas G., and Warneck P. (1986) Temperature dependence of the equilibrium $CH_2(OH)_2 + HSO_3^- = CH_2(OH)SO_3^- + H_2O$ in aqueous solution. *J. Phys. Chem.* **90**, 3213–3217.

Deveez D. and Rumpf P. (1964) Spectrophotometric study of aqueous SO_2 in various acid buffers. *C.r. Acad. Sci. Paris* **258**, 6135–6138.

Freiberg J.E. and Schwartz S.E. (1981) Oxidation of SO_2 in aqueous droplets: Mass–transport limitation in laboratory studies and the ambient atmosphere. *Atmos. Environ.* **15**, 1145–1154.

Green L.R. and Hine J. (1974) The pH independent equilibrium constants and rate constants for formation of the bisulfite addition compound of isobutyraldehyde in water. *J. Org. Chem.* **39**, 3896–3901.

Grosjean D. (1982) Formaldehyde and other carbonyls in Los Angeles ambient air. *Environ. Sci. Technol.* **16**, 254–262.

Grosjean D. and Wright B. (1983) Carbonyls in urban fog, ice fog, cloudwater, and rainwater. *Atmos. Environ.* **17**, 2093–2096.

Gubareva M.A. (1947) *J. Gen. Chem. USSR* **17**, 649–651.

Hayon E., Treinin A., and Wilf J. (1972) Electronic spectra, photochemistry and autoxidation mechanism of the sulfite–bisulfite–pyrosulfite systems. The SO_4^-, and SO_5^- radicals. *J. Am. Chem. Soc.* **94**, 47–57.

Himmelblau D.M. (1964) Diffusion of dissolved gases in liquids. *Chem. Rev.* **64**, 527–550.

Hoffmann M.R. and Calvert J.G. (1985) Chemical transformation modules for Eulerian acid deposition models. USEPA Rep., Office of Research and Development, Research Triangle Park, N.C.

Hoigne J., Bader H., Haag W.R., and Staehelin, J. (1985) Rate constants of reactions of ozone with organic and inorganic compounds in water – III. *Water Res.* **19**, 993–1004.

Igawa M, Munger J.W., and Hoffmann M.R. (1988) Analysis of aldehydes in natural water samples by HPLC with a postcolumn reaction detector. *Anal. Chem.* (in review).

Jencks W.P. (1964) Mechanism and catalysis of simple carbonyl group reactions. *Progr. Phys. Org. Chem.* **2**, 63–118.

Johnstone H.F. and Leppla P.W. (1934) The solubility of sulfur dioxide. *J. Am. Chem. Soc.* **56**, 2233–2238.

Kawamura K., and Kaplan I.R. (1983) Organic compounds in the rainwater of Los Angeles. *Environ. Sci. Technol.* **17**, 497–501.

Klippel W., and Warneck P. (1980) The formaldehyde content of the atmospheric aerosol. *Atmos. Environ.* **14**, 809–818.

Kok G.L., Gitlin S.N., and Lazrus A.L. (1986) Kinetics of the formation and decomposition of hydroxymethanesulfonate. *J. Geophys. Res.* **91**, 2801–2804.

Kuta, J (1959) Polarographic study of dehydration of glyoxylic acid. *Collec. Czech. Chem. Commun.* **24**, 2532–2543.

Munger J.W., Jacob D.J. and Hoffmann M.R. (1984) The occurrence of bisulfite–aldehyde addition products in fog– and cloudwater. *J. Atmos. Chem.* **1**, 335–350.

Munger J.W., Tiller C., and Hoffmann M.R. (1986) Identification of hydroxy–methanesulfonate in fogwater. *Science* **231**, 247–249.

National Research Council (1981) *Formaldehyde and Other Aldehydes*, National Academy Press, Washington, D.C.

Olson T.M. (1988) The formation kinetics, mechanisms, and thermodynamics of S(IV)–aldehyde addition compounds. Appendix B, Ph.D. Thesis; Calif. Inst. of Tech.

Olson T.M., Boyce S.D., and Hoffmann M.R. (1986) Kinetics, thermodynamics and mechanism of the formation of benzaldehyde–S(IV) adducts. *J. Phys. Chem.* **90**, 2482–2488.

Olson T.M. and Hoffmann M.R. (1986) On the kinetics of formaldehyde–S(IV) adduct formation in slightly acidic solution. *Atmos. Environ.* **20**, 2277–2278.

Olson T.M. and Hoffmann M.R. (1988a) The kinetics, mechanism, and thermodynamics of glyoxal–S(IV) adduct formation. *J. Phys. Chem.* **92**, 533–540.

Olson T.M. and Hoffmann M.R. (1988b) Formation kinetics, mechanism and thermodynamics of glyoxylic acid – S(IV) adduct formation. *J. Phys. Chem.* (in press).

Olson T.M., Torry L.A., and Hoffmann M.R. (1988) Kinetics of the formation of hydroxyacetaldehyde–bisulfite adducts at low pH. *Environ. Sci. Technol.* (in review).

Perrin D.D., Dempsey B., and Serjeant E.P. (1981) pK_a Prediction for organic acids and bases. Chapman and Hall, London.

Richards L.W., Anderson J.A., Blumenthal D.L., McDonald J.A., Kok G.L., and Lazrus A.L. (1983) Hydrogen peroxide and sulfur(IV) in Los Angeles cloud–water. *Atmos. Environ.* **17**, 911–914.

Schwartz S.E. (1984) Gas aqueous reactions of sulfur and nitrogen oxides in liquid–water clouds. In: *SO_2, NO, and NO_2 Oxidation Mechanisms: Atmospheric Considerations.* Calvert, J.G., Ed.; Butterworth Publishers: Boston, pp. 173–208.

Schwartz S.E. and Freiberg J.E. (1981) Mass–transport limitation to the rate of reaction of gases in liquid droplets: Application to oxidation of SO_2 in aqueous solutions. *Atmos. Environ.* **15**, 1129–1144.

Sørensen P.E. (1972) The reversible addition of water to glycolaldehyde in aqueous solution. *Acta Chem. Scand.* **26**, 3357–3365.

Sørensen P.E., Bruhn K., and Lindeløv F. (1974) Kinetics and equilibria for the reversible hydration of the aldehyde group in glyoxylic acid. *Acta Chem. Scand.* **28**, 162–168.

Snider J.R., and Dawson G.A. (1985) Tropospheric light alcohols, carbonyls, and acetonitrile: Concentrations in the southwestern United States and Henry's law data. *J. Geophys. Res.* **90**, 3797–3805.

Steinberg S., and Kaplan I.R (1984) The determination of low molecular weight aldehydes in rain, fog and mist by reversed phase liquid chromatography of the 2,4–dinitrophenylhydrazone derivatives. *Intern. J. Environ. Anal. Chem.* **18**, 253–266.

Steinberg S., Kawamura K., and Kaplan I.R. (1985) The determination of α–keto acids and oxalic acid in rain, fog, and mist by HPLC. *Intern. J. Environ. Anal. Chem.* **19**, 251–260.

Tuazon E.C., Atkinson R., Mac Leod H., Biermann H.W., Winer A.M., Carter W.P.L. and Pitts, J.N. Jr. (1984) Yields of glyoxal and methylglyoxal from the NO_x – air photooxidations of toluene and m– and p–xylene. *Environ. Sci. Technol.* **18**, 981–984.

Tuazon E.C., Mac Leod H., Atkinson R., and Carter W.P.L. (1986) α–Dicarbonyl yields from the NO_x – air photooxidations of a series of aromatic hydrocarbons in air. *Environ. Sci. Technol.* **20**, 383–387.

Wasa T. and Musha S. (1970) Polarographic behavior of glyoxal and its related compounds. *Bull. Univ. Osaka Prefect Ser. A* **19**, 169–180.

TABLE 1. Addition Compound Structures and Abbreviations

Aldehyde	Hydroxyalkylsulfonate	Structure	Abbr.
Formaldehyde	hydroxymethanesulfonate	$CH_2(OH)SO_3^-$	HMS
Acetaldehyde	1–hydroxy–1–ethanesulfonate	$CH_3CH(OH)SO_3^-$	HES
Hydroxyacetaldehyde	1,2–dihydroxy–1–ethanesulfonate	$CH_2(OH)CH(OH)SO_3^-$	DHES
Benzaldehyde	hydroxyphenylmethanesulfonate	$C_6H_5CH(OH)SO_3^-$	HPMS
Glyoxal	1–hydroxy–2,2–diol–1–ethane–sulfonate (or glyoxal mono–bisulfite)	$CH(OH)_2CH(OH)SO_3^-$	GMBS
	1,2–dihydroxy–1,2–ethane–sulfonate (or glyoxal di–bisulfite)	$(CH(OH)SO_3^-)_2$	GDBS
Methylglyoxal	hydroxyacetylmethanesulfonate	$CH_3COCH(OH)SO_3^-$	HAMS
Glyoxylic Acid	2–hydroxy–2–sulfo–ethanoic acid	$HO_2CCH(OH)SO_3^-$	HSEA

TABLE 2. Forward Rate Constants (25°C) and Activation Energy Parameters

$$RCHO + HSO_3^- \xrightarrow{k_1}$$

$$RCHO + SO_3^{2-} \xrightarrow{k_2}$$

	$M^{-1}\ s^{-1}$		kJ mol^{-1}		J $mol^{-1}\ deg^{-1}$	
RCHO	k_1	k_2	$\Delta H_1^{\neq}$	$\Delta H_2^{\neq}$	$\Delta S_1^{\neq}$	$\Delta S_2^{\neq}$
CH_3COCHO[a]	3.44×10^3	3.66×10^7	29.0	18.2	–77.7	–22.6
HCHO[b]	7.90×10^2	2.50×10^7	24.9	20.4	–108.	–31.7
HO_2CCHO[c]	4.43×10^2	1.98×10^7	21.4	N.D.[d]	–141.	N.D.
$CH_2(OH)CHO$[e]	1.74	5.02×10^4	29.9	17.7	–156.	–117.
C_6H_5CHO[f]	7.10×10^{-1}	2.15×10^4	36.6	36.0	–142.	–58.1
$(CH_3)_2CHCHO$[g]	N.D.	1.4×10^4	N.D.	N.D.	N.D.	N.D.
CHOCHO[h]	1.30×10^{-1}[i]	2.08×10^3[i]	N.D.	N.D.	N.D.	N.D.

[a] Betterton and Hoffmann (1987).
[b] Boyce and Hoffmann (1984).
[c] Olson and Hoffmann (1988b).
[d] Not determined.
[e] Olson *et al.* (1988).
[f] Olson *et al.* (1986).
[g] Green and Hine (1974).
[h] Olson and Hoffmann (1988a).
[i] Rate constants are $k_{1,app}$ and $k_{2,app}$ as defined in Equations 14 and 15.

TABLE 3. Hydroxyalkylsulfonate Stability Constants (25° C)

R_1	R_2	$\Sigma\sigma^{*}$†	K_1‡ M^{-1}	ΔH_1° *kJ/mol*	$^{app}K_1$§ M^{-1}	Ref.
Aldehydes						
H	COO^-	–0.57	5.3×10^6		3.3×10^5	*a*
H	$(CH_3)_2CH$	0.30	4.8×10^4		2.9×10^4	*b*
H	CH_3	0.49	6.8×10^5		1.2×10^5	*c*
H	H	0.98	6.6×10^9	–21.1	3.6×10^6	*d*
H	$CH_2(OH)$	1.11	2.0×10^6		2.0×10^5	*c*
H	C_6H_5	1.24	4.8×10^3	–64.6	4.8×10^3	*e*
H	$CH(OH)SO_3^-$	N.A.*			1.4×10^4	*f*
H	$CH(OH)_2$	1.86	1.4×10^8		2.8×10^4	*f*
H	CH_3CO	2.30	8.1×10^8	–54.5	3.1×10^5	*g*
H	CO_2H	2.57	7.1×10^7		2.4×10^5	*a*
Ketones						
CH_3	COO^-	–1.06	4.8×10^3		5.0×10^3	*h*
CH_3	CH_3	0.00	2.9×10^2		2.9×10^2	*i*
CH_3	CO_2H	2.08	4.6×10^4		7.4×10^4	*h*

Refs.: (*a*) Olson and Hoffmann (1988b); (*b*) Green and Hine (1974); (*c*) Betterton *et al.* (1988); (*d*) Deister *et al.* (1986); (*e*) Olson *et al.* (1986); (*f*) Olson and Hoffmann (1988a); (*g*) Betterton and Hoffmann (1987); (*h*) calculated in Olson (1988) from Burroughs and Sparks (1973); (*i*) Gubareva (1947).

*N.A. = Not available

†$\Sigma\sigma^* = \sigma^*_{R_1} + \sigma^*_{R_2}$

‡Defined in Equation 22.

§Defined in Equation 23.

TABLE 4. Dehydration Constants, Diffusion Coefficients, Henry's Law Constants, and Acid Dissociation Constants at 25° C.

Process	Constant	Ref.
$RCHO_{(g)} + H_2O \rightleftharpoons RCH(OH)_2$		
R = H	$H^* = 2.97 \times 10^3$ M atm^{-1}	*a*
R = CH_3CO	$H^* = 3.71 \times 10^3$ M atm^{-1}	*a*
R = CHO	$H^* = 3 \times 10^5$ M atm^{-1}	*a*
R = $CH_2(OH)$	$H^* = 4.14 \times 10^4$ M atm^{-1}	*a*
R = CO_2H	$H^* \approx 3 \times 10^2$ M atm^{-1}	*b*
$SO_{2(g)} \rightleftharpoons SO_{2(aq)}$	H = 1.26 M atm^{-1}	*c*
$H_2O \cdot SO_2 \rightleftharpoons HSO_3^- + H^+$	$K_{a1} = 1.45 \times 10^{-2}$ M	*d*
$HSO_3^- \rightleftharpoons SO_3^{2-} + H^+$	$K_{a2} = 6.31 \times 10^{-8}$ M	*e*
$RCH(OH)_2 \rightarrow RCHO + H_2O$		
R = H	$k_0 = 5.1 \times 10^{-3}$ s^{-1}	*f*
R = CH_3CO	$k_0 = 9 \times 10^{-3}$ s^{-1}	*g*
R = $CH(OH)_2$	$k_0 = 9.6 \times 10^{-3}$ s^{-1}	*h*
R = CO_2H	$k_0 = 2.5 \times 10^{-2}$ s^{-1}	*i*
R = CO_2^-	$k_0 = 5.5 \times 10^{-3}$ s^{-1}	*i*
$RCH(OH)_2 + H^+ \rightarrow RCHO + H_2O + H^+$		
R = H	$k_H = 2.7$ M^{-1} s^{-1}	*f*
R = CH_3CO	$k_H = 28$ M^{-1} s^{-1}	*g*
R = $CH_2(OH)$	$k_H = 8.3$ M^{-1} s^{-1}	*h*
R = CO_2H	$k_H = 7.6 \times 10^{-2}$ M^{-1} s^{-1}	*i*
$RCH(OH)_2 + OH^- \rightarrow RCHO + H_2O + OH^-$		
R = H	$k_{OH} = 1.58 \times 10^3$ M^{-1}s^{-1}	*f*
R = CH_3CO	$k_{OH} = 3.1 \times 10^4$ M^{-1}s^{-1}	*g*
R = $CH_2(OH)$	$k_{OH} = 6 \times 10^3$ M^{-1} s^{-1}	*h*
R = CO_2^-	$k_{OH} = 9 \times 10^3$ M^{-1}s^{-1}	*i*
$RCH(OH)_2 \rightleftharpoons RCHO + H_2O$		
R = H	$K_d = 5.5 \times 10^{-4}$	*j*
R = CH_3CO	$K_d = 3.7 \times 10^{-4}$	*k*
R = $CH_2(OH)$	$K_d = 0.11$	*h*
R = CO_2H	$K_d = 3.3 \times 10^{-3}$	*i*
R = CO_2^-	$K_d = 6.6 \times 10^{-2}$	*i*
Aqueous Diffusion		
SO_2	$\mathscr{D}_{aq} = 1.8 \times 10^{-5}$ cm^2 s^{-1}	*l*
RCHO	$\mathscr{D}_{aq} \approx 1 \times 10^{-5}$ cm^2 s^{-1}	*m*

TABLE 4. (Continued)

Process	Constant	Ref.
Gas–phase Diffusion		
SO_2	$\mathscr{D}_g = 0.126$ cm^2 s^{-1}	*n*
RCHO	$\mathscr{D}_g \approx 0.1$ cm^2 s^{-1}	*m*

Refs. (*a*) Betterton and Hoffmann (1988); (*b*) H* estimated by assuming intrinsic Henry's law constant, H ≈ 1 M atm^{-1}; (*c*) Johnstone and Leppla (1934); (*d*) Deveez and Rumpf (1964); (*e*) Hayon *et al.* (1972); (*f*) Bell and Evans (1966); (*g*) Betterton and Hoffmann (1987); (*h*) Sørensen (1972); (*i*) Sørensen *et al.* (1974); (*j*) Bell (1966); (*k*) Wasa and Musha (1970); (*l*) Himmelblau (1964); (*m*) Assumed; (*n*) Andrew (1955).

Figure Captions

Figure 1. Correlation of rate constants, k_1 (•) and k_2 (○), with Taft's σ^* parameter. $\Sigma\sigma^*_{R_1COR_2} = \sigma^*_{R_1} + \sigma^*_{R_2}$.

Figure 2. Correlation between the second–order rate constants, k_1 and k_2 (M^{-1} s^{-1}), corresponding to the addition of HSO_3^- and SO_3^{2-} with RCHO. The solid line is a linear least–squares fit to the data.

Figure 3. Linear–free–energy correlation between hydroxyalkylsulfonate stability constants, K_1, and hydration constants, K_h, of the aldehyde. The solid line is a linear–least–squares fit to the data.

Figure 4. Adduct formation rates in an open atmosphere as a function of pH. Steady–state saturation was assumed with respect to the the reagent gases, SO_2 and RCHO. Adduct abbreviations are defined in Table 1.

Figure 5. Comparison of the characteristic times for gas transfer and the chemical formation rate of hydroxyacetaldehyde–bisulfite addition compounds (DHES). The time scales, τ, are defined in Equations 25–29.

Figure 6. Boundary lines between the regions where hydroxyalkylsulfonate formation is governed by chemical reaction rates and by mass transport limitations for (a) HMS, a = 10 μ; (b) HMS, a = 100 μ ; (c) DHES, a = 10 μ; and (d) DHES, a = 100 μ. Steady–state saturation assumptions are valid below the curves. Typical fog– and cloudwater conditions are shown by the crosshatched area.

Figure 7. ***Solid lines:*** Macroscopic removal rates, $d\rho/dt$, of SO_2 from the atmosphere due to HMS formation for two liquid water contents, L (volume fraction). Removal rates become dependent on the gas–phase concentration of SO_2 above pH 5, since the rate of dehydration of $CH_2(OH)_2$ becomes rate–limiting. ***Dashed lines:*** Macroscopic removal rates of SO_2 that are due to oxidation by H_2O_2.

Figure 8. Sulfur(IV) enrichment factors at equilibrium due to hydroxyalkyl–sulfonate formation in an open atmosphere. The factor f_e is defined in Equation 35.

Figure 9. Fraction of total S(IV) bound as the aldehyde–bisulfite adduct as a function of pH for P_{SO_2} = 1 ppbv, (a) P_{RCHO} = 1 ppbv, LWC = .01 g/m^3; (b) P_{RCHO} = 1 ppbv, LWC = 0.1 g/m^3; and (c) P_{RCHO} = 10 ppbv, LWC = 0.1 g/m^3. An equation for ρ is given in Equation 37.

Figure 10. Calculated equilibrium pH after hydroxymethanesulfonate (HMS) formation in an open atmosphere containing 3.2×10^{-4} atm CO_2 and varying concentrations of SO_2 and HCHO.

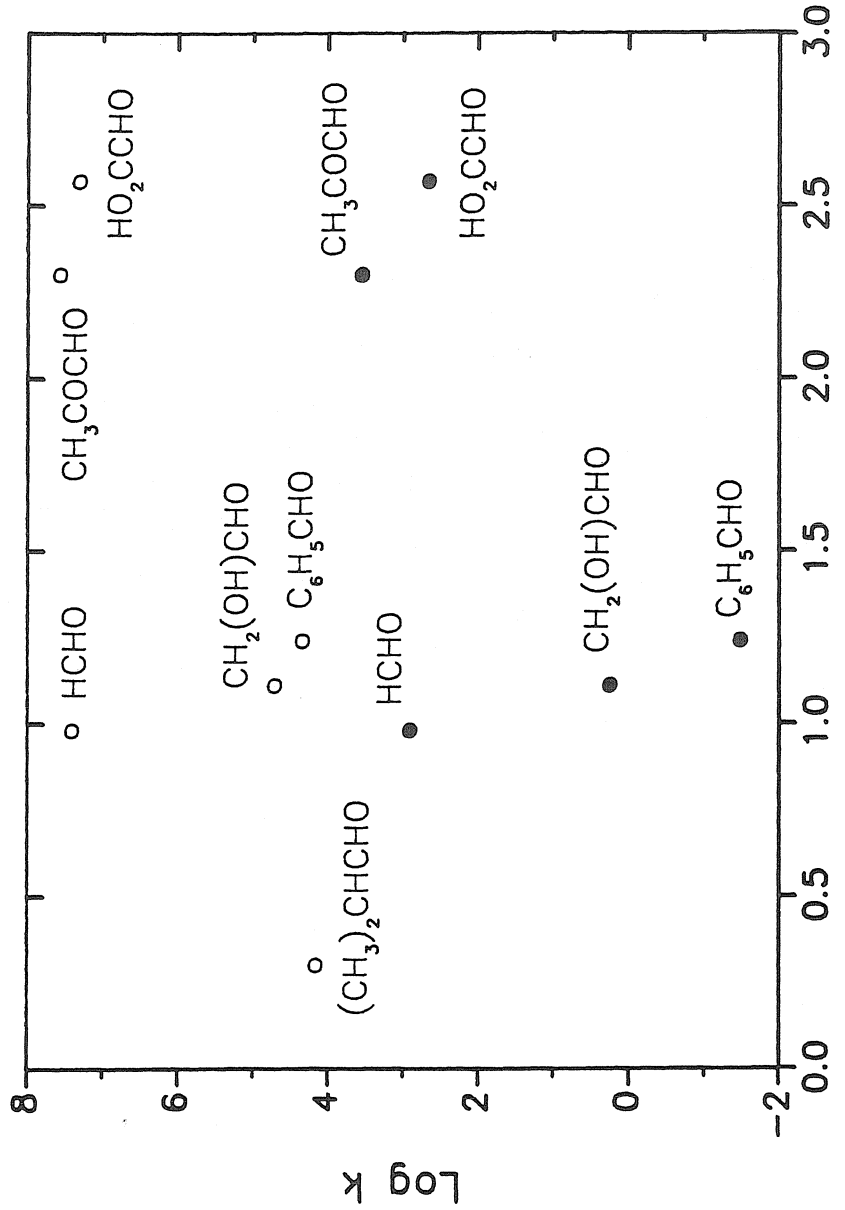
Log k
8
6
4
2
0
−2
0.0
0.5
1.0
1.5
2.0
2.5
3.0
Σσ*
HCHO
CH3COCHO
HO2CCHO
CH2(OH)CHO
C6H5CHO
(CH3)2CHCHO
HCHO
CH3COCHO
HO2CCHO
CH2(OH)CHO
C6H5CHO

Figure 1

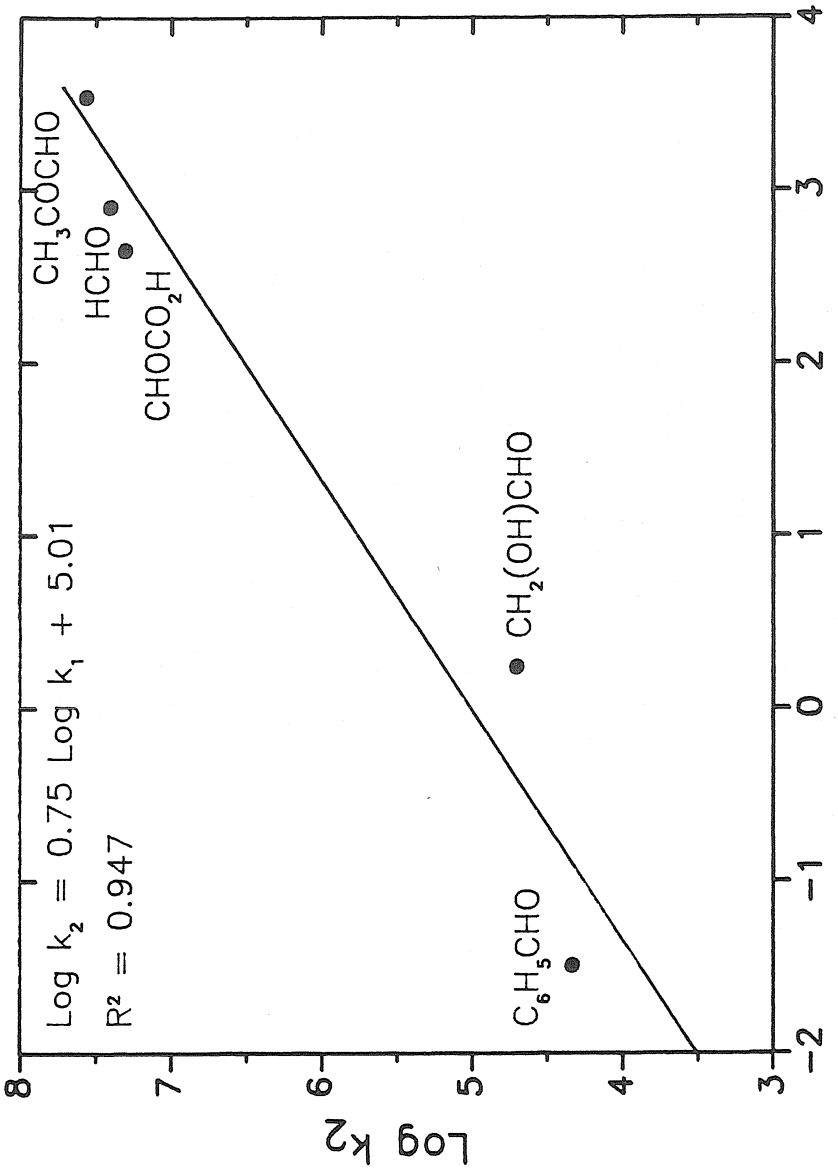
Log k2
Log k1
Log k2 = 0.75 Log k1 + 5.01
R2 = 0.947
CH3COCHO
HCHO
CHOCO2H
CH2(OH)CHO
C6H5CHO
8
7
6
5
4
3
-2
-1
0
1
2
3
4

Figure 2

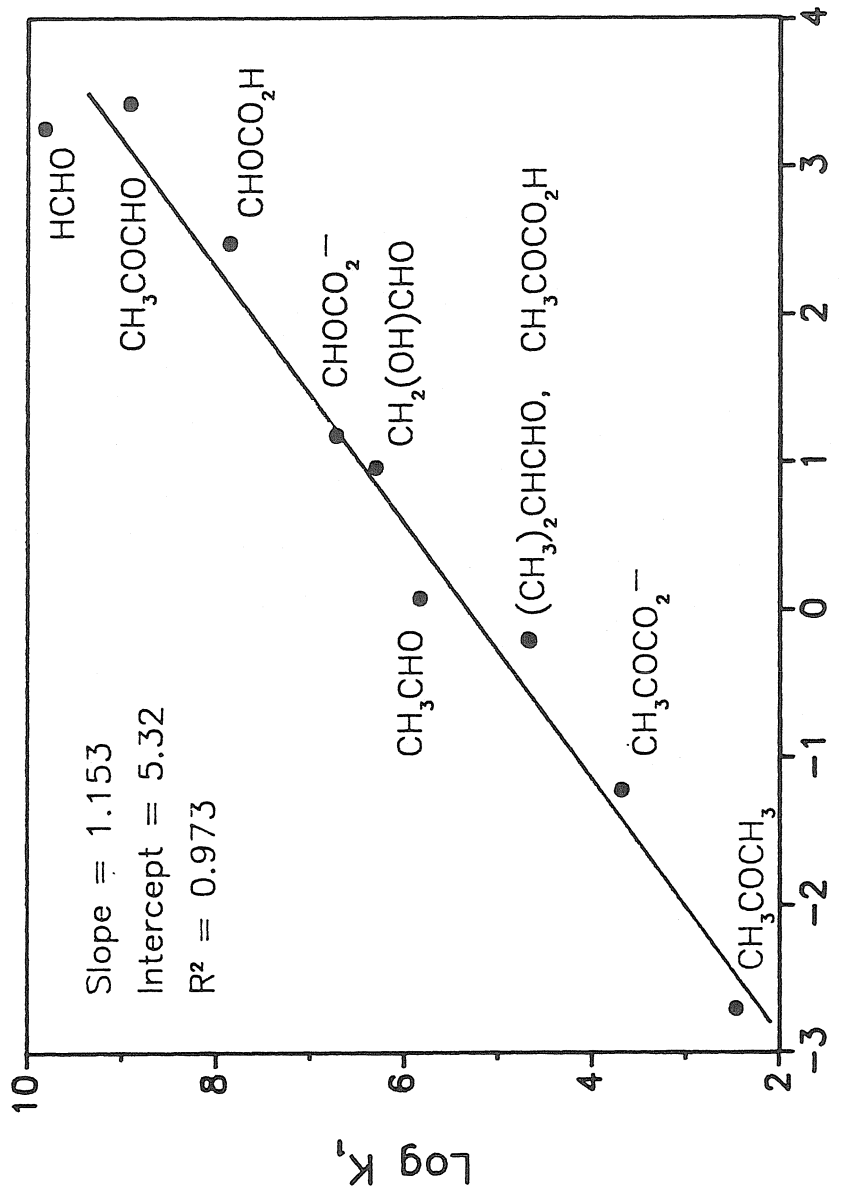
Slope = 1.153
Intercept = 5.32
R² = 0.973
HCHO
CH3COCHO
CHOCO2H
CHOCO2−
CH2(OH)CHO
CH3CHO
(CH3)2CHCHO, CH3COCO2H
CH3COCO2−
CH3COCH3
Log K
Log (Kh)
10
8
6
4
2
−3
−2
−1
0
1
2
3
4

Figure 3

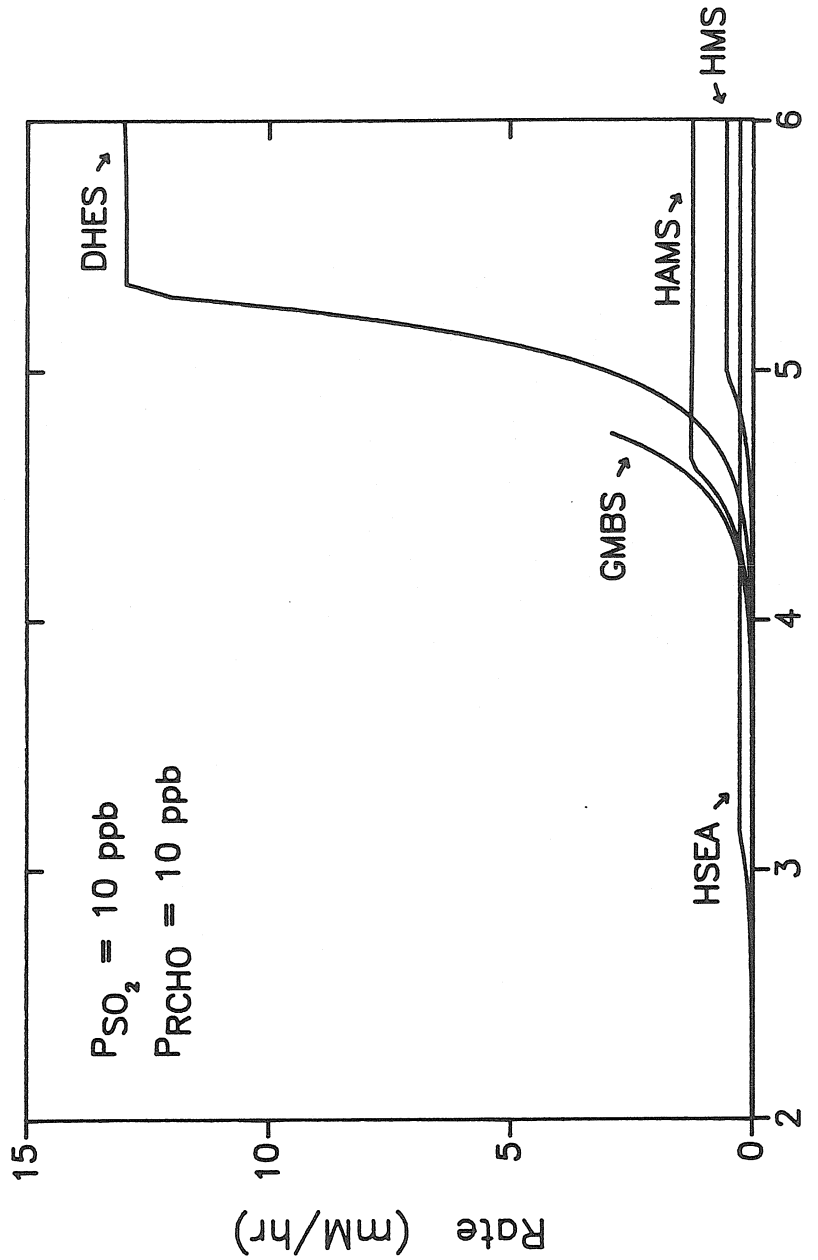
Rate (mM/hr)
pH
DHES
HAMS
HMS
GMBS
HSEA
P_{SO_2} = 10 ppb
P_{RCHO} = 10 ppb
0
5
10
15
2
3
4
5
6

Figure 4

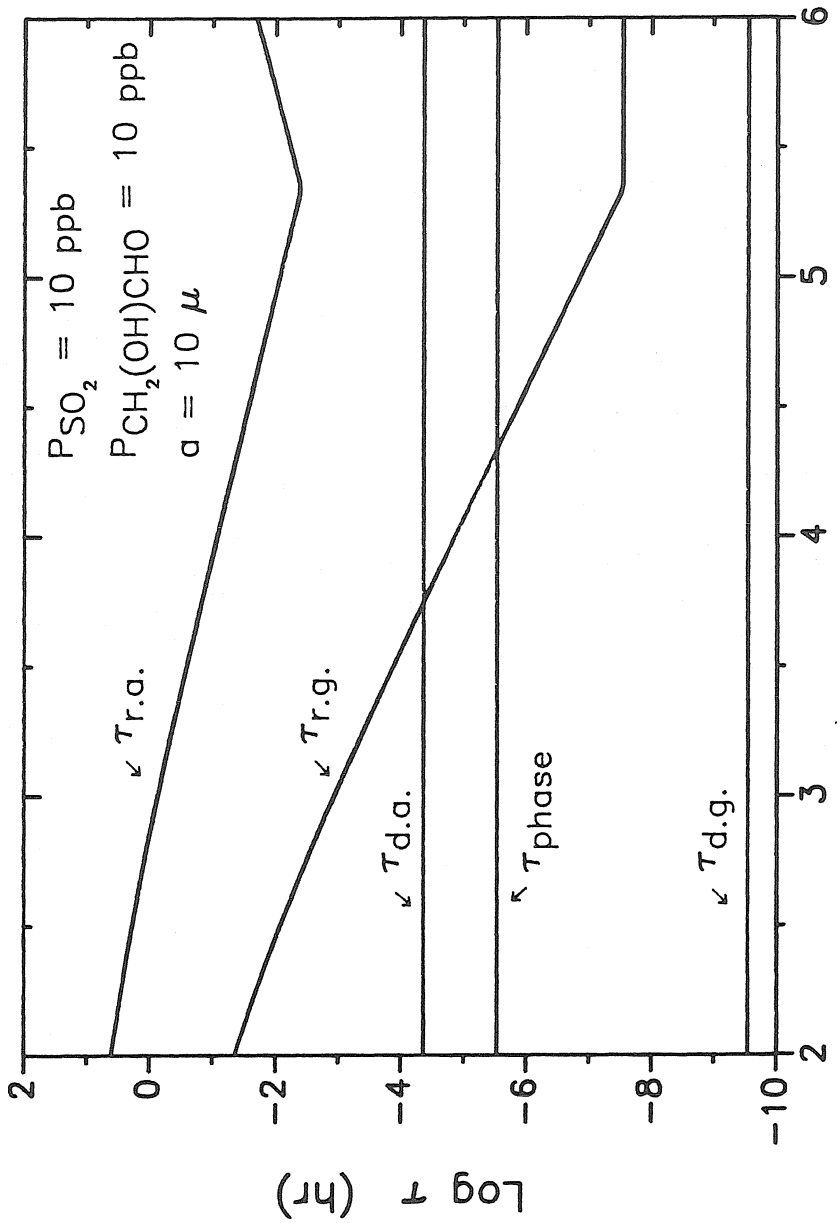
P_{SO_2} = 10 ppb
$P_{CH_2(OH)CHO}$ = 10 ppb
a = 10 μ
$\tau_{r.a.}$
$\tau_{r.g.}$
$\tau_{d.a.}$
τ_{phase}
$\tau_{d.g.}$
Log τ (hr)
pH
2
0
−2
−4
−6
−8
−10
2
3
4
5
6

Figure 5

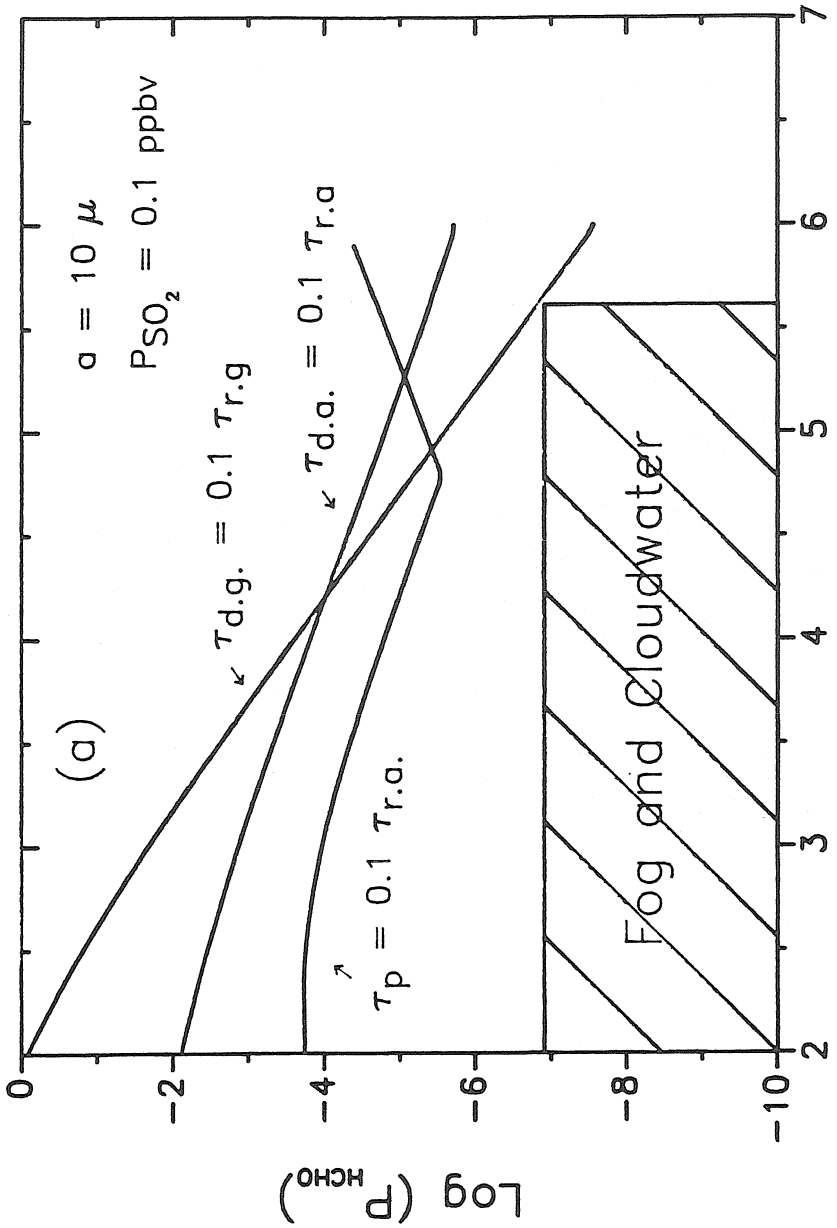
(a)
a = 10 μ
P_{SO_2} = 0.1 ppbv
$\tau_{d.g.}$ = 0.1 $\tau_{r.g}$
$\tau_{d.a.}$ = 0.1 $\tau_{r.a}$
τ_p = 0.1 $\tau_{r.a.}$
Fog and Cloudwater
Log (P_{HCHO})
pH
0
-2
-4
-6
-8
-10
2
3
4
5
6
7

Figure 6a

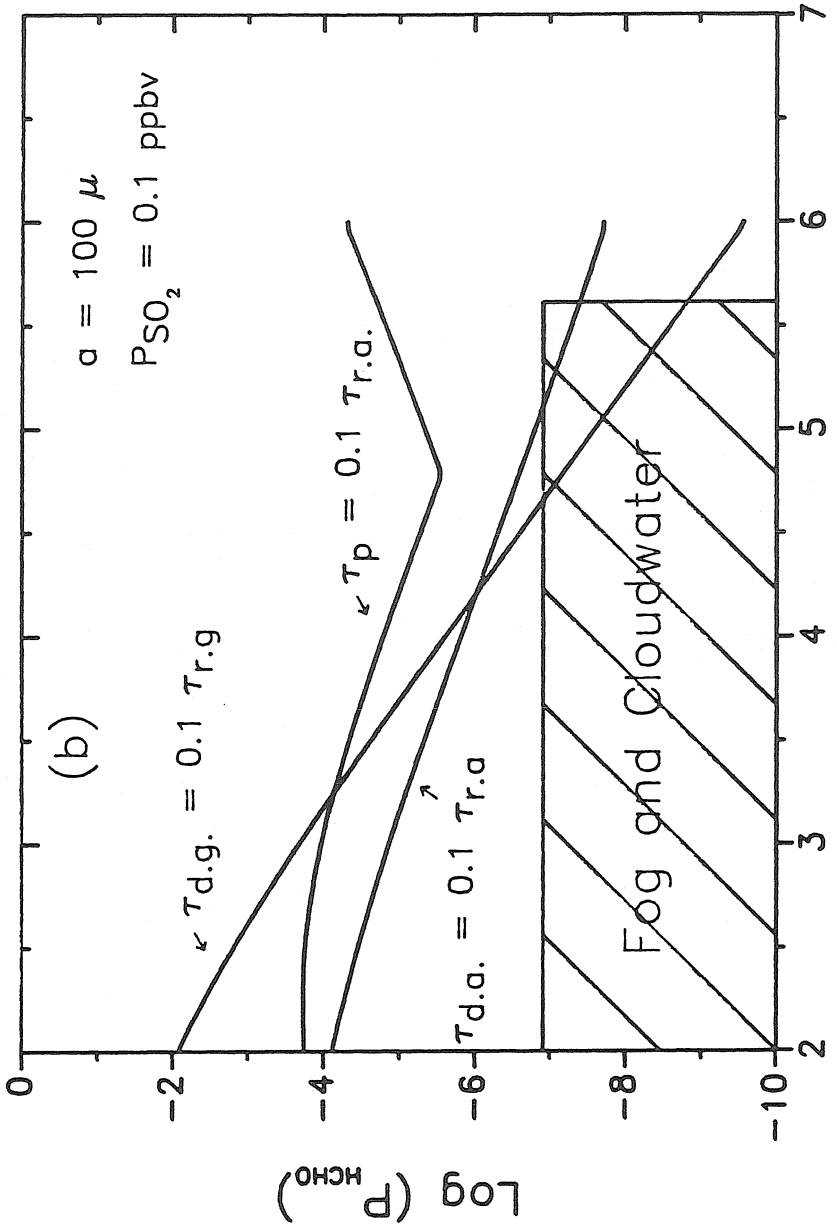
(b)
a = 100 μ
P_{SO_2} = 0.1 ppbv
$\tau_{d.g.}$ = 0.1 $\tau_{r.g}$
τ_p = 0.1 $\tau_{r.a.}$
$\tau_{d.a.}$ = 0.1 $\tau_{r.a}$
Fog and Cloudwater
Log (P_{HCHO})
pH
0
-2
-4
-6
-8
-10
2
3
4
5
6
7

Figure 6b

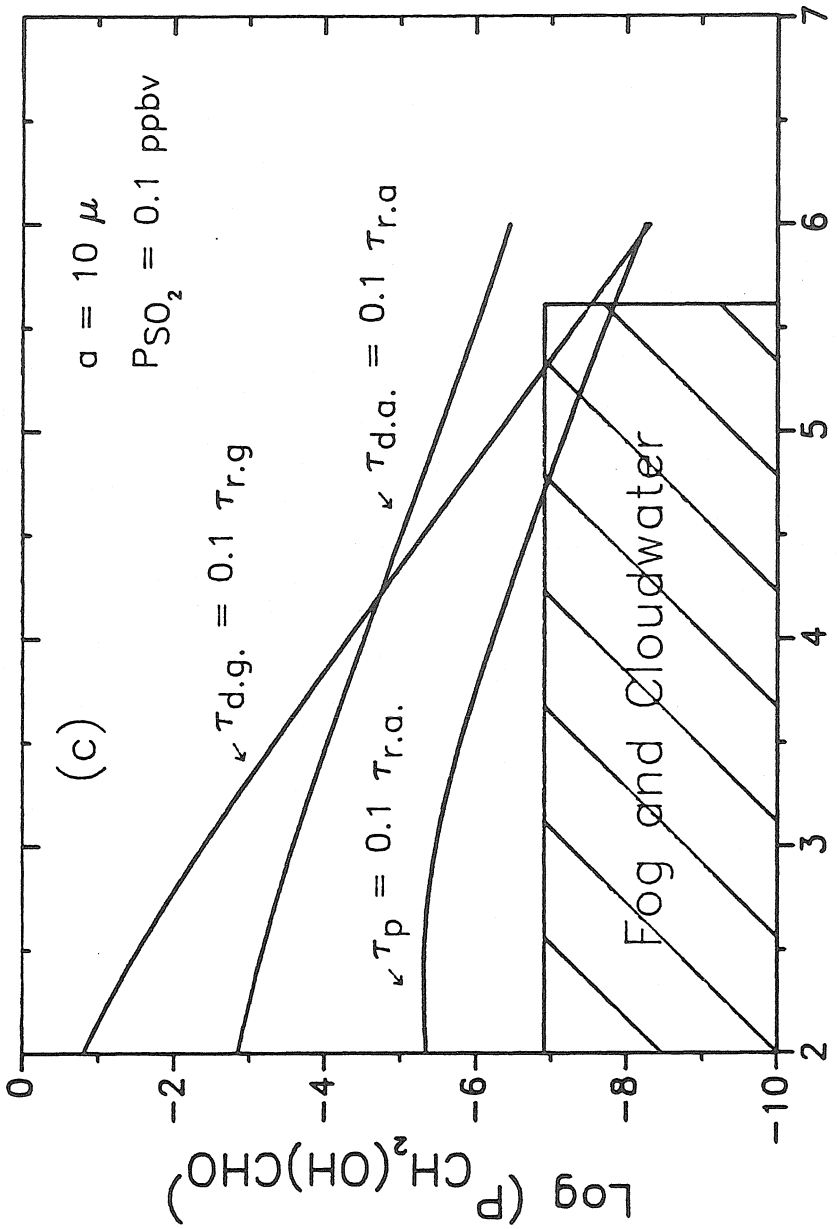
(c)
a = 10 μ
P_{SO_2} = 0.1 ppbv
$\tau_{d.g.} = 0.1\ \tau_{r.g}$
$\tau_{d.a.} = 0.1\ \tau_{r.a}$
$\tau_p = 0.1\ \tau_{r.a.}$
Fog and Cloudwater
Log ($P_{CH_2(OH)CHO}$)
pH
0
-2
-4
-6
-8
-10
2
3
4
5
6
7

Figure 6c

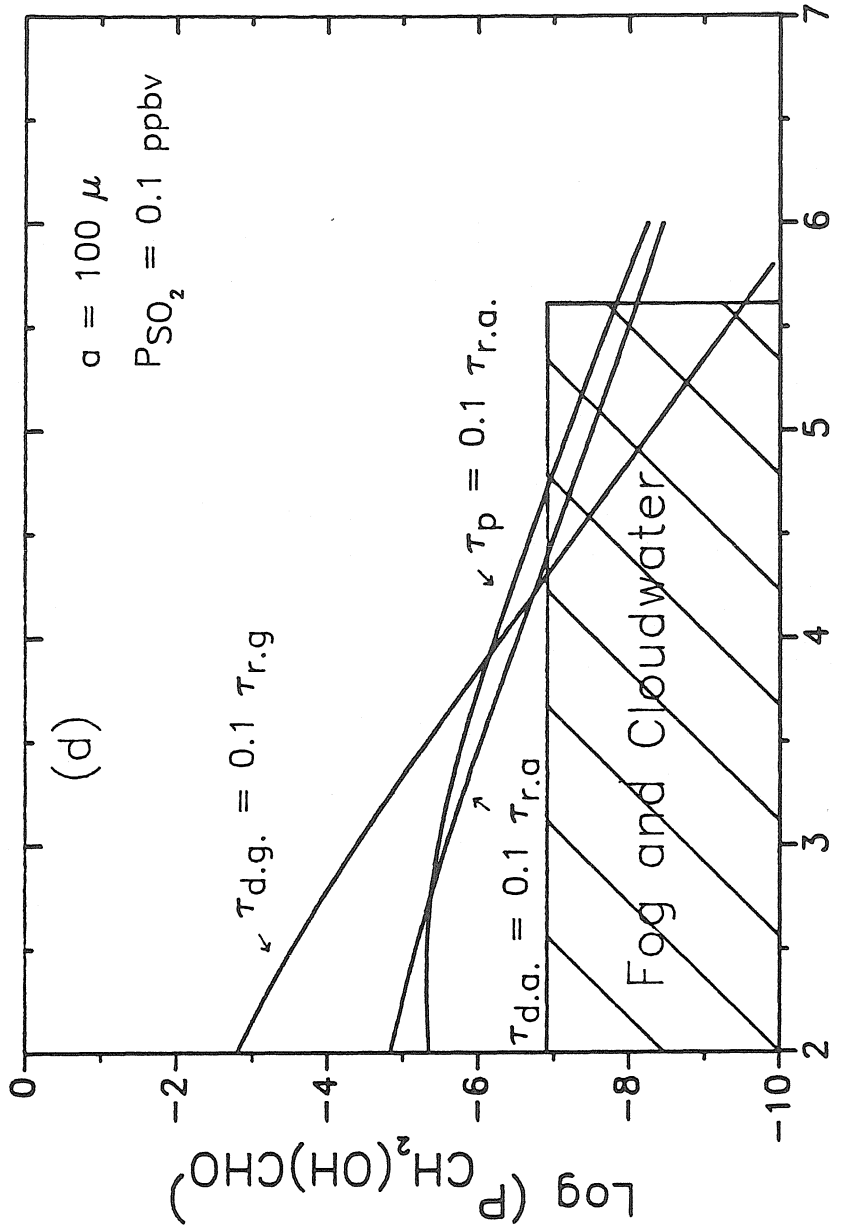
(d)
a = 100 μ
P_{SO_2} = 0.1 ppbv
$\tau_{d.g.}$ = 0.1 $\tau_{r.g}$
τ_p = 0.1 $\tau_{r.a.}$
$\tau_{d.a.}$ = 0.1 $\tau_{r.a}$
Fog and Cloudwater
Log ($P_{CH_2(OH)CHO}$)
pH
0
-2
-4
-6
-8
-10
2
3
4
5
6
7

Figure 6d

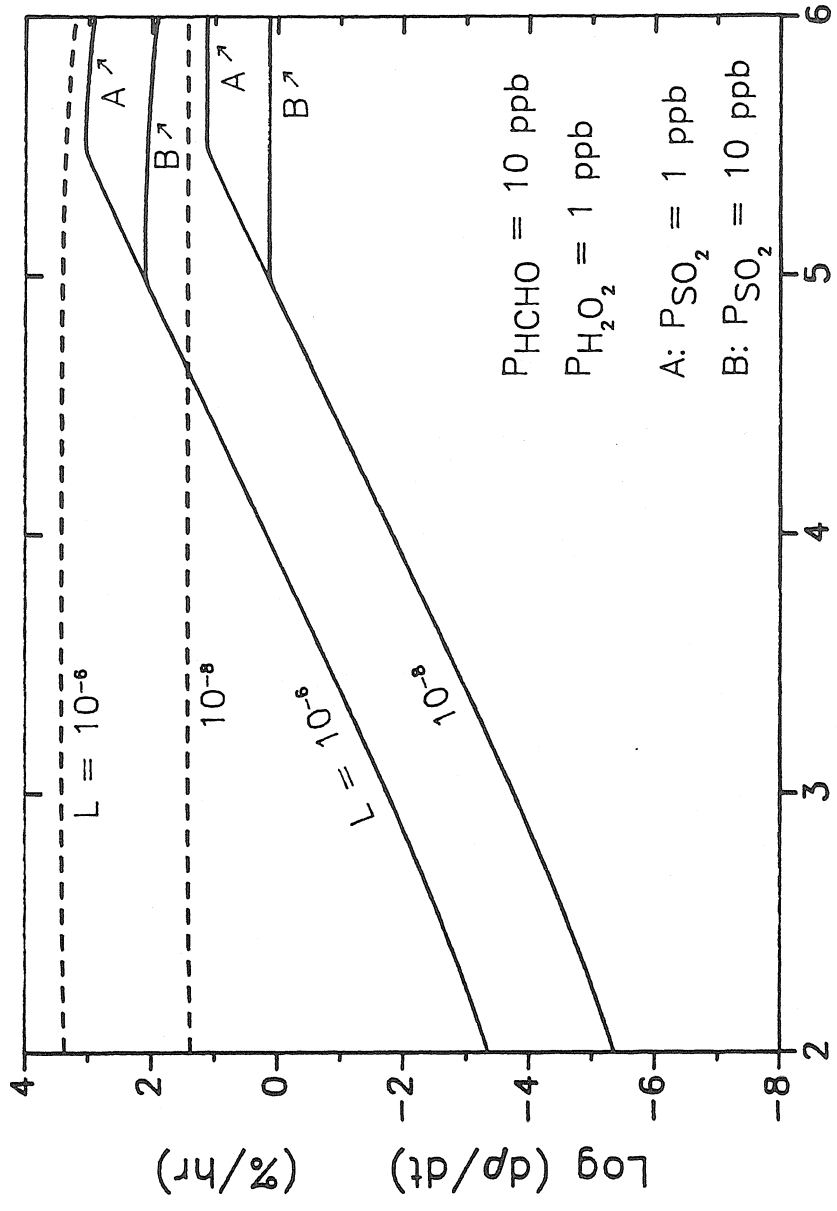
Log (dp/dt) (%/hr)
pH
P_{HCHO} = 10 ppb
$P_{H_2O_2}$ = 1 ppb
A: P_{SO_2} = 1 ppb
B: P_{SO_2} = 10 ppb
L = 10^{-6}
10^{-8}
L = 10^{-6}
10^{-8}
A
B
A
B

Figure 7

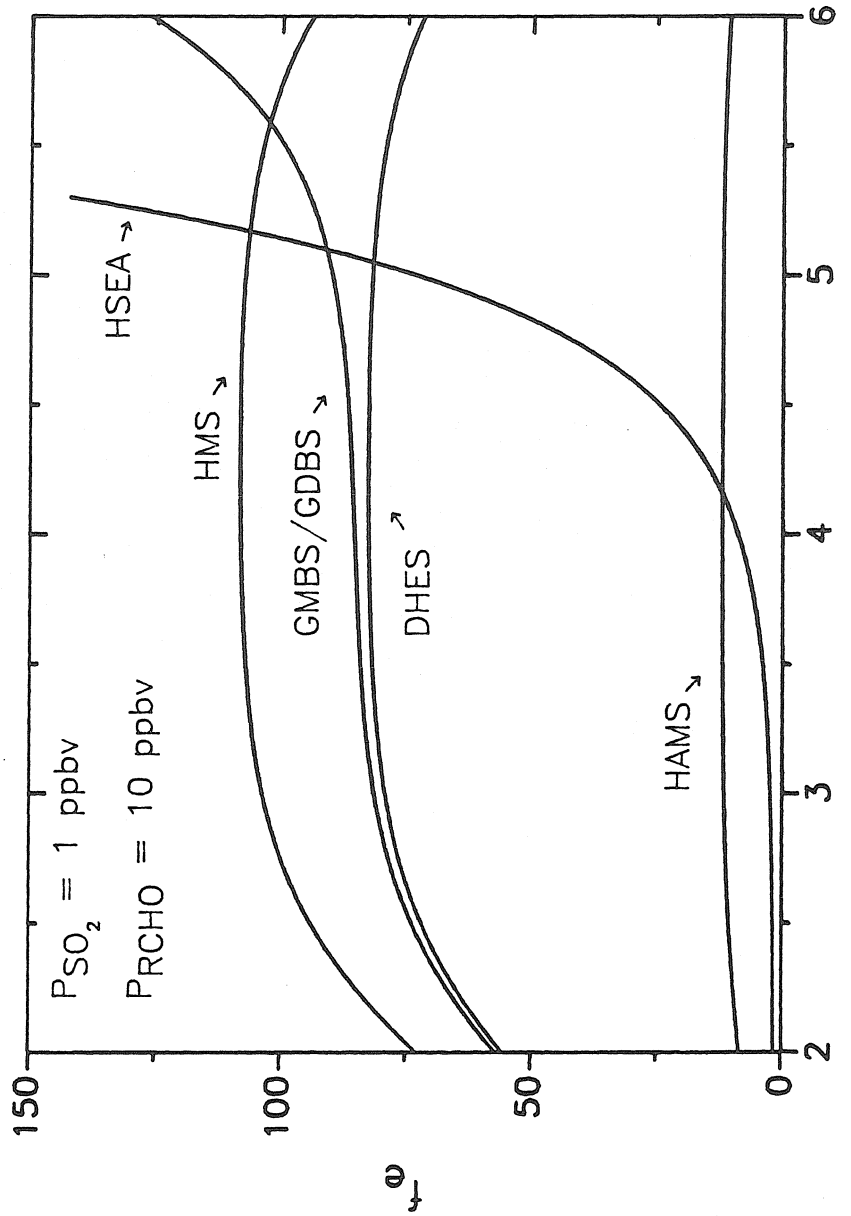
150
100
50
0
ω_f
2
3
4
5
6
pH
P_{SO_2} = 1 ppbv
P_{RCHO} = 10 ppbv
HSEA
HMS
GMBS/GDBS
DHES
HAMS

Figure 8

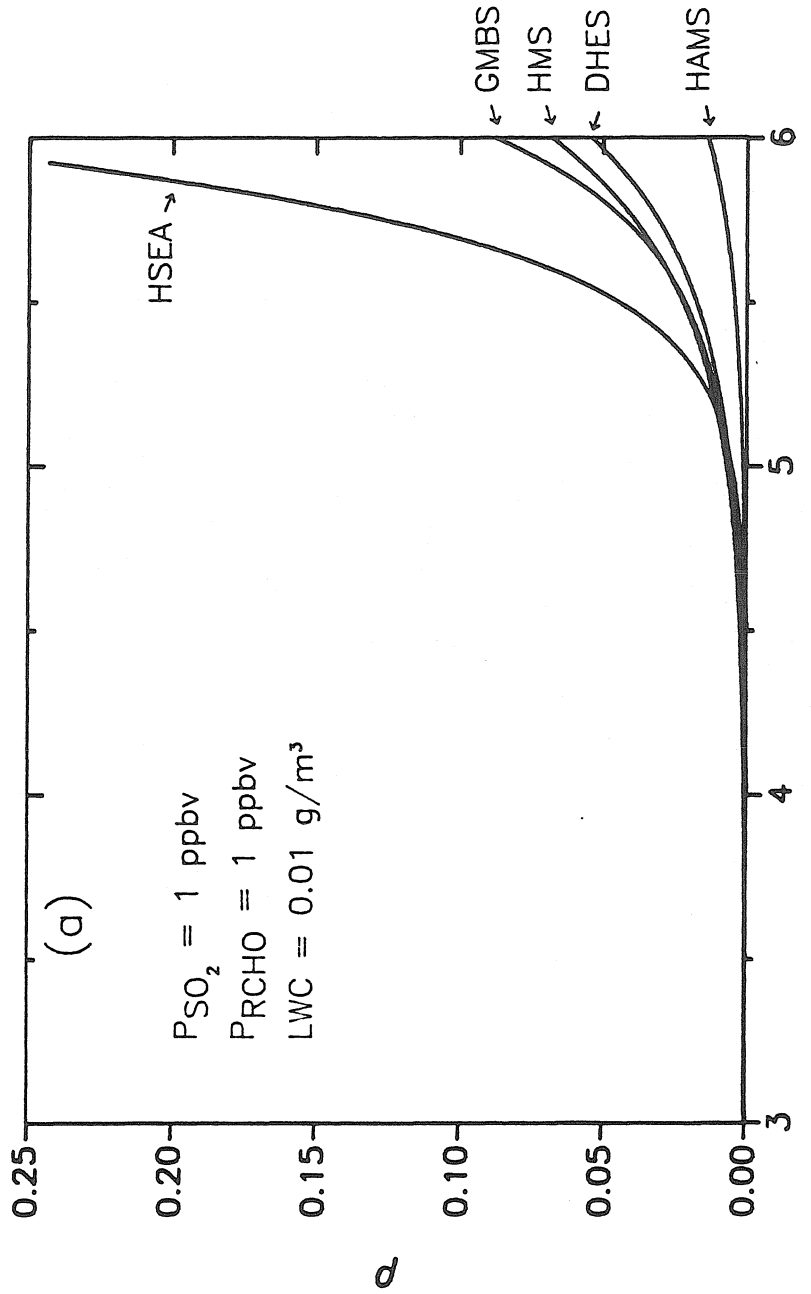
0.25
0.20
0.15
0.10
0.05
0.00
α
3
4
5
6
pH
(a)
P_{SO_2} = 1 ppbv
P_{RCHO} = 1 ppbv
LWC = 0.01 g/m³
HSEA
GMBS
HMS
DHES
HAMS

Figure 9a

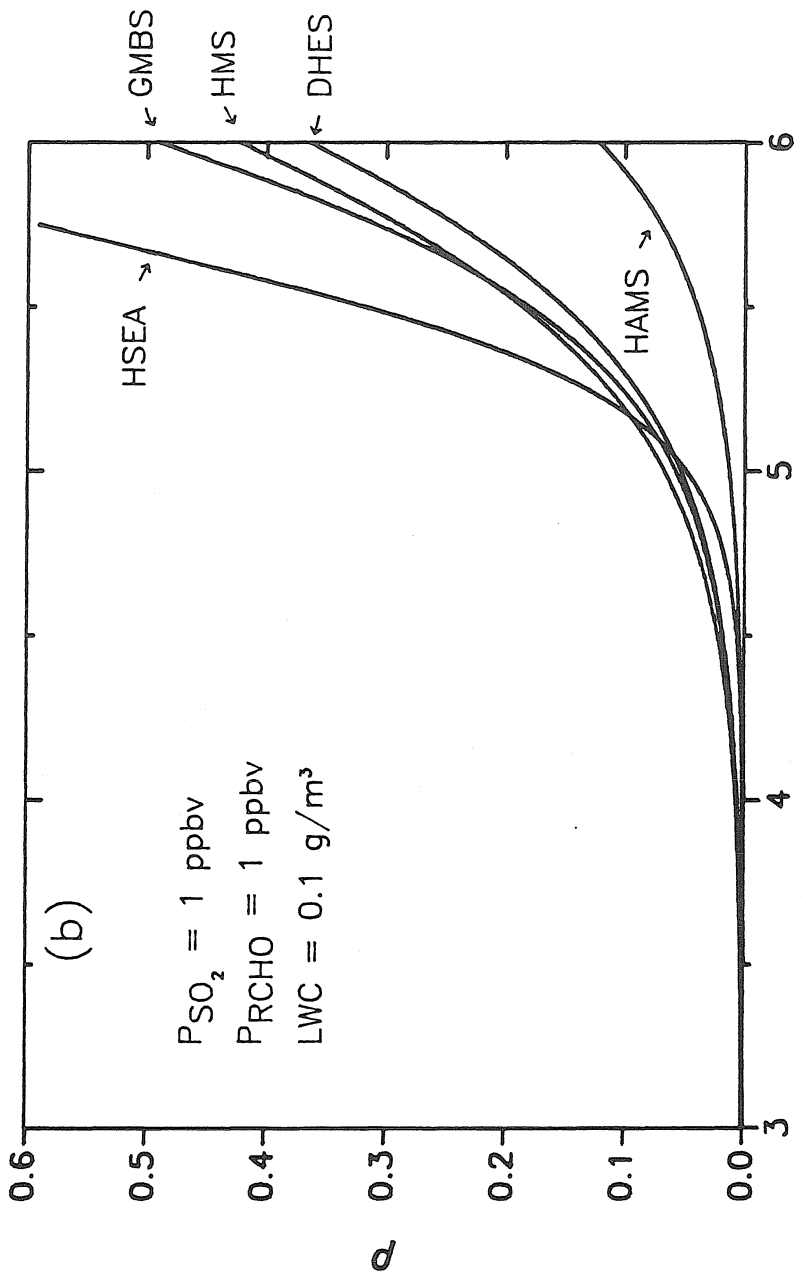
GMBS
HMS
DHES
HSEA
HAMS
(b)
P_{SO_2} = 1 ppbv
P_{RCHO} = 1 ppbv
LWC = 0.1 g/m³
α
pH
0.0
0.1
0.2
0.3
0.4
0.5
0.6
3
4
5
6

Figure 9b

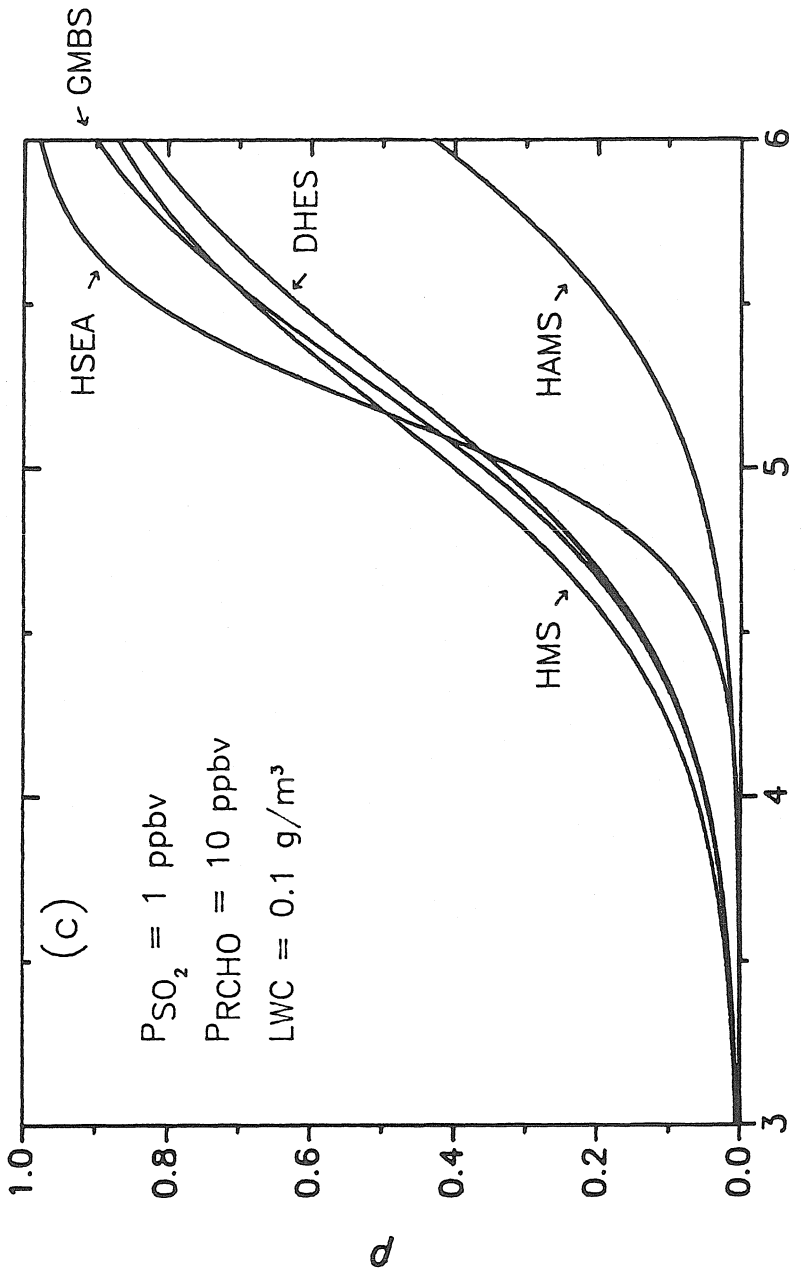
GMBS
HSEA
DHES
HAMS
HMS
(c)
P_{SO_2} = 1 ppbv
P_{RCHO} = 10 ppbv
LWC = 0.1 g/m³
α
pH
1.0
0.8
0.6
0.4
0.2
0.0
3
4
5
6

Figure 9c

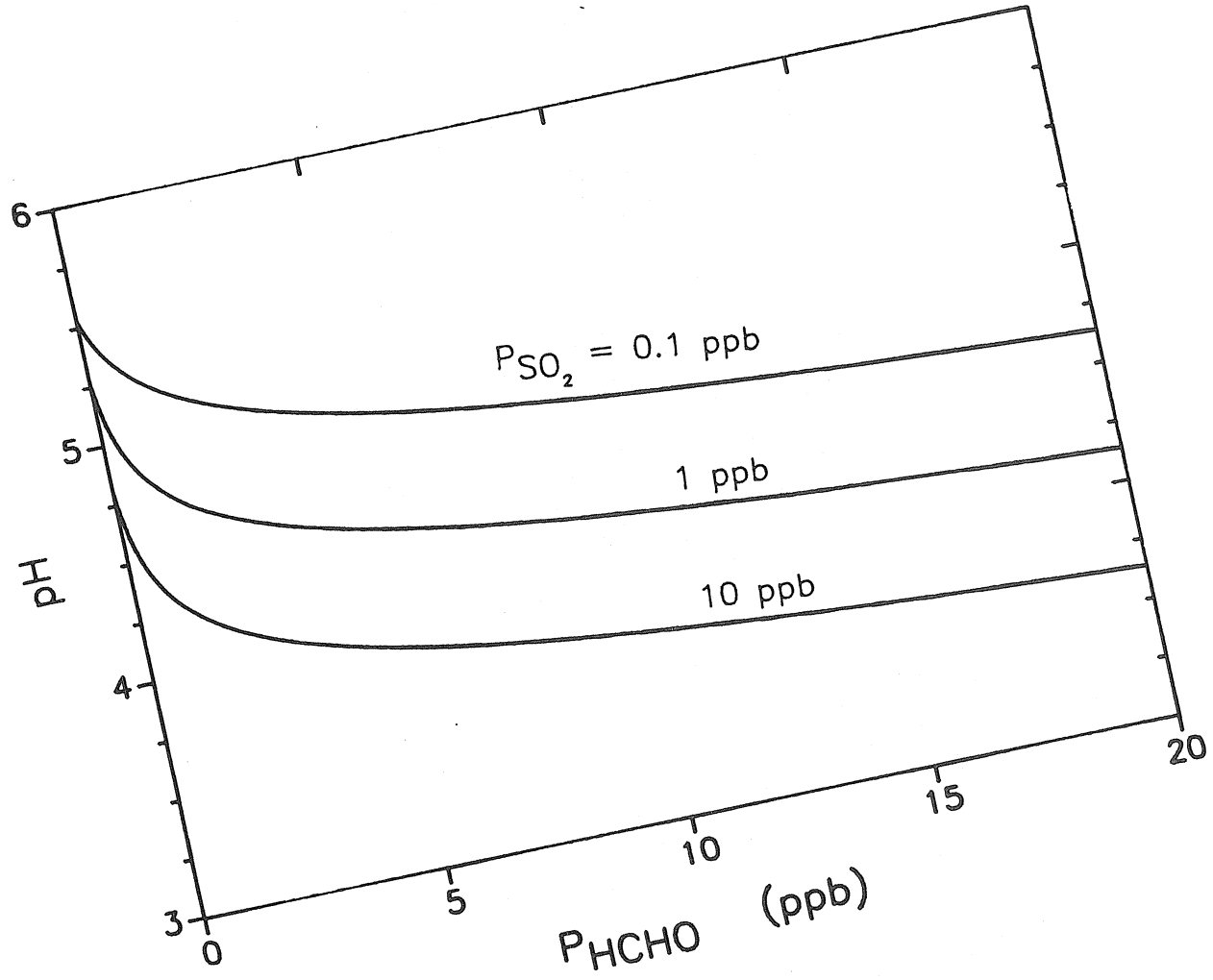

Figure 10

CHAPTER 3

Kinetics, Thermodynamics, and Mechanism of the Formation of Benzaldehyde–S(IV) Adducts

by

Terese M. Olson, Scott D. Boyce, and Michael R. Hoffmann

Journal of Physical Chemistry, 90, 2482–2488 (1986)

Reprinted from The Journal of Physical Chemistry, 1986, 90, 2482

Kinetics, Thermodynamics, and Mechanism of the Formation of Benzaldehyde–S(IV) Adducts

Terese M. Olson, Scott D. Boyce, and Michael R. Hoffmann*

Department of Environmental Engineering Science, W. M. Keck Laboratories, California Institute of Technology, Pasadena, California 91125 *(Received: October 11, 1985; In Final Form: January 8, 1986)*

The kinetics and mechanism of the formation of α-hydroxyphenylmethanesulfonate (HPMS) by the addition of bisulfite to benzaldehyde were studied at low pH. A three-term rate law was observed as $d[HPMS]/dt = \{k_1\alpha_2 + (k_2 + k_3K_H\{H^+\})\alpha_1\}[S(IV)][C_6H_5CHO]$ where $\alpha_1 = [HSO_3^-]/[S(IV)]$, $\alpha_2 = [SO_3^{2-}]/[S(IV)]$, and K_H is the proton association constant of benzaldehyde. The rate-limiting steps of each term appeared to be the nucleophilic attack of SO_3^{2-} on the carbonyl carbon of benzaldehyde, the attack of HSO_3^- on the carbonyl carbon, and the attack by HSO_3^- on the protonated carbon of the carbocation, $C_6H_5C^+H(OH)$, respectively. Over the pH range of most natural systems, only the k_1 and k_2 steps contribute to adduct formation while the k_3 term becomes important for pH < 1. At 25 °C and μ = 1.0 M, the intrinsic rate constants were determined to be $k_1 = (2.15 \pm 0.09) \times 10^4$ M^{-1} s^{-1}, $k_2 = (0.71 \pm 0.03)$ M^{-1} s^{-1}, $k_3 \simeq 2.5 \times 10^7$ M^{-1} s^{-1}. Para-substitution on the benzaldehyde ring resulted in a slight increase in reactivity for p-NO_2– and p-Cl–, and a decrease for p-OH–, p-OCH_3–, and p-CH_3–C_6H_5CHO. The equilibrium association constant, $K = [C_6H_5CH(OH)SO_3^-]/[HSO_3^-][C_6H_5CHO]$, at 25 °C was determined to be 4.8 (±0.8) × 10^3 at μ = 0.1 M and 0.98 (±0.11) × 10^3 M^{-1} at μ = 1.0 M. ΔH° and ΔS° were determined to be −64.6 kJ mol^{-1} and −146 J mol^{-1} deg^{-1}, respectively.

Introduction

Benzaldehyde has been found to be present in fogs, clouds, and rain at substantial levels.[1-3] In aqueous solution, benzaldehyde reacts with SO_2 to form α-hydroxyphenylmethanesulfonate (HPMS). Formation of S(IV)–carbonyl adducts such as HPMS leads to the apparent stabilization and enhancement of S(IV) in atmospheric water droplets. Previously, we established that hydroxymethanesulfonate (HMS, the formaldehyde–bisulfite adduct) is often present in fogwater in appreciable concentrations.[4a-c]

The kinetics[5-7] and thermodynamics[5,7-11] of bisulfite addition to benzaldehyde have been studied previously. Stewart and Donnally[5a,b] proposed a three-term rate law for the dissociation of HPMS over the pH range 0–13. In their proposed mechanism, three discrete forms of the diprotic hydroxyphenylmethanesulfonic acid dissociate to give benzaldehyde and SO_3^{2-}, HSO_3^-, or $H_2O{\cdot}SO_2$, respectively. Blackadder and Hinshelwood[6] reported overall dissociation rate constants for the release of HSO_3^- at pH 3 (1.55×10^{-4} s^{-1}) and pH 5 (7.76×10^{-3} s^{-1}); their values were consistent with those reported by Stewart and Donnally,[5] which were $\sim 1.7 \times 10^{-4}$ and $\sim 1 \times 10^{-2}$ s^{-1} for pH 3 and 5, respectively. Iodometric titration was used as an analytical method by both groups. However, a rate constant of 1.7×10^{-2} s^{-1} (13 °C), which appears to be at least an order of magnitude higher than that reported by Stewart and Donnally[5] at pH ~ 4.1 for the dissociation of $HPMS^-$ to HSO_3^- and C_6H_5CHO, was reported by Sousa and Margerum,[7] based on spectroscopic measurements.

Values for the formation constant of the bisulfite–benzaldehyde adduct are compiled in Table I. In some cases, pH was not reported; therefore some of the cited values, which vary by more than an order of magnitude, may be apparent constants. In addition, iodometric titration as used by Kerp,[8] Gubareva,[9] and Stewart and Donnally[5a,b] may have led to errors in that rapid dissociation of the complex most likely occurred during titration. Kokesh and Hall[11] examined this possibility by measuring K_{obsd} vs. pH spectrophotometrically and found that the titration method yielded inaccurate equilibrium constants above pH 8.

TABLE I: Literature Values for the Equilibrium Association Constant of HSO_3^- and Benzaldehyde

$10^{-3}K$, M^{-1}	conditions	method	ref
11.3	20.9 °C, pH 5.21	iodometric titration	5b
4.7	23 °C	UV spectrophotometry	7
10.0	15–17 °C, $\mu \simeq 0.1$ M	iodometric titration	8
0.44	30 °C	iodometric titration	9
1.27	20 °C, pH 4.3	UV spectrophotometry	10
6.4	21 °C, μ = 1.0 M, pH 3.5–5.3	UV spectrophotometry	11
4.8	25 °C, μ = 0.1 M	UV spectrophotometry	this work

In view of the above uncertainties, a thorough investigation of the kinetics, mechanism, and thermodynamics of bisulfite–benzaldehyde was conducted by using spectrophotometric methods. The rate of adduct formation was studied over the pH range 0–4.4, which is typical of acidic fogs, clouds, and haze aerosols.[12,13] The formation constant for HSO_3^- and benzaldehyde was determined as a function of ionic strength and temperature.

Experimental Procedures

Materials. Reagent grade sodium sulfite (Mallinkrodt), sodium bisulfite (Mallinkrodt), hydrochloric acid (Mallinkrodt), sodium hydroxide (Mallinkrodt), chloroacetic acid (MCB), dichloroacetic acid (MCB), glacial acetic acid (Dupont), formic acid (Mallinkrodt), and phosphoric acid (Spectrum) were utilized without further purification. Benzaldehyde (MCB) was redistilled periodically. Stock solutions of para-substituted benzaldehydes (p-Cl, NO_2, OH, CH_3, and CH_3O) were prepared by dissolving analytical grade Aldrich reagents in 60% (v/v) methanol/H_2O. The sodium salt of the benzaldehyde–bisulfite addition compound, which was used in equilibrium constant determinations, was prepared according to Blackadder and Hinshelwood.[6] Elemental analysis of the salt (Galbraith Laboratories) suggested a stoichiometry of $Na{\cdot}C_6H_5CH(OH)SO_3{\cdot}^1/_2(H_2O)$. Ionic strength was maintained (μ = 1.0 M) with sodium chloride (Mallinkrodt). All water used

(1) Grosjean, D.; Wright, B. *Atmos. Environ.* **1983**, *17*, 2093–96.
(2) Kawamura, K.; Kaplan, I. R. *Environ. Sci. Technol.* **1983**, *17*, 497–501.
(3) Lunde, G.; Gether, J.; Gjos, N.; Lunde, M. B. S. *Atmos. Environ.* **1977**, *11*, 1007–14.
(4) (a) Munger, J. W.; Jacob, D. J.; Waldman, J. M.; Hoffmann, M. R. *J. Geophys. Res.* **1983**, *88*, 5109–21. (b) Munger, J. W.; Jacob, D. J.; Hoffmann, M. R. *J. Atmos. Chem.* **1984**, *11*, 335–50. (c) Munger, J. W.; Tiller, C.; Hoffmann, M. R. *Science* **1986**, *231*, 247–249.
(5) (a) Stewart, T. D.; Donnally, L. H. *J. Am. Chem. Soc.* **1932**, *54*, 2333–40. (b) Stewart, T. D.; Donnally, L. H. *Ibid.* **1932**, *54*, 3555–69.
(6) Blackadder, D. A.; Hinshelwood, C. *J. Chem. Soc.* **1958**, 2720–27.
(7) Sousa, J. A.; Margerum, J. D. *J. Am. Chem. Soc.* **1960**, *82*, 3013–16.
(8) Kerp, W. *Chem. Zentralbl.* **1904**, *75/II*, 56–59.
(9) Gubareva, M. A. *J. Gen. Chem.* **1947**, *17*, 2259–64.
(10) Arai, K. *Nippon Kagaku Zasshi* **1962**, *83*, 765–767.
(11) Kokesh, F. C.; Hall, R. E. *J. Org. Chem.* **1975**, *40*, 1632–36.
(12) Jacob, D. J.; Waldman, J. M.; Munger, J. W.; Hoffmann, M. R. *Environ. Sci. Technol.* **1985**, *19*, 730–36.
(13) Waldman, J. M.; Munger, J. W.; Hoffmann, M. R. *Tellus* **1985**, *37B*, 91–108.

0022-3654/86/2090-2482$01.50/0

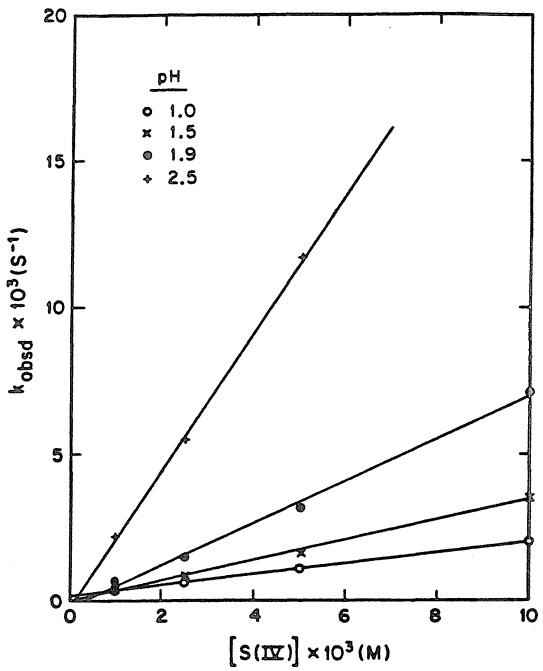

Figure 1. Dependence of the pseudo-first-order rate constant on [S(IV)] over the pH (−log $[H^+]$) range 1.3–4.4. The solid line denotes the linear least-squares fit to the data. Reaction conditions: $[C_6H_5CHO]_t$ = 0.05–0.1 mM, $[S(IV)]_t$ = 0.5–10 mM, T = 25 °C, μ = 1.0 M.

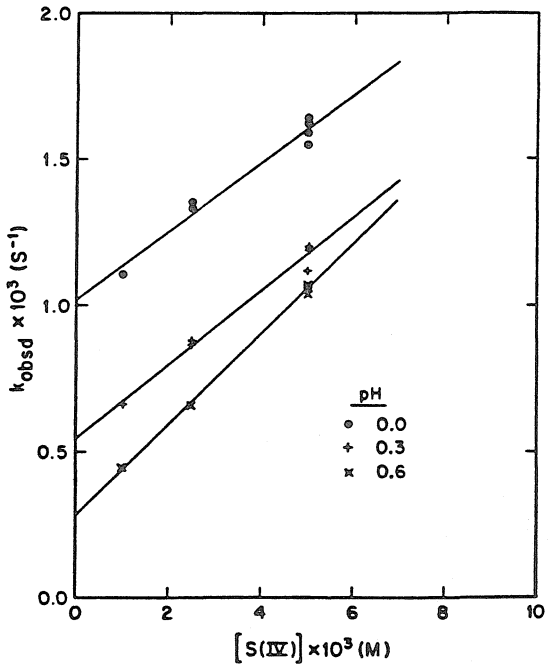

Figure 2. Dependence of pseudo-first-order rate constant on [S(IV)] over the pH range 0–1. Reaction conditions are same as given in Figure 1.

to prepare the solutions was deionized (18 MΩ cm resistivity; Milli RO-4/Milli Q) and deoxygenated by purging with N_2. Reagent solutions were prepared daily in a glovebox under a N_2 atmosphere. Hydrogen ion activities were measured with a Beckman Altex Model Φ71 pH meter and Radiometer glass electrode.

Methods. Reaction rates were determined by monitoring the disappearance of benzaldehyde with a Hewlett-Packard Model 8450A UV/visible spectrophotometer at 249 nm (λ_{max}). These measurements were made in a 1-cm quartz cell. Temperature was held constant (25 °C unless otherwise stated) with a Haake Model FK-2 water recirculation bath and temperature controller. Between 15 and 200 absorbance measurements were collected for each kinetic analysis and an average of four determinations for each pseudo-first-order rate constant was obtained. Sulfur(IV) concentrations ranged from 0.5 to 10 mM, while total benzaldehyde concentrations in the samples varied from 0.05 to 0.1 mM.

The equilibrium constant was determined by dissolving the sodium salt of the addition compound in solution and measuring the absorbance of the equilibrated solution at 250 nm in a 1-cm cell. Published values of the extinction coefficients of the complex (ϵ = 152 L/(mol cm)) and benzaldehyde ($\epsilon = 1.26 \times 10^3$ L/(mol cm)) at this wavelength were then used to calculate the equilibrium constant. Our independent determination of ϵ for benzaldehyde did not differ significantly from the literature value; the absorptivity of benzaldehyde varied by less than 1.5% over the temperature range 15–35 °C. The pH of each solution was adjusted to 3.9 ± 0.1 with HCl. Thermodynamic parameters were determined by varying the cell temperature with a Hewlett-Packard Model 89100A temperature controller. The averages of four absorbance measurements at three different concentrations of the addition compound were used to calculate the equilibrium constant. Total sulfonate concentrations ranged from 41.0 to 92.0 μM.

Results

Kinetic Studies. Pseudo-first-order conditions were maintained throughout the kinetic study whereby $[S(IV)]_t \gg [C_6H_5CHO]_t$, with a minimum tenfold excess of S(IV). Plots of $\ln \{(A - A_\infty)/(A_0 - A_\infty)\}$ vs. time were linear ($r^2 \geq 0.99$) for better than 90% of the reaction, confirming that the reaction is first-order in benzaldehyde. At constant pH the observed pseudo-first-order rate constant was also a linear function of the total S(IV) concentration, as Figures 1 and 2 illustrate. Above pH 1.0 (see Figure 1), k_{obsd} increased with increasing pH, a phenomenon also characteristic of the formation of hydroxymethanesulfonate[14] and other carbonyl–S(IV) adducts.[15] For pH greater than 2.5, the pH dependence of reaction rate can be made linear by plotting $k_{obsd}/[S(IV)]_t$ vs. the reciprocal of the hydrogen ion activity. A least-squares fit (Figure 3) of data from Table II demonstrates this pH dependence.

Below pH 1.0, however, k_{obsd} increases with decreasing pH (see Figure 2) and the y intercept steadily increases above zero. A similar dissociation rate minimum near pH 1.0 was found by Stewart and Donnally.[5b] Between pH 0.0 and 1.0 there is no

TABLE II: Kinetic Data for the Reaction of S(IV) and Benzaldehyde in Aqueous Solution

pH	$10^3[S(IV)]_t$, M	$10^4[C_6H_5CHO]_t$, M	$10^3 k_{obsd}$ ($\pm\sigma$),[a] s^{-1}	$10^3 k_{calcd}$, s^{-1}
0.0	5.0	1.0	1.60 ± 0.03	1.87
0.3	5.0	1.0	1.17 + 0.02	1.17
0.6	5.0	1.0	1.06 ± 0.02	0.91
1.0	5.0	1.0	1.08 ± 0.02	1.03
1.3	5.0	1.0	1.29 ± 0.01	1.46
1.51	5.0	1.0	1.63 ± 0.03	1.97
1.87	5.0	1.0	3.16 ± 0.03	3.45
2.12	5.0	1.0	4.69 ± 0.06	5.20
2.55	2.5	1.0	5.38 ± 0.07	5.66
2.84	2.5	1.0	10.1 ± 0.10	10.1
3.10	2.5	1.0	18.0 ± 0.20	17.5
3.42	1.0	1.0	15.5 ± 0.20	14.2
4.43	0.5	0.5	70.0 ± 2.1	70.0

[a] $\sigma = [\{(k_{obsd} - \bar{k}_{obsd})^2/N\}]^{1/2}$ where $N = 4$.

(14) Boyce, S.; Hoffmann, M. R. *J. Phys. Chem.* **1984**, *88*, 4740–46.
(15) Jencks, W. P. *Prog. Phys. Org. Chem.* **1964**, *2*, 63–118.

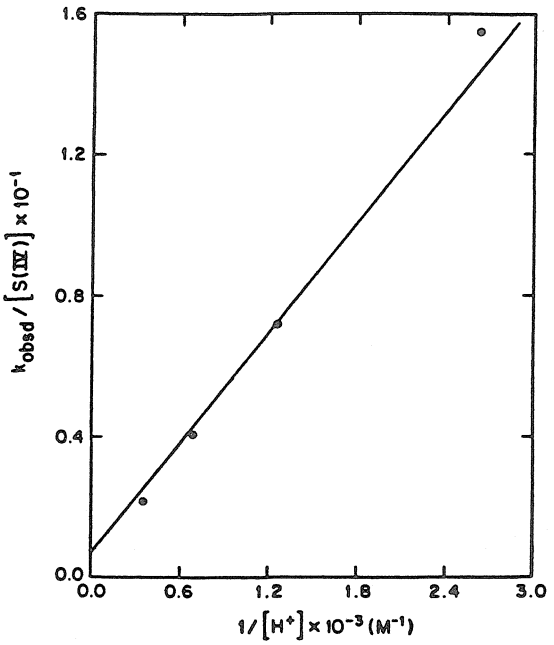

Figure 3. Dependence of $k_{obsd}/[S(IV)]_t$ vs. $1/[H^+]$ for pH ≥ 2.5. Solid line denotes linear least-squares fit to the data taken from Table II.

simple dependence on the hydrogen ion activity. Instead Figure 2 suggests that the slope of k_{obsd} vs. [S(IV)], approaches a constant value as the pH approaches zero. The intercepts, when divided by $\{H^+\}$, yield a constant value (1.08 (±0.06) × 10^{-3} M^{-1} s^{-1}) at very low pH. A decrease of $[C_6H_5CHO]$ at pH ≤ 1, that could be attributed to either a slow decarbonylation or a specific acid-catalyzed hydration, in the absence of S(IV), was not observed over 2 h. Sulfur(IV) solutions at pH 0 (without benzaldehyde) were also stable over the same time period.

The possibility of general acid catalysis by the various buffers used herein was examined by measuring the reaction rate over a tenfold range of buffer concentrations. To correct for small variations in the pH of the sample solutions, the observed pseudo-first-order rate constant was normalized as $k_{obsd}\{H^+\}/[S(IV)]_t$. No buffer dependence was found for formate, acetate, chloroacetate, or dichloroacetate. However, the reaction was catalyzed slightly by phosphoric acid. In this case, general acid catalysis may occur in the presence of relatively strong acids. General base catalysis of the dissociation of ketone bisulfite compounds has been demonstrated and the mechanism is said to involve the formation of an encounter complex with the oxocarbonium ion, >C=O⁺H, bisulfite and buffer, and subsequent removal of a proton from bisulfite.[16] At the phosphate concentration used in these studies (0.1 M), less than a 7–8% change in the pseudo-first-order rate constant was attributed to phosphate catalysis and consequently k_{obsd} values were not corrected.

Based on the preceding kinetic data, the following reaction mechanism is proposed for the pH range of 0–4:

$$H_2O{\cdot}SO_2 \overset{K_{a1}}{\rightleftharpoons} H^+ + HSO_3^- \quad \text{(fast)} \qquad (1)$$

$$HSO_3^- \overset{K_{a2}}{\rightleftharpoons} H^+ + SO_3^{2-} \quad \text{(fast)} \qquad (2)$$

$$C_6H_5CHO + SO_3^{2-} \underset{k_{-1}}{\overset{k_1}{\rightleftharpoons}} C_6H_5CH(O^-)SO_3^- \quad \text{(slow)} \qquad (3)$$

$$C_6H_5CHO + HSO_3^- \underset{k_{-2}}{\overset{k_2}{\rightleftharpoons}} C_6H_5CH(OH)SO_3^- \quad \text{(slow)} \qquad (4)$$

$$C_6H_5CH(OH)SO_3H \overset{K_{a1(HPMS)}}{\rightleftharpoons} C_6H_5CH(OH)SO_3^- + H^+ \quad \text{(fast)} \qquad (5)$$

$$C_6H_5CH(OH)SO_3^- \overset{K_{a2(HPMS)}}{\rightleftharpoons} C_6H_5CH(O^-)SO_3^- + H^+ \quad \text{(fast)} \qquad (6)$$

$$C_6H_5CHO + H^+ \overset{K_H}{\rightleftharpoons} C_6H_5C^+H(OH) \quad \text{(fast)} \qquad (7)$$

$$C_6H_5C^+H(OH) + HSO_3^- \underset{k_{-3}}{\overset{k_3}{\rightleftharpoons}} C_6H_5CH(OH)SO_3^- + H^+ \quad \text{(slow)} \qquad (8)$$

$$C_6H_5C^+H(OH) + H_2O \underset{k_{-h}}{\overset{k_h}{\rightleftharpoons}} C_6H_5CH(OH)O^+H_2 \quad \text{(slow)} \qquad (9)$$

$$C_6H_5CH(OH)O^+H_2 \rightleftharpoons H^+ + C_6H_5CH(OH)_2 \quad \text{(fast)} \qquad (10)$$

Steps 3 and 4 involve the rate-limiting nucleophilic attack by bisulfite and sulfite on the carbonyl carbon of benzaldehyde to form the sulfonate. A specific acid-catalyzed pathway for bisulfite addition is also proposed in steps 7 and 8 to account for the increased reactivity of S(IV) at low pH. Reaction 7 leads to the rapid formation of a carbocation and the enhanced positive character of its carbon center facilitates the rate-limiting nucleophilic attack of bisulfite in eq 8. Analogous acid-catalyzed pathways have been proposed for the dissociation of acetophenone bisulfites.[16] Specific acid catalysis has not been observed in the formation of formaldehyde–S(IV) adducts,[14] but since formaldehyde is present primarily as the *gem*-diol, $CH_2(OH)_2$, very little of the probable intermediate, $C^+H_2(OH)$, will form.

The nonzero *y* intercepts of Figure 2 suggest a loss of benzaldehyde by a pathway that does not involve S(IV) in the rate-determining step. Even though we were not able to detect any loss of benzaldehyde at pH 0 in the absence of S(IV), we believe these intercepts are due to the acid-catalyzed hydrolysis of the aldehyde as shown in steps 9 and 10. Between pH 0 and 1 the apparent equilibrium constant for adduct formation is quite small. At pH 0 with the lowest concentration of S(IV) which was used (1 mM), the overall change in absorbance was approximately 5%. By these techniques alone, therefore, it probably was not possible to detect hydrolysis of benzaldehyde in the absence of S(IV).

The predominant sulfonic acid species between pH ~ 1–10 will be $C_6H_5CH(OH)SO_3^-$. Some confusion exists regarding the value of $K_{a1(HPMS)}$, however. Stewart and Donnally's initial estimate, based on titration data, was 3.7 × 10^{-2} M.[5b] They later found that their proposed mechanism was inconsistent with this value and it was then assumed that the sulfonic acid was a much stronger acid. A new $K_{a1(HPMS)}$ value was estimated as ca. 1 × 10^3 M by fitting this constant to their kinetic data. Based on a fit of our own titration data which was analyzed with the computer code MINEQL,[17] $pK_{a1(HPMS)}$ is approximately 0.7.

From the above mechanism, the rate of disappearance of benzaldehyde over the pH range 0–4 is written as

$$\nu = -d[C_6H_5CHO]/dt = k_1[SO_3^{2-}][C_6H_5CHO] + k_2[HSO_3^-][C_6H_5CHO] + k_3K_H\{H^+\}[HSO_3^-][C_6H_5CHO] + k_hK_H\{H^+\}[C_6H_5CHO] \qquad (11)$$

while the rate expression for the rate of formation of the sulfonic acid is

$$\nu' = d\textstyle\sum[HPMS]/dt = (k_1[SO_3^{2-}] + k_2[HSO_3^-] + k_3K_H\{H^+\}[HSO_3^-])[C_6H_5CHO] \qquad (12)$$

Terms that describe the decomposition of HPMS were not included in the theoretical rate expression of eq 11 since the equilibrium for the reaction is displaced far to the right. Equation

(16) Young, P. R.; Jencks, W. P. *J. Am. Chem. Soc.* **1978**, *100*, 1228–35.

(17) Westall, J. C.; Zachary, J. L.; Morel, F. M. *Technical Note No. 18*, Ralph M. Parsons Laboratory for Water Resources and Environmental Engineering, Massachusetts Institute of Technology, 1976.

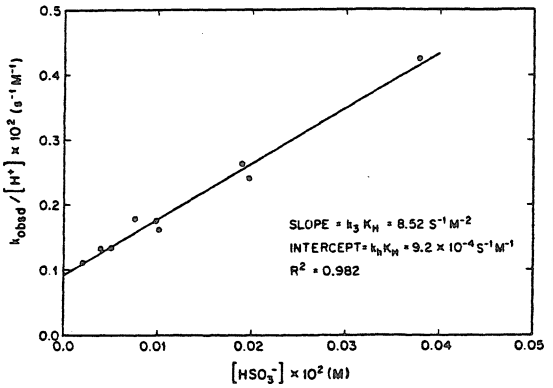

Figure 4. Dependence of $k_{obsd}/[H^+]$ vs. $[HSO_3^-]$ for pH 0–0.6. Solid line represents linear least-squares fit to the data.

11 may be rewritten in terms of total S(IV) and benzaldehyde to yield

$$v = ((k_1\alpha_2 + (k_2 + k_3K_H\{H^+\})\alpha_1)[S(IV)] + k_hK_H\{H^+\}) \times [C_6H_5CHO] \quad (13)$$

where

$$[S(IV)] = [H_2O{\cdot}SO_2] + [HSO_3^-] + [SO_3^{2-}] \quad (14)$$

$$[HSO_3^-] = \alpha_1[S(IV)] \quad (15)$$

$$[SO_3^{2-}] = \alpha_2[S(IV)] \quad (16)$$

$$\alpha_1 = K_{a1}\{H^+\}/D \quad (17)$$

$$\alpha_2 = K_{a1}K_{a2}/D \quad (18)$$

$$D = \{H^+\}^2 + K_{a1}\{H^+\} + K_{a1}K_{a2} \quad (19)$$

The activity scale is retained in the above equations for the hydrogen ion since only H^+ activities were measured and because activity coefficients are difficult to estimate at μ = 1.0 M. If S(IV) is in sufficient excess and pH is held constant, then

$$k_{obsd} = \{k_1\alpha_2 + (k_2 + k_3K_H\{H^+\})\alpha_1\}[S(IV)]_t + k_hK_H\{H^+\} \quad (20)$$

The intrinsic rate constants, k_1 and k_2, and the apparent constant, k_3K_H, were estimated initially from analysis of rate data at low and high pH. In the pH region of 2.5–4.4, $K_{a1}\{H^+\} \gg \{H^+\}^2$ and $K_{a1}K_{a2}$. Furthermore, if $k_3K_H\{H^+\}$ and $k_hK_H\{H^+\}/[S(IV)]_t \ll k_2$, then

$$k_{obsd} = (k_1K_{a2}/\{H^+\} + k_2)[S(IV)]_t \quad (21)$$

and a plot of $k_{obsd}/[S(IV)]_t$ vs. $\{H^+\}^{-1}$ will be linear; the slope and intercept of this plot provides an estimate of k_1 and k_2. This linearity was previously demonstrated in Figure 3. These estimates of k_1 and k_2 were refined by a nonlinear least-squares fitting of the data in Table II (for pH > 1.3) with a routine described by Moore and Pearson.[18] Each data point was weighted in accordance with its statistical variance and values of K_{a1} (1.45 × 10^{-2} M)[19] and K_{a2} (6.31 × 10^{-8} M)[20] were held constant. The intrinsic constants, k_1 and k_2, were determined to be k_1 = 2.15 (±0.09) × 10^4 M^{-1} s^{-1} and k_2 = 0.71 (±0.03) M^{-1} s^{-1}.

For pH ≤ 1.0, $\{H^+\}^2 \gg K_{a1}\{H^+\}$ and $K_{a1}K_{a2}$; and if $k_3K_HK_{a1} \gg k_2K_{a1}/\{H^+\}$ and $k_1K_{a1}K_{a2}/\{H^+\}^2$, k_{obsd} becomes

$$k_{obsd} = k_3K_H\{H^+\}[S(IV)]_t + k_hK_H\{H^+\} \quad (22)$$

Initial estimates of k_3K_H and k_hK_H were obtained from the slope ($k_3K_H \cong$ 8.52 M^{-1} s^{-1}) and intercept/$\{H^+\}$ ($k_hK_H \cong$ 9.2 × 10^{-4} M^{-1} s^{-1}) of Figure 4. These two constants were then refined by using eq 20, the initial estimates of k_1 and k_2, and the data from Table II (pH 0–1.3). The refined values of k_3K_H and k_hK_H are 2.5 (±1.5) M^{-1} s^{-1} and 1.54 (±0.47) × 10^{-3} M^{-1} s^{-1}, respectively. From our estimate of k_3K_H and a reported value of $K_H \sim 10^{-7}$,[21] the intrinsic constant k_3 is ~2.5 × 10^7 s^{-1} M^{-1}. The source of error in the value k_3K_H is unknown. A possible source of error is in the uncertainties of the molar absorptivities of $C_6H_5CH(OH)SO_3H$ and $C_6H_5CH(OH)SO_3^-$ at 249 nm.

Since the above rate constants have been determined for the mixed concentration/activity scales used in eq 13, literature values of K_{a1} and K_{a2} (at μ = 0) were corrected to μ = 1.0 M in computing the intrinsic rate constants. Activity coefficients, $\gamma_{SO_3^{2-}}$ and $\gamma_{HSO_3^-}$, were computed by using the Davies approximation for conditions of μ = 0.5 M, as recommended by Butler.[22] The corrected acidity constants were ${}^cK_{a1} = K_{a1}\gamma_{H_2O{\cdot}SO_2}/\gamma_{HSO_3^-}$ = 0.021 M and ${}^cK_{a2} = K_{a2}\gamma_{HSO_3^-}/\gamma_{SO_3^{2-}}$ = 2.43 × 10^{-7} M. A sensitivity analysis to test the effect of using the Davies approximation for conditions outside its limits of applicability indicated that the maximum introduced errors for k_1 and k_2 would be 12% and 8%, respectively.

The temperature dependence of k_2 and k_1 over the range 15–40 °C was determined at pH 1.3 (Figure 5a) and at pH 2.5 (Figure 5b), respectively. From these experiments, ΔH_1^* = 36.0, ΔH_2^* = 36.6 kJ/mol, ΔS_1^* = −58.1, and ΔS_2^* = −142 J/mol/°C at μ = 1.0 M.

Substituent effects for para-substituted benzaldehydes were determined for k_2 at pH 1.3 and k_1 at pH 2.5; results are presented in Table III. For each substituted benzaldehyde, plots of k_{obsd} vs. $[S(IV)]_t$ were linear. The magnitude of k_1 increased in the order –OH < $-OCH_3$ < $-CH_3$ < –H < –Cl < $-NO_2$, while for k_2, the order was $-CH_3$ < –H < –Cl < $-NO_2$. A change in the mechanism of HSO_3^- addition was suspected for *p*-OH– and *p*-OCH_3–C_6H_5CHO (vide infra). Activation parameters are summarized in Table III.

Formation Constant. Over the pH region of 3–5, the predominant S(IV) species are $C_6H_5CH(OH)SO_3^-$ and HSO_3^-. Stewart and Donnally showed that

$$K_{app} = \frac{(\Sigma HPMS)}{(\Sigma H_2SO_3)(\Sigma C_6H_5CHO)} \quad (23)$$

was pH-independent over the same pH range, and therefore K can be approximated by

$$^cK = \frac{[C_6H_5CH(OH)SO_3^-]}{[HSO_3^-][C_6H_5CHO]} \quad (24)$$

TABLE III: Rate Constants[a] and Activation Parameters[b] for Bisulfite and Sulfite Ion Addition Reactions with Benzaldehyde and Para-Substituted Benzaldehydes

X	$10^{-4}k_1$, M^{-1} s^{-1}	k_2, M^{-1} s^{-1}	ΔH_1^*, kJ mol^{-1}	ΔS_1^* J mol^{-1} deg^{-1}	ΔH_2^*, kJ mol^{-1}	ΔS_2^*, J mol^{-1} deg^{-1}
OCH_3	0.777	N/A[d]	41.5	−50.2	N/A	N/A
CH_3	1.56	0.68	43.0	−39.5	42.0	−126
H	2.15	0.71	36.0	−58.1	36.6	−142
Cl	5.53	1.05	37.4	−47.9	32.7	−154
OH[c]	0.582	N/A	30.4	−89.9	N/A	N/A
NO_2[c]	5.66	5.31	37.4	−12.8	29.0	−153

[a] Rate constants k_1 and k_2 correspond to the following reactions at 25 °C and μ = 1.0 M:

$$X\text{–}C_6H_5CHO + SO_3^{2-} \xrightarrow{k_1} X\text{–}C_6H_5CH(O^-)SO_3^-$$

$$X\text{–}C_6H_5CHO + HSO_3^- \xrightarrow{k_2} X\text{–}C_6H_5CH(OH)SO_3^-$$

where X refers to the para-substituted functional group. [b] Activation parameters based on reaction rate temperature dependence over the range 15–40 °C unless otherwise stated. [c] Activation parameters based on temperature dependence between 15–33 °C. [d] N/A = not applicable; measured activation parameters indicate a change in mechanism.

(18) Moore, J. W.; Pearson, R. G. *Kinetics and Mechanism, A Study of Homogeneous Chemical Reactions*, 3rd ed.; Wiley-Intersience: New York, 1981; pp 69–70.
(19) Deveze, D.; Rumpf, P. *C. R. Acad. Sci. Paris* **1964**, *258*, 6135–38.
(20) Hayon, E.; Treinin, A.; Wilf, J. *J. Am. Chem. Soc.* **1972**, *94*, 47–57.
(21) Yates, K.; Stewart, R. *Can. J. Chem.* **1959**, *37*, 664–7.
(22) Butler, J. *Ionic Equilibrium, A Mathematical Approach*; Addison-Wesley: Reading, MA, 1964; pp 431–39.

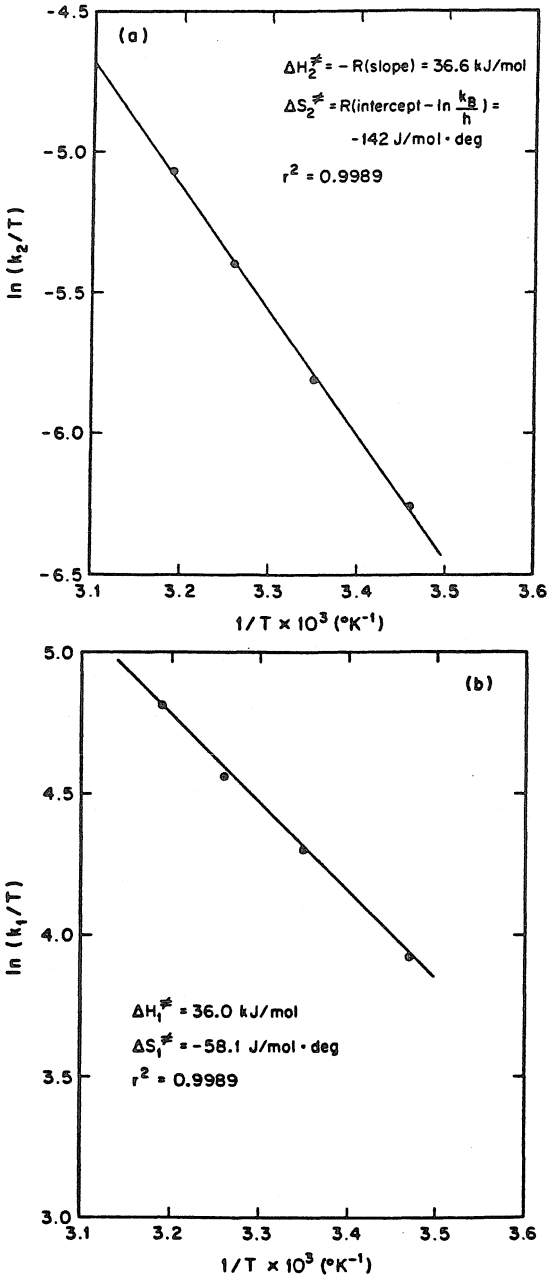

Figure 5. Temperature dependencies of (a) the intrinsic rate constant, k_2, for the nucleophilic addition of bisulfite ion to benzaldehyde, and (b) the intrinsic rate constant, k_1, for the addition of sulfite ion to benzaldehyde. Solid lines denote least-squares fit to the data. Reaction conditions: μ = 1.0 M, T = 25 °C; (a) [S(IV)] = 5.0 mM, [C_6H_5CHO] = 0.1 mM, pH 1.3, and (b) [S(IV)] = 1.0 mM, [C_6H_5CHO] = 0.1 mM, pH 3.41.

at pH 4. Dissolution of the sodium sulfonate salt results in [HSO_3^-] = [C_6H_5CHO] at equilibrium; and consequently eq 24 can be reduced to

$$^cK = \frac{[\text{HPMS}]_0 - [C_6H_5CHO]_e}{[C_6H_5CHO]_e^2} \quad (25)$$

where $[\text{HPMS}]_0$ is the initial concentration of the dissolved sulfonate salt and $[C_6H_5CHO]_e$ is the equilibrium concentration

TABLE IV: Thermodynamic Data for the Reaction[a] $C_6H_5CHO + HSO_3^- \rightleftharpoons C_6H_5CH(OH)SO_3^-$

T, °C	μ, M	$10^{-3} K_{eq}$ ($\pm\sigma$), M^{-1}
15	0.1	11.6 ± 0.6
20	0.1	7.6 + 0.7
25	0.1	4.81 + 0.8
30	0.1	3.21 + 0.8
35	0.1	1.99 + 0.7
25	1.0	0.98 ± 0.11

[a] Determinations were made at pH 3.9 ± 0.1 with [$NaC_6H_5CH(OH)SO_3$], = 41.0–92.0 μM.

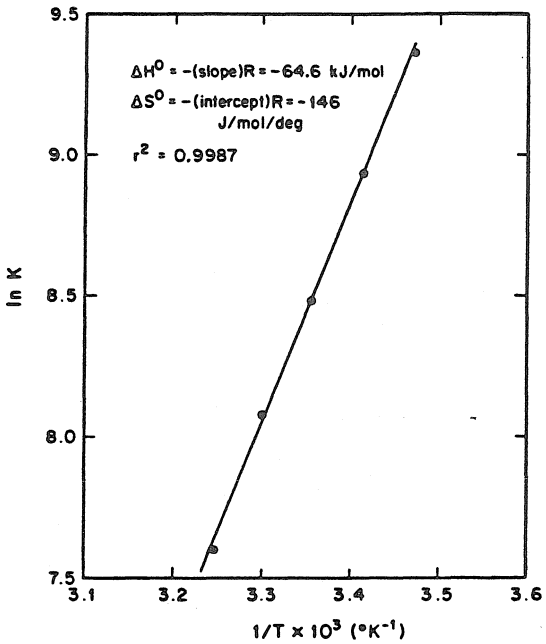

Figure 6. Temperature dependence of the equilibrium association constant, K, for the bisulfite–benzaldehyde addition complex. Solid line represents least-squares fit to the data. Reaction conditions: [$NaC_6H_5CH(OH)SO_3$], = 0.043–0.095 mM, μ = 0.1 M.

of benzaldehyde. The absorbance at 250 nm is given by the following relationship

$$A_{250} = \epsilon_{C_6H_5CHO}[C_6H_5CHO]_e + \epsilon_{\text{HPMS}}([\text{HPMS}]_0 - [C_6H_5CHO]_e) \quad (26)$$

since ϵ of $H_2O{\cdot}SO_2$, HSO_3^-, and SO_3^{2-} at pH ~ 4.0 is negligible. At equilibrium, $[C_6H_5CHO]_e$ was calculated from eq 26 and substituted into eq 25 to yield the values of ^cK reported in Table IV. At μ = 0.1 M (25 °C), ^cK was determined to 4810 (±770) M^{-1}, which is in close agreement with Sousa and Margerum's[7] value of K = 4700 M^{-1} (dilute solution conditions, 23 °C). Values of $\Delta H°$ and $\Delta S°$ were calculated to be −64.6 kJ/mol and −146 J/mol/deg, respectively (Figure 6). If the activity coefficients of the ionic species are determined by the Davies equation, and $\gamma_{C_6H_5CHO} \cong 1$, then the formation constant

$$^cK = {}^aK\left[\frac{\gamma_{HSO_3^-}\gamma_{C_6H_5CHO}}{\gamma_{\text{HPMS}^-}}\right] \quad (27)$$

should be relative insensitive to ionic strength. However, when μ was increased to 1 M, ^cK decreased to 980 (±110) M^{-1}. This suggests that $\gamma_{C_6H_5CHO}$ is considerably less than one.

Discussion

The intrinsic rate constants, k_1 and k_2, obtained for the steps leading to the production of HPMS are in fair agreement with

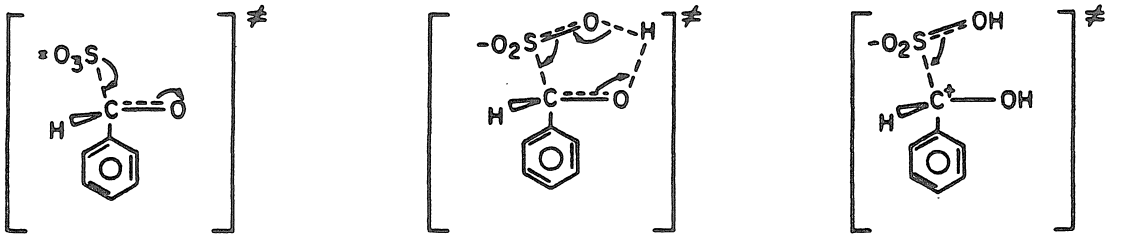

(a) (b) (c)

Figure 7. Possible structures for the activated complexes formed by the nucleophilic addition of (a) SO_3^{2-} and (b) HSO_3^- to benzaldehyde, and (c) HSO_3^- to $C_6H_5C^+H(OH)$.

TABLE V: Comparison of Intrinsic Rate Constants with Literature Values for the Formation of S(IV)–Benzaldehyde Addition Compounds

reaction	rate constant, M^{-1} s^{-1}	source/ref
C_6H_5CHO + SO_3^{2-} (k_1)	1.25 × 10^4 (21 °C)	5b
	2.15 × 10^4 (μ = 1 M, 25 °C)	this work
C_6H_5CHO + HSO_3^- (k_2)	0.43 (21 °C)	5b
	245 (13 °C)	7
	0.71 (μ = 1 M, 25 °C)	this work
C_6H_5CHO + $H_2O{\cdot}SO_2$ (k')	0.097 (21 °C)	5b
$C_6H_5C^+H(OH)$ + HSO_3^- (k_3)	2.5 × 10^7 (μ = 1 M, 25 °C)	this work

the corresponding constants determined by Stewart and Donnally[5b] (see Table V). Our higher values of k_1 and k_2 may be due to the higher temperature used in our study. Based on our ΔH^* and ΔS^* values, however, the 4 °C difference is too small to account for the entire difference in the rate constants. The effect of the higher ionic strength used in our experiments on k_1 and k_2 is not known and activity corrections would be difficult to apply since ionic strength was apparently not held constant in their study. The larger disagreement in k_1 suggests that a portion of the difference may be due to kinetic limitations of their iodometric method at neutral and high pH.

An alternative reaction mechanism for the formation of HPMS in which eq 8 is replaced with the following rate-limiting reaction

$$H_2O{\cdot}SO_2 + C_6H_5CHO \underset{k_{-3}'}{\overset{k_3'}{\rightleftharpoons}} C_6H_5CH(OH)SO_3H \quad (28)$$

as Stewart and Donnally have proposed,[5b] leads to the kinetically equivalent rate law

$$d[\Sigma HPMS]/dt = (k_1\alpha_2 + k_2\alpha_1 + k_3'\alpha_0)[S(IV)]_t[C_6H_5CHO] \quad (29)$$

where $\alpha_0 = [H_2O{\cdot}SO_2]/[S(IV)]$. (The third term in the sum can also be expressed in the form $k'[H^+]\alpha_1$.) Their mechanistic interpretation of the kinetics at very low pH appears improbable particularly because the species, $H_2O{\cdot}SO_2$, has not been observed to react with other aldehydes such as HCHO.[14] Since the difference between our mechanism and Stewart and Donnally's is evident only at extremely low pH, the discrepancy is of negligible importance in virtually all natural systems of interest.

Sulfite ion is predicted to be the strongest nucleophile among the S(IV) species for a wide variety of reactions with organic and inorganic substrates.[23-25] The observed order of increasing reactivity among the species, $SO_3^{2-} \gg HSO_3^- \gg H_2O{\cdot}SO_2$, was also demonstrated in our previous study of the formation of hydroxymethanesulfonate.[14] The ratio, k_1/k_2, was ~3 × 10^4 for the formation of HPMS and HMS. Rate constants for the reaction of SO_3^{2-} and HSO_3^- with formaldehyde were 2.48 × 10^7 and 790 M^{-1} s^{-1}, respectively, and are roughly 3 orders of magnitude greater than the corresponding constants for benzaldehyde. The greater reactivity of formaldehyde is probably due to (1) the greater ordering required to form the benzaldehyde–S(IV) activated complexes and (2), the increased steric hindrance to the formation of the transition-state complex by the phenyl group. Clearly the ΔS^* values for both the benzaldehyde–sulfite and –bisulfite adducts were more negative than those for the corresponding formaldehyde adducts (ΔS_1^* = −40.2 J mol^{-1} K^{-1} and ΔS_2^* = −121.3 J mol^{-1} K^{-1} for HMS).

From our estimate of the rate constant for the addition of HSO_3^- and the carbocation, $C_6H_5C^+H(OH)$, the latter is at least 7 orders of magnitude more reactive than the unprotonated benzaldehyde. A possible activated complex for the addition of HSO_3^- to the carbonyl group is the cyclic structure shown in Figure 7b. Bisulfite addition to the electron deficient carbon atom of the carbocation most likely occurs without this structural constraint. Instead, the activated state (Figure 7c) is postulated to resemble the complex formed by benzaldehyde and SO_3^{2-} (Figure 7a).

Substituent effects resulted in less than an order of magnitude change in the rate constants, k_2 and k_3, relative to benzaldehyde. Blackadder and Hinshelwood have also demonstrated that para-substituent effects on the dissociation rate are slight.[6] Substantial differences in ΔH_2^* and ΔS_2^* for the *p*-OH and *p*-OCH_3 substituents suggest that there may be a change in mechanism.[26] These substituents may induce substitution of HSO_3^- directly on the phenyl ring. The *p*-NO_2 group exhibited the greatest reactivity, followed by the *p*-Cl group. The combined effect of electron withdrawal from the carbonyl center and a favorable dipole moment will result in enhanced nucleophilic addition.[27] The decreased reactivity of *p*-CH_3, *p*-OH, and *p*-OCH_3 in the k_1 step may be attributed to increased electron density on the carbonyl carbon due to inductive effects.

Substitution of a phenyl group for the proton of HCHO should lead to a less stable bisulfite–aldehyde adduct due to steric hindrance. Comparison of the HMS and HPMS equilibrium constants supports this notion. Deister et al.[28] have reported that the association constant for HSO_3^- and HCHO (25 °C) is 3.78 × 10^6 M^{-1}; this is nearly a factor of 10^3 larger than the value for K_{HPMS}.

Conclusions for Atmospheric Systems. Based on the above kinetic and thermodynamic results, certain conclusions can be drawn regarding the importance of these reactions in atmospheric water droplets. A rough estimate of the maximum concentration

(23) Schroeter, L. C. *Sulfur Dioxide, Applications in Foods, Beverages, and Pharmaceuticals*; Pergamon: New York, 1966, pp 105–67.
(24) Edwards, J. O. *Inorganic Reaction Mechanisms*; Benjamin: New York, 1965; pp 51–71.
(25) Hoffmann, M. R.; Edwards, J. O. *Inorg. Chem.* **1977**, *16*, 3333–8.
(26) Geissman, T. A. *Principles of Organic Chemistry*, 3rd ed.; W. H. Freeman: San Francisco, 1968; pp 547–59.
(27) Brown, R. F. *Organic Chemistry*; Wadsworth: Belmont, CA, 1975; pp 445–51.
(28) Deister, U.; Neeb, R.; Helas, G.; Warneck, P. *J. Phys. Chem.*, in press.

of aqueous HPMS which might be formed in a polluted open atmosphere was calculated by assuming a concentration of 0.2 μM free benzaldehyde, a SO_2 partial pressure, P_{SO_2}, of 20 ppb, and a pH of 4.0. A P_{SO_2} of 20 ppb is common in some urban areas. The benzaldehyde concentration was chosen from the highest values cited for Los Angeles rainwater by Kawamura and Kaplan,[2] although it is not clear whether their analytical method measures free or total benzaldehyde. Our estimate would overpredict potential HPMS concentrations if complexed benzaldehyde was also detected by their analysis. A free aqueous benzaldehyde concentration calculated on the basis of a gas-phase–liquid equilibrium assumption leads to comparable concentrations. Solving the following equations for [HPMS]

$$[HSO_3^-] = \frac{P_{SO_2} H_{SO_2} K_{a1}}{\{H^+\}} \quad (30)$$

$$[HPMS] = K_{HPMS}[C_6H_5CHO]_{free}[HSO_3^-] \quad (31)$$

where H_{SO_2} (1.26 M atm^{-1} at 25 °C) is the Henry's law constant for SO_2, yields [HPMS] = 5.8 nM. This calculation indicates that only a small fraction of the benzaldehyde and S(IV) would be present as the adduct. The contribution of benzaldehyde to the speciation of S(IV) in atmospheric water droplets will be less important than that due to formaldehyde since benzaldehyde is less abundant and its adduct is less stable. Further research on other carbonyl–S(IV) systems is under way.

Acknowledgment. We gratefully acknowledge the Electric Power Research Institute (RP1630-47) and the Environmental Protection Agency (R811496-01-1) for providing financial support for this research. We also thank Drs. Detlef W. Bahnemann, Eric A. Betterton, and the reviewers for their helpful insight.

Registry No. *p*-$MeOC_6H_4CHO$, 123-11-5; *p*-MeC_6H_4CHO, 104-87-0; PhCHO, 100-52-7; *p*-ClC_6H_4CHO, 104-88-1; *p*-HOC_6H_4CHO, 123-08-0; *p*-$NO_2C_6H_4CHO$, 555-16-8; sodium bisulfite, 7631-90-5; sodium sulfite, 7757-83-7.

CHAPTER 4

The Kinetics, Mechanism, and Thermodynamics of Glyoxal–S(IV) Adduct Formation

by

Terese M. Olson and Michael R. Hoffmann

Journal of Physical Chemistry, 92, 533–540 (1988)

Abstract

The reversible addition of glyoxal (ethanedial) and S(IV) to form glyoxal–monobisulfite (GMBS) was studied spectrophotometrically over the pH range of 0.7 to 3.3. Far from equilibrium, the rate of GMBS formation is given by: $d[GMBS]/dt = (k_{1,app}\alpha_1 + k_{2,app}\alpha_2)[C_2H_2O_2][S(IV)]$, where $[C_2H_2O_2] = [(CH(OH)_2)_2] + [CH(OH)_2CHO] + [CHOCHO]$, $[S(IV)] = [H_2O\cdot SO_2] + [HSO_3^-] + [SO_3^{2-}]$, $\alpha_1 = [HSO_3^-]/[S(IV)]$ and $\alpha_2 = [SO_3^{2-}]/[S(IV)]$. The apparent rate constants, $k_{1,app} = 0.13\ M^{-1}\ s^{-1}$ and $k_{2,app} = 2.08 \times 10^3\ M^{-1}\ s^{-1}$, are pH–independent functions of the dehydration equilibrium constants of $(CH(OH)_2)_2$ and $CHOCH(OH)_2$, and intrinsic rate constants for the reaction of HSO_3^- and SO_3^{2-} with unhydrated and singly hydrated glyoxal. Glyoxal–dibisulfite (GDBS) and GMBS were shown to dissociate with a rate given by: $\frac{d[S(IV)]}{dt} = \left(k_{-1}' + k_{-1}''K_{D3} + \frac{k_{-2}'K_{a2}' + k_{-2}''K_{a2}K_{D3}}{\{H^+\}}\right)[GMBS]_t + \left(k_{-3} + \frac{k_{-4}K_{a3}}{\{H^+\}}\right)[GDBS]_t$; where k_{-1} and k_{-2} correspond to the release of bisulfite and sulfite, respectively, from unhydrated and hydrated GMBS species; k_{-3} and k_{-4} correspond to the release of bisulfite and sulfite from GDBS; K_{D3} is the dehydration constant for GMBS; and K_{a2}', K_{a2}'' and K_{a3} are acid–dissociation constants. Stability constants for the formation of GMBS and GDBS were determined to be ${}^cK_1 = [CH(OH)_2CH(OH)SO_3^-]/([(CH(OH)_2)_2][HSO_3^-]) = 2.81 \times 10^4\ M^{-1}$ and ${}^cK_2 = [(CH(OH)SO_3^-)_2]/([CH(OH)_2CH(OH)SO_3^-][HSO_3^-]) = 1.45 \times 10^4\ M^{-1}$ at 25° C and $\mu = 0.2$ M.

Introduction

Aldehyde–bisulfite adducts are believed to form at appreciable concentrations in atmospheric water droplets of polluted environments and are thought to play an important role in stabilizing SO_2 in the aqueous phase (1,2). To predict which aldehydes represent significant S(IV) reservoirs, we have previously examined the formation kinetics and stability of formaldehyde–, benzaldehyde–, methylglyoxal–, acetaldehyde–, and hydroxyacetaldehyde–S(IV) adducts (3–5). Formaldehyde and methylglyoxal (CH_3COCHO), both of which have large effective Henry's Law constants, were found to form highly stable S(IV) addition compounds and are likely to be important when they are present in the environment. Conversely, hydroxyphenylmethanesulfonate, the benzaldehyde adduct, will be much less important since it is less stable and since benzaldehyde is predominantly unhydrated (hence, it is unlikely to have a large Henry's Law constant).

The objective of this work has been to investigate the reaction of S(IV) with another predominantly hydrated α–dicarbonyl, glyoxal (ethanedial, CHOCHO). Recent experimental evidence has shown that dicarbonyls, such as glyoxal and methylglyoxal, are primary gas–phase oxidation products of aromatic hydrocarbons after free radical attack (6a,b). Theoretical calculations by Calvert and Madronich (7) suggest that α–dicarbonyls account for a substantial mole fraction of the initial oxidation product distribution of an aromatic hydrocarbon mixture. Dicarbonyls, including glyoxal, have also been identified in fog– and rainwater samples (8).

Only one determination of the stability constants for the glyoxal – mono– and dibisulfite adducts, 1–hydroxy–2,2–diol–ethanesulfonate and 1,2–dihydroxy–1,2–ethanedisulfonate, (hereafter respectively denoted with the acronyms GMBS

and GDBS) is known. Salomaa reported a value of the apparent stability constant of GDBS as 3.7×10^3 M^{-1} at pH 7.3 and an unspecified ionic strength, and that the formation constant for GMBS must be greater than 3.7×10^3 M^{-1} (9). He also described the kinetics of the addition of sulfite to the first glyoxal carbonyl group as being comparable to the rate of addition of formaldehyde and sulfite.

Since the pH conditions of fogs, clouds and haze aerosols are typically acidic, the kinetic and thermodynamic parameters obtained in this work were determined at pH $\leq$ 4.0. Conventional and stopped–flow spectrophotometric methods were employed to obtain the rate constants for adduct formation (GMBS only) and dissociation (GMBS and GDBS). Spectrophotometry was also used to determine the successive adduct stability constants. An independent calculation of the stability constant for GMBS was possible from the ratio of forward/reverse rate constants.

Experimental Procedures

Materials. Stock solutions of glyoxal were prepared from a 40% reagent grade glyoxal–in–water solution (Aldrich), which was periodically filtered and standardized by an alkalimetric titration technique described by Salomaa (9). The filtering step was necessary to remove the solid polymer that formed slowly at room temperature. Since the depolymerization process was apparently quite slow, buffered or acidified glyoxal stock solutions (at approximately twice the sample concentration) were heated to 35° C for 30 minutes and allowed to stand for several days in a N_2 atmosphere glovebox before use. Buffer solutions were prepared with reagent–grade sodium hydroxide (Baker), hydrochloric acid (Baker), chloroacetic acid (Kodak), dichloroacetic acid (MCB), phosphoric acid (Spectrum), sodium acetate (Baker), glacial acetic acid (Mallinckrodt) and monobasic potassium

phosphate (Baker). Small amounts of disodium–EDTA were added to the buffers to inhibit possible metal–catalyzed oxidation of S(IV).

The disodium salt of the glyoxal–bisulfite addition compound was synthesized and recrystallized using a method adapted from Ronzio and Waugh (10). Based on an elemental analysis of the salt (Galbraith Laboratories), its stoichiometry was $(NaCH(OH)SO_3)_2 \cdot H_2O$.

Stock S(IV) solutions were prepared fresh before use from A.R. grade disodium sulfite (Baker). All solutions were prepared in a glovebox with deoxygenated, 18 MΩ·cm resistivity water (Millipore). Oxygen was purged by degassing with high purity N_2 gas. Ionic strength was held constant at $\mu = 0.2$ M with sodium chloride.

Methods. The kinetics of adduct formation was studied by monitoring the disappearance of free S(IV) (i.e., $H_2O \cdot SO_2$, HSO_3^- and SO_3^{2-}) at 280 nm ($\lambda_{max' H_2O \cdot SO_2}$) with a Hewlett–Packard Model 8450A UV/Vis spectrophotometer linked to an IBM Model XT computer. The quartz, 10 cm reaction cell was water–jacketed and a Haake water recirculation bath was used to maintain a constant temperature of 25° C. Usually four replications were performed at each pH with a minimum of 200 absorbance measurements being collected in each data set.

Adduct dissociation was studied indirectly by dissolving the salt of the addition compound, mixing this fresh solution with a pH–buffered iodine solution (containing excess KI), and monitoring the disappearance of triiodide at 351 nm (λ_{max} for I_3^-). Since the oxidation reaction of S(IV) to S(VI) by iodine is extremely rapid, the rate of disappearance of iodine therefore is equal to the rate of liberation of free S(IV). At pH 1.3 and 1.8, absorbance measurements of aliquots were taken manually in a 1 cm cell over several days. Between pH 1.8 and 5.0, the

reaction was conducted directly in a 1 cm mixing cell, and continuous absorbance measurements were made. Cell temperature (25° C) was maintained with a Hewlett–Packard Model 89100A Temperature Controller. Above pH 5.0, the reaction was studied using a stopped–flow spectrophotometer (Dionex). In these experiments, buffered I_2/KI solutions were placed in one syringe, while freshly prepared GDBS solutions (acidified to approximately pH 2) were placed in another. Acidification of the adduct reagent was necessary to quench the dissociation rate of the adduct. The pH of the reaction mixture was determined by analyzing samples of the stopped–flow effluent stream. No loss of iodine was evident in the absence of S(IV).

The apparent stability constant for GMBS, K_1, was determined by three independent methods. An estimate was first calculated from the previously determined forward and reverse rate constants (Method "A"). A second, direct determination (Method "B") involved measuring the concentration of unbound S(IV) in equilibrated solutions containing a tenfold excess of glyoxal; the formation of GDBS was thereby minimized. Free S(IV) concentrations were determined by mixing the equilibrated mixture with an acidified I_2/KI solution and spectrophotometrically measuring the residual I_3^- concentration. The change in absorbance at 351 nm relative to light absorption by I_3^- in the absence of S(IV) was used to calculate the amount of I_3^- consumed (i.e., amount of free S(IV) present). Beer's Law calibration curves were used to relate light absorption to I_3^- concentrations. Although the pH of the resulting I_2/KI/adduct mixture was approximately 1.7, even slight extents of adduct dissociation that occurred over the initial ~30 seconds seriously interfered with the measurement. Stopped–flow mixing of the two reagents was therefore employed. During these experiments the stopped–flow apparatus was housed in a N_2–atmosphere glovebox. Stock I_2

solutions were protected from light and analyzed with a primary standard As_2O_3 solution after each experiment.

The third method (Method "C") involved measuring the concentration of unbound S(IV) in equilibrated solutions of the disodium dibisulfite salt and fitting the single and double association constants to the data with a nonlinear least–squares fitting routine. The technique for determining $[S(IV)]_{unbound}$ was similar to the second method above except that the reagents were mixed in a 1 cm mixing cell and the absorbance that was due to residual I_3^- was measured by conventional spectrophotometry. Adduct dissociation under these conditions ($[CHOCHO]_{tot}$: $[(S(IV)]_{tot}$ = 1:2) was insignificant even several minutes after mixing.

Results

GMBS Formation Kinetics. Under the imposed condition, $[CHOCHO]_t \gg [S(IV)]_t$, pseudo–first–order plots of $\ln\{(A-A_\infty)/(A_o-A_\infty)\}$ vs time were linear ($r^2 \geq 0.99$) for reaction extents up to 90%. The formation of GMBS is therefore first–order with respect to $[S(IV)]_{free}$ (which shall hereafter be denoted simply as [S(IV)]) below pH 3.2. This pseudo–first–order behavior further implies that the amount of GDBS formed was indeed insignificant. The reaction order with respect to glyoxal was examined by varying the aldehyde concentration at constant pH. The pseudo–first–order rate constant, k_{obsd}, exhibited a linear dependence on $[C_2H_2O_2]_t$. Slope values close to unity obtained from logarithmic plots of the data (see Fig. 1) demonstrate this relationship.

The pseudo–first–order rate constants obtained as a function of pH are tabulated in Table 1. Over the pH range studied, the overall pH dependence of k_{obsd} closely resembled earlier trends established for formaldehyde– and benzaldehyde–S(IV) addition compounds (3,4). In these studies, the reaction rate

increase with increasing pH was explained by two rate–determining steps for adduct formation: the nucleophilic attack by HSO_3^- and SO_3^{2-} on the carbonyl carbon atom. To test whether or not the data in Table 1 obeyed such a mechanism, $k_{obsd}/(\alpha_1[CHOCHO]_t) = \nu/[HSO_3^-][CHOCHO]_t$, where $\alpha_1 = [HSO_3^-]/[S(IV)]$, was first plotted against pH (Fig. 2). This pseudo–second–order rate constant became invariant below pH 2, suggesting that bisulfite addition is the dominant rate–determining pathway over this pH range. Between pH 2.5 and 3.2, the pseudo–second–order rate constant, $k_{obsd}/[CHOCHO]_t$, was inversely dependent on the hydrogen ion activity as shown in Fig. 3. Since the concentration of SO_3^{2-} also varies inversely with $\{H^+\}$ over this pH range, a second pathway involving SO_3^{2-} addition is implied. The following reaction mechanism for GMBS formation is therefore proposed for the pH range of 0.7 to 3.2:

$$H_2O \cdot SO_2 \overset{K_{a1}}{\rightleftharpoons} H^+ + HSO_3^- \qquad \text{(fast)} \quad (1a)$$

$$HSO_3^- \overset{K_{a2}}{\rightleftharpoons} H^+ + SO_3^{2-} \qquad \text{(fast)} \quad (1b)$$

$$(CH(OH)_2)_2 \overset{K_{D1}}{\rightleftharpoons} CH(OH)_2CHO + H_2O \qquad \text{(fast)} \quad (2a)$$

$$CH(OH)_2CHO \overset{K_{D2}}{\rightleftharpoons} CHOCHO + H_2O \qquad \text{(fast)} \quad (2b)$$

$$CH(OH)_2CHO + HSO_3^- \underset{k'_{-1}}{\overset{k'_1}{\rightleftharpoons}} CH(OH)_2CH(OH)SO_3^- \qquad \text{(slow)} \quad (3a)$$

$$CHOCHO + HSO_3^- \underset{k''_{-1}}{\overset{k''_1}{\rightleftharpoons}} CHOCH(OH)SO_3^- \qquad \text{(slow)} \quad (3b)$$

$$CH(OH)_2CHO + SO_3^{2-} \underset{k'_{-2}}{\overset{k'_2}{\rightleftharpoons}} CH(OH)_2CH(O^-)SO_3^- \quad \text{(slow)} \quad (4a)$$

$$CHOCHO + SO_3^{2-} \underset{k''_{-2}}{\overset{k''_2}{\rightleftharpoons}} CHOCH(O^-)SO_3^- \quad \text{(slow)} \quad (4b)$$

$$CH(OH)_2CH(OH)SO_3^- \overset{K'_{a2,GMBS}}{\rightleftharpoons} H^+ + CH(OH)_2CH(O^-)SO_3^- \quad \text{(fast)} \quad (5a)$$

$$CHOCH(OH)SO_3^- \overset{K''_{a2,GMBS}}{\rightleftharpoons} H^+ + CHOCH(O^-)SO_3^- . \quad \text{(fast)} \quad (5b)$$

Although glyoxal is assumed to be present primarily as the dihydrate, $(CH(OH)_2)_2$, values of K_{D1} and K_{D2} are not well known. Wasa and Musha (11) obtained a value of the product, $K_{D1}K_{D2} = [CHOCHO]/ [(CH(OH)_2)_2]$, as 4.6×10^{-6} at 25° C, using polarography and 2.52 M glyoxal solutions. They admitted, however, that their results may have been affected by the presence of polymers. Such interference seems likely in view of what is now known about other β–hydroxyaldehydes such as hydroxyacetaldehyde ($CH_2(OH)CHO$). Proton NMR studies have revealed that at least two dimer forms of hydroxyacetaldehyde,

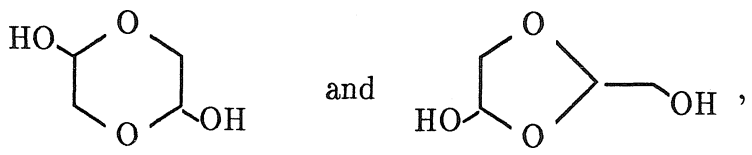

are present in 0.1 M aldehyde–in–D_2O solutions at concentrations of 9 and 17%, respectively, at 35° C (12,13).

Estimates of K_{D1} and K_{D2} can be calculated from linear–free–energy relationships, such as the Taft equation:

$$pK_D = pK_D^\circ + \rho^*\sigma^* , \qquad (6)$$

where K_D° is the dehydration constant for acetaldehyde, σ^* are the Taft polar substituent constants for group R in $RCH(OH)_2$, and ρ^* is the characteristic slope for the reaction. Using literature values of K_D (14–18) and σ^* (19) for carbonyl compounds with a single α–hydrogen, the correlation in Fig. 4 was developed. Estimates of K_{D1} and K_{D2} are 2.0×10^{-4} and 4.2×10^{-3}, respectively, and the product, $K_{D1}K_{D2}$, is more than an order of magnitude smaller than Wasa and Musha's experimental value. The correlation estimates support the assumption that $(CH(OH)_2)_2$ is the predominant glyoxal species. Further supporting evidence is the absence of the characteristic carbonyl $n \longrightarrow \pi^*$ absorption band near 280 nm (20) in glyoxal's absorbance spectrum.

The acid–dissociation constants, K'_{a2} and K''_{a2}, for GMBS are also not well known. However, pK_{a2} values for other aldehyde–S(IV) addition compounds are typically in the range of 9 – 12 (5b) so that under our pH conditions, the adducts are expected to exist primarily as the singly protonated species.

Under conditions that lie far to the left of equilibrium, Eqs. 1–5 give the following rate expression for GMBS formation:

$$v = \frac{d[GMBS]}{dt} = (k_1'[CH(OH)_2CHO] + k_1''[CHOCHO])[HSO_3^-] + (k_2'[CH(OH)_2CHO] + k_2''[CHOCHO])[SO_3^{2-}] , \qquad (7)$$

which may be further simplified as

$$v = \left\{(k_1'\beta_1 + k_1''\beta_2)\alpha_1 + (k_2'\beta_1 + k_2''\beta_2)\alpha_2\right\} [S(IV)][C_2H_2O_2] , \qquad (8)$$

where

$$\beta_1 = \frac{[CH(OH)_2CHO]}{[C_2H_2O_2]} = \frac{K_{D1}}{1 + K_{D1} + K_{D1}K_{D2}} \qquad (9)$$

$$\beta_2 = \frac{[\,CHOCHO\,]}{[\,C_2H_2O_2\,]} = \frac{K_{D1}K_{D2}}{1 + K_{D1} + K_{D1}K_{D2}} \tag{10}$$

$$[S(IV)] = [H_2O\cdot SO_2] + [HSO_3^-] + [SO_3^{2-}] \tag{11a}$$

$$[C_2H_2O_2] = [CHOCHO] + [CHOCH(OH)_2] + [(CH(OH)_2)_2] \tag{11b}$$

$$\alpha_1 = \frac{[HSO_3^-]}{[S(IV)]} = \frac{K_{a1}\{H^+\}}{\{H^+\}^2 + K_{a1}\{H^+\} + K_{a1}K_{a2}} \tag{12}$$

$$\alpha_2 = \frac{[SO_3^{2-}]}{[S(IV)]} = \frac{K_{a1}K_{a2}}{\{H^+\}^2 + K_{a1}\{H^+\} + K_{a1}K_{a2}}. \tag{13}$$

When a large excess of glyoxal is present, $[C_2H_2O_2] \approx [C_2H_2O_2]_t$ and the observed rate constant becomes:

$$k_{obsd} = \left\{(k_1'\beta_1 + k_1''\beta_2)\alpha_1 + (k_2'\beta_1 + k_2''\beta_2)\alpha_2\right\}[C_2H_2O_2]_t. \tag{14}$$

In aqueous solutions alone it is not possible to determine the intrinsic rate constants, k_1', k_1'', k_2' and k_2''. Consequently, the following substitution in Eq. 14 will be made to simplify the notation:

$$k_{1,app} = k_1'\beta_1 + k_1''\beta_2 \tag{15a}$$

$$k_{2,app} = k_2'\beta_1 + k_2''\beta_2\,, \tag{15b}$$

giving:

$$k_{obsd} = (k_{1,app}\,\alpha_1 + k_{2,app}\,\alpha_2)[C_2H_2O_2]_t\,. \tag{16}$$

Dividing k_{obsd} by $\alpha_1[C_2H_2O_2]_t$ gives:

$$\frac{k_{obsd}}{\alpha_1[C_2H_2O_2]_t} = k_{1,app} + k_{2,app}\left(\frac{\alpha_2}{\alpha_1}\right), \tag{17}$$

and an estimate of $k_{1,app} \approx 0.15\ M^{-1}\ s^{-1}$ therefore can be obtained from the intercept of Fig. 2. Since the magnitudes of K_{a1} and K_{a2} (25° C, $\mu = 0$) are 1.45×10^{-2} M (21) and 6.31×10^{-8} M (22), respectively, the approximations that $K_{a1}\{H^+\}$, $\gg \{H^+\}^2$ and $K_{a1}\{H^+\} \gg K_{a1}K_{a2}$ can be made in the pH region of 2.5 – 3.2. Equation (16) then can be approximated as

$$k_{obsd} \approx \left\{ k_{1,app} + k_{2,app} \frac{K_{a2}}{\{H^+\}} \right\} [C_2H_2O_2]_t \,. \tag{18}$$

An estimate of $k_{2,app} \approx 2.21 \times 10^3\ M^{-1}s^{-1}$ was obtained by plotting $k_{obsd}/[C_2H_2O_2]_t$ vs $1/\{H^+\}$ as shown in Fig. 3 and dividing the slope by K_{a2}.

Refined estimates of $k_{1,app}$ and $k_{2,app}$ were obtained by fitting all of the data in Table 1 to Eq. 16 with a nonlinear least–squares regression routine (23a). Our rough estimates of the rate constants were supplied as initial guesses to the fitting program. The values of K_{a1} and K_{a2} were held fixed in the regression analysis but were corrected for an ionic strength of 0.2 M. The corrected acidity constants were ${}^cK_{a1} = K_{a1}\gamma_{H_2O\cdot SO_2}/\gamma_{HSO_3^-} = 1.99 \times 10^{-2}$ M and ${}^cK_{a2} = K_{a2}\gamma_{HSO_3^-}/\gamma_{SO_3^{2-}} = 1.63 \times 10^{-7}$ M, where K_{a1} and K_{a2} refer to acidity constants at infinite dilution. Activity coefficients, γ, were computed with the Davies equation (24):

$$\log \gamma = -Az^2 \left(\frac{\sqrt{\mu}}{\sqrt{\mu} + 1} - 0.2\mu \right) \tag{19}$$

where A = 0.509 (for water at 25° C), z is the ionic charge, and μ is the ionic strength. From the regression analysis, the refined estimates are $k_{1,app} = 0.130$ (± 0.014) $M^{-1}s^{-1}$ and $k_{2,app} = 2.08$ (± 0.05) $\times 10^3\ M^{-1}s^{-1}$. A comparison of observed and calculated pseudo–first–order rate constants (based on the fitted values of $k_{1,app}$ and $k_{2,app}$) is presented in Table 1.

The ionic strength dependence of $k_{1,app}$ and $k_{2,app}$ between $\mu = 0.2$ and

1.0 M was expected to be slight since both constants correspond to the addition of an anion or dianion with a neutral molecule. This assumption was experimentally tested and as Fig. 5 demonstrates, $k_{1,app}$ and $k_{2,app}$ are nearly independent of μ between $\mu = 0.2$ and 1.0 M.

Although the possibility of general acid catalysis by the buffers used herein was not tested, such catalysis has not been found for the addition of bisulfite and sulfite with other aldehydes (3,4). In addition, an absence of general acid or base catalysis is a well–known characteristic for the reaction of strong nucleophilic reagents with the carbonyl group (25). Buffer effects in the glyoxal–S(IV) system are therefore expected to be minimal over the pH range used here.

Adduct Dissociation Kinetics. By monitoring the dissociation of GDBS and GMBS in the presence of I_2, the reaction proceeded irreversibly as follows:

$$\text{GDBS} \xrightarrow{k_{-1,obsd}} \text{GMBS} + \text{S(IV)} \qquad \text{(slow)} \quad (20)$$

$$\text{GMBS} \xrightarrow{k_{-2,obsd}} \text{Glyoxal} + \text{S(IV)} \qquad \text{(slow)} \quad (21)$$

$$I_2 + \text{S(IV)} \longrightarrow 2I^- + \text{S(VI)}\,, \qquad \text{(fast)} \quad (22)$$

and hence the kinetic analysis was greatly simplified. At constant pH, the corresponding rate equation is

$$\nu = \frac{-d[I_3^-]}{dt} = k_{-1,obsd}[GDBS]_t + k_{-2,obsd}[GMBS]_t, \qquad (23)$$

where

$$[GMBS]_t = [CH(OH)_2CH(OH)SO_3^-] + [CH(OH)_2CH(O^-)SO_3^-] + [CHOCH(OH)SO_3^-] + [CHOCH(O^-)SO_3^-] \qquad (24a)$$

$$[GDBS]_t = [(CH(OH)SO_3^-)_2] + [CH(OH)SO_3^-CH(O^-)SO_3^-], \quad (24b)$$

and is subject to the initial conditions:

$$[GDBS]_o = C_o$$
$$[GMBS]_o = 0$$
$$[S(IV)]_o = 0 .$$

Equation (23) is readily integrable and the solution satisfying the initial conditions can be written in the form:

$$\frac{A - A_\infty}{A_o - A_\infty} = \frac{1}{2}\left\{\left[1 + \frac{k_{-2,obsd}}{(k_{-2,obsd} - k_{-1,obsd})}\right] e^{-(k_{-1,obsd}\, t)} - \left[\frac{k_{-1,obsd}}{(k_{-2,obsd} - k_{-1,obsd})}\right] e^{-(k_{-2,obsd}\, t)}\right\}. \quad (25)$$

The two first–order rate constants were fit to each data set with a nonlinear least–squares regression routine (23a). Results of this analysis as a function of pH are tabulated in Table 2. Plots of log $k_{-1,obsd}$ and log $k_{-2,obsd}$ vs pH have slopes of approximately unity above pH 4 and are nearly pH–independent near pH 1 as shown in Fig. 6. This pH dependence was also observed for the dissociation of benzaldehyde– and methylglyoxal–S(IV) addition compounds (5,26) and can be explained with the following mechanism and Eqs. (5a,b):

$$(CH(OH)SO_3^-)_2 \xrightarrow{k_{-3}} CHOCH(OH)SO_3^- + HSO_3^- \quad \text{(slow)} \quad (26)$$

$$CH(OH)SO_3^-CH(O^-)SO_3^- \xrightarrow{k_{-4}} CH(OH)SO_3^-CHO + SO_3^{2-} \quad \text{(slow)} \quad (27)$$

$$CH(OH)_2CH(OH)SO_3^- \xrightarrow{k_{-1}'} CH(OH)_2CHO + HSO_3^- \quad \text{(slow)} \quad (28a)$$

$$CHOCH(OH)SO_3^- \xrightarrow{k_{-1}''} CHOCHO + HSO_3^- \qquad \text{(slow)} \quad (28b)$$

$$CH(OH)_2CH(O^-)SO_3^- \xrightarrow{k_{-2}'} CH(OH)_2CHO + SO_3^{2-} \qquad \text{(slow)} \quad (29a)$$

$$CHOCH(O^-)SO_3^- \xrightarrow{k_{-2}''} CHOCHO + SO_3^{2-} \qquad \text{(slow)} \quad (29b)$$

$$CH(OH)_2CH(OH)SO_3^- \overset{K_{D3}}{\rightleftharpoons} CHOCH(OH)SO_3^- + H_2O \qquad \text{(fast)} \quad (30)$$

$$(CH(OH)SO_3^-)_2 \overset{K_{a3,GDBS}}{\rightleftharpoons} H^+ + CH(OH)SO_3^-CH(O^-)SO_3^- . \qquad \text{(fast)} \quad (31)$$

The rate expression governing the rate of release of S(IV),

$$\begin{aligned} \nu = \; & k_{-1}'[CH(OH)_2CH(OH)SO_3^-] + k_{-1}''[CHOCH(OH)SO_3^-] + \\ & k_{-2}'[CH(OH)_2CH(O^-)SO_3^-] + k_{-2}''[CHOCH(O^-)SO_3^-] + \\ & k_{-3}[(CH(OH)SO_3^-)_2] + k_{-4}[CH(OH)SO_3^-CH(O^-)SO_3^-] \end{aligned} \qquad (32)$$

can be rewritten in terms of $[GMBS]_t$ and $[GDBS]_t$ to give:

$$\nu = \left\{ k_{-1}' + k_{-1}''K_{D3} + \frac{\left(k_{-2}'K_{a2,GMBS}' + k_{-2}''K_{a2,GMBS}''K_{D3} \right)}{\{H^+\}} \right\} [GMBS]_t$$

$$+ \left\{ k_{-3} + \frac{k_{-4}\, K_{a3,GDBS}}{\{H^+\}} \right\} [GDBS]_t . \qquad (33)$$

In deriving Eq. (33) , it was assumed that $[CH(OH)_2CH(OH)SO_3^-] \approx [GMBS]_t$ and $[(CH(OH)SO_3^-)_2] \approx [GDBS]_t$, Although the former assumption depends on the magnitude of K_{D3}, an unknown, GMBS is likely to have a relatively large σ^* value and hence to be predominantly hydrated. The proposed mechanism leads to the following representations for the observed rate constants:

$$k_{-1,obsd} = k_{-3} + \left(\frac{k_{-4}\, K_{a3,GDBS}}{\{H^+\}} \right) \qquad (34a)$$

$$k_{-2,obsd} = (k_{-1}' + k_{-1}''K_{D3}) + (k_{-2}'K'_{a2,GMBS} + k_{-2}'' K_{a2,GMBS}K_{D3})/\{H^+\} , \quad (34b)$$

and these are consistent with the data in Fig. 6. Plots of $k_{-1,obsd}$ and $k_{-2,obsd}$ vs $1/\{H^+\}$ over the entire pH range were linear ($R^2 > 0.9999$), and the slopes were used to estimate the apparent constants $k_{-2}'K'_{a2} + k_{-2}'' K''_{a2,GMBS}K_{D3}$ and $k_{-4}K_{a3,GDBS}$, given in Table 3. The values of k_{-3} and $k_{-1}' + k_{-1}'' K''_{a2,GMBS}$ in Table 3 were obtained from the intercepts, using only the data below pH 4.

Adduct Stability Constants. The predominant adduct, S(IV), and glyoxal species remain the same between pH 3 to 5 and hence measurements of $K_{1,app}$ and $K_{2,app}$, where

$$K_{1,app} = \frac{[GMBS]}{[C_2H_2O_2][S(IV)]} \quad (35a)$$

$$K_{2,app} = \frac{[GDBS]}{[GMBS][S(IV)]} \quad (35b)$$

should be pH–independent over this pH range and approximately given by

$$K_{1,app} \approx {}^cK_1 = \frac{[CH(OH)_2CH(OH)SO_3^-]}{[(CH(OH)_2)_2][HSO_3^-]} \quad (36a)$$

$$K_{2,app} \approx {}^cK_2 = \frac{[(CH(OH)SO_3^-)_2]}{[CH(OH)_2CH(OH)SO_3^-][HSO_3^-]} . \quad (36b)$$

Furthermore, when $[C_2H_2O_2]_t$ is sufficiently greater than $[S(IV)]_t$, [GDBS] is negligible and hence,

$${}^cK_1 \approx \frac{([S(IV)]_t - [S(IV)]_{eq})}{\{[C_2H_2O_2]_t - ([S(IV)]_t - [S(IV)]_{eq})\}[S(IV)]_{eq}} . \quad (37)$$

With a tenfold excess of glyoxal, measurements of $[S(IV)]_{eq}$ at three different pH's were used in Eq. 37 to obtain an average ${}^{c}K_1 = 2.81 \times 10^4\ M^{-1}$ at 25° C and $\mu = 0.2$ M.

In solutions of the disodium glyoxal dibisulfite salt (i.e., $[S(IV)]_t = 2[C_2H_2O_2]_t$), both GMBS and GDBS species may be present. Mass balance and mass action relationships can be shown to yield the following expression for ${}^{c}K_2$ under these conditions:

$$ {}^{c}K_2 = \frac{{}^{c}K_1[S(IV)]_{eq}^2 + [S(IV)]_{eq}(1 - {}^{c}K_1[C_2H_2O_2]_t) - 2[C_2H_2O_2]_t}{- {}^{c}K_1[S(IV)]_{eq}^3} . \qquad (38) $$

The concentration of free S(IV) at equilibrium is therefore a root of the cubic equation:

$$ {}^{c}K_1{}^{c}K_2[S(IV)]_{eq}^3 + {}^{c}K_1[S(IV)]_{eq}^2 + (1 - {}^{c}K_1[C_2H_2O_2]_t)[S(IV)]_{eq} - 2[C_2H_2O_2]_t = 0 . \qquad (39) $$

The magnitudes of ${}^{c}K_1$ and ${}^{c}K_2$ were obtained by fitting the data in Table 4 to Eq. 39. Since it was not possible to write an analytic expression for $[S(IV)]_{eq}$ in terms of ${}^{c}K_1$, ${}^{c}K_2$ and $[C_2H_2O_2]_t$, the nonlinear least–squares regression routine had to be coupled to an algorithm that could solve for the zeroes of Eq. 39 (23a,b). Estimates for ${}^{c}K_1$ and ${}^{c}K_2$ at 25° C and $\mu = 0.2$ M were $3.57 \times 10^4\ M^{-1}$ and $1.45 \times 10^4\ M^{-1}$, respectively. Measured free S(IV) concentrations are compared with the calculated function in Fig. 7.

Formation constants at infinite dilution, ${}^{a}K$, can be computed using Eqs. 40a,b and the Davies equation to estimate the activity coefficients of the ionic species.

$$ {}^{a}K_1 = {}^{c}K_1 \left\{ \frac{\gamma_{GMBS^-}}{\gamma_{(CH(OH)_2)_2}\ \gamma_{HSO_3^-}} \right\} \tag{40a} $$

$$ {}^{a}K_2 = {}^{c}K_2 \left\{ \frac{\gamma_{GDBS^{2-}}}{\gamma_{GMBS^-}\ \gamma_{HSO_3^-}} \right\} \tag{40b} $$

If $\gamma_{(CH(OH)_2)_2} \approx 1$, use of the Davies equation in (40a) implies that ${}^{c}K_1$ should be relatively insensitive to ionic strength, and hence ${}^{a}K_1 \approx 3.57 \times 10^4\ M^{-1}$. A separate determination of ${}^{c}K_1$ (see Table 5) at $\mu = 1.0$ M suggests that this hypothesis is approximately correct since ${}^{c}K_1$ increased by only 30% over a fivefold increase in μ. Based on Eq. 40b and our estimate of ${}^{c}K_2$ at $\mu = 0.2$ M, ${}^{a}K_2 = 7.70 \times 10^3\ M^{-1}$ at 25° C. Standard enthalpy ($\Delta H_1^\circ = -29.0$ and $\Delta H_2^\circ = -40.0$ kJ/mol) and entropy ($\Delta S_1^\circ = -10.1$ and $\Delta S_2^\circ = -60.0$ J/mol/deg) changes were calculated from the results of temperature studies and the Vant Hoff plot shown in Fig. 8.

Discussion

The mechanism outlined in Eqs. 1–5 is similar to those we have proposed for the formation of other aldehyde–S(IV) adducts (3–5) over the same pH range (0.7 – 3.2). Outside this pH domain, however, other rate–determining steps are possible and have been observed with other aldehydes. Above pH 4.0, for example, dehydration of the methylglyoxal diol species becomes the rate–limiting step for adduct formation (5), and similar predictions have been made for formaldehyde (27). We are unable to make the analogous prediction for GMBS formation since reliable values of the necessary dehydration rate constants are not available. Below pH 0.7, other adduct formation pathways may be important. Specific acid catalysis was observed at very low pH for both benzaldehyde and methylglyoxal. This catalysis was attributed to the protonation of the carbonyl carbon, which

thereby provides a more electrophilic site for attack by bisulfite.

The magnitudes of $k_{1,app}$ and $k_{2,app}$ reported in this study reflect the large difference in reactivity between HSO_3^- and SO_3^{2-} with aldehydes. The ratio of $k_{2,app}/k_{1,app}$ for GMBS is 1.6×10^4, which is slightly lower than the corresponding ratios of other aldehydes (CH_3COCHO: 1.14×10^5, C_6H_5CHO: 3.02×10^4, HCHO: 3.14×10^4). Our lower value for glyoxal may be due to the fact that the rate constants were not intrinsic. Other investigators have also found SO_3^{2-} to be the strongest nucleophile among S(IV) species in reactions with a wide variety of inorganic and organic substrates (28,29). Besides the expected difference in nucleophilicity of SO_3^{2-} and HSO_3^-, the greater reactivity of sulfite may involve structural differences in the transition state complexes. In our previous studies with formaldehyde, benzaldehyde and methylglyoxal, we proposed that bisulfite addition requires the formation of a cyclic, activated complex, whereas sulfite addition does not. Measured activation parameters in these studies supported this hypothesis since a much larger activation entropy was found for HSO_3^- addition than the $\Delta S^{\neq}$ for SO_3^{2-}.

Above pH 3, the decomposition of $RCH(O^-)SO_3^-$ species governs the dissociation kinetics of GMBS and GDBS. This behavior reflects the large difference in rate constants for the release of HSO_3^- and SO_3^{2-}. A minimum value of the ratio, $k_{-4}/k_{-3} > 10^6$, can be estimated, for example, using the data in Table 3 and assuming a conservative limit of $K_{a3,GDBS} < 10^{-9}$. The more rapid dissociation of $RCH(O^-)SO_3^-$ species may be attributed to the inductive effect of its electron–donating O^- group. The release of bisulfite would be less favorable since the hydroxy group withdraws electrons from the carbon center.

Applying the principle of microscopic reversibility, a third independent estimate of the stability constant for GMBS is ${}^cK_1 = k_{1,app}/(k'_{-1} + k''_{-1}K_{D3}) =$

2.81×10^4 M^{-1} (25° C, μ = 0.2 M). This value of ${}^cK_1$ agrees closely with the one determined by Method "B" but is slightly less than the stability constant obtained by Method "C" (see Table 5). Since the standard error associated with the Method "C" value of ${}^cK_1$ is also quite large, we believe the more reliable estimate of ${}^cK_1$ to be 2.81×10^4 M^{-1}.

Reasonable agreement was also found between our value of the second association constant, ${}^aK_2 = 7.70 \times 10^3$ M^{-1} (25° C, μ = 0), and Salomaa's data (9). The apparent constant cited by Salomaa at pH 7.3 (equivalent to $K_{2,app}$ defined in Eq. 35b) gives a value of ${}^cK_2 = 8.61 \times 10^3$ M^{-1} at 20° C. Temperature corrections based on our reported values of $\Delta H_2°$ and $\Delta S_2°$ increase ${}^aK_2$ to 1.00×10^4 M^{-1} at 20° C; however, direct comparison of this number with Salomaa's is still not exact since the ionic strength in his study is not known.

In Fig. 9 a linear–free–energy plot relates S(IV)–aldehyde adduct stability constants (now expressed in terms of the *unhydrated* aldehyde concentration) and Taft polar substituent constants. In order to include the formation constant for glyoxal monobisulfite in this correlation, values of $K_{D1} \approx 2.0 \times 10^{-4}$ and $K_{D2} \approx 4.2 \times 10^{-3}$ were assumed (*vide supra*). The stability constant for GDBS was not compared in the correlation since the σ^* parameter for the substituent, $-CH(OH)SO_3^-$, has not been established. Taft correlations for K_D (Fig. 4) and K_1 (Fig. 9) are strikingly similar in that aliphatic carbonyl substrates with a single α–hydrogen are linear in σ^*. Formaldehyde, which has two α–hydrogen atoms, forms more stable adducts ($CH_2(OH)_2$ and $CH_2(OH)SO_3^-$) than the lines in Figs. 4 and 9 would predict. The enhanced stability observed when methyl groups are replaced by hydrogen atoms may be due to an increase in hydrogen bonding with the solvent water and the subsequent increased polarization of the carbonyl group.

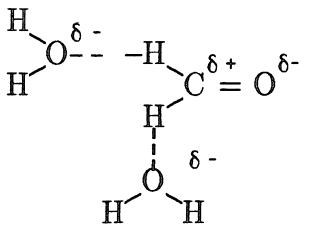

Similar hydrogen bonding arguments have been invoked to explain Taft correlations for acidity constants of primary, secondary, and tertiary amines (19). Benzaldehyde–water and –bisulfite addition compounds are substantially less stable than the lines in Figs. 4 and 9 would predict. The lack of correlation in this case may be due to resonance stabilization of free benzaldehyde and/or to steric hindrance by the phenyl group.

Conclusions for Atmospheric Systems. With the above thermodynamic data it is now possible to examine the importance of glyoxal–S(IV) adducts as reservoirs for S(IV) and glyoxal. Maximum concentrations of aqueous GMBS and GDBS, which could form in a polluted open atmosphere, were calculated with the following mass balances and Henry's Law relationships:

$$[S(IV)]_t = [H_2O \cdot SO_2] + [HSO_3^-] + [SO_3^{2-}] + [GMBS]_t + 2[GDBS]_t \quad (41a)$$

$$[C_2H_2O_2]_t = [(CH(OH)_2)_2] + [GMBS]_t + [GDBS]_t \quad (41b)$$

$$[H_2O \cdot SO_2] = P_{SO_2} H^*_{SO_2} \quad (42a)$$

$$[HSO_3^-] = P_{SO_2} H^*_{SO_2} K_{a1}/\{H^+\} \quad (42b)$$

$$[SO_3^{2-}] = P_{SO_2} H^*_{SO_2} K_{a1} K_{a2}/\{H^+\} \quad (42c)$$

$$[(CH(OH)_2)_2] = P_{CHOCHO} H^*_{CHOCHO} \quad (42d)$$

$$[GMBS]_t \simeq [CH(OH)_2CH(OH)SO_3^-]$$

$$= {}^cK_1 P_{CHOCHO} H^*_{CHOCHO} P_{SO_2} H^*_{SO_2} K_{a1} / \{H^+\} \quad (42e)$$

$$[GDBS]_t \simeq [(CH(OH)SO_3^-)_2]$$

$$= {}^cK_1 {}^cK_2 P_{CHOCHO} H^*_{CHOCHO} \left[P_{SO_2} H^*_{SO_2} K_{a1} / \{H^+\} \right]^2 , \quad (42f)$$

where P_{CHOCHO} and P_{SO_2} are the partial pressures of gas–phase species, and H^*_{CHOCHO} and $H^*_{SO_2}$ are apparent Henry's Law constants.

Since ambient SO_2 levels in polluted atmospheres generally range from 0 to 50 ppbv (1), a typical SO_2 partial pressure of 20 ppbv was selected. Typical gas–phase concentrations of glyoxal have not been established; however, a value of 0.1 ppbv leads to an aqueous concentration of 30 μM glyoxal if the apparent Henry's Law constant is approximately 3×10^5 M atm^{-1} (32). Although glyoxal photolyzes quite rapidly in the gas phase, with predicted atmospheric lifetimes of a few hours (33), the above aqueous glyoxal concentration is comparable to those reported in mist and fogwater (8).

Adduct concentrations and S(IV) and glyoxal enrichment factors (i.e., $[S(IV)]_t/[S(IV)]_{free}$ and $[C_2H_2O_2]_t/[(CH(OH)_2)_2]$) corresponding to the above conditions are tabulated in Table 6 for four pH conditions. Below pH 5, GDBS concentrations are negligible and GMBS formation leads to nearly twice the total S(IV) concentration, which would be present in the absence of glyoxal. Above pH 5, GDBS formation leads to even larger S(IV) enrichment factors. In this pH range glyoxal–S(IV) adducts are also a significant reservoir for glyoxal.

Although a rather simplistic set of conditions was chosen, our calculations suggest that glyoxal–S(IV) adduct formation potentially leads to greater scavenging of glyoxal and S(IV) by atmospheric water droplets. Scavenging of SO_2

is particularly enhanced under slightly acidic conditions because of the unique ability of glyoxal to form the dibisulfite adduct.

Acknowledgements. We gratefully acknowledge the Electric Power Research Institute (RP1630–47) and the Environmental Protection Agency (R811496–01–1) for their financial support.

REFERENCES

(1) Munger, J.W.; Tiller, C.; Hoffmann, M.R. *Science* **1986**, *231*, 247–249.

(2) Ang, C.C.; Lipari, F.; Swarin, S.W. *Environ. Sci. Technol.* **1987**, *21*, 102–105.

(3) Boyce, S.D.; Hoffmann, M.R. *J. Phys. Chem.* **1984**, *88*, 4740–4746.

(4) Olson, T.M.; Boyce, S.D.; Hoffmann, M.R. *J. Phys. Chem.* **1986**, *90*, 2482–2488.

(5a) Betterton, E.A.; Hoffmann, M.R. *J. Phys. Chem.* **1987**, *91*, 3011–3020.

(5b) Betterton, E.A.; Erel, Y.; Hoffmann, M.R. *Environ. Sci. Technol.* **1988**, *22*, 92–99.

(6a) Tuazon, E.C.; Atkinson, R.; MacLeod, H.; Biermann, H.W.; Winer, A.M.; Carter, W.P.L.; Pitts, J.N. *Environ. Sci. Technol.* **1984**, *18*, 981–84.

(6b) Tuazon, E.C.; MacLeod, H.; Atkinson, R.; Carter, W.P.L. *Environ. Sci. Technol.* **1986**, *20*, 383–387.

(7) Calvert, J.G.; Madronich, S. *J. Geophys. Res.*, **1987**, *92*, 2211–2220.

(8) Steinberg, S.; Kaplan, I.R. *Internat. J. Environ. Anal. Chem.*, **1984**, *18*, 253–266.

(9) Salomaa, P. *Acta Chemica Scand.* **1956**, *10*, 306–310.

(10) Ronzio, A.R.; Waugh, T.D. *Organic Syntheses Col.*; Vol. 3, **1944**, 438–440.

(11) Wasa, T.; Musha, S. *Bull. Univ. Osaka Prefect Ser. A* **1970**, *19*, 169–180.

(12) Collins, G.C.S.; George, W.O. *J. Chem. Soc.* (B) **1971**, 1352–1355.

(13) Kobayashi, Y.; Takahashi, H. *Spectrochimica Acta* **1979**, *35A*, 307–314.

(14) Hine, J.; Houston, J.G.; Jensen, J.H. *J. Org. Chem.* **1965**, *30*, 1184–1188.

(15) Buschmann, H.J.; Füldner, H.H.; Knoche, W. *Ber. Bunsenges Phys. Chem.* **1980**, *84*, 41–44.

(16) Sørensen, P.E. *Acta Chem. Scand.* **1972**, *26*, 3357–3365.

(17) Bell, R.P. In: *Advances in Physical Organic Chemistry*, Gold, V., Ed.; Academic Press: London, **1966**; Vol. 4., pp. 1–29.

(18) Gruen, L.C.; McTigue, P.T. *J. Chem. Soc.* **1963**, 5224–5229.

(19) Perrin, D.D.; Dempsey, B.; Serjeant, E.P. *pKa Prediction for Organic Acids and Bases*; Chapman and Hall: London, **1981**, pp. 37–38, 109–125.

(20) Rao, C.N.R. *Ultra–Violet and Visible Spectroscopy*, 2nd ed.; Butterworth and Co.: London, **1967**, p. 15.

(21) Deveze, D.; Rumpf, P. *C.R. Acad. Sc. Paris* **1964**, *258*, 6135–6138.

(22) Hayon, E.; Treinin, A.; Wilf, J. *J. Amer. Chem. Soc.* **1972**, *94*, 47–57.

(23a) *STAT/LIBRARY FORTRAN Subroutines for Statistical Analysis On a Personal Computer*, IMSL User Manual, **1984**.

(23b) *MATH/LIBRARY Problem–Solving Software System for Mathematical FORTRAN Programming*, IMSL User Manual, **1984**.

(24) Stumm, W.; Morgan, J.J.; *Aquatic Chemistry*, 2nd ed.; Wiley–Interscience: New York, **1981**, p. 135.

(25) Jencks, W.P. *Prog. Phys. Chem.* **1964**, *2*, 63–118.

(26) Stewart, T.D.; Donnally, L.H. *J. Amer. Chem. Soc.* **1932**, *54*, 2333–2340.

(27) Olson, T.M.; Hoffmann, M.R. *Atmos. Environ.* **1986**, *11*, 2277–2278.

(28) Schroeter, L.C. *Sulfur Dioxide, Applications in Foods, Beverages, and Pharmaceuticals*; Pergamon: New York, **1966**, pp. 119–120.

(29) Edwards, J.O. *Inorganic Reaction Mechanisms*; Benjamin: New York, **1965**, pp. 54–56.

(30) Deister, U.; Neeb, R.; Helas, G.; Warneck, P. *J. Phys. Chem.* **1986**, *90*, 3213–3217.

(31) Green, L.R.; Hine, J. *J. Org. Chem.* **1974**, *39*, 3896–3901.

(32) This Henry's Law constant is a minimum value, which was experimentally determined by E. Betterton. Details of these experiments will be published elsewhere.

(33) Plum, C.N.; Sanhueza, E.; Atkinson, R.; Carter, W.P.L.; Pitts, J.N. *Environ. Sci. Technol.* **1983**, *17*, 479–484.

TABLE 1. Kinetic Data for the Formation of Glyoxal–Monobisulfite.

pH	10^2[CHOCHO], M	10^3[S(IV)], M	$10^3 k_{obsd}$ ($\pm\sigma$), s^{-1}	$10^3 k_{calc}$ s^{-1}
0.74	2.0	0.15	0.280 (0.005)	0.262
0.87	2.0	0.20	0.331 (0.013)	0.337
0.98	2.0	0.20	0.448 (0.010)	0.420
1.31	2.0	0.20	0.769 (0.042)	0.790
1.55	2.0	0.25	1.25 (0.05)	1.16
1.79	2.0	0.50	1.79 (0.05)	1.65
2.00	2.0	0.50	2.26 (0.12)	2.18
2.29	2.0	1.0	3.21 (0.10)	3.11
2.59	2.0	1.0	4.68 (0.14)	4.63
2.92	2.0	1.0	6.78 (0.15)	7.72
3.06	1.5	1.5	8.26 (0.18)	7.44
3.26	1.5	1.5	10.8 (0.4)	10.8

TABLE 2. Kinetic Data for the Dissociation of Glyoxal–Monobisulfite and Glyoxal–Dibisulfite Addition Compounds.

pH	$k_{-1,obsd}(\pm\sigma)$ (s^{-1})	$k_{-2,obsd}(\pm\sigma)$ (s^{-1})
1.26	1.24 (0.03) × 10^{-5}	4.01 (0.01) × 10^{-6}
1.80	1.49 (0.13) × 10^{-5}	4.22 (0.04) × 10^{-6}
3.00	8.37 (0.37) × 10^{-5}	1.85 (0.21) × 10^{-5}
3.88	5.65 (0.18) × 10^{-4}	9.27 (0.12) × 10^{-5}
4.53	2.16 (0.16) × 10^{-3}	4.25 (0.10) × 10^{-4}
4.87	5.85 (0.23) × 10^{-3}	9.08 (0.03) × 10^{-4}
5.09	1.05 (0.07) × 10^{-2}	1.38 (0.03) × 10^{-3}
5.92	7.58 (0.30) × 10^{-2}	8.22 (0.11) × 10^{-2}
6.49	0.278 (0.004)	3.00 (0.12) × 10^{-2}
6.99	0.858 (0.001)	9.53 (0.35) × 10^{-2}

TABLE 3. Dissociation Rate Constant Estimates at 25° C, μ = 0.2 M.

Constant Term	Value
$k_{-1}' + k_{-1}'' K_{D3}$	4.62×10^{-6} s^{-1}
$k'_{-2} K'_{a2} + k''_{-2} K''_{a2,GMBS} K_{D3}$	9.74×10^{-9} s^{-1} M
k_{-3}	1.07×10^{-5} s^{-1}
$k_{-4} K_{a3,GDBS}$	8.80×10^{-8} s^{-1} M

TABLE 4. S(IV) Concentrations in Equilibrated Disodium Glyoxal–Dibisulfite Solutions at 25° C, $\mu = 0.2$ M, pH 3.4 – 3.6.

$10^5[(NaCH(OH)SO_3)_2]_t$ (M)	$10^5[S(IV)]_{eq,meas}$ (M)	$10^5[S(IV)]^{(a)}_{eq,calc}$ (M)
1.0	1.59	1.53
2.0	2.60	2.58
3.0	3.37	3.42
4.0	4.18	4.14
5.0	4.70	4.77
6.0	5.33	5.34
7.0	5.89	5.87
8.0	6.39	6.36

(a) Based on ${}^cK_1 = 3.57 \times 10^4$ M^{-1} and ${}^cK_2 = 1.45 \times 10^4$ M^{-1}.

TABLE 5. Apparent Stability Constants for Glyoxal Mono– and Dibisulfite Addition Compounds.

Method[a]	T(°C)	μ (M)	10^{-4} $^{c}K_1(\pm\sigma)$ (M^{-1})	10^{-4} $^{c}K_2(\pm\sigma)$ (M^{-1})
A	25	0.2	2.81	N/A
B	25	0.2	2.81 (0.14)	N/A
C	25	0.2	3.57 (0.42)	1.45 (0.15)
C	25	1.0	4.66 (0.89)	2.44 (0.34)
C	30	0.2	2.95 (0.46)	1.08 (0.16)
C	35	0.2	2.44 (0.51)	0.87 (0.22)

[a]Method "A": $^{c}K_1$ calculated from forward and reverse rate constants.
Method "B": $[S(IV)]_{eq}$ measured with a tenfold excess of glyoxal.
Method "C": $[S(IV)]_{eq}$ measured in dissolved $Na_2(CH(OH)SO_3)_2$ solutions.

TABLE 6. Potential Aqueous Glyoxal–S(IV) Adduct Concentrations in an Open Atmosphere (P_{SO_2} = 20 ppbv, P_{CHOCHO} = 0.1 ppbv, T = 25° C).

	(μM)					
pH	[GMBS]	[GDBS]	$[S(IV)]_t^{(a)}$	$[C_2H_2O_2]_t^{(b)}$	$\frac{[C_2H_2O_2]_t}{[(CH(OH)_2)_2]}$	$\frac{[S(IV)]_t}{[S(IV)]_{free}}$
3	0.308	0.0009	0.70	30.3	1.01	1.79
4	3.08	0.087	6.93	33.2	1.11	1.89
5	30.9	8.67	84.7	69.5	2.32	2.32
6	308	867	2430	1200	40.0	6.26

(a) $[S(IV)]_t = [H_2O \cdot SO_2] + [HSO_3^-] + [SO_3^{2-}] + [GMBS]_t + 2[GDBS]_t$

(b) $[C_2H_2O_2]_t = [(CH(OH)_2)_2] + [GMBS] + [GDBS]$

Figure Captions

Figure 1. Dependence of pseudo–first–order rate constants for glyoxal monobisulfite formation on $[CHOCHO]_t$. Solid lines are linear least–square fits to the data. Reaction conditions: $[S(IV)]_t$ = 0.1 – 2.5 mM, T = 25° C, μ = 0.2 M.

Figure 2. Dependence of $k_{obsd}/(\alpha_1[CHOCHO]_t) = \nu/([HSO_3^-][CHOCHO]_t)$ on pH. Data are taken from Table 1.

Figure 3. Dependence of $k_{obsd}/[CHOCHO]$ on $1/\{H^+\}$ between pH 2.6 – 3.2. Solid line represents a linear least–squares fit to the data taken from Table 1.

Figure 4. Linear–free–energy relationship between pK_D and the Taft σ^* parameter. Key: 1 = $(CH_3)_2CHCHO$ (Ref. 14); 2 = CH_3CH_2CHO (15); 3 = CH_3CHO (15); 4 = $CH_2(OH)CHO$ (16); 5 = $ClCH_2CHO$ (17); 6 = CH_3COCHO (11); 7 = Cl_3CCHO (18). Formaldehyde (σ^*_{HCHO} = 0.49, $pK_{D,HCHO}$ = 3.26 (Ref. 17)) lies well above the least–squares regression line and was not included.

Figure 5. Ionic strength dependence of the apparent rate constants for bisulfite and sulfite addition with glyoxal species, $k_{1,app}$ and $k_{2,app}$ (25° C).

Figure 6. Dissociation rate constants for glyoxal – di– and monobisulfite, $k_{-1,obsd}$ and $k_{-2,obsd}$, respectively, as a function of pH. Solid lines are linear least–squares regression fits to the data in Table 2.

Figure 7. Measured free [S(IV)] at equilibrium as a function of total $[Na_2(CH(OH)SO_3)_2]$. Conditions: T = 25° C, μ = 0.2 M, pH = 3.6. Solid line represents nonlinear least–squares regression fit of ${}^cK_1$ and ${}^cK_2$ to the data in Table 4 using Eq. 39.

Figure 8. Temperature dependence of glyoxal – mono– and dibisulfite stability constants (${}^aK_1$ and ${}^aK_2$, respectively). Stability constants in Table 5 have been corrected from μ = 0.2 to μ = 0 with Eq. 19.

Figure 9. Linear–free–energy plot of aldehyde–S(IV) stability constants (K_1 = $[RCH(OH)SO_3^-]/([RCHO][HSO_3^-])$) vs the Taft σ^* parameter at 25° C. Key: 1 = CH_3COCHO (Ref. 5a); 2 = $CH(OH)_2CHO$ (This work); 3 = C_6H_5CHO (4); 4 = $CH_2(OH)CHO$ (5b); 5 = HCHO (5b); 6 = $(CH_3)_2CHCHO$ (31); 7 = CH_3CHO (30). The solid line was calculated from a least–squares fit of data for points 1,2,4,6 and 7 only.

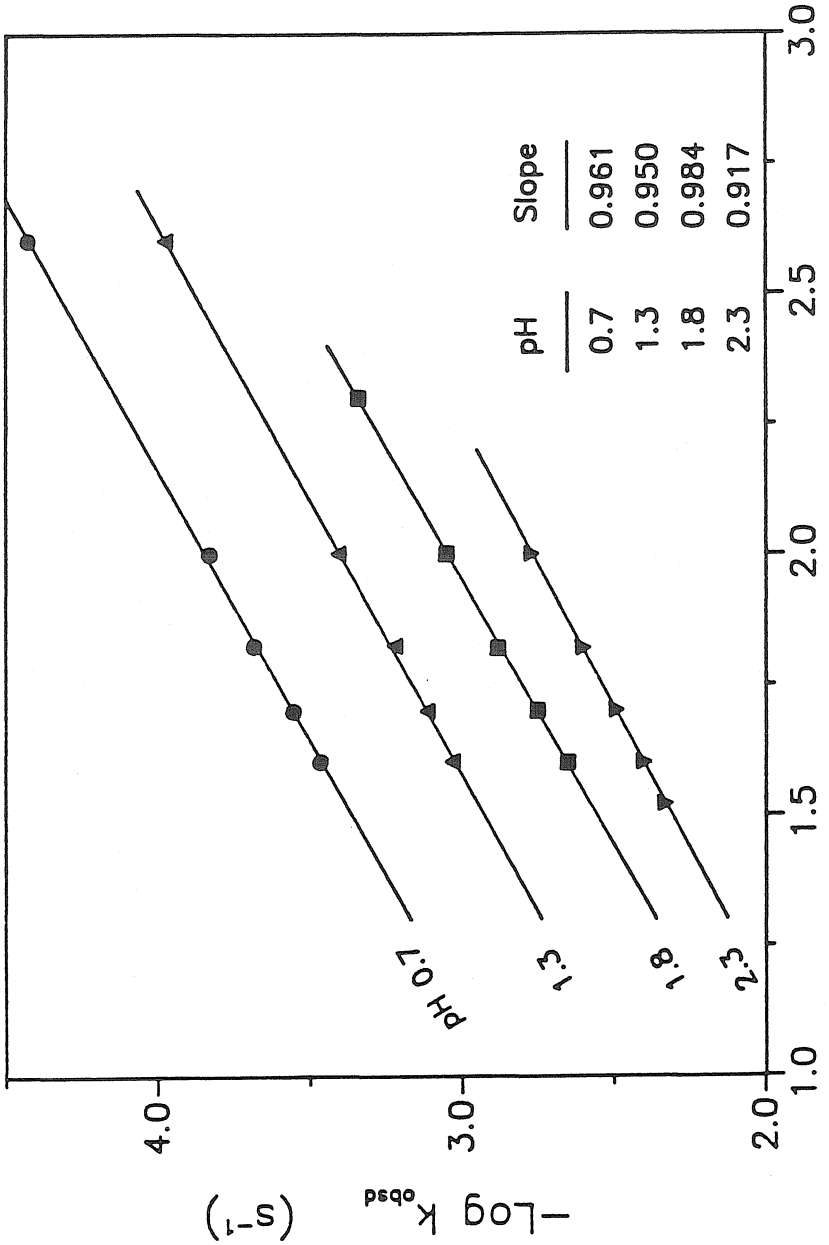
−Log k_{obsd} (s^{-1})
4.0
3.0
2.0
1.0
1.5
2.0
2.5
3.0
−Log $[CHOCHO]_T$ (M)
pH 0.7
1.3
1.8
2.3
pH Slope
0.7 0.961
1.3 0.950
1.8 0.984
2.3 0.917

Figure 1

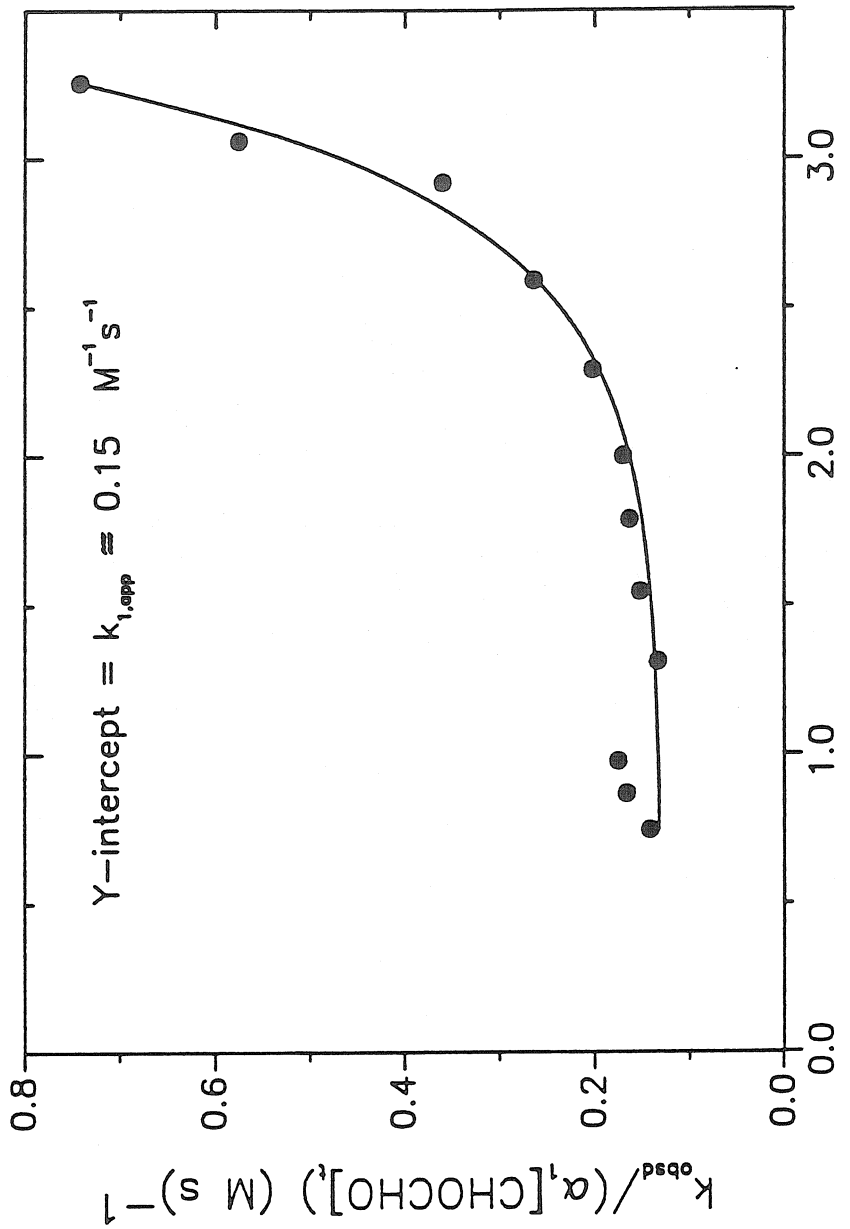
Y–intercept = $k_{1,app}$ = 0.15 $M^{-1}s^{-1}$
$k_{obsd}/(\alpha_1[CHOCHO]_t)$ (M s)$^{-1}$
pH
0.0
0.2
0.4
0.6
0.8
1.0
2.0
3.0

Figure 2

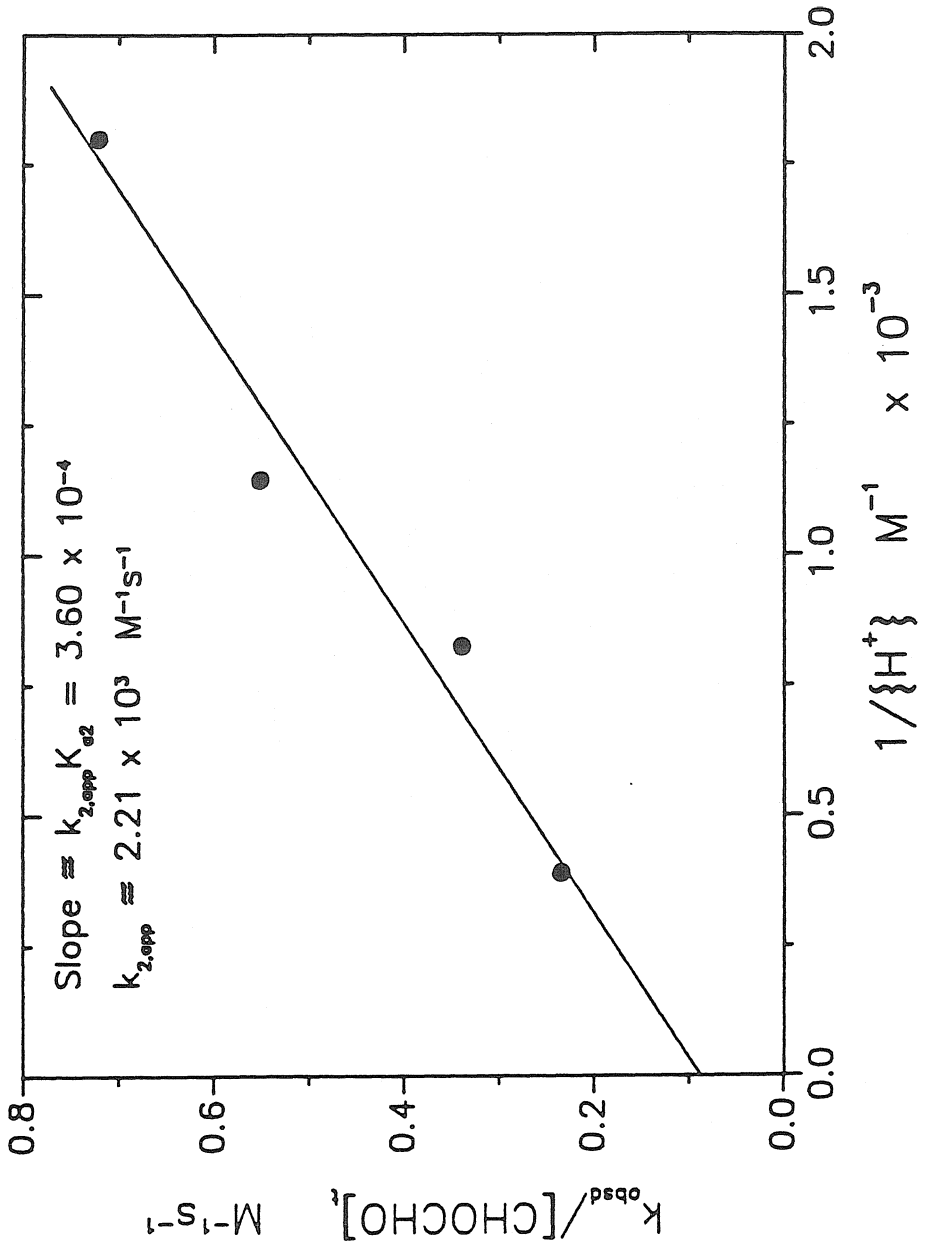
Slope ≡ $k_{2,app}K_{a2}$ = 3.60 x 10^{-4}
$k_{2,app}$ ≡ 2.21 x 10^{3} $M^{-1}s^{-1}$
$k_{obsd}/[CHOCHO]_t$ $M^{-1}s^{-1}$
0.0
0.2
0.4
0.6
0.8
0.0
0.5
1.0
1.5
2.0
$1/\{H^+\}$ M^{-1} x 10^{-3}

Figure 3

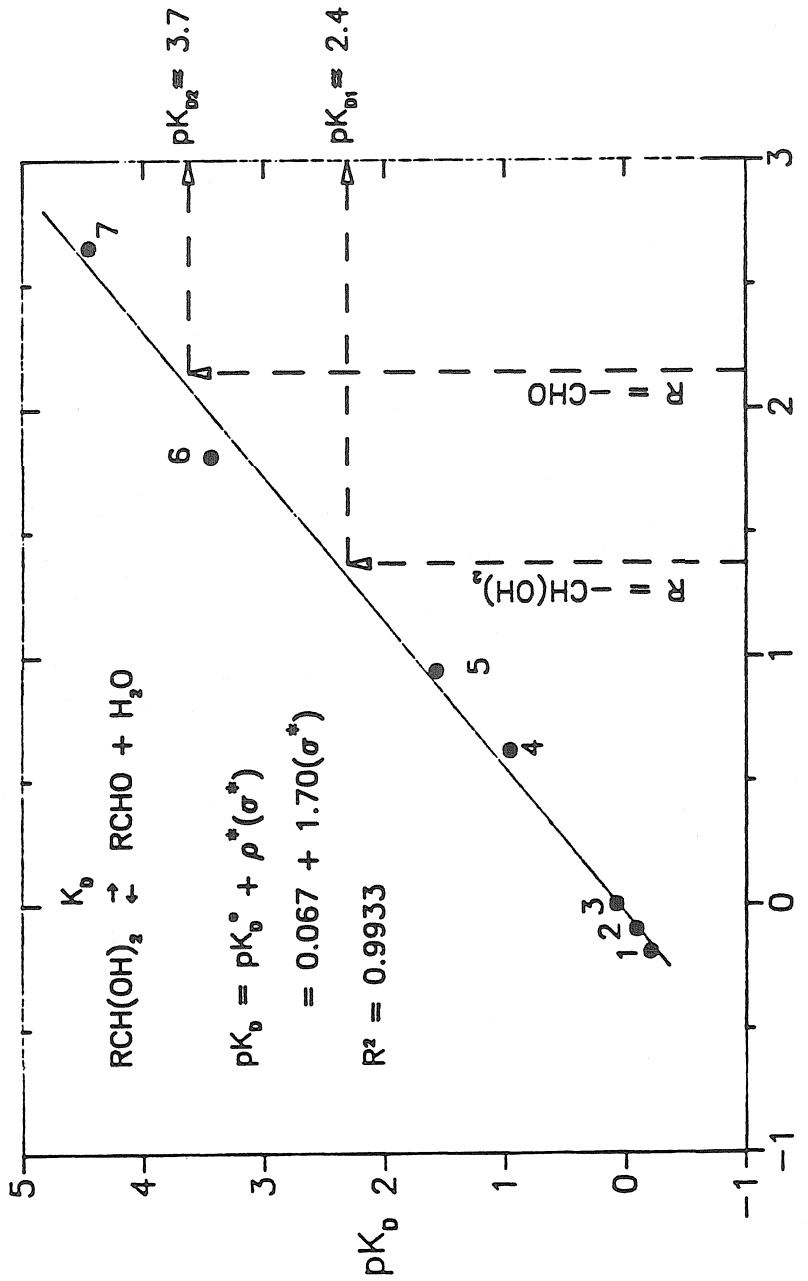
pK_b2 ≅ 3.7
pK_b1 ≅ 2.4
R = –CHO
R = –CH(OH)2
K_b
RCH(OH)2 ⇄ RCHO + H2O
pK_b = pK_b° + ρ*(σ*)
= 0.067 + 1.70(σ*)
R² = 0.9933
pK_b
σ*
1
2
3
4
5
6
7

Figure 4

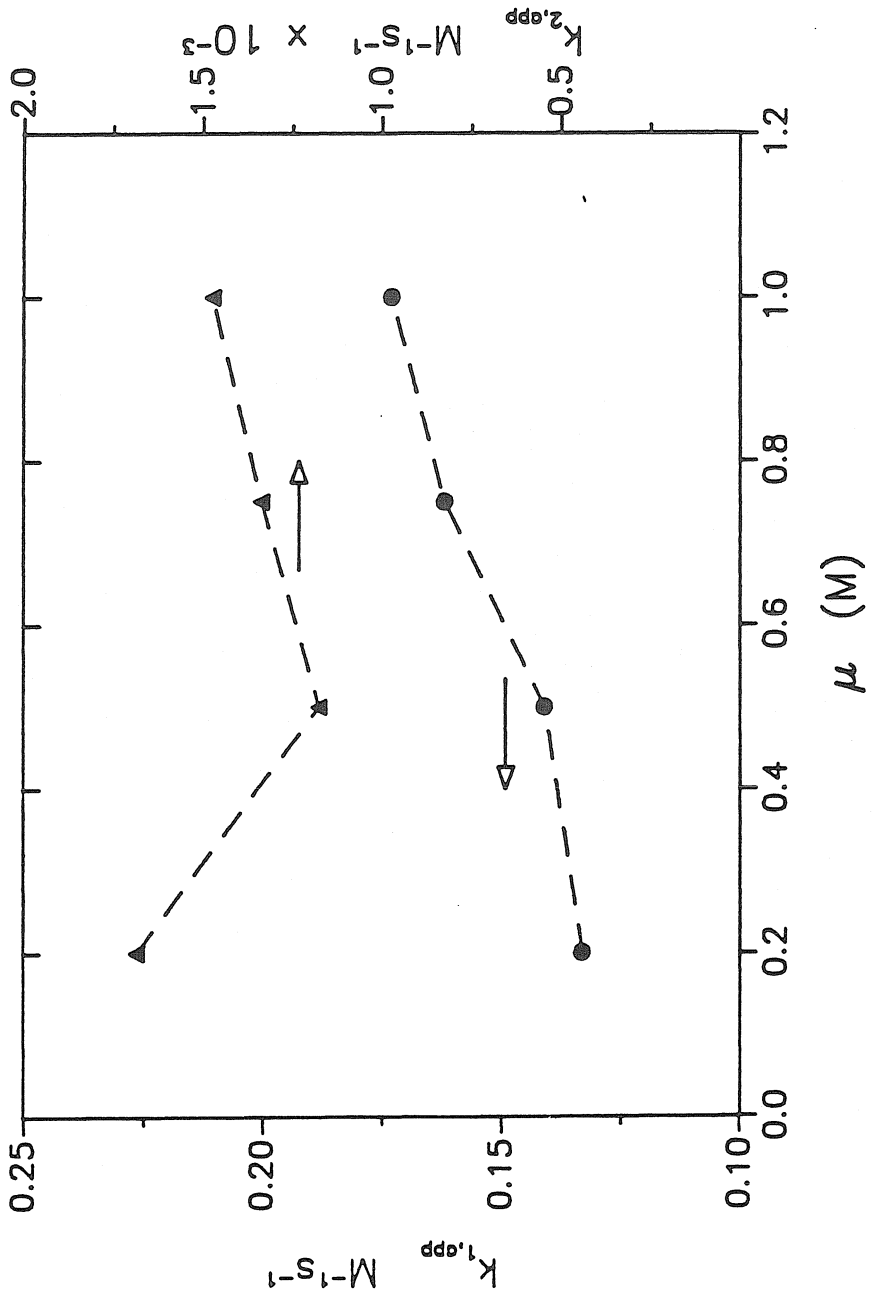
0.25
0.20
0.15
0.10
$k_{1,app}$ $M^{-1}s^{-1}$
0.0
0.2
0.4
0.6
0.8
1.0
1.2
μ (M)
2.0
1.5
1.0
0.5
$k_{2,app}$ $M^{-1}s^{-1}$ x 10^{-3}

Figure 5

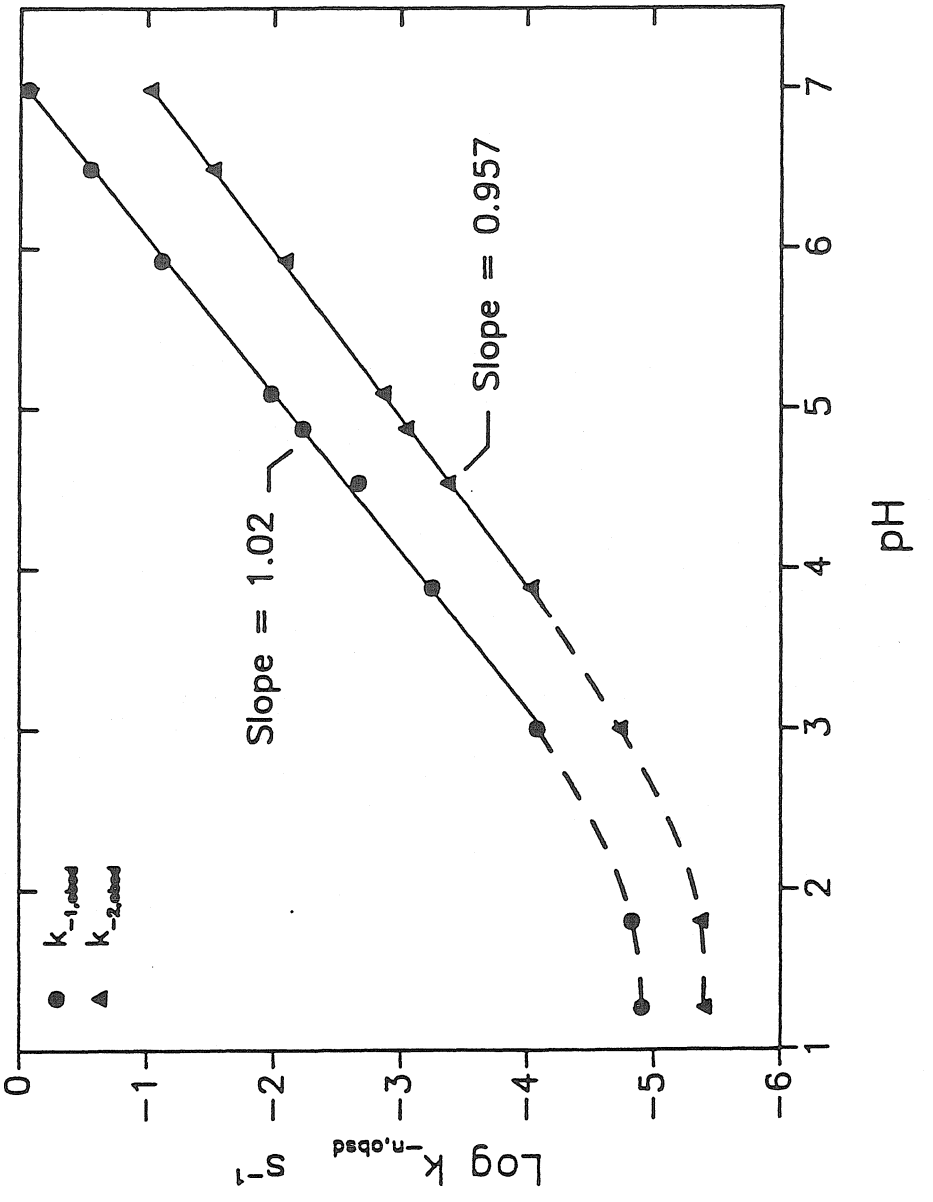

Figure 6

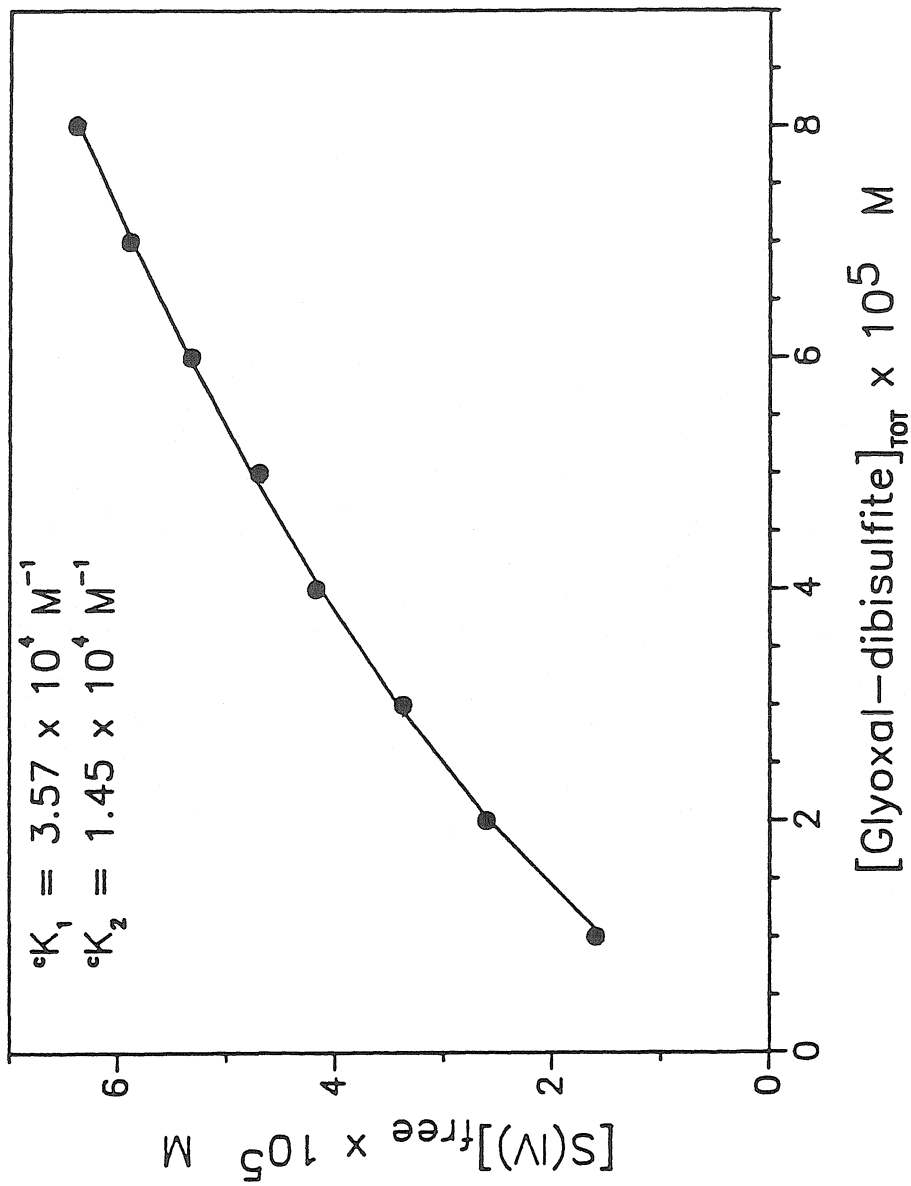
$^{c}K_1$ = 3.57 x 10^4 M^{-1}
$^{c}K_2$ = 1.45 x 10^4 M^{-1}
$[S(IV)]_{free}$ x 10^5 M
[Glyoxal−dibisulfite]$_{TOT}$ x 10^5 M
0
2
4
6
8

Figure 7

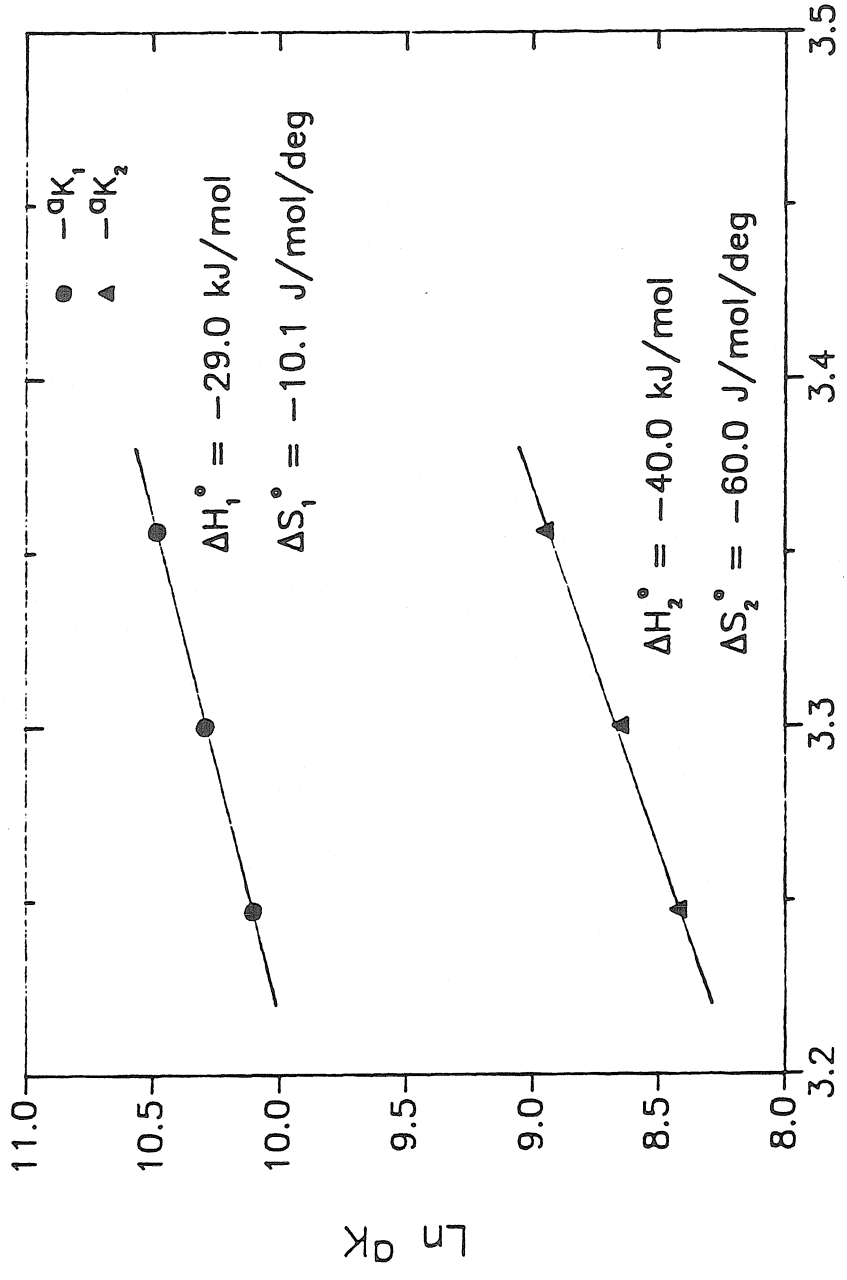
$-^{a}K_1$
$-^{a}K_2$
$\Delta H_1^\circ = -29.0$ kJ/mol
$\Delta S_1^\circ = -10.1$ J/mol/deg
$\Delta H_2^\circ = -40.0$ kJ/mol
$\Delta S_2^\circ = -60.0$ J/mol/deg
Ln ^{a}K
1/T ($^\circ K^{-1}$) x 10^3
11.0
10.5
10.0
9.5
9.0
8.5
8.0
3.2
3.3
3.4
3.5

Figure 8

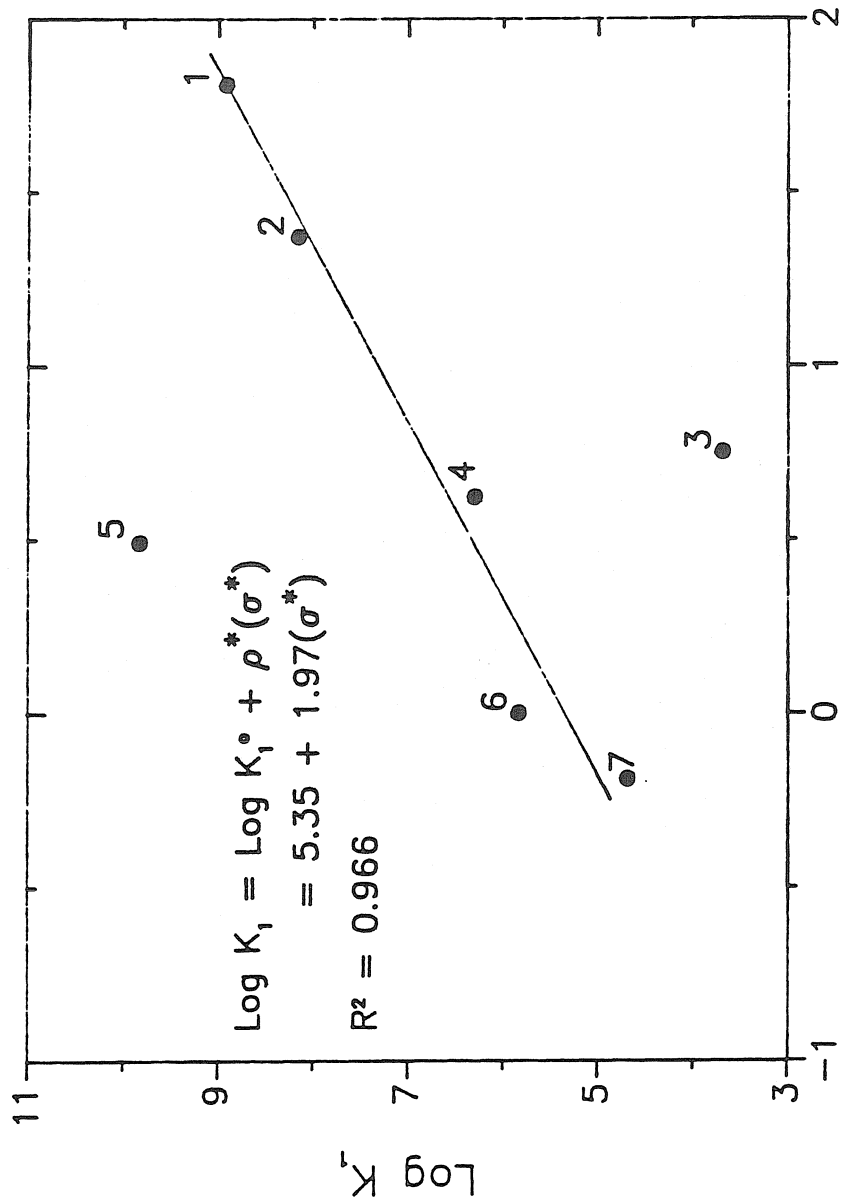

Figure 9

CHAPTER 5

The Formation Kinetics, Mechanism, and Thermodynamics of Glyoxylic Acid - S(IV) Adducts

by

Terese M. Olson and Michael R. Hoffmann

Submitted to: *Journal of Physical Chemistry*, November 1987

Abstract

A spectrophotometric study of the reversible addition of glyoxylic acid and S(IV) was conducted over the pH range of 0.7 to 2.9. Formation rates of the adduct, 2–hydroxy–2–sulfo–ethanoic acid (HSEA), and its conjugate base were consistent with the following rate expression: $-d[S(IV)]/dt = (k_1\alpha_1\beta_1 + k_3\alpha_2\beta_1)[C_2H_2O_3][S(IV)]$, where $[C_2H_2O_3] = [CHOCO_2H] + [CHOCO_2^-] + [CH(OH)_2CO_2H] + [CH(OH)_2CO_2^-]$, $[S(IV)] = [H_2O\cdot SO_2] + [HSO_3^-] + [SO_3^{2-}]$, $\alpha_1 = [HSO_3^-]/[S(IV)]$, $\alpha_2 = [SO_3^{2-}]/[S(IV)]$, and $\beta_1 = [CHOCO_2H]/[C_2H_2O_3]$. The rate constants k_1 and k_3 correspond to the respective addition steps of HSO_3^- and SO_3^{2-} with $CHOCO_2H$. A study of the pH dependence gave $k_1 = 443$ (±21.2) M^{-1} s^{-1} and $k_3 = 1.98 \times 10^7$ M^{-1} s^{-1}. Temperature studies of the reaction showed that the $\Delta S^{\ddagger}$ for the addition of bisulfite and glyoxylic acid is significantly more negative than activation entropies for other low molecular weight aldehydes. A transition state was proposed that involves intramolecular hydrogen bonding. Adduct stability constants were determined as ${}^cK_1 = [HO_2CCH(OH)SO_3^-]/([CHOCO_2H][HSO_3^-]) = 7.09 \times 10^7$ M^{-1} and ${}^cK_2 = [^-O_2CCH(OH)SO_3^-]/([CHOCO_2^-][HSO_3^-]) = 5.27 \times 10^6$ M^{-1} at 25° C and $\mu = 0.2$ M. Correlations of these and other α–hydroxyalkylsulfonate stability constants with the Taft σ^* parameter and with carbonyl hydration constants are presented. The acid dissociation constant for the HSEA carboxyl group was estimated by potentiometric titration to be $pK_{a5} = 2.99$. The importance of glyoxylic acid as a reservoir for S(IV) in atmospheric water droplets was evaluated based on these thermodynamic constants.

Introduction

The reaction of aldehydes, especially formaldehyde, with S(IV) to form hydroxyalkylsulfonate salts has recently gained recognition as a pathway for stabilizing sulfur dioxide in fog and rainwater (1a–c). Previously we have studied the formation kinetics and stability of several aldehyde–bisulfite adducts, including those derived from formaldehyde (2), benzaldehyde (3), methylglyoxal (CH_3COCHO) (4), glyoxal (CHOCHO) (5), acetaldehyde (6), and hydroxy–acetaldehyde (6). Since the primary pool of carbonyl compounds in polluted environments is the gas phase (1a,7), aldehydes with large effective Henry's law constants ($H^* = (\{RCHO\}+\{RCH(OH)_2\})/ P_{RCHO}$) are the most abundant in the droplet phase. Aldehyde substrates that meet this criterion and that also form highly stable aldehyde–bisulfite adducts represent potentially important S(IV) reservoirs. Based on these criteria, formaldehyde–, glyoxal–, and methylglyoxal–bisulfite adducts have been found to be important species in clouds and fogs. The contribution of hydroxyacetaldehyde–bisulfite adduct formation is expected to be smaller but perhaps not negligible. Benzaldehyde and acetaldehyde, however, do not satisfy either constraint and hence do not significantly affect the distribution of S(IV).

The presence of α–keto acids such as glyoxylic ($CHOCO_2H$) and pyruvic acid (CH_3COCO_2H) in fog and cloudwater has recently been hypothesized since significant concentrations of oxalate $(COO^-)_2$ have been measured (8) and since these acids have been observed as oxidation products of aromatic hydrocarbons in aqueous solution (9). In addition, at least one set of fog and rain samples was reported to contain glyoxylic and pyruvic acid in the range of $4 - 40\ \mu M$ (10).

Alternately, if the primary source of α–keto acids in droplets is from the gas

phase, glyoxylic acid and glyoxylate are predominantly hydrated (see Table 1) and are therefore expected to have large effective Henry's law constants. The apparent solubility of an α–keto acid such as glyoxylic acid will also be pH–dependent at pH $\geq$ pK_a of the *gem*–diol form ($CH(OH)_2CO_2H$). Published values of this acid dissociation constant (see Table 1) range from $10^{-2.98}$ to $10^{-3.46}$ M at 25° C.

Very little is known about the stability, formation kinetics or acid/base characteristics of glyoxylic acid – bisulfite, $HO_2CCH(OH)SO_3^-$ (2–hydroxy–2–sulfo–ethanoic acid, which will hereafter be referred to as HSEA), although this keto acid has been used in a patented process to remove SO_2 from flue gases (11). Glyoxylic acid's expected solubility and affinity to bind SO_2, imply that it is a potentially important S(IV) reservoir, and with this motivation we undertook a kinetic and thermodynamic study of the reaction. Ultimately, our objective was to use these data to predict its importance under atmospheric conditions.

The approach employed was to study the association and dissociation kinetics as well as to determine directly the stability and acid dissociation constants of the adduct. Although these efforts lead to a redundant set of constants, i.e., equilibrium, forward and reverse rate constants, this duplication was believed to be necessary in view of the difficulty in measuring formation constants of highly stable adducts. The formation kinetic studies were conducted at pH $\leq$ 3, a pH range, which overlaps with the acidic pH range frequently observed in fogs, clouds and haze aerosols.

Experimental Procedures

Materials. All solutions were prepared from A.R. grade reagents and deoxygenated, high purity water (18 MΩ·cm), which was de–ionized with a Millipore MilliRO–4 MilliQ system. Oxygen was purged either by degassing under

vacuum or by bubbling with high purity N_2 gas. Stock solutions of glyoxylic acid were prepared from a 50% aqueous solution (Aldrich) and stored under an N_2 atmosphere, protected from light. Stock S(IV) solutions were prepared fresh before use from disodium sulfite (Baker) under an N_2 atmosphere. An ionic strength of 0.2 M was maintained in all experiments by adding appropriate electrolyte (NaCl, Baker). Studies of the forward reaction rates were buffered in the pH range of 1.6 – 3 with sufficient NaOH (Baker) and 0.1 M concentrations of $Cl_2CHCOOH$ (MCB) or $ClCH_2COOH$ (Kodak). Hydrochloric acid (Baker) was used to acidify solutions below pH 1.6. Dissociation kinetic experiments were buffered above pH 4.0 with mixtures of glacial acetic acid (Mallinckrodt)/NaOH, $NaCH_3COO$ (Baker)/HCl or KH_2PO_4 (Baker)/NaOH; below pH 4, only HCl was added. All buffer and electrolyte solutions were filtered before use through a 0.2 μm Millipore filter.

The disodium salt of the glyoxylate–bisulfite addition compound was synthesized by mixing 0.16 mole $NaHSO_3$ from a 25% w/w filtered solution with a slight excess of glyoxylic acid. Approximately 0.15 mole NaOH (from a concentrated solution) was then slowly added while the mixture was stirred. Sufficient ethanol was added to obtain a 40% EtOH solution, which was then stirred for three hours in a glovebox. The precipitate was filtered and washed with two 30 ml volumes of anhydrous ethanol and 30 ml of anhydrous ether. The solid was dried for three days in a vacuum desiccator containing P_2O_5. Results of the elemental analyses (Galbraith Laboratories), C: 11.88%, H: 1.24%, S: 16.34%, Na: 22.82%, indicated that the stoichiometry of the salt was $NaO_2CCH(OH)SO_3Na$, where oxygen was assumed to make up the balance (47.72%). This stoichiometry corresponds to a theoretical composition of C: 12.00%, H: 1.08%, S: 16.01%, Na: 22.96%, O: 47.95%, and agrees well with the experimental results.

Methods. The forward reaction kinetics was studied by spectrophotometrically monitoring the disappearance of unbound S(IV) at 280 nm (λ_{max} for $H_2O \cdot SO_2$). Reactions were conducted in a 10 cm quartz, water–jacketed cell, and a Haake water recirculation bath was used to maintain a constant temperature. A conventional Hewlett–Packard Model 8450A UV/Vis spectrophotometer was used throughout the entire pH range. Above pH 2.6, however, the rates were quite fast and hence it was not possible to observe a substantial initial portion of the reaction by conventional spectrophotometry. Two stopped–flow experiments at pH 2.68 and 2.79 were therefore conducted in order to monitor the entire reaction. The optical path length of the stopped–flow spectrophotometer (Dionex) was 2 cm., and reactant concentrations were increased because of the shorter cell dimensions. These reactions could also be monitored under anoxic conditions since the stopped–flow apparatus was housed in an N_2–atmosphere glovebox. Usually four replications were performed at each pH and a minimum of 200 absorbance measurements were collected in each data set. The raw data were transferred directly from the spectrophotometer to a computer.

Above pH 2, adduct dissociation was monitored by scavenging techniques. Acidified solutions containing HSEA were mixed with pH–buffered iodine solutions (containing excess KI) in a 1 cm mixing cell, and the disappearance of triiodide at 351 nm (λ_{max} for I_3^-, $\epsilon = 2.5 \times 10^4$ M^{-1} cm^{-1}) was recorded. The rate of disappearance of I_3^- was assumed equal to the rate of liberation of free S(IV) since the oxidation of S(IV) to S(VI) by I_2 and I_3^- is extremely rapid (12). Below pH 2, the rate of oxidation of I^- to I_2 was no longer negligible compared to the slow rate of adduct dissociation. Experiments in this pH range were conducted in the absence of KI to eliminate this interference, and the disappearance of I_2 was followed at 460 nm ($\epsilon = 7 \times 10^2$ M^{-1} cm^{-1}). Absorbance measurements of aliquots

were recorded manually in a 10–cm cell over the course of several days.

Apparent stability constants of HSEA were calculated as a function of pH by measuring the concentration of unbound S(IV) at equilibrium. The addition compound was dissolved in deoxygenated water in which the pH was adjusted with appropriate amounts of HCl and equilibrated in an N_2–atmosphere glovebox. Free S(IV) concentrations were determined by mixing the equilibrated mixture with an acidified I_2/KI solution, and by spectrophotometrically measuring the residual I_3^- concentration. Beer's Law calibration curves were used to relate light absorption at 351 nm to I_3^- concentrations. Stock I_2 solutions were protected from light and analyzed with a primary standard As_2O_3 solution after each experiment.

The acid dissociation constants, K_{a5} and K_{a6} of Eqs. 11–12, were determined by potentiometric titration of a 0.01 M $NaO_2CCH(OH)SO_3Na$, 0.2 M NaCl solution with 0.2 M NaOH (CO_2–free) and HCl standards. The titration vessel was water–jacketed for temperature control and a stream of N_2, pretreated to remove residual oxygen and CO_2, was continually blown through the head space. pH measurements were obtained with a Radiometer PHM 80 portable pH meter.

Results

Formation Kinetics. Since adduct formation was monitored with an imposed large excess of glyoxylic acid, a first–order dependence in free S(IV) was tested by plotting ln $[(A-A_\infty)/(A_o-A_\infty)]$ vs time. These plots were linear ($r^2 \geq 0.999$) for reaction extents up to 90%, and the pseudo–first–order rate constants, k_{obsd}, are tabulated in Table 2. Above pH 2.9, the reaction became too fast to study by conventional spectrophotometry, and the absorbance signal was too weak to monitor in the shorter (2 cm) stopped–flow cell. The reaction order with respect to glyoxylic acid was determined by varying the total aldehyde concentration at

constant pH. Values of k_{obsd} varied linearly with the concentration of glyoxylic acid, as shown in Figure 1, thus demonstrating a first–order reaction dependence with respect to glyoxylic acid.

In our previous studies with formaldehyde and glyoxal, the pH dependence of adduct formation at pH $\leq$ 3 was governed by two rate–determining steps: the addition of HSO_3^- and SO_3^{2-} at the carbonyl carbon atom (2,5). The formation kinetics of benzaldehyde– and methylglyoxal–bisulfite addition compounds were also governed by these two addition steps, but some specific acid catalysis was observed below pH 1 (3,4). For glyoxylic acid, we initially proposed the following mechanism:

$$H_2O \cdot SO_2 \overset{K_{a1}}{\rightleftharpoons} H^+ + HSO_3^- \quad \text{(fast)} \quad (1)$$

$$HSO_3^- \overset{K_{a2}}{\rightleftharpoons} H^+ + SO_3^{2-} \quad \text{(fast)} \quad (2)$$

$$CH(OH)_2CO_2H \overset{K_{d1}}{\rightleftharpoons} CHOCO_2H + H_2O \quad \text{(fast)} \quad (3)$$

$$CH(OH)_2CO_2^- \overset{K_{d2}}{\rightleftharpoons} CHOCO_2^- + H_2O \quad \text{(fast)} \quad (4)$$

$$CHOCO_2H \overset{K_{a3}}{\rightleftharpoons} H^+ + CHOCO_2^- \quad \text{(fast)} \quad (5)$$

$$CH(OH)_2CO_2H \overset{K_{a4}}{\rightleftharpoons} H^+ + CH(OH)_2CO_2^- \quad \text{(fast)} \quad (6)$$

$$CHOCO_2H + HSO_3^- \underset{k_{-1}}{\overset{k_1}{\rightleftharpoons}} HO_2CCH(OH)SO_3^- \quad \text{(slow)} \quad (7)$$

$$CHOCO_2^- + HSO_3^- \underset{k_{-2}}{\overset{k_2}{\rightleftharpoons}} {}^-O_2CCH(OH)SO_3^- \quad \text{(slow)} \quad (8)$$

$$CHOCO_2H + SO_3^{2-} \underset{k_{-3}}{\overset{k_3}{\rightleftharpoons}} HO_2CCH(O^-)SO_3^- \quad \text{(slow)} \quad (9)$$

$$CHOCO_2^- + SO_3^{2-} \underset{k_{-4}}{\overset{k_4}{\rightleftharpoons}} {}^-O_2CCH(O^-)SO_3^- \quad \text{(slow)} \quad (10)$$

$$HO_2CCH(OH)SO_3^- \overset{K_{a5}}{\rightleftharpoons} H^+ + {}^-O_2CCH(OH)SO_3^- \quad \text{(fast)} \quad (11)$$

$${}^-O_2CCH(OH)SO_3^- \overset{K_{a6}}{\rightleftharpoons} H^+ + {}^-O_2CCH(O^-)SO_3^- . \quad \text{(fast)} \quad (12)$$

When Eqs. 7–10 are displaced far to the left of equilibrium, the corresponding rate expression for HSEA formation is

$$\nu = \frac{d[HSEA]_t}{dt} = (k_1[CHOCO_2H] + k_2[CHOCO_2^-])[HSO_3^-] + (k_3[CHOCO_2H] + k_4[CHOCO_2^-])[SO_3^{2-}], \quad (13)$$

where

$$[HSEA]_t = [HO_2CCH(OH)SO_3^-] + [{}^-O_2CCH(OH)SO_3^-] + [{}^-O_2CCH(O^-)SO_3^-] + [HO_2CCH(O^-)SO_3^-] . \quad (14)$$

Equation 13 may be rewritten as

$$\nu = (k_1\alpha_1\beta_1 + k_2\alpha_1\beta_2 + k_3\alpha_2\beta_1 + k_4\alpha_2\beta_2)\,[C_2H_2O_3]\,[S(IV)], \quad (15)$$

where

$$[S(IV)] = [H_2O \cdot SO_2] + [HSO_3^-] + [SO_3^{2-}] \quad (16)$$

$$[C_2H_2O_3] = [CHOCO_2H] + [CHOCO_2^-] + [CH(OH)_2CO_2H] + [CH(OH)_2CO_2^-] \quad (17)$$

$$\alpha_1 = \frac{[HSO_3^-]}{[S(IV)]} = \frac{{}^cK_{a1}\{H^+\}}{\{H^+\}^2 + {}^cK_{a1}\{H^+\} + {}^cK_{a1}{}^cK_{a2}} \tag{18}$$

$$\alpha_2 = \frac{[SO_3^{2-}]}{[S(IV)]} = \frac{{}^cK_{a1}\,{}^cK_{a2}}{\{H^+\}^2 + {}^cK_{a1}\{H^+\} + {}^cK_{a1}{}^cK_{a2}} \tag{19}$$

$$\beta_1 = \frac{[CHOCO_2H]}{[C_2H_2O_3]} = \frac{{}^cK_{d1}{}^cK_{d2}\{H^+\}}{{}^cK_{d2}(1+{}^cK_{d1})\{H^+\} + {}^cK_{a3}{}^cK_{d1}(1+{}^cK_{d2})} \tag{20}$$

$$\beta_2 = \frac{[CHOCO_2^-]}{[C_2H_2O_3]} = \frac{{}^cK_{d1}{}^cK_{d2}{}^cK_{a3}}{{}^cK_{d2}(1+{}^cK_{d1})\{H^+\} + {}^cK_{a3}{}^cK_{d1}(1+{}^cK_{d2})}. \tag{21}$$

The notation "^cK" in the above expressions denotes thermodynamic constants that have been corrected for ionic strength effects. Since a large excess of glyoxylic acid was present, $[C_2H_2O_3] \approx [C_2H_2O_3]_t$, where $[C_2H_2O_3]_t$ is the total concentration of bound and unbound glyoxylic acid and glyoxylate. The observed rate constant is therefore

$$k_{obsd} = (k_1\alpha_1\beta_1 + k_2\alpha_1\beta_2 + k_3\alpha_2\beta_1 + k_4\alpha_2\beta_2)[C_2H_2O_3]_t\,. \tag{22}$$

Dividing Eq. 22 by $\alpha_1\beta_1[C_2H_2O_3]_t$ gives

$$\frac{k_{obsd}}{\alpha_1\beta_1[C_2H_2O_3]_t} = k_1 + \frac{k_2K_{a3} + k_3K_{a2}}{\{H^+\}} + \frac{k_4K_{a3}K_{a2}}{\{H^+\}^2}. \tag{23}$$

At sufficiently low pH, therefore, $k_{obsd}/(\alpha_1\beta_1[C_2H_2O_3]_t)$ should be inversely proportional to $\{H^+\}$. The corresponding plot of data from Table 2 (see Figure 2) yielded a straight line for the entire pH range studied. Our kinetic data are therefore consistent with the mechanism of Eqs. 1–12, although Eq. 10 does not contribute at pH $\leq$ 2.9. Estimates of the intrinsic constant, k_1, and the apparent constant, $k_2K_{a3} + k_3K_{a2}$, were obtained from the intercept and slope of this line,

respectively. From a linear least–squares regression fit of the data, $k_1 = 443$ (± 21.2) $s^{-1}\ M^{-1}$ and $k_2K_{a3} + k_3K_{a2} = 3.22$ (± 0.06) s^{-1} at 25° C with $\mu = 0.2$ M. The thermodynamic constants, $K_{a1} = 1.45 \times 10^{-2}$ M (22), $K_{a2} = 6.31 \times 10^{-8}$ M (23), $K_{a3} = 1 \times 10^{-2}$ M (19), $K_{d1} = 3.33 \times 10^{-3}$ (19), and $K_{d2} = 6.61 \times 10^{-2}$ (19) were corrected to an ionic strength of 0.2 M such that ${}^cK_{a1} = K_{a1}\gamma_{H_2O\cdot SO_2}/\gamma_{HSO_3^-} = 1.99 \times 10^{-2}$ M, ${}^cK_{a2}\gamma_{HSO_3^-}/\gamma_{SO_3^{2-}} = 1.63 \times 10^{-7}$ M, ${}^cK_{a3} = K_{a3}\gamma_{CHOCO_2H}/\gamma_{CHOCO_2^-} = 1.4 \times 10^{-2}$, ${}^cK_{d1} = K_{d1}\gamma_{CH(OH)_2CO_2H}/\gamma_{CHOCO_2H} = 3.3 \times 10^{-3}$, and ${}^cK_{d2} = K_{d2}\gamma_{CH(OH)_2CO_2^-}/\gamma_{CHOCO_2^-} = 6.6 \times 10^{-2}$. A mixed concentration/activity scale was chosen since hydrogen ion activities were measured in the experiments. Activity coefficients were calculated with the Davies equation (24).

In order to estimate activation energy parameters, the temperature dependence of k_1 was studied between 15 and 35° C at pH 0.7, since $k_1 \approx k_{obsd}/\alpha_1\beta_1[C_2H_2O_3]_t$ under these conditions. The ionization fraction, α_1, was computed with temperature–corrected values of ${}^cK_{a1}$ and ${}^cK_{a2}$; standard state enthalpies from the literature are $\Delta H^\circ_{a1} = -16.2$ kJ/mol (22) and $\Delta H^\circ_{a2} = -11.7$ kJ/mol (23). To calculate β_1, Eq. 20 was first rewritten as

$$\beta_1 = \frac{{}^cK_{d1}\{H^+\}}{(1+{}^cK_{d1})\{H^+\} + {}^cK_{a4}(1+{}^cK_{d2})}, \tag{24}$$

with the substitution, ${}^cK_{a3} = {}^cK_{a4}{}^cK_{d2}/{}^cK_{d1}$. Furthermore, since ${}^cK_{d2} \ll 1$, β_1 is approximately

$$\beta_1 = \frac{{}^cK_{d1}\{H^+\}}{(1+{}^cK_{d1})\{H^+\} + {}^cK_{a4}}. \tag{25}$$

${}^cK_{a4}$ can be corrected for temperature since ΔH°_{a4} is known (2.22 kJ/mol (14)); however, the temperature dependence of K_{d1} has not been studied. It was assumed that $\Delta H^\circ_{d1} \approx 30$ kJ/mol, since standard dehydration enthalpies for formaldehyde

and pyruvic acid (CH_3COCO_2H) are 33.5 (25) and 32.6 (26) kJ/mol, respectively. The measured values of k_1 as a function of temperature are given in Table 3. Activation energy parameters for this reaction step were obtained by plotting ln (k_1/T) vs 1/T. This plot was linear ($r^2 = 0.9955$), with $\Delta H_1^{\ddagger} = (-\text{slope} \cdot R) = 21.4$ kJ/mol and $\Delta S_1^{\ddagger} = (\text{intercept} - \ln k_B/\hbar)R = -141$ J mol^{-1} deg^{-1}, where k_B is Boltzmann's constant, $\hbar$ is Planck's constant and R is the gas constant.

HSEA Acid Dissociation Constants. The acid dissociation constants, K_{a5} and K_{a6}, were calculated from titration data by methods adapted from Albert and Serjeant (13). Mass and charge balance relationships governing the titration of HSEA by HCl yield the following equation for ${}^cK_{a5}$ ($\mu = 0.2$ M):

$$\text{Log } {}^cK_{a5} = \text{Log } \theta_1 - \text{pH} , \tag{26}$$

where

$$\theta_1 = \left\{ \frac{[H^+] + [Na^+] - C_1 - [Cl^-]}{2C_1 - [H^+] - [Na^+] - [Cl^-]} \right\} \tag{27}$$

$$C_1 = [HO_2CCH(OH)SO_3^-] + [^-O_2CC(OH)SO_3^-]. \tag{28}$$

Based on Eq. 26, a plot of pH vs Log θ_1 should be linear with unit slope and y–intercept = p^cK_{a5}. The resulting plots of duplicate titration data sets were linear ($r^2 > 0.99$), with average slopes of 1.001 (± 0.006) and y–intercepts equal to 2.988 (± 0.004). The quotient, θ_1, was calculated using H^+ concentrations estimated with the Davies approximation. At an ionic strength of 0.2 M, our estimate of ${}^cK_{a5}$, defined as

$${}^cK_{a5} = \frac{\{H^+\}\ [^-O_2CCH(OH)SO_3^-]}{[HO_2CCH(OH)SO_3^-]} , \tag{29}$$

is therefore 1.03×10^{-3} M (25° C). Correction to infinite dilution gives $K_{a5} = 3.98 \times 10^{-4}$ M.

Similar analysis of the HSEA titration by NaOH leads to the following equation for ${}^{c}K_{a6}$:

$$\text{Log } {}^{c}K_{a6} = \text{Log } \theta_2 - \text{pH} , \tag{30}$$

where

$$\theta_2 = \frac{[Na^+] - 2C_2 - [Cl^-] - [OH^-]}{[Cl^-] + [OH^-] + 3C_2 - [Na^+]} \tag{31}$$

$$C_2 = [{}^-O_2CCH(OH)SO_3^-] + [{}^-O_2CCH(O^-)SO_3^-] . \tag{32}$$

A plot of pH vs Log θ_2 was linear between pH 7.7 and 10.0 with y–intercept = 10.05 (± 0.01); however, the average slope was 1.83 (± 0.01). The deviation of the slope from the expected value of one is probably due to some dissociation of HSEA; the conjugate base, ${}^-O_2CCH(O^-)SO_3^-$, is expected to be much less stable than ${}^-O_2CCH(OH)SO_3^-$. Because of these complications, the true error in our estimate of $p{}^{c}K_{a6} \approx 10.05$ is probably greater than the standard error cited above.

HSEA Dissociation Kinetics. In the presence of iodine, the dissociation of HSEA proceeds irreversibly as follows:

$$HO_2CCH(OH)SO_3^- \xrightarrow{k_{-1}} CHOCO_2H + HSO_3^- \quad \text{(slow)} \tag{33}$$

$${}^-O_2CCH(OH)SO_3^- \xrightarrow{k_{-2}} CHOCO_2^- + HSO_3^- \quad \text{(slow)} \tag{34}$$

$$HO_2CCH(O^-)SO_3^- \xrightarrow{k_{-3}} CHOCO_2H + SO_3^{2-} \quad \text{(slow)} \tag{35}$$

$${}^-O_2CCH(O^-)SO_3^- \xrightarrow{k_{-4}} CHOCO_2^- + SO_3^{2-} \quad \text{(slow)} \tag{36}$$

$$I_2 + S(IV) \longrightarrow 2I^- + S(VI)\,, \qquad \text{(fast)} \quad (37)$$

where the rate of disappearance of I_2 (or I_3^-) is equal to the dissociation rate of HSEA

$$\begin{aligned} \nu &= \frac{-d[I_3^-]}{dt} = \frac{-d[HSEA]_t}{dt} \\ &= k_{-1}[HO_2CCH(OH)SO_3^-] + k_{-2}[^-O_2CCH(OH)SO_3^-] + \\ &\quad k_{-3}[HO_2CC(O^-)SO_3^-] + k_{-4}[^-O_2CCH(O^-)SO_3^-]\,. \end{aligned} \qquad (38)$$

Equation 38 may be rewritten as

$$\nu = (k_{-1}\phi_1 + k_{-2}\phi_2 + k_{-3}\phi_3 + k_{-4}\phi_4)[HSEA]_t\,, \qquad (39)$$

where

$$\begin{aligned} [HSEA]_t = {} & [HO_2CC(OH)SO_3^-] + [^-O_2CCH(OH)SO_3^-] + \\ & [HO_2CCH(O^-)SO_3^-] + [^-O_2CCH(O^-)SO_3^-] \end{aligned} \qquad (40)$$

$$\begin{aligned} \phi_1 &= [HO_2CCH(OH)SO_3^-]/[HSEA]_t = \\ &= \frac{\{H^+\}^2}{\{H^+\}^2 + (K_{a5}+K_{a7})\{H^+\} + K_{a5}K_{a6}} \end{aligned} \qquad (41)$$

$$\begin{aligned} \phi_2 &= [^-O_2CCH(OH)SO_3^-]/[HSEA]_t \\ &= \frac{K_{a5}\{H^+\}}{\{H^+\}^2 + (K_{a5}+K_{a7})\{H^+\} + K_{a5}K_{a6}} \end{aligned} \qquad (42)$$

$$\begin{aligned} \phi_3 &= [HO_2CCH(O^-)SO_3^-]/[HSEA]_t \\ &= \frac{K_{a7}\{H^+\}}{\{H^+\}^2 + (K_{a5}+K_{a7})\{H^+\} + K_{a5}K_{a6}} \end{aligned} \qquad (43)$$

$$\phi_4 = [^-O_2CCH(O^-)SO_3^-]/[HSEA]_t$$

$$= \frac{K_{a5}K_{a6}}{\{H^+\}^2 + (K_{a5}+K_{a7})\{H^+\} + K_{a5}K_{a6}} \quad (44)$$

$$^cK_{a7} = \frac{\{H^+\}\,[HO_2CCH(O^-)SO_3^-]}{[HO_2CCH(OH)SO_3^-]} . \quad (45)$$

At constant pH, pseudo–first–order conditions are established such that

$$k'_{obsd} = (k_{-1}\phi_1 + k_{-2}\phi_2 + k_{-3}\phi_3 + k_{-4}\phi_4) . \quad (46)$$

Least–squares regression plots of ln $(A-A_\infty)/(A_o-A_\infty)$ vs time were linear over the pH range 0.7 – 7.0, confirming a pseudo–first–order reaction. The observed rate constants are tabulated in Table 4. Since Eq. 46 can be rewritten as

$$\frac{k'_{obsd}}{\phi_2} = \frac{k_{-1}\{H^+\}}{K_{a5}} + k_{-2} + k_{-3}K_{a7}/K_{a5} + \frac{k_{-4}K_{a6}}{\{H^+\}} , \quad (47)$$

k'_{obsd}/ϕ_2 must be directly and inversely proportional to $\{H^+\}$ at low pH and high pH, respectively. Figures 3 and 4 demonstrate that the data are consistent with both of these predicted pH trends. Estimates of the intrinsic constants, k_{-1} and k_{-4}, were obtained from the slopes of linear least–squares fits to the data in Figures 3 and 4, respectively. An estimate of the lumped constant, $k_{-2} + k_{-3}K_{a7}/K_{a5}$, was obtained by averaging the intercepts of the two fitted lines. A Taylor's method (27), nonlinear least–squares regression routine was used to fit the entire set of data to Eq. 46 and the above preliminary estimates of the rate constants were supplied as initial guesses in the program. The thermodynamic constants, K_{a5} and K_{a6}, were held fixed in this analysis to the values we experimentally determined (*vide infra*). Although the magnitude of K_{a7} is not known, we assumed that $K_{a7} \ll K_{a5}$, and hence $\phi_2 \approx K_{a5}\{H^+\}/(\{H^+\}^2+K_{a5}\{H^+\}+K_{a5}K_{a6})$. Refined estimates were

obtained as $k_{-1} = 6.32\ (\pm\ 0.32) \times 10^{-6}\ s^{-1}$, $k_{-2} + k_{-3}K_{a7}/K_{a5} = 5.68\ (\pm\ 0.30) \times 10^{-5}\ s^{-1}$, and $k_{-4} = 63.0\ (\pm\ 1.8)\ s^{-1}$. Pseudo–first–order rate constants, which were calculated using the results of the regression analysis, are compared to the experimentally measured values of k'_{obsd} in Figure 5.

HSEA Stability Constants. Apparent stability constants for simple hydroxy–alkylsulfonates, such as hydroxymethanesulfonate, are pH–independent over the pH range of 3 to 5 since the predominant adduct, aldehyde, and S(IV) species do not change under these conditions. The speciation of keto acids and their bisulfite adducts, such as HSEA, however, changes over this pH range, and hence it cannot be assumed that the apparent stability constant of HSEA,

$$K_{app} = \frac{[HSEA]_t}{[C_2H_2O_3]\ [S(IV)]}, \tag{48}$$

is pH–independent. Direct determinations of K_{app} were obtained as a function of pH by measuring the concentration of unbound S(IV) at equilibrium. Dissolution of the disodium HSEA salt leads to the constraint, $[S(IV)]_{unbound,eq} = [C_2H_2O_3]_{unbound,eq}$, so that K_{app} can be calculated as

$$K_{app} = \frac{[NaO_2CCH(OH)SO_3Na]_o - [S(IV)]_{unbound,eq}}{([S(IV)]_{unbound,eq})^2}, \tag{49}$$

where $[NaO_2CCH(OH)SO_3Na]_o$ is the initial concentration of the salt. Measured values of K_{app} are given in Table 5 and plotted in Figure 6.

The apparent formation constant can be re–expressed in terms of a pH–independent equilibrium constant, ${}^cK_1$, as

$$K_{app} = \frac{[HO_2CCH(OH)SO_3^-]/\phi_1}{([CHOCO_2H]/\beta_1)\ ([HSO_3^-]/\alpha_1)} \tag{50}$$

$$= {}^{c}K_1 \left[\frac{\alpha_1 \beta_1}{\phi_1}\right], \tag{51}$$

where

$${}^{c}K_1 = \frac{[HO_2CCH(OH)SO_3^-]}{[CHOCO_2H]\ [HSO_3^-]}. \tag{52}$$

The magnitude of ${}^{c}K_1$ was estimated as 7.09 (± 0.17) × 10^7 M^{-1} by fitting the data in Table 5 to Eq. 51 with a nonlinear least–squares regression routine. A second estimate of ${}^{c}K_1$ was calculated from the previously determined forward and reverse rate constants, k_1 and k_{-1}. By this method, ${}^{c}K_1 = 7.01 \times 10^7$ M^{-1} ($\mu = 0.2$ M) and is within the standard error of the first estimate.

Discussion

Although the pH dependence of HSEA formation at pH ≤ 2.9 appears to yield only the intrinsic constant k_1 and the apparent constant, $k_2K_{a3} + k_3K_{a2}$, it is possible to show that the k_2 term can be dropped. Based on our estimated value of the sum, $k_2K_{a3} + k_3K_{a2}$, and published values of K_{a2} and K_{a3}, upper limits can be calculated as $k_2 \leq 2 \times 10^2$ and $k_3 \leq 2 \times 10^7$ M^{-1} s^{-1}. Rate constants for the proton transfer

$$CHOCO_2^- + HSO_3^- \rightleftharpoons CHOCO_2H + SO_3^{2-}, \tag{53}$$

however, would be much larger than $k_{2,max}$, and thus Eq. 8 is not a competitive pathway. By setting $k_3{}^{c}K_{a2}$ equal to our estimate of the apparent constant, a value of $k_3 = 1.98 \times 10^7$ M^{-1} s^{-1} is obtained. Since neither the k_2 or k_4 steps of our originally proposed mechanism are important below 2.9, the rate expression of Eq. 15 may be simplified as

$$\nu = (k_1\alpha_1\beta_1 + k_3\alpha_2\beta_1)\,[C_2H_2O_3]\,[S(IV)]. \tag{54}$$

The magnitudes of k_1 and k_3 are comparable to the rate constants given in Table 6 for methylglyoxal and formaldehyde. With all other previous aldehyde substrates, SO_3^{2-} was observed to react much more rapidly than HSO_3^-. Where rate constants for both addition steps are available, the data in Table 6 indicate that the ratio, k_{II}/k_I (defined in Table 6), ranges between 3×10^4 to 1×10^5. These large ratios are consistent with the known greater nucleophilicity of SO_3^{2-} relative to HSO_3^-.

A comparison of the activation energy parameters, $\Delta H_I^{\ddagger}$ and $\Delta S_I^{\ddagger}$, for glyoxylic acid with those of other aldehyde substrates (see Table 7) suggests that there may be some difference in the HSEA transition state structure. The $\Delta S_I^{\ddagger}$ value for HSEA formation is significantly more negative than the $\Delta S_I^{\ddagger}$ for methylglyoxal and formaldehyde and is comparable to the $\Delta S_I^{\ddagger}$ for aldehydes with bulky α–substituents such as benzaldehyde. In previous studies we have demonstrated that the activation entropy of HSO_3^- addition is typically more negative than the $\Delta S^{\ddagger}$ of SO_3^{2-} addition for the aldehydes listed in Table 7. To explain this difference, we postulated that bisulfite addition requires a cyclic activated complex, whereas sulfite addition does not. The large $\Delta S_I^{\ddagger}$ for HSEA suggests that its transition state may be further constrained. Additional steric restrictions perhaps arise as a result of intramolecular hydrogen bonding with the carboxylic acid group, as shown here.

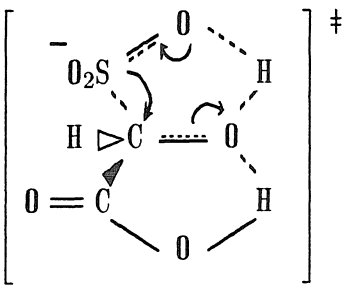

The possibility of general acid catalysis by the buffers used in this study was not tested; however, addition reactions involving a strong nucleophile, such as SO_3^{2-}, at a carbonyl center are not generally subject to this type of catalysis (28). In the case of benzaldehyde and formaldehyde, for example, adduct formation rates were independent of the buffer concentration (2,3).

Another mechanism giving an equivalent rate law for adduct formation can be hypothesized. For example, it is impossible to distinguish kinetically between our proposed mechanism and one in which the following catalyzed dehydration steps are rate–determining:

$$CH(OH)_2CO_2H \overset{HSO_3^-,SO_3^{2-}}{\rightleftharpoons} CHOCO_2H + H_2O \qquad (55)$$

$$CH(OH)_2CO_2^- \overset{HSO_3^-,SO_3^{2-}}{\rightleftharpoons} CHOCO_2^- + H_2O\,. \qquad (56)$$

Sørensen *et al.* (19) have reported that the dehydration of $CH(OH)_2CO_2^-$ is catalyzed by SO_3^{2-} but not by HSO_3^-. Spontaneous dehydration or catalysis by H^+ or OH^- was found to be faster. Using their rate constants, the rate of dehydration at pH $<$ 3 is much faster than the adduct formation rates we observed. Reactions 55 and 56 can be ruled out on this basis. At pH $\gg$ 3, however, we expect that the dehydration of $CH(OH)_2CO_2^-$ will become rate–determining. Similar changes in the mechanism have been predicted for hydroxymethanesulfonate (28) and demonstrated for methylglyoxal–S(IV) adduct formation (4).

The rapid dissociation of HSEA in slightly acidic or neutral pH solution is due to the large difference in rate constants for the release of SO_3^{2-} over HSO_3^-. Although k_{-2} and k_{-3} were not calculable, it is expected that k_{-2} is greater than k_{-1} (6.32×10^{-2} s^{-1}) and that k_{-3} is less than k_{-4} (63 s^{-1}), since electronic effects would

favor dissociation when the carboxyl group is deprotonated. Our estimate of $k_{-2} + k_{-3}K_{a7}/K_{a5}$ also provides an upper limit for k_{-2}, so that $6.32 \times 10^{-6} \leq k_{-2} \leq 5.68 \times 10^{-5}$ s^{-1}. The ratio, k_{-4}/k_{-2} is therefore greater than or equal to 10^6 and the dissociation rate of $^-O_2CCH(OH)SO_3^-$ is at least six orders of magnitude slower than the dissociation of its conjugate base, $^-O_2CCH(O^-)SO_3^-$. Deprotonation of the hydroxy group increases the electron density at the tetrahedral carbon; thus, electronic effects may partially account for its facile dissociation. The large difference in rate constants may also reflect the different degrees of structural complexity between the two transition states as we proposed above.

The carboxylic acid strength of $HO_2CCH(OH)SO_3^-$ ($pK_{a5} = 3.4$, $\mu = 0$) was found here to be similar to that of $HO_2CCH(OH)_2$ ($pK_{a4} \approx 3.3$). Formation of the bisulfite addition compound, therefore, should not significantly change the pH, even in unbuffered solutions.

Contrary to our expectations, the apparent stability of HSEA increased slightly (see Figure 6) at pH greater than pK_{a5}, and attained a maximum between pH 4 – 5. Based on the greater positive inductive effect of the $-CO_2H$ substituent compared to $-CO_2^-$, we expected the carboxylic acid form of the adduct to be more stable. There is some scatter to the data in Figure 6, particularly at higher pH. We believe it is due to the difficulty of measuring low concentrations of free S(IV) at pH conditions where the adduct dissociates rapidly. Despite the scatter, the fitted formation constant, K_1, was in close agreement with the independent calculation of K_1 derived from the forward and reverse rate constants.

Linear–free–energy correlations relating carbonyl hydration constants with the Taft polar substituent parameter, σ^*, have been developed, wherein carbonyl compounds with the same number of α–hydrogen atoms were found to correlate with σ^* (30–32). Although these correlations do not contain hydration data for

any α–keto acids, constants for at least seven, including glyoxylic (19), pyruvic (26), oxo–malonic (20), α–keto glutaric (33), phenylpyruvic (33), 2–oxo–butanoic (34), and 3–methyl–2–oxo–butanoic acid (34), are available. When these carbonyls are included in a log K_H vs $\Sigma\sigma^*$ plot, the deprotonated keto acids consistently form more stable *gem*–diols than the correlation would predict, as Figure 7a demonstrates. Therefore, factors other than the simple electronic field effects considered by this Taft plot must influence the hydration of $RCOCO_2^-$.

The stability constants of carbonyl–bisulfite addition compounds expressed as

$$K = \frac{[R_1CR_2(OH)SO_3^-]}{[R_1COR_2]\ \ [HSO_3^-]} \tag{57}$$

were also correlated with $\Sigma\sigma^*$ in our earlier studies (5,6). A pattern similar to hydration correlations was observed in that aldehydes with a single α–hydrogen atom were linear with respect to $\Sigma\sigma^*$. However, the formaldehyde–bisulfite adduct was found to be substantially more stable than predicted from the LFER.

In addition to K_1 ($HO_2CCH(OH)SO_3^-$), we can obtain an estimate for K_2 ($^-O_2CCH(OH)SO_3^-$), as follows:

$$^cK_2 = \frac{[^-O_2CCH(OH)SO_3^-]}{[^-O_2CCHO]\ \ [HSO_3^-]} = {}^cK_1\frac{^cK_{a5}}{^cK_{a3}}; \tag{58}$$

thus, $^cK_2$ is 5.27×10^6 M^{-1} at 25° C, with μ = 0.2 M. When K_1 and K_2 are included in the Taft plot of Figure 7b, they appear to deviate from the line correlating other aldehydes having a single α–hydrogen atom, in a manner resembling the hydration data in Figure 7a. The magnitude of log K_1 falls slightly below the line, while log K_2 lies well above it.

From the raw data reported by Burroughs and Sparks (34), we were also able

to calculate the stability constant for the pyruvate–bisulfite addition compound (35). Since pyruvate forms a more stable adduct than acetone (see Figure 7b), pyruvate appears to be another example of a keto acid adduct whose stability can not be solely explained in terms of inductive effects.

Glyoxylate–bisulfite and other deprotonated α–keto acid – S(IV) adducts may be stabilized by intramolecular hydrogen bonding between the hydroxy and carboxylate group as shown here.

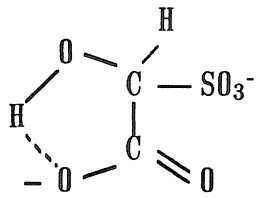

Being nearly symmetrical, this hydrogen bond should be quite strong (36), and in order to form our proposed activated complex prior to dissociation, it must be broken. Intramolecular hydrogen bonding is also possible when the carboxyl group is protonated; however, these unsymmetrical bonds would be weaker.

The similarities between Figures 7a and 7b suggest that a linear–free–energy relationship exists between hydration and bisulfite addition. A log–log plot of hydroxyalkylsulfonate stabilities vs K_h was indeed linear (see Figure 8), with a slope of 1.15 and y–intercept of 5.32. This relationship suggests that the steric, inductive, solvent bonding and hydrogen bonding characteristics of the substituent have similar effects on the degree of hydration of a carbonyl or its tendency to form stable bisulfite adducts.

Atmospheric Implications. The importance of glyoxylic acid as a reservoir for S(IV) can be assessed by estimating the maximum aqueous concentrations of HSEA that would form in an open polluted atmosphere. Typical gas–phase

concentrations of glyoxylic acid have not been established, however, so we have assumed a partial pressure of 1 ppbv in our calculations. This concentration is still an order of magnitude less than the typical partial pressure range reported for formaldehyde in photochemically polluted environments (7). Another assumption must be made regarding the value of the unknown intrinsic Henry's law constant of $CHOCO_2H$. We have assumed that its magnitude is approximately 1 M atm^{-1}, since Betterton and Hoffmann (37) have found that the intrinsic Henry's law constants for several short chain aldehydes are close to this value. A gas–phase SO_2 concentration of 20 ppbv was used, since SO_2 levels in polluted atmospheres range from 0 – 50 ppbv (1b). From mass balance and Henry's law relationships, the equilibrium concentrations of unbound S(IV), glyoxylic acid and total HSEA are

$$[S(IV)] = P_{SO_2} H_{SO_2} / \alpha_0 \tag{59}$$

$$[C_2H_2O_3] = P_{CHOCO_2H} H_{CHOCO_2H} / \beta_1 \tag{60}$$

$$[HSEA]_t = \frac{K_1 \alpha_1}{\phi_1 \alpha_0} P_{CHOCO_2H} H_{CHOCO_2H} P_{SO_2} H_{SO_2}, \tag{61}$$

where α_0 is the ionization fraction of $H_2O \cdot SO_2$, P_{CHOCO_2H}, and P_{SO_2} are the partial pressures of gas–phase species, and H_{CHOCO_2H} and H_{SO_2} are the intrinsic Henry's law constants.

Sulfur(IV) enrichment factors, defined as $([S(IV)] + [HSEA]_t)/[S(IV)]$, were tabulated for five pH conditions in Table 8. This ratio compares the total amount of sulfur dioxide incorporated into the liquid phase when both substrates are present to the amount dissolved when glyoxylic acid is absent. Our calculations indicate that HSEA formation does not lead to significant S(IV) enrichment below pH 4. At pH greater than 4, the solubility of glyoxylic acid increases, and

consequently, HSEA becomes a potential S(IV) reservoir in cloud–, fog–, or rainwater. By comparison, the S(IV) enrichment factor that is due to a 1 ppbv concentration of formaldehyde is approximately 23 and is pH–independent between pH 3 – 5.5. Glyoxylic acid is therefore at least as effective as formaldehyde in stabilizing S(IV) at pH $\geq$ 5.4 when the gas–phase aldehyde concentrations are the same.

These studies have shown that glyoxylic acid may be a significant S(IV) reservoir in weakly acidic droplets, primarily because of the unusually high stability of the *glyoxylate*–bisulfite adduct and because of the expected greater solubility of $CHOCO_2H$ at pH greater than its pK_a. Predictions of the importance of other carbonyl–bisulfite addition compounds with unknown stabilities are now possible with the linear–free–energy correlations we have developed.

Acknowledgements. We thank Eric Betterton for his helpful advice and we gratefully acknowledge the Electric Power Research Institute (RP1630–47), the Environmental Protection Agency (R811496–01–1), and the Public Health Service (ES04635–01) for their financial support.

REFERENCES

(1a) Munger, J.W.; Jacob, D.J.; Hoffmann, M.R. *J. Atmos. Chem.* **1984**, *1*, 335–350.

(1b) Munger, J.W.; Tiller, C.; Hoffmann, M.R. *Science* **1986**, *231*, 247–249.

(1c) Ang, C.C.; Lipari, F.; Swarin, S.J. *Environ. Sci. Technol.* **1987**, *21*, 102–105.

(2) Boyce, S.D.; Hoffmann, M.R. *J. Phys. Chem.* **1984**, *88*, 4740–4746.

(3) Olson, T.M.; Boyce, S.D.; Hoffmann, M.R. *J. Phys. Chem.* **1986**, *90*, 2482–2488.

(4) Betterton, E.A.; Hoffmann, M.R. *J. Phys. Chem.* **1987**, *91*, 3011–3020.

(5) Olson, T.M.; Hoffmann, M.R. *J. Phys. Chem.* **1988**, *92*, 533–540.

(6) Betterton, E.A.; Erel, Y.; Hoffmann, M.R. *Environ. Sci. Technol.* **1988**, *22*, 92–99.

(7) Grosjean, D. *Environ. Sci. Technol.* **1982**, *16*, 254–262

(8) Norton, R.B.; Roberts, J.M.; Huebert, B.J. *Geophys. Res. Letts.* **1983**, *10*, 517–520.

(9) Leitis, E. *An Investigation into the Chemistry of the U.V. Ozone Purification Process*; Annual Report to the Natl. Sci. Foundation, NTIS Doc. No. PB 296485, 1979.

(10) Steinberg, S.; Kawamura, K.; Kaplan, I.R. *Int. J. Environ. Anal. Chem.* **1985**, *19*, 251–260.

(11) Stark, W.H.; Syme, H.A.; Chu, J.C.H. *The Spring–Nobel Hoechst Process for Sulfur Dioxide Recovery from Stack Gases*; Proc. Symp. Flue Gas Desulfurization, Vol. 2, USEPA Offc. Res. Dev., [Rep] EPA–600/2–76–136b, 1976.

(12) Bunau, G.v.; Eigen, M. *Z. Phys. Chem (Frankfurt/Main)* **1962**, *32*, 25–50.

(13) Albert, A.; Serjeant, E.P. *The Determination of Ionization Constants*, 3rd ed.; Chapman and Hall: London, 1984; pp. 40–69.

(14) Öjelund, G.; Wadsö, I. *Acta Chem. Scand.* **1967**, *21*, 1408–1414.

(15) Powell, J.E.; Suzuki, Y. *Inorg. Chem.* **1964**, *3*, 690–692.

(16) Kůta, J. *Collect. Czech. Chem. Commun.* **1959**, *24*, 2532–2543.

(17) Leussing, D.L.; Hanna, E.M. *J. Amer. Chem. Soc.* **1966**, *88*, 696–699.

(18) Tur'jan, J.I.v. *Z. Phys. Chem. (Leipzig)* **1965**, *229*, 305–310.

(19) Sørensen, P.E.; Bruhn, K.; Lindeløv, F. *Acta Chem. Scand.* **1974**, *28*, 162–168.

(20) Ahrens, M.L. *Ber Bunsenges Phys. Chem.* **1968**, *72*, 691–696.

(21) Cooper, A.J.L.; Redfield, A.G. *J. Biol. Chem.* **1975**, *250*, 527–532.

(22) Deveze, D.; Rumpf, P. *C. R. Acad. Sci. Paris,* **1964**, *258*, 6135–6138.

(23) Hayon, E.; Treinin, A.; Wilf, J. *J. Amer. Chem. Soc.* **1972**, *94*, 47–57.

(24) Stumm, W.; Morgan, J.J. *Aquatic Chemistry*, 2nd ed.; Wiley–Interscience: New York, 1981; pp. 134–135.

(25) Iliceto, A. *Gazz. Chim. Ital.* **1954**, *84*, 536–552.

(26) Pocker, Y.; Meany, J.E.; Nist, B.J.; Zadorojny, C. *J. Phys. Chem.* **1969**, *73*, 2879–2882.

(27) Draper, N.R.; Smith, H. *Applied Regression Analysis*, 2nd ed.; John Wiley & Sons: New York, 1981; pp. 458–465.

(28) Jencks, W.P. *Prog. Phys. Org. Chem.* **1964**, *2*, 63–118.

(29) Olson, T.M.; Hoffmann, M.R.; *Atmos. Environ.* **1986**, *11*, 2277–2278.

(30) Bell, R.P. *Adv. Phys. Org. Chem.* **1966**, *4*, 1–29.

(31) Guthrie, J.P. *Can. J. Chem.* **1975**, *53*, 898–906.

(32) Fleury, M.B.; Letellier, S.; Dufresne, J.C.; Moiroux, J. *J. Electroanal. Chem.* **1978**, *88*, 123–135.

(33) Strehlow, V.H. *Z. Elecktrochem.* **1962**, *66*, 392–396.

(34) Burroughs, L.F.; Sparks, A.H. *J. Sci. Fd. Agric.* **1973**, *24*, 187–198.

(35) Olson, T.M.; Ph.D. Thesis, Appendix B; California Institute of Technology, 1988.

(36) Ferguson, L.N. *Organic Molecular Structure*; Willard Grant Press: Boston, 1975; pp. 28–29.

(37) Betterton, E.A.; Hoffmann, M.R.; submitted to *Environ. Sci. Technol.*

(38) Valenta, P. *Collect. Czech. Chem. Commun.* 1960, *25*, 853–861.

(39) Deister, U.; Neeb, R.; Helas, G.; Warneck, P.J. *J. Phys. Chem.* **1986**, *90*, 3213–3217.

(40) Lewis, C.A.; Wolfenden, R. *J. Amer. Chem. Soc.* **1973**, *95*, 6685–6688.

(41) Hine, J.; Houston, J.G.; Jensen, J.H. *J. Org. Chem.* **1965**, *30*, 1184–1188.

(42) Green, L.R.; Hine, J. *J. Org. Chem.* **1974**, *39*, 3896–3901.

(43) Gruen, L.C.; McTigue, P.T. *J. Chem. Soc.* **1963**, 5217–5223.

(44) Buschmann, H.J.; Füldner, H.H.; Knoche, W. *Ber. Bunsenges Phys. Chem.* **1980**, *84*, 41–44.

(45) Sørensen, P.E.; *Acta Chem. Scand.* **1972**, *26*, 3357–3365.

(46) Federlin, P. *Compt. rend.* **1952**, *235*, 44–46.

(47) Wasa, T.; Musha, S. *Bull. Univ. Osaka Prefect. Ser. A* **1970**, *19*, 169–180.

(48) Hine, J.; Redding, R.W. *J. Org. Chem.* **1970**, *35*, 2769–2772.

(49) Gubareva, M.A. *J. Gen. Chem. USSR* **1947**, *17*, 2259–2264.

(50) LeHenaff, P. *Bull. Soc. Chim. Fr.* **1968**, *11*, 4687–4700.

(51) Stewart, R.; Dyke, J.D.v. *Can. J. Chem.* **1970**, *48*, 3961–3963.

TABLE 1. Acid Dissociation Constants and Hydration Constants for Glyoxylic Acid (25° C, $\mu = 0$).

$$RCO_2H \overset{K_a}{\rightleftharpoons} RCO_2^- + H^+$$

$$RCHO + H_2O \overset{K_h}{\rightleftharpoons} RCH(OH)_2$$

R	pK_a	K_h	Ref.
$-CH(OH)_2$	3.46		14
	3.18†		15
	3.30		16
	2.98		17
$-CHO$	1.89		18
	2.00‡		19
$-CO_2H$		300.	19
$-CO_2^-$		15.1	19
		16.7	20
		19.2	21

†20° C

‡Calculated.

TABLE 2. Kinetic Data for the Addition of S(IV) and Glyoxylic Acid (25° C, μ = 0.2 M).

pH	10^2 $[CHOCO_2H]_t$ M	10^3 $[S(IV)]_t$ M	10^3 k_{obsd}† ($\pm\sigma$) s^{-1}	10^3 k_{calc} s^{-1}
0.71	2.0	0.15	2.84 (±0.05)	2.80
0.94	2.0	0.15	4.56 (±0.06)	4.58
1.14	2.0	0.15	7.04 (±0.05)	6.92
1.36	2.0	0.20	10.2 (±0.2)	10.5
1.65	1.0	0.25	7.94 (±0.05)	8.89
1.77	1.0	0.30	9.71 (±0.16)	10.8
2.00	1.0	0.375	17.0 (±0.3)	15.9
2.22	1.0	1.0	22.5 (±0.4)	22.5
2.36	1.0	1.0	29.1 (±0.3)	27.8
2.57	1.0	1.0	40.4 (±0.97)	38.7
2.68‡	2.5	2.5	113 (±1.0)	111.
2.74	1.0	1.0	49.0 (±2.6)	48.4
2.79‡	3.0	3.0	149 (±3)	157.
2.89	1.0	1.0	60.1 (±2.2)	59.9

†Values are averages of at least four replications.

‡Data obtained by stopped–flow spectrophotometry.

TABLE 3. Temperature Dependence of the Rate Constant for the Addition of HSO_3^- and $CHOCO_2H$ ($\mu = 0.2$ M).

T °C	k_1† s^{-1}
15	338
20	396
25	463
30	565
35	635

†Estimated as $k_1 \approx k_{obsd}/\alpha_1\beta_1[C_2H_2O_3]$ where k_{obsd} is the average of at least two determinations.

TABLE 4. Kinetic Data for the Dissociation of 2–Hydroxy–2–sulfo–ethanoic acid (25° C, μ = 0.2 M).

pH	k'_{obsd} ($\pm\sigma$) s^{-1}	k'_{calc} s^{-1}
0.66	7.06×10^{-6}	6.55×10^{-6}
1.00	7.00×10^{-6}	6.83×10^{-6}
1.60	7.76×10^{-6}	8.32×10^{-6}
2.01	1.05×10^{-5}	1.12×10^{-5}
2.99	3.32×10^{-5}	3.44×10^{-5}
3.62	6.58×10^{-5}	6.63×10^{-5}
4.48	$2.34(\pm0.04) \times 10^{-4}$	2.18×10^{-4}
4.95	$6.26(\pm0.06) \times 10^{-4}$	5.53×10^{-4}
5.39	$1.39(\pm0.01) \times 10^{-3}$	1.44×10^{-3}
6.11	$6.98(\pm0.07) \times 10^{-3}$	7.22×10^{-3}
6.54	$1.84(\pm0.07) \times 10^{-2}$	1.96×10^{-2}
6.97	$4.81(\pm0.05) \times 10^{-2}$	5.20×10^{-2}

TABLE 5. Apparent HSEA Stability Constants.

pH	$K^{\dagger}_{app}$, M^{-1}
1.06	5.51×10^4
1.63	1.26×10^5
2.05	1.90×10^5
2.31	2.13×10^5
2.67	2.33×10^5
3.20	2.70×10^5
3.63	2.86×10^5
4.36	3.09×10^5
4.62	3.17×10^5
5.48	3.57×10^5
5.49	2.91×10^5

$$\dagger K_{app} = \frac{[HSEA]_t}{[C_2H_2O_3]\ [S(IV)]}$$

TABLE 6. Comparison of Forward Rate Constants for Hydroxyalkyl–sulfonate Formation (25° C):

$$RCHO + HSO_3^- \xrightarrow{k_I} RCH(OH)SO_3^-$$

$$RCHO + SO_3^{2-} \xrightarrow{k_{II}} RCH(O^-)SO_3^- .$$

R	μ, M	k_I, $M^{-1}\,s^{-1}$	k_{II}, $M^{-1}\,s^{-1}$	Ref.
$-CO_2H$	0.2	4.43×10^2	1.98×10^7	This work
$-COCH_3$	0.2	3.44×10^3	3.66×10^7	4
$-H$	1.0	7.90×10^2	2.50×10^7	2
$-C_6H_5$	1.0	7.1×10^{-1}	2.15×10^4	3

TABLE 7. Comparison of Activation Parameters for Hydroxyalkylsulfonate Formation:

$$RCHO + HSO_3^- \xrightarrow{k_I} RCH(OH)SO_3^-$$

$$RCHO + SO_3^{2-} \xrightarrow{k_{II}} RCH(O^-)SO_3^- .$$

R	$\Delta H^{\ddagger}_{I}$ kJ/mol	$\Delta S^{\ddagger}_{I}$ kJ/(mol·deg)	$\Delta H^{\ddagger}_{II}$ kJ/mol	$\Delta S^{\ddagger}_{II}$ kJ/(mol·deg)	Ref.
$-CO_2H$	21.4	−141.	N.D.†	N.D.	This work
$-COCH_3$	29.0	−77.7	18.2	−22.6	4
−H	24.9	−108.	20.4	−31.7	2
$-C_6H_5$	36.6	−142	36.0	−58.1	3

†N.D. = Not determined.

TABLE 8. Potential S(IV) Enrichment Due to HSEA Formation in an Open Atmosphere (P_{SO_2} = 20 ppbv, P_{CHOCO_2H} = 1 ppbv, T = 25° C).

pH	$[HSEA]_t$† M	$([S(IV)] + [HSEA]_t)/[S(IV)]$
2	3.95×10^{-9}	1.05
3	7.53×10^{-8}	1.14
4	4.34×10^{-6}	1.86
5	4.02×10^{-4}	8.88
6	3.98×10^{-2}	69.3

†$[HSEA]_t = [HO_2CCH(OH)SO_3^-] + [^-O_2CCH(OH)SO_3^-] + [HO_2CCH(O^-)SO_3^-] + [^-O_2CCH(O^-)SO_3^-]$.

Figure Captions

Figure 1. Dependence of pseudo–first–order rate constant for HSEA formation on $[CHOCO_2H]_t$. Solid lines are linear least–squares fits to the data. Reaction conditions: $[S(IV)]_t = 0.15 - 1$ mM, T = 25° C, $\mu = 0.2$ M. Correlation coefficients are $R^2 = 0.9987$ (pH 0.7), 0.9987 (pH 1.4), and 0.9968 (pH 2.2).

Figure 2. Dependence of $k_{obsd}/(\alpha_1\beta_1[CHOCO_2H]_t)$ on $1/\{H^+\}$. Solid line is a linear least–squares fit to the data in Table 2.

Figure 3. Dependence of k'_{obsd}/ϕ_2 on $\{H^+\}$. Data were obtained from the five lowest pH entries in Table 4. Least–squares slope and intercept parameters correspond to initial estimates of k_{-1}/K_{a5} and $k_{-2} + k_{-3}K_{a7}/K_{a5}$, respectively.

Figure 4. Dependence of k'_{obsd}/ϕ_2 on $1/\{H^+\}$. Data were taken from the five entries in Table 4 between pH 3.6 – 5.4. Least–squares slope and intercept parameters correspond to initial estimates of $k_{-4}K_{a6}$ and $k_{-2} + k_{-3}K_{a7}/K_{a5}$, respectively.

Figure 5. Comparison of measured and calculated pseudo–first–order dissociation rate constants. Solid line represents a nonlinear least–squares regression fit to the data by Taylor's method (Ref. 27).

Figure 6. Comparison of measured and calculated apparent adduct stability constants as a function of pH. Solid line represents a nonlinear least–squares fit to the data by Taylor's method (Ref. 27). Reaction conditions: $[NaO_2CCH(OH)SO_3Na]$ = 0.033 mM, T = 25° C, μ = 0.2 M.

Figure 7. Correlations of stability constants for (a) carbonyl hydration and (b) bisulfite addition with Taft's σ^* parameter. $K_h = [R_1C(OH)_2R_2]/([R_1COR_2]\ [HSO_3^-])$ and $K = [R_1R_2C(OH)SO_3^-]/([R_1COR_2][HSO_3^-])$. Key: 1 – HCHO (Refs. 38,39); 2 – $CHOCO_2^-$ (19, this work); 3 – $(CH_3)_3CCHO$ (40); 4 – $(CH_3)_2CHCHO$ (41,42); 5 – CH_3CH_2CHO (43); 6 – CH_3CHO (44,6); 7– $CH_2(OH)CHO$ (45,6); 8 – CH_2ClCHO (46); 9 – $CHOCO_2H$ (19, this work); 10 – CH_3COCHO (47,4); 11 – C_6H_5COCHO (32); 12 – Cl_3CCHO (43); 13 – $CH_3COCO_2^-$ (26,34); 14 – $C_6H_5COCO_2^-$ (21); 15 – $HO_2CCOCO_2^-$ (20); 16 – CH_3COCH_3 (48,49); 17 – CH_3COCH_2Cl (44); 18 – CH_3COCH_2F (44); 19 – $CH_2ClCOCH_2Cl_2$ (50); 20 – CH_3COCO_2H (26); 21 – $CH_3COCHCl_2$ (44); 22 – $CH_3COCOCH_3$ (47); 23 – $HO_2CCOCH(CH_3)_2$ (33); 24 – $HO_2CCOCH_2CH_3$ (33); 25 – $CH_3COC_2H_5CO_2$ (26); 26 – $HO_2CCO(CH_2)_2CO_2H$ (21); 27 – $C_6H_5COCO_2H$ (21); 28 – CH_3COCF_3 (31); 29 – $C_6H_5COCF_3$ (51); 30 – CF_3COCF_3 (51); 31 – $CH(OH)_2CHO$ (5); 32 – C_6H_5CHO (3). Solid lines in (a) are least–squares fits to the data as follows: "RCHO" = (▲), slope = 1.58, intercept = –0.759; "R_1COR_2" = (•), slope = 1.53, intercept = –2.72. Dashed line in (a) was drawn through point 1 with slope = 1.5. Dashed line in (b) is a

least–squares fit of points 4,6,7,9,10, and 31, with slope = 1.57 and intercept = 4.70. Open symbols correspond to compounds with a $-CO_2^-$ substituent.

Figure 8. Linear–free–energy correlation of carbonyl–bisulfite adduct stabilities, K, with carbonyl hydration constants, K_h. Solid line is a least–squares regression fit.

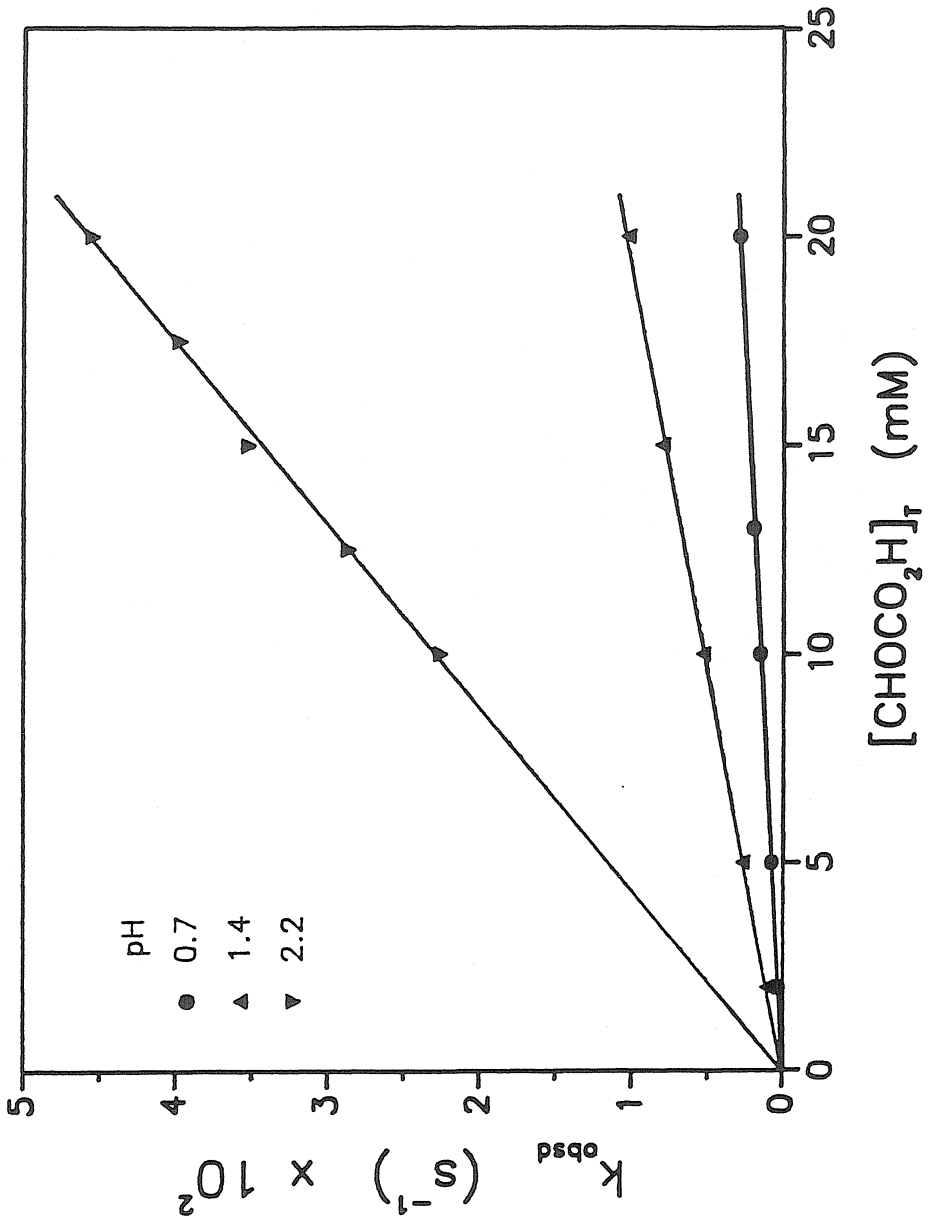

Figure 1

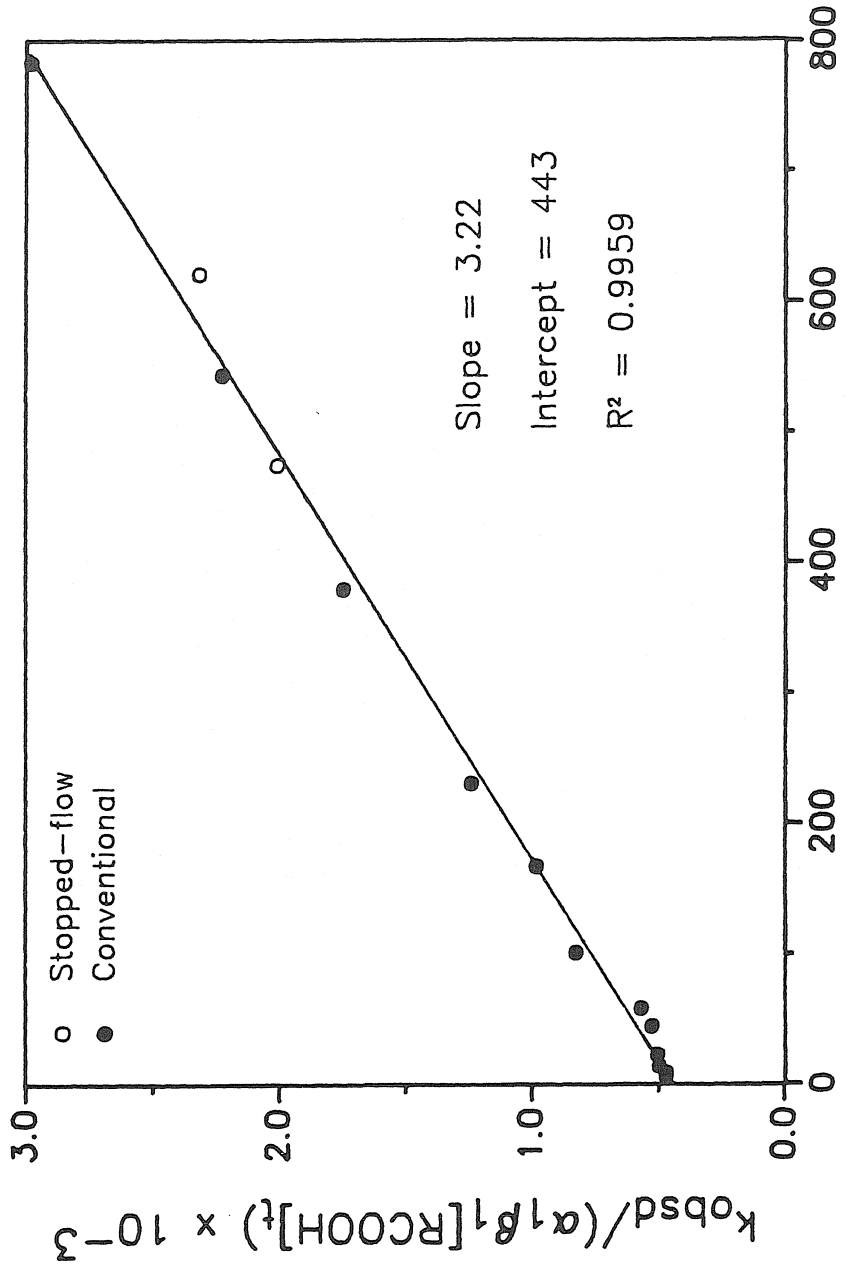
Stopped−flow
Conventional
Slope = 3.22
Intercept = 443
R² = 0.9959
3.0
2.0
1.0
0.0
0
200
400
600
800
1/{H+} M⁻¹
kobsd/(α1β1[RCOOH]t) x 10⁻³

Figure 2

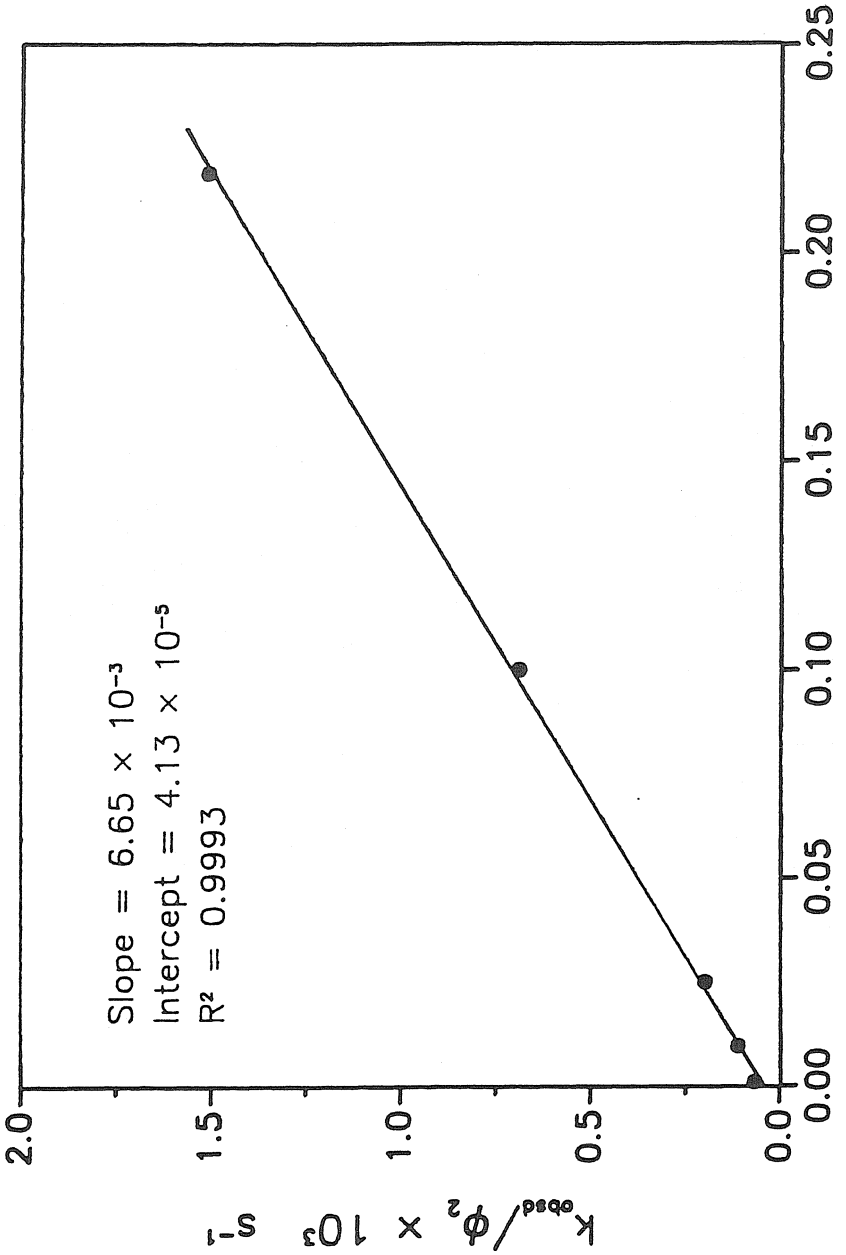
Slope = 6.65 × 10⁻³
Intercept = 4.13 × 10⁻⁵
R² = 0.9993
k_obsd/φ₂ × 10³ s⁻¹
{H⁺} (M)
0.0
0.5
1.0
1.5
2.0
0.00
0.05
0.10
0.15
0.20
0.25

Figure 3

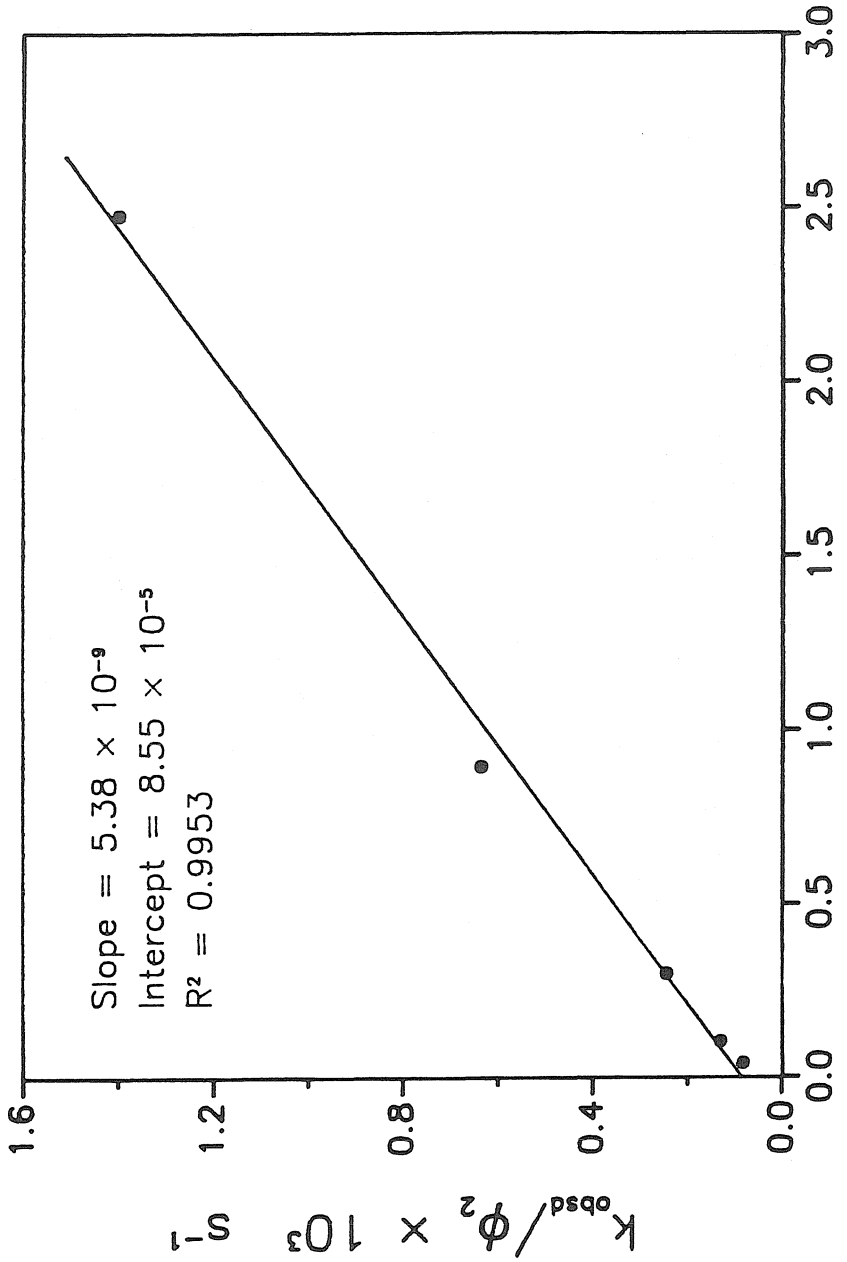
Slope = 5.38 × 10⁻⁹
Intercept = 8.55 × 10⁻⁵
R² = 0.9953
k_obsd/φ₂ × 10³ s⁻¹
1/{H⁺} × 10³ M⁻¹
0.0
0.4
0.8
1.2
1.6
0.0
0.5
1.0
1.5
2.0
2.5
3.0

Figure 4

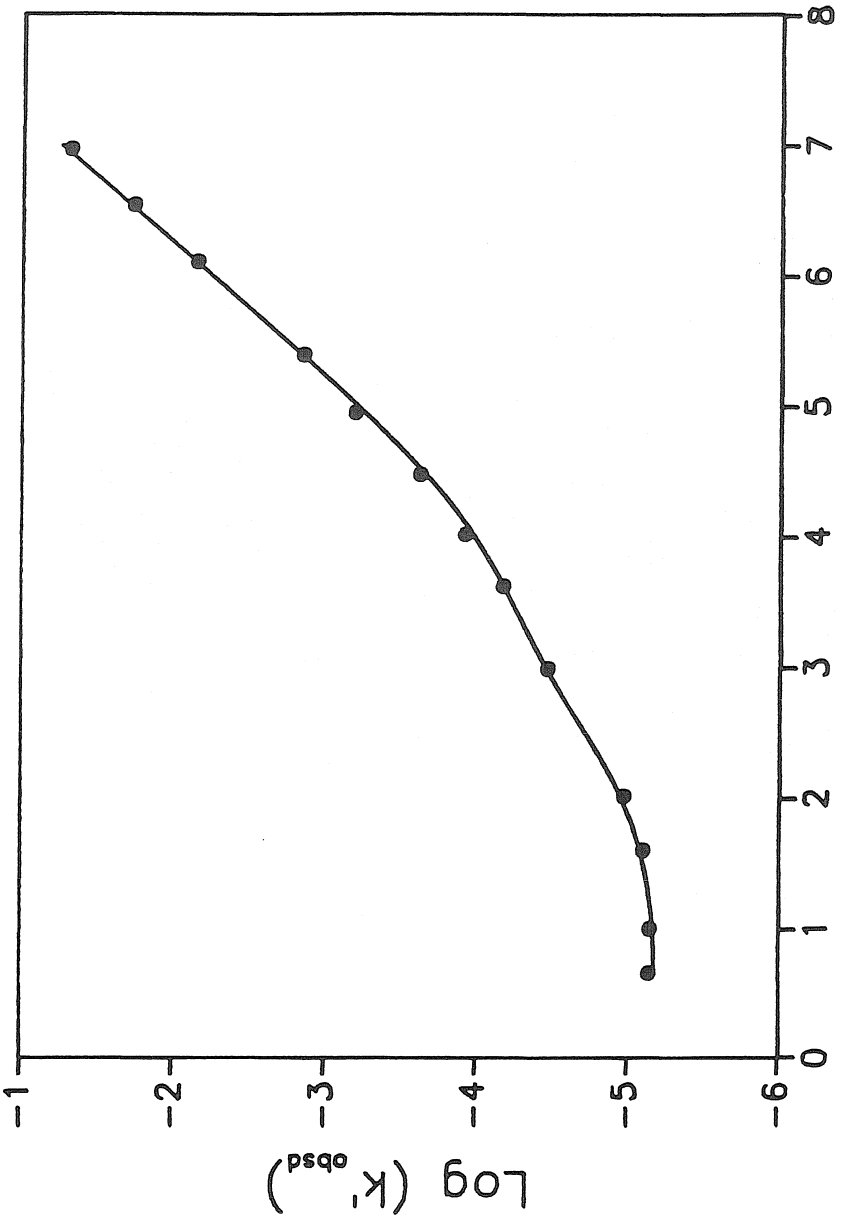

Figure 5

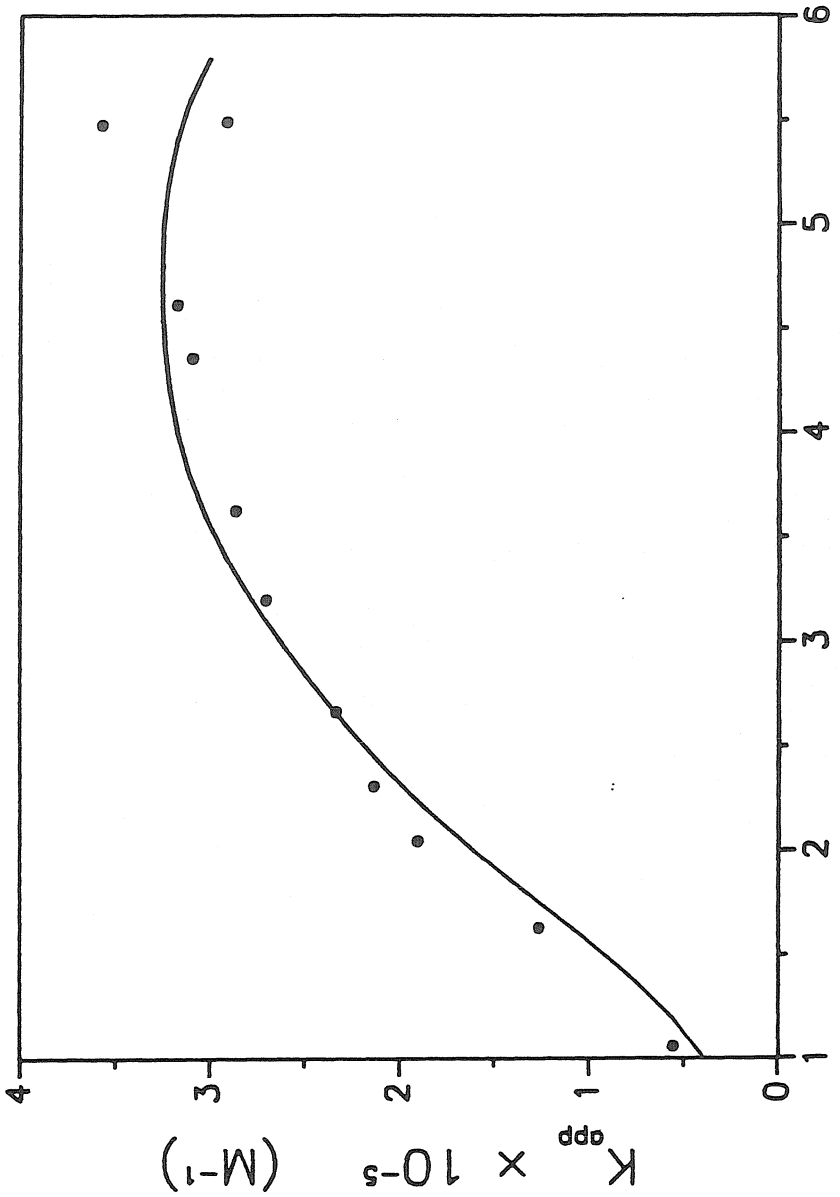

Figure 6

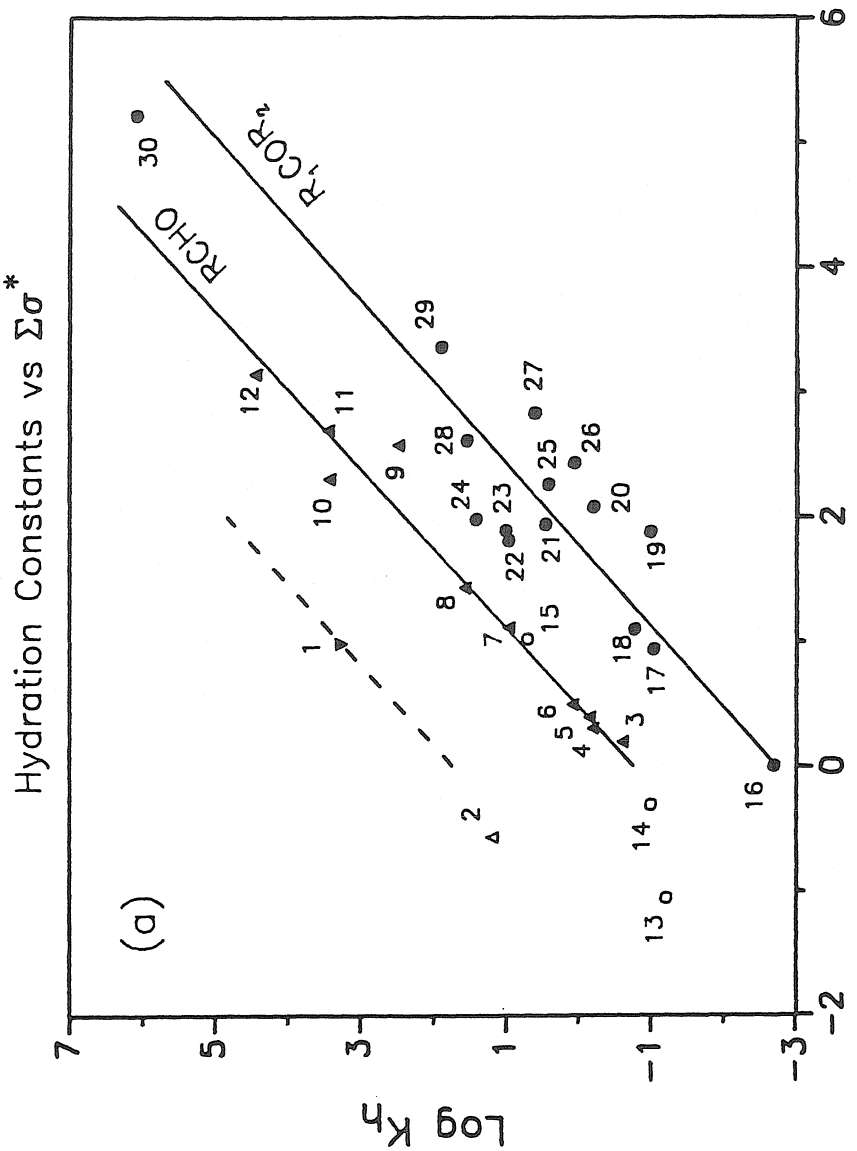
Hydration Constants vs Σσ*
(a)
RCHO
R'COR
Log Kh
Σσ*
7
5
3
1
−1
−3
−2
0
2
4
6
1
2
3
4
5
6
7
8
9
10
11
12
13
14
15
16
17
18
19
20
21
22
23
24
25
26
27
28
29
30

Figure 7a

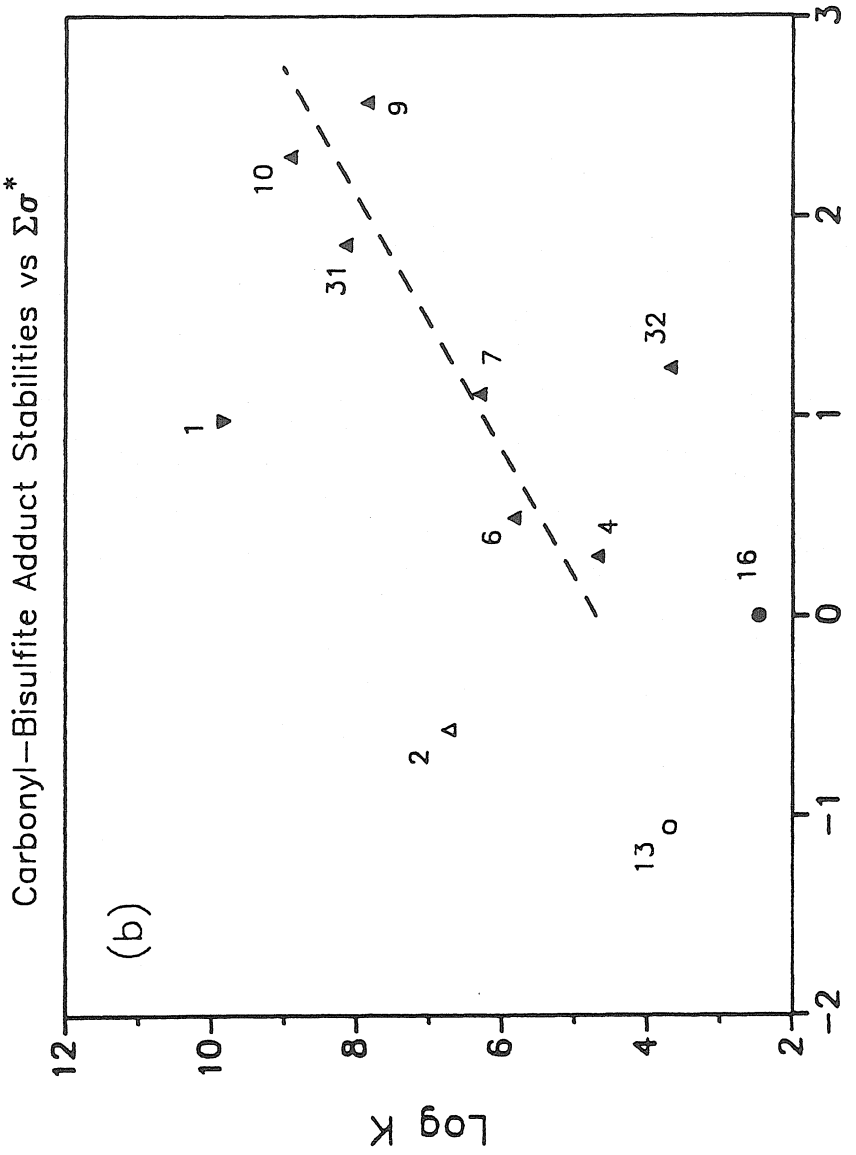
Carbonyl–Bisulfite Adduct Stabilities vs Σσ*
(b)
Log K
Σσ*
12
10
8
6
4
2
-2
-1
0
1
2
3
1
2
13
6
4
16
7
32
31
10
9

Figure 7b

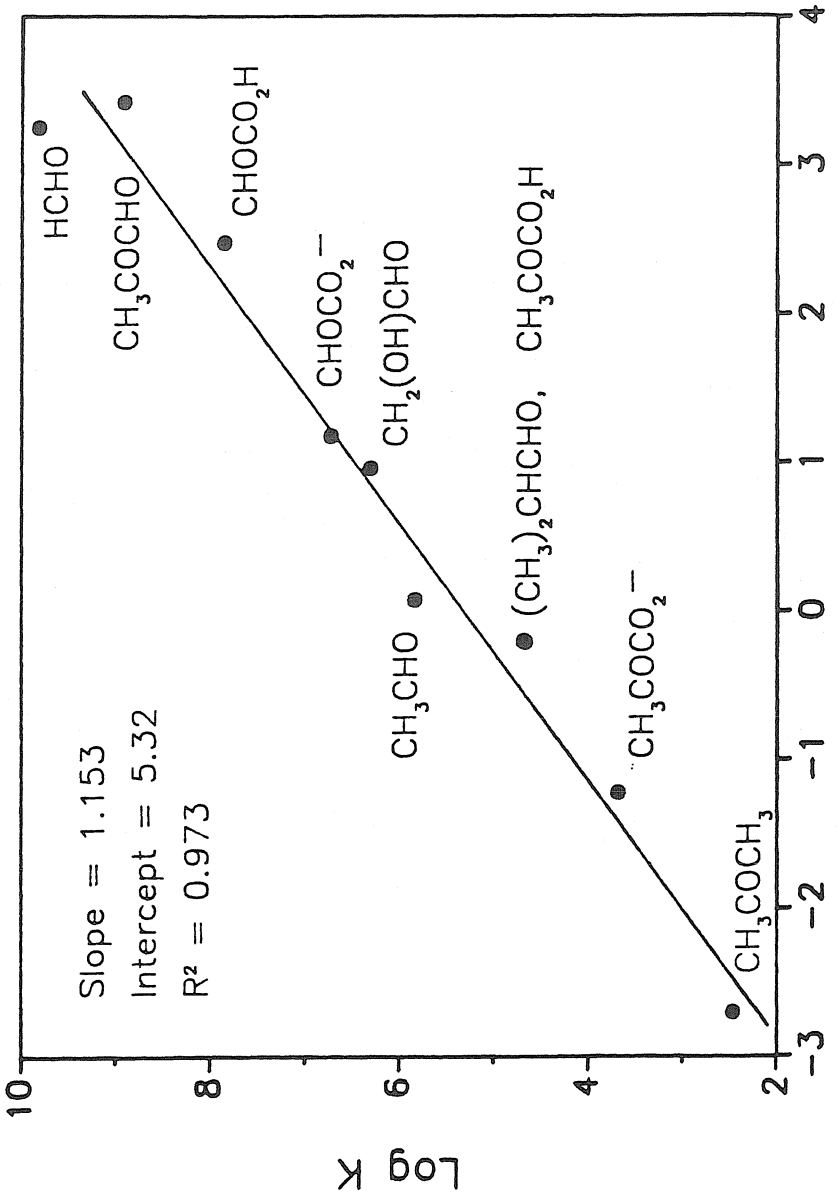
Slope = 1.153
Intercept = 5.32
R² = 0.973
HCHO
CH3COCHO
CHOCO2H
CHOCO2−
CH2(OH)CHO
CH3CHO
(CH3)2CHCHO, CH3COCO2H
CH3COCO2−
CH3COCH3
Log K
Log (Kh)
10
8
6
4
2
−3
−2
−1
0
1
2
3
4

Figure 8

CHAPTER 6

Kinetics of the Formation of Hydroxyacetaldehyde-S(IV) Adducts at Low pH

by

Terese M. Olson, Lori A. Torry, and Michael R. Hoffmann

Submitted to: *Environmental Science and Technology*, February 1988

Abstract

The kinetics of the addition of hydroxyacetaldehyde and S(IV) was studied spectrophotometrically over the pH range of 0.7 to 3.3. Formation rates of the adduct, 1,2 dihydroxy–1–ethanesulfonate (DHES), were consistent with the following three–term rate expression: $d[DHES]/dt = (k_0\{H^+\}\alpha_1/K_{a0} + k_1\alpha_1 + k_2\alpha_2)[C_2H_3O_2]_t[S(IV)]$, where $[C_2H_3O_2]_t = [CH_2(OH)CHO] + [CH_2(OH)CH(OH)_2]$, $[S(IV)] = [H_2O\cdot SO_2] + [HSO_3^-] + [SO_3^{2-}]$, $\alpha_1 = [HSO_3^-]/[S(IV)]$, $\alpha_2 = [SO_3^{2-}]/[S(IV)]$, and K_{a0} is the acid dissociation constant for $CH_2(OH)C^+HOH$. The rate constant k_0 corresponds to a proton–catalyzed pathway in which bisulfite reacts with the carbocation, $CH_2(OH)C^+HOH$. A value for the constant k_0/K_{a0} was determined as 5.4 (± 2.0) $M^{-2}\ s^{-1}$ (25° C, μ = 0.2 M). The intrinsic constants, k_1 and k_2, are the respective rate constants for the reactions of HSO_3^- and SO_3^{2-} with unhydrated hydroxyacetaldehyde, where it was determined that k_1 = 1.74 (± 0.16) $M^{-1}\ s^{-1}$ and k_2 = 5.02 (± 0.12) × $10^4\ M^{-1}\ s^{-1}$. From temperature–dependence studies, activation energy parameters for the k_1 and k_2 steps were calculated. For k_1, $\Delta H_1^{\neq}$ = 29 kJ mol^{-1} and $\Delta S_1^{\neq}$ = –156 J mol^{-1} deg^{-1}; for k_2, $\Delta H_2^{\neq}$ = 17.7 kJ mol^{-1} and $\Delta S_2^{\neq}$ = –117 J mol^{-1} deg^{-1}. Both values of $\Delta S^{\neq}$ were significantly more negative than the previously determined activation entropies of other hydroxyalkylsulfonates. Transition state structures were proposed to explain these differences. A correlation between k_1 and k_2 is also presented. Because of the high intrinsic solubility of $CH_2(OH)CHO$, calculated DHES formation rates in fog– and cloudwater are faster than the addition rate of formaldehyde and S(IV). DHES is shown to satisfy the criteria of a significant S(IV) reservoir in atmospheric droplets.

Introduction

As part of a continuing study of the addition of S(IV) species ($H_2O \cdot SO_2$, HSO_3^-, and SO_3^{2-}) with carbonyl compounds, we have investigated the kinetics of hydroxyacetaldehyde–S(IV) adduct formation at low pH. This study was motivated by the identification of hydroxymethanesulfonate ($CH_2(OH)SO_3^-$, HMS) in fog– and rainwater at concentrations exceeding 100 μM (1,2). The formation of hydroxyalkylsulfonates in atmospheric droplets leads to an enrichment of S(IV) and aldehydes relative to the concentrations predicted by simple Henry's law equilibria. These adducts are also stable in the presence of compounds that readily oxidize S(IV), such as H_2O_2 and O_3 (3–5). Carbonyl–bisulfite addition compounds are therefore potential reservoirs for S(IV) in atmospheric water droplets.

Based on our previous studies with formaldehyde (6), benzaldehyde (7), acetaldehyde (8), glyoxal (CHOCHO) (9), methylglyoxal (CH_3COCHO) (10), and glyoxylic acid ($CHOCO_2H$) (11), criteria were formulated for predicting which hydroxyalkylsulfonates are potentially important S(IV) reservoirs. Carbonyls that effectively stabilize S(IV) are those with high solubilities (*i.e.*, large apparent Henry's law constants) and significant sources in the environment. The bisulfite addition compounds derived from these carbonyls must also be highly stable. Finally, bisulfite adduct formation rates must be rapid relative to the lifetime of a fog event.

Already, there is sufficient data to show that hydroxyacetaldehyde satisfies two of the above criteria. Betterton and Hoffmann (12) have reported that its apparent Henry's law constant, $H^* = ([CH_2(OH)CHO]_{aq} + [CH_2(OH)CH(OH)_2]_{aq}) / [CH_2(OH)CHO]_g)$, is 4.14×10^4 M atm^{-1}. Since $H^*_{HCHO} = 2.97 \times 10^3$ M atm^{-1} (12), hydroxyacetaldehyde is an order of magnitude more soluble than

formaldehyde. Betterton *et al.* also determined the stability constant for the hydroxyacetaldehyde–bisulfite adduct (1,2–dihydroxy–1–ethanesulfonate, hereafter referred to as DHES) as $K_1 = [CH_2(OH)CH(OH)SO_3^-]/ [CH_2(OH)CHO][HSO_3^-] = 2.0 \times 10^6\ M^{-1}$ (8). Since hydroxyacetaldehyde is approximately 90% hydrated in solution (13), the apparent adduct stability constant, $^{app}K_1 = [CH_2(OH)CH(OH)SO_3^-]/([CH_2(OH)CHO] + [CH_2(OH)CH(OH)_2])[HSO_3^-]$, is $2 \times 10^5\ M^{-1}$. Compared with the apparent formation constant of hydroxymethane–sulfonate, $3.6 \times 10^6\ M^{-1}$ (14), the hydroxyacetaldehyde–bisulfite adduct is an order of magnitude less stable. Although the apparent Henry's law constants and bisulfite adduct stabilities are similar, it is not known how their ambient gas–phase concentrations compare. Hydroxyacetaldehyde is, however, a predicted important component of the gas–phase product mixtures resulting from alkene oxidation (15).

Thermodynamic calculations therefore suggest that hydroxyacetaldehyde is a potentially important reservoir for S(IV). With this motivation, we undertook a study of the kinetics and mechanism of the reaction. These experiments were conducted at pH < 3.3; a pH range, which overlaps with the acidic pH range frequently observed in fogs, clouds and haze aerosols (16 a–c).

Experimental Procedures

Materials. Unless otherwise specified, all solutions were prepared from A.R. grade reagents and deoxygenated, high purity water (18 MΩ·cm; Millipore). Oxygen was purged by bubbling with high purity N_2 gas. Stock solutions of hydroxyacetaldehyde (0.1 M) were prepared from the anhydrous solid (glycolaldehyde; Sigma, laboratory grade) in an N_2 atmosphere glovebox and stored there protected from light. Since hydroxyacetaldehyde exists in concentrated solution as a dimer (17a,b), we allowed the stock solution to

equilibrate at least 24 hours before use. In a 0.1 M solution, 74% of the aldehyde exists as either the unhydrated or *gem*–diol monomers; the remaining 26% are dimer species (17a). The most concentrated aldehyde solutions in our experiments were 0.02 M and the dimer fraction at this concentration is estimated as $\leq 5\%$.

Stock S(IV) solutions were prepared fresh before use from disodium sulfite (Baker) under an N_2 atmosphere. The ionic strength in all experiments was maintained as 0.2 M by adding sufficient sodium chloride (Baker). Reactant mixtures were buffered in the pH range of 1.6 – 3.3 with sufficient NaOH (Baker) and 0.1 M concentrations of Cl_2CHCO_2H (MCB) or $ClCH_2CO_2H$ (Kodak). Hydrochloric acid (Baker) was used to adjust the acidity below pH 1.6. All buffer and electrolyte solutions were filtered before use through a 0.2 μm Millipore filter.

Methods. The forward reaction kinetics were studied by monitoring the disappearance of unbound S(IV) at 280 nm (λ_{max} for $H_2O \cdot SO_2$) with a Hewlett–Packard Model 8450A UV/Vis spectrophotometer. In all experiments, pseudo–first–order conditions were imposed by maintaining at least a tenfold excess of hydroxyacetaldehyde. Reactions were conducted in a 10 cm quartz, water–jacketed cell and a Haake water recirculation bath was used to maintain a constant temperature. For each of the kinetic runs at least 200 data points were collected. Above pH 3.3, the reaction became too fast to study by conventional spectrophotometry and the concentration of $H_2O \cdot SO_2$ was too small to monitor by stopped–flow techniques. Hydrogen ion activities were measured with a Radiometer Model PHM85 pH meter and a combination glass electrode.

Results

Formation Kinetics. Under the pseudo–first–order conditions of our experiments, $[CH_2(OH)CHO]_t \gg [S(IV)]$, a first–order dependence in free S(IV) was

tested by plotting ln $[(A-A_\infty)/(A_o-A_\infty)]$ vs time. These plots were linear ($r^2 > 0.999$) for reaction extents up to 90%. The pseudo–first–order rate constants, k_{obsd}, which correspond to the slopes of these lines averaged from at least four replications, are tabulated in Table 1. At pH 1.4 and 2.1, k_{obsd} was measured as a function of $[CH_2(OH)CHO]_t$ to test the reaction order dependence on hydroxy–acetaldehyde. Plots of the data, shown in Fig. 1, are linear and the y–intercepts are not significantly different from zero. The reaction is first–order, therefore, with respect to $[CH_2(OH)CHO]$.

Our previous studies with other aldehyde substrates have shown that hydroxyalkylsulfonate formation rates below pH 3 are governed by the two addition steps of HSO_3^- and SO_3^{2-} at the carbonyl carbon atom (6,7,9–11). Specific acid catalysis was also observed below pH 1 for the formation of benzaldehyde– and methylglyoxal–bisulfite addition compounds (7,10). Using the data in Table 1, we initially tested the simpler, two–step mechanism which did not contain a proton–catalyzed pathway. This mechanism did not fit the data at low pH, so the following mechanism, which considers specific acid catalysis, was proposed:

$$H_2O\cdot SO_2 \overset{K_{a1}}{\rightleftharpoons} HSO_3^- + H^+ \qquad \text{(fast)} \qquad (1)$$

$$HSO_3^- \overset{K_{a2}}{\rightleftharpoons} SO_3^{2-} + H^+ \qquad \text{(fast)} \qquad (2)$$

$$CH_2(OH)CH(OH)_2 \underset{H^+}{\overset{K_d}{\rightleftharpoons}} CH_2(OH)CHO + H_2O \qquad \text{(fast)} \qquad (3)$$

$$CH_2(OH)CHO + HSO_3^- \underset{k_{-1}}{\overset{k_1}{\rightleftharpoons}} CH_2(OH)CH(OH)SO_3^- \qquad \text{(slow)} \qquad (4)$$

$$CH_2(OH)CHO + SO_3^{2-} \underset{k_{-2}}{\overset{k_2}{\rightleftharpoons}} CH_2(OH)CH(O^-)SO_3^- \qquad \text{(slow)} \quad (5)$$

$$CH_2(OH)CHO + H^+ \overset{1/K_{a0}}{\rightleftharpoons} CH_2(OH)CHOH^+ \qquad \text{(fast)} \quad (6)$$

$$CH_2(OH)CHOH^+ + HSO_3^- \underset{k_{-0}}{\overset{k_0}{\rightleftharpoons}} CH_2(OH)CH(OH)SO_3H \qquad \text{(slow)} \quad (7)$$

$$CH_2(OH)CH(OH)SO_3H \overset{K_{a3}}{\rightleftharpoons} CH_2(OH)CH(OH)SO_3^- + H^+ \qquad \text{(fast)} \quad (8)$$

$$CH_2(OH)CH(OH)SO_3^- \overset{K_{a4}}{\rightleftharpoons} CH_2(OH)CH(O^-)SO_3^- + H^+ . \qquad \text{(fast)} \quad (9)$$

The above scheme leads to a three–term rate expression for the formation of DHES:

$$\nu = \frac{d[DHES]_t}{dt} = k_0[CH_2(OH)CHOH^+][HSO_3^-] + k_1[CH_2(OH)CHO][HSO_3^-] + k_2[CH_2(OH)CHO][SO_3^{2-}] , \quad (10)$$

where

$$[DHES]_t = [CH_2(OH)CH(OH)SO_3H] + [CH_2(OH)CH(OH)SO_3^-] + [CH_2(OH)CH(O^-)SO_3^-] . \quad (11)$$

An equivalent expression for Eq. 10 in terms of the ionization fractions of S(IV) species may be written as

$$\nu = \{k_0\alpha_1[CH_2(OH)CHOH^+] + (k_1\alpha_1 + k_2\alpha_2)[CH_2(OH)CHO]\}\,[S(IV)] , \quad (12)$$

where

$$[S(IV)] = [H_2O\cdot SO_2] + [HSO_3^-] + [SO_3^{2-}] \quad (13)$$

$$\alpha_1 = \frac{[SO_3^{2-}]}{[S(IV)]} = \frac{K_{a1}\{H^+\}}{\{H^+\}^2 + K_{a1}\{H^+\} + K_{a1}K_{a2}} \quad (14)$$

$$\alpha_2 = \frac{[HSO_3^-]}{[S(IV)]} = \frac{K_{a1}K_{a2}}{\{H^+\}^2 + K_{a1}\{H^+\} + K_{a1}K_{a2}} . \quad (15)$$

Based on the typical acid strengths of other sulfonic acids, we expect that $pK_{a3} < -1$ (18). The second acid dissociation constant of DHES has also been determined as $pK_{a4} = 10.3$ (8), so consequently the dominant adduct species over the pH range of this study is $CH_2(OH)CH(OH)SO_3^-$. The magnitude of K_{a0} is not known, however, the carbonyl species is expected to be a very weak base. Oxygen bases such as acetone and benzaldehyde, for example, have pK_{a0}'s of –7.5 and –6.9, respectively (19). The total aldehyde concentration therefore, may be approximated as

$$[C_2H_3O_2]_t \approx [CH_2(OH)CHO] + [CH_2(OH)CH(OH)_2] , \quad (16)$$

since the concentration of $CH_2(OH)CHOH^+$ is negligible. When Eq. 12 is rewritten in terms of $[C_2H_3O_2]_t$, rates are given as

$$\nu = \left(\frac{k_0\{H^+\}}{K_{a0}}\alpha_1 + k_1\alpha_1 + k_2\alpha_2\right)\left(\frac{K_d}{1 + K_d}\right)[C_2H_3O_2]_t[S(IV)] , \quad (17)$$

and the observed rate constant is, therefore,

$$k_{obsd} = \left(\frac{k_0\{H^+\}}{K_{a0}}\alpha_1 + k_1\alpha_1 + k_2\alpha_2\right)\left(\frac{K_d}{1 + K_d}\right)[C_2H_3O_2]_t . \quad (18)$$

Dividing Eq. 18 by $\alpha_1[C_2H_3O_2]_tK_d/(1+K_d)$ gives an equation that can be used to examine the pH–dependence of the reaction:

$$\frac{k_{obsd}\ (1+K_d)}{\alpha_1[C_2H_3O_2]_t K_d} = \frac{k_0\{H^+\}}{K_{a0}} + k_1 + \frac{k_2 K_{a2}}{\{H^+\}}. \qquad (19)$$

A plot of $k_{obsd}(1+K_d)/\alpha_1[C_2H_3O_2]_tK_d$ vs $\{H^+\}$ at sufficiently low pH, therefore, should be linear with a slope of k_0/K_{a0} and a y–intercept of k_1. At sufficiently high pH, Eq. 19 predicts that $k_{obsd}(1+K_d)/\alpha_1K_d[C_2H_3O_2]_t$ will vary inversely with $\{H^+\}$. Estimates of the constants k_2K_{a2} and k_1 can be calculated from the slope and intercept of this second plot. Figures 2 and 3 demonstrate, therefore, that the kinetic data are consistent with these trends. Refined estimates of $k_0/K_{a0} = 5.4$ (± 2.0) $M^{-2}s^{-1}$, $k_1 = 1.74$ (± 0.16) $M^{-1}s^{-1}$, and $k_2 = 5.02$ (± 0.12) × 10^4 $M^{-1}s^{-1}$ were obtained by fitting the entire set of data in Table 1 to Eq. 19 with a Taylor's method, nonlinear regression routine (20). The previous rough estimates were supplied as initial guesses to the program. Values of the thermodynamic constants (at infinite dilution), $K_{a1} = 1.45 \times 10^{-2}$ M (21), $K_{a2} = 6.31 \times 10^{-8}$ M (22) and $K_d = 0.11$ (13), were held fixed in the regression analysis and were corrected to an ionic strength of 0.2 M. Since hydrogen ion activities were measured in our experiments, a mixed concentration/activity scale was chosen, and hence the corrected equilibrium constants are given by ${}^cK_{a1} = K_{a1}\ \gamma_{H_2O\cdot SO_2}/\gamma_{HSO_3^-} = 1.99 \times 10^{-2}$ M, ${}^cK_{a2} = K_{a2}\ \gamma_{HSO_3^-}/\gamma_{SO_3^{2-}} = 1.63 \times 10^{-7}$ M, and ${}^cK_d = K_d\ \gamma_{CH_2(OH)CH(OH)_2}/\gamma_{CH_2(OH)CHO} = 0.11$. Activity coefficients were calculated with the Davies equation (23). A comparison of the fitted values of $k_{obsd}K_d/(1+K_d)\alpha_1[C_2H_3O_2]_t$ with the experimental data is presented in Fig. 4 and calculated pseudo–first–order rate constants are tabulated in Table 1.

The possibility of general acid or base catalysis by the buffers used was not examined in this study. In previous studies with formaldehyde (6) and benzaldehyde (7), however, no buffer dependence was found. Furthermore, Jencks (24) has reported that addition reactions to the carbonyl group by strong

nucleophiles, such as sulfite, are not catalyzed by general acids or bases.

Temperature Dependence. Kinetic studies between 15° and 35°C at pH 1.4 and 2.7 were performed in order to obtain the temperature dependence of k_1 and k_2. At each temperature, these constants were estimated by assuming that a plot of $k_{obsd}K_d/(1+K_d)\alpha_1[C_2H_3O_2]_t$ vs $1/\{H^+\}$ was linear between the two data points. Values of k_1 and k_2K_{a2} were then calculated from the intercepts and slopes of these lines. The ionization fraction α_1 was computed with temperature–corrected values of ${}^cK_{a1}$ and ${}^cK_{a2}$, based on the standard state enthalpies of $\Delta H^\circ_{a1} = 16.2$ kJ mol^{-1} (21) and $\Delta H^\circ_{a2} = =11.7$ kJ mol^{-1} (22). The standard dehydration enthalpy for hydroxyacetaldehyde is not known; however, it was assumed that $\Delta H^\circ_d \approx 30$ kJ mol^{-1}, since the corresponding enthalpies for formaldehyde and pyruvic acid are 33.5 (25) and 32.6 (26), respectively. Activation energy parameters corresponding to k_1 and k_2 were determined by plotting ln(k/T) vs 1/T. These plots were linear (see Figs. 5a,b) with $\Delta H_1^{\neq} = (-\text{slope}\cdot R) = 29.9$ kJ mol^{-1}, $\Delta S_1^{\neq} = (\text{intercept} - \ln k_B/h\,)R = -156$ J mol^{-1} deg^{-1}, $\Delta H_2^{\neq} = 17.7$ kJ mol^{-1} and $\Delta S_2^{\neq} = -117$ J mol^{-1} deg^{-1}, where k_B is Boltzmann's constant, h is Planck's constant, and R is the gas constant.

Discussion

A comparison of the forward rate constants, k_1 and k_2, for several carbonyl substrates is presented in Table 2. It is evident from this comparison that hydroxyacetaldehyde reacts much more slowly than methylglyoxal, formaldehyde, and glyoxylic acid. Since an overall increase in k_1 and k_2 is apparent as the α–substituent group to the carbonyl becomes more electron–withdrawing, we tested a correlation of k_1 and k_2 with Taft's σ^* parameter. The Taft parameter is a measure of the polarizing ability of a substituent, and in the case of several

substituents, it has the property that $\Sigma\sigma^*_{R_1COR_2} = \sigma^*_{R_1} + \sigma^*_{R_2}$. With the limited available kinetic data, however, Fig. 6 indicates that neither k_1 or k_2 correlates closely with $\Sigma\sigma^*$. It is likely, therefore, that steric effects among the substrates considered are not constant; under these conditions the Taft equation is not valid. Varying steric effects are also suggested by the wide range of $\Delta S^{\neq}$ values.

The similarities between the plots of log k_1 vs $\Sigma\sigma^*$ and log k_2 vs $\Sigma\sigma^*$, as well as the nearly constant ratio of k_2/k_1 ($\sim 3 \times 10^4 - 1 \times 10^5$) imply that a better correlation exists between log k_1 and log k_2. This correlation, shown in Fig. 7, contains some scatter; however, the relatively good fit ($r^2 = 0.947$) suggests that steric effects on the addition of HSO_3^- and SO_3^{2-} at the carbonyl carbon atom are comparable.

Large differences have been observed between the activation entropies of the k_1 and k_2 steps for all of the bisulfite addition compounds we have studied. To explain the more negative $\Delta S_1^{\neq}$ we postulated that bisulfite addition requires a more ordered, cyclic transition state (see Fig 8a) than the activated complex of the k_2 step (Fig 8b). The most negative $\Delta S^{\neq}$ values for both k_1 and k_2 were obtained for the hydroxyacetaldehyde–bisulfite adducts. One explanation for this may be that additional steric hindrance is introduced because of solvent bonding with the hydroxy group (as shown in Figs. 8a,b).

An alternative mechanism could be invoked to explain the kinetics of DHES formation at pH $\leq$ 1. Replacement, for example, of the proton–catalyzed pathway with the steps,

$$H_2O\cdot SO_2 + CH_2(OH)CHO \underset{k_{-0}'}{\overset{k_0'}{\rightleftharpoons}} CH_2(OH)CH(OH)SO_3H \qquad (20)$$

$$CH_2(OH)CH(OH)SO_3H \rightleftharpoons CH_2(OH)CH(OH)SO_3^- + H^+, \qquad (21)$$

leads to the kinetically indistinguishable rate expression:

$$\nu = \left(\frac{k_0'\{H^+\}}{K_{a1}}\alpha_1 + k_1\alpha_1 + k_2\alpha_2\right)\left(\frac{K_d}{1 + K_d}\right)[C_2H_3O_2]_t\,[S(IV)]. \qquad (22)$$

The value of k_0' would then be ~ 0.1 $M^{-1}s^{-1}$, which is only an order of magnitude less than k_1. A much greater difference in the nucleophilicity of HSO_3^- over $H_2O \cdot SO_2$, however, is expected.

Rough calculations were also made to ensure that the rate constant of Eq. 7 in our proposed mechanism does not exceed diffusion–controlled rates. Assuming that the pK_{a0} of hydroxyacetaldehyde is within the range of –8 to –6, the value of k_0 is between $6 \times 10^6 - 6 \times 10^8$ $M^{-1}s^{-1}$. The proposed k_0 step, therefore, is well below the diffusion limit.

Atmospheric Implications. The rate constants obtained in this study allow us to calculate the formation rates of DHES under atmospheric conditions. Assuming that steady–state saturation is achieved in an open atmosphere containing hydroxyacetaldehyde and SO_2, the rate of DHES formation is given by

$$\frac{d[DHES]}{dt} = \left(\frac{k_0\{H^+\}}{K_{a0}}\alpha_1 + k_1\alpha_1 + k_2\alpha_2\right)\left(\frac{K_d}{1 + K_d}\right)P_{RCHO}H^*_{RCHO}\frac{P_{SO_2}H_{SO_2}}{\alpha_0}\,, \qquad (23)$$

where α_0 is the ionization fraction of $H_2O \cdot SO_2$, P refers to the partial pressure of the reagent gases, and H* and H are the apparent and intrinsic Henry's law constants. Previously we have shown for these conditions that dehydration of the *gem*–diol, $CH_2(OH)CH(OH)_2$, becomes rate–limiting at pH > 5.0 (29). Over the pH region of 4–5, therefore, Eq. 23 still applies and only the k_2 term is important. Since $\alpha_2/\alpha_0 = K_{a1}K_{a2}/\{H^+\}^2$, Eq. 23 can be approximated as

$$\frac{d[DHES]}{dt} \approx \left(\frac{k_2K_{a1}K_{a2}}{\{H^+\}^2}\right)\left(\frac{K_d}{1 + K_d}\right)P_{RCHO}H^*_{RCHO}P_{SO_2}H_{SO_2}$$

$$(\text{for } 4 < pH < 5)\,. \qquad (24)$$

Assuming gas–phase concentrations of $P_{SO_2} = P_{RCHO} = 10$ ppbv, the rate of DHES formation at pH 4 is 8.4×10^{-9} M s^{-1} (~ 30 μM hr^{-1}), and at pH 5 the rate is 100 times faster. The Henry's law constants used in these calculations were $H^*_{CH_2(OH)CHO} = 4.14 \times 10^4$ M atm^{-1} (12) and $H_{SO_2} = 1.26$ M atm^{-1} (30). By comparison, the rate of HMS formation at pH 4 is 1.7×10^{-9} M s^{-1} (~ 6 μM hr^{-1}). Despite the fact that the intrinsic rate constants, k_1 and k_2, for hydroxyacetaldehyde are smaller than the corresponding constants for formaldehyde, apparent formation rates of DHES are faster than HMS. This result is due to the anomalously high solubility of $CH_2(OH)CHO$. Therefore, hydroxyacetaldehyde–bisulfite adduct formation is not kinetically limited at pH > 4. Our results suggest that DHES is a potentially significant reservoir for S(IV).

Acknowledgements. We gratefully acknowledge the Electric Power Research Institute (RP1630–47), the Environmental Protection Agency (R811496–01–1), and the Public Health Service (ES04635–01) for their financial support.

REFERENCES

(1) Munger, J.W.; Tiller, C.; Hoffmann, M.R. *Science* **1986**, *231*, 247–249.

(2) Ang, C.C.; Lipari, F.; Swarin, S.J. *Environ. Sci. Technol.* **1987**, *21*, 102–105.

(3) Richards, L.W.; Anderson, J.A.; Blumenthal, D.L.; McDonald, J.A.; Kok, G.L.; Lazrus, A.L. *Atmos. Environ.* **1983**, *17*, 911–914.

(4) Kok, G.L.; Gitlin, S.N.; Lazrus, A.L. *J. Geophys. Res.* **1986**, *91*, 2801–2804.

(5) Hoigne, J.; Bader, H.; Haag, W.R.; Staehlin, J. *Water Res.* **1985**, 19, 993–1004.

(6) Boyce, S.D.; Hoffmann, M.R. *J. Phys. Chem.* **1984**, *88*, 4740–4746.

(7) Olson, T.M.; Boyce, S.D.; Hoffmann, M.R. *J. Phys. Chem.* **1986**, *90*, 2482–2488.

(8) Betterton, E.A.; Erel, Y.; Hoffmann, M.R. *Environ. Sci. Technol.* **1988**, *22*, 92–99.

(9) Olson, T.M.; Hoffmann, M.R. *J. Phys. Chem.* **1988**, *92*, 533–540.

(10) Betterton, E.A.; Hoffmann, M.R. *J. Phys. Chem.* **1987**, *91*, 3011–3020.

(11) Olson, T.M.; Hoffmann, M.R. *J. Phys. Chem.* **1988**, *92* (in press).

(12) Betterton, E.A.; Hoffmann, M.R. *Environ. Sci. Technol.* (in review).

(13) Sørensen, P.E. *Acta Chem. Scand.* **1972**, *26*, 3357–3365.

(14) Deister, U.; Neeb, R.; Helas, G.; Warneck, P. *J. Phys. Chem.* **1986**, *90*, 3213–3217.

(15) Calvert, J.G.; Madronich, S. *J. Geophys. Res.* **1987**, *92*, 2211–2220.

(16a) Jacob, D.; Waldman, J.M.; Munger, J.W.; Hoffmann, M.R. *Environ. Sci. Technol.* **1985**, *19*, 730–740.

(16b) Munger, J.W.; Jacob, D.J.; Waldman, J.M.; Hoffmann, M.R. *J. Geophys. Res.* **1983**, *88*, 5109–5121.

(16c) Hegg, D.A.; Hobbs, P.V. *Atmos. Environ.* **1981**, *15*, 1597–1604.

(17a) Collins, G.C.S.; George, W.O. *J. Chem. Soc. (B)* **1971**, 1352–1355.

(17b) Kobayashi, Y.; Takahashi, H. *Spectrochim. Acta* **1979**, *35A*, 307–314.

(18) Stewart, R. *The Proton: Applications to Organic Chemistry*; Academic Press: New York, 1985.

(19) Albert, A.; Serjeant, E.P. *The Determination of Ionization Constants*, 3rd ed.; Chapman and Hall: London, 1984; pp. 40–69.

(20) Draper, N.R.; Smith, H. *Applied Regression Analysis*, 2nd ed.; John Wiley and Sons: New York, 1981; pp. 458–465.

(21) Deveez, D.; Rumpf, P. *C.R. Acad. Sci. Paris* **1964**, *258*, 6135–6138.

(22) Hayon, E.; Treinin, A.; Wilf, J. *J. Amer. Chem. Soc.* **1972**, *94*, 47–57.

(23) Stumm, W.; Morgan, J.J. *Aquatic Chemistry*, 2nd ed.; Wiley–Interscience: New York, 1981; pp. 134–135.

(24) Jencks, W.P. *Prog. Phys Org. Chem.* **1964**, *2*, 63–118.

(25) Iliceto, A. *Gazz. Chim. Ital.* **1954**, *84*, 536–552.

(26) Pocker, Y.; Meany, J.E.; Nist, B.J.; Zadorojny, C. *J. Phys. Chem.* **1969**, *73*, 2879–2882.

(27) Green, L.R.; Hine, J. *J. Org. Chem.* **1974**, *39*, 3896–3901.

(28) Perrin, D.D; Dempsey, B.; Serjeant, E.P. *pK_a Prediction for Organic Acids and Bases*; Chapman and Hall: London, 1981.

(29) Olson, T.M.; Hoffmann, M.R. *Atmos. Environ.* **1988**, (in review).

(30) Johnstone, H.F.; Leppla, P.W. *J. Am. Chem. Soc.* **1934**, *56*, 2233–2238.

TABLE 1. Kinetic Data for the Addition of Hydroxyacetaldehyde and S(IV) at 25° C (μ = 0.2 M).

pH	10^2 $[CH_2(OH)CHO]_t$ M	10^3 $[S(IV)]_t$ M	10^3 k_{obsd}† ($\pm\sigma$) s^{-1}	10^3 k_{calc} s^{-1}
0.73	2.0	0.15	0.509 (±0.011)	0.532
0.95	2.0	0.15	0.756 (±0.013)	0.724
1.18	2.0	0.15	1.052 (±0.014)	1.021
1.41	1.0	0.20	0.747 (±0.024)	0.726
1.67	1.0	0.25	1.094 (±0.081)	1.073
1.90	1.0	0.30	1.646 (±0.067)	1.496
2.15	1.0	0.60	2.250 (±0.054)	2.129
2.42	1.0	1.0	3.32 (±0.12)	3.23
2.69	1.0	1.0	4.92 (±0.24)	5.21
2.98	1.0	1.0	8.25 (±0.25)	9.02
3.27	2.0	1.0	33.7 (±6.2)	32.8

†Values are averages of at least four replications.

TABLE 2. Forward Rate Constants (25° C) and Activation Energy Parameters for Hydroxyalkylsulfonates.

$$R_1COR_2 + HSO_3^- \xrightarrow{k_1}$$

$$R_1COR_2 + SO_3^{2-} \xrightarrow{k_2}$$

		$M^{-1}\,s^{-1}$		kJ mol^{-1}		J $mol^{-1}\,deg^{-1}$		
R_1COR_2	$\Sigma\sigma^{*}$(a)	k_1	k_2	$\Delta H_1^{\neq}$	$\Delta H_2^{\neq}$	$\Delta S_1^{\neq}$	$\Delta S_2^{\neq}$	Ref.
CH_3COCHO	2.30	3.44×10^3	3.66×10^7	29.0	18.2	–77.7	–22.6	10
HCHO	0.98	7.90×10^2	2.50×10^7	24.9	20.4	–108.	–31.7	6
HO_2CCHO	2.57	4.43×10^2	1.98×10^7	21.4	N.D.(b)	–141.	N.D.	11
$CH_2(OH)CHO$	1.11	1.74	5.02×10^4	29.9	17.7	–156.	–117.	This work
C_6H_5CHO	1.24	7.10×10^{-1}	2.15×10^4	36.6	36.0	–142.	–58.1	7
$(CH_3)_2CHCHO$	0.30	N.D.	1.4×10^4	N.D.	N.D.	N.D.	N.D.	27

(a) $\Sigma\sigma^*_{R_1COR_2} = \sigma^*_{R_1} + \sigma^*_{R_2}$. Values of σ^*_R were obtained from ref. 28.

(b) Not determined.

Figure Captions

Figure 1. Dependence of the pseudo–first–order rate constant on $[CH_2(OH)CHO]_t$. Solid lines are least–squares fits to the data with the following parameters: (pH 1.4) slope = 7.57×10^{-2}, intercept = -1.88×10^{-5}, $\sigma = 3.07 \times 10^{-5}$, $R^2 = 0.9977$; (pH 2.1) slope = 0.227, intercept = -5.24×10^{-5}, $\sigma = 4.91 \times 10^{-5}$, $R^2 = 0.9998$. Reaction conditions: $[S(IV)]_t = 0.2 - 0.6$ mM, T = 25° C, $\mu = 0.2$ M.

Figure 2. Dependence of the variable, $k_{obsd}(1+K_d)/\alpha_1[CH_2(OH)CHO]_tK_d$ on $\{H^+\}$ for the pH range 0.7 – 1.4. Data were taken from Table 1. The solid line denotes a linear least–squares fit.

Figure 3. Dependence of the variable $k_{obsd}(1+K_d)/\alpha_1[CH_2(OH)CHO]_tK_d$ on $1/\{H^+\}$ for the pH range 1.9 – 3.3. Data were taken from Table 1. The solid line denotes a linear least–squares fit.

Figure 4. Comparison of the calculated (solid line) and experimental values of $k_{obsd}(1+K_d)/\alpha_1[CH_2(OH)CHO]_tK_d$. The solid line was calculated with the fitted values of $k_0/K_{a0} = 5.4\ M^{-2}s^{-1}$, $k_1 = 1.74\ M^{-1}s^{-1}$, $k_2K_{a2} = 8.19 \times 10^{-3}\ s^{-1}$, and Eq. 19.

Figure 5. Temperature dependence of the rate constants for the addition of hydroxyacetaldehyde with (a) bisulfite and (b) sulfite. Solid lines were calculated from linear least–squares regressions.

Figure 6. Correlation of the rate constants, k_1 (•) and k_2 (○), with Taft's σ^* parameter. $\Sigma\sigma^*_{R_1COR_2} = \sigma^*_{R_1} + \sigma^*_{R_2}$.

Figure 7. Correlation between the second–order rate constants, k_1 and k_2 ($M^{-1}s^{-1}$), corresponding to the addition of HSO_3^- and SO_3^{2-} with the carbonyl, respectively. The solid line is a linear least–squares fit to the data.

Figure 8. Proposed activated complexes for the bimolecular addition of $CH_2(OH)CHO$ with **(a)** bisulfite and **(b)** sulfite.

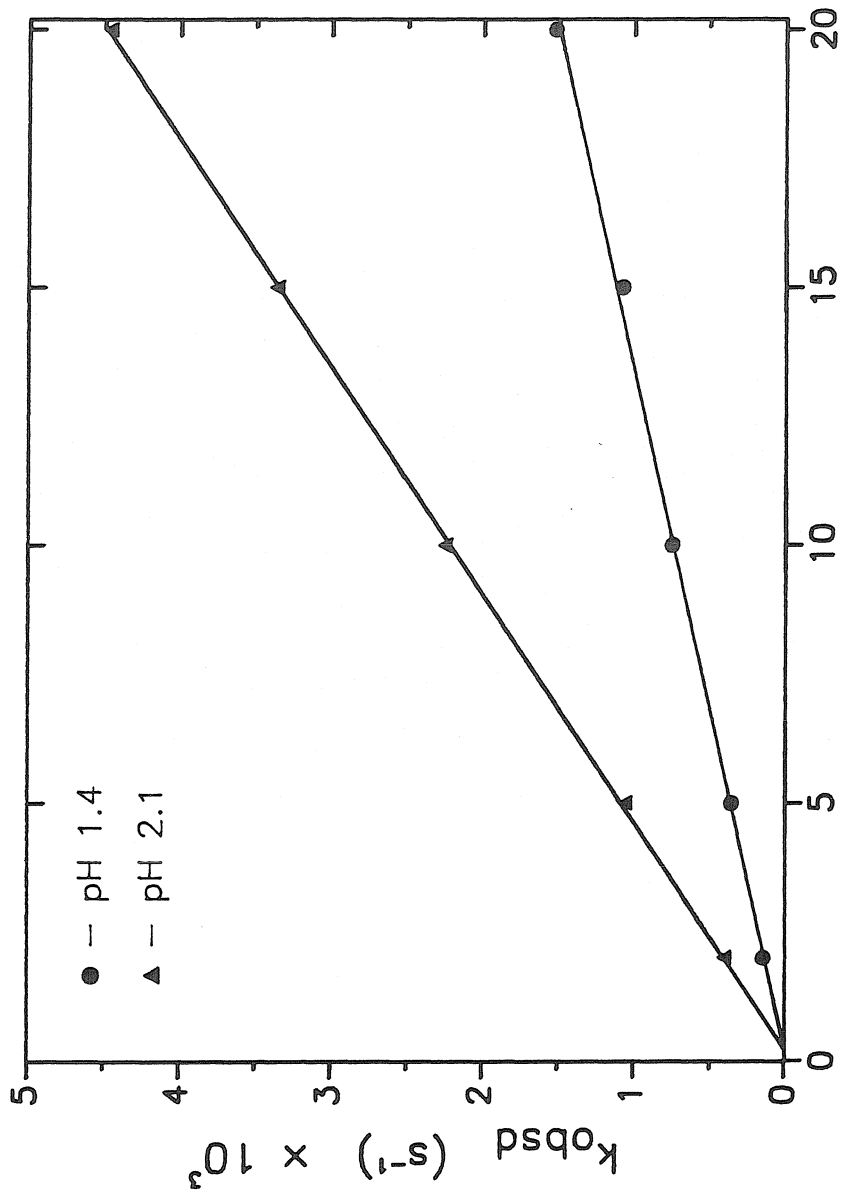

Figure 1

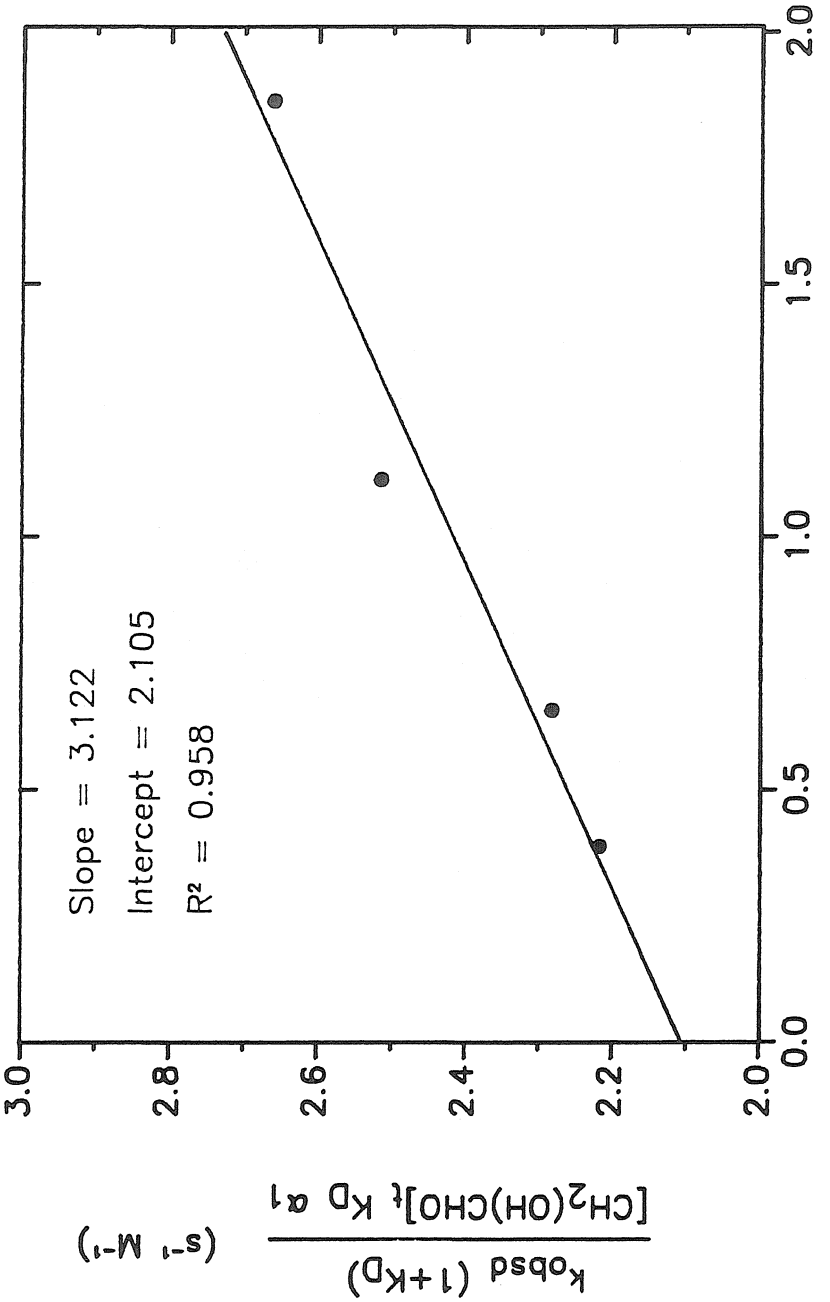
Slope = 3.122
Intercept = 2.105
R² = 0.958
3.0
2.8
2.6
2.4
2.2
2.0
0.0
0.5
1.0
1.5
2.0
{H+} x 10¹ (M)
kobsd (1+KD) / [CH2(OH)CHO]t KD α1 (s⁻¹ M⁻¹)

Figure 2

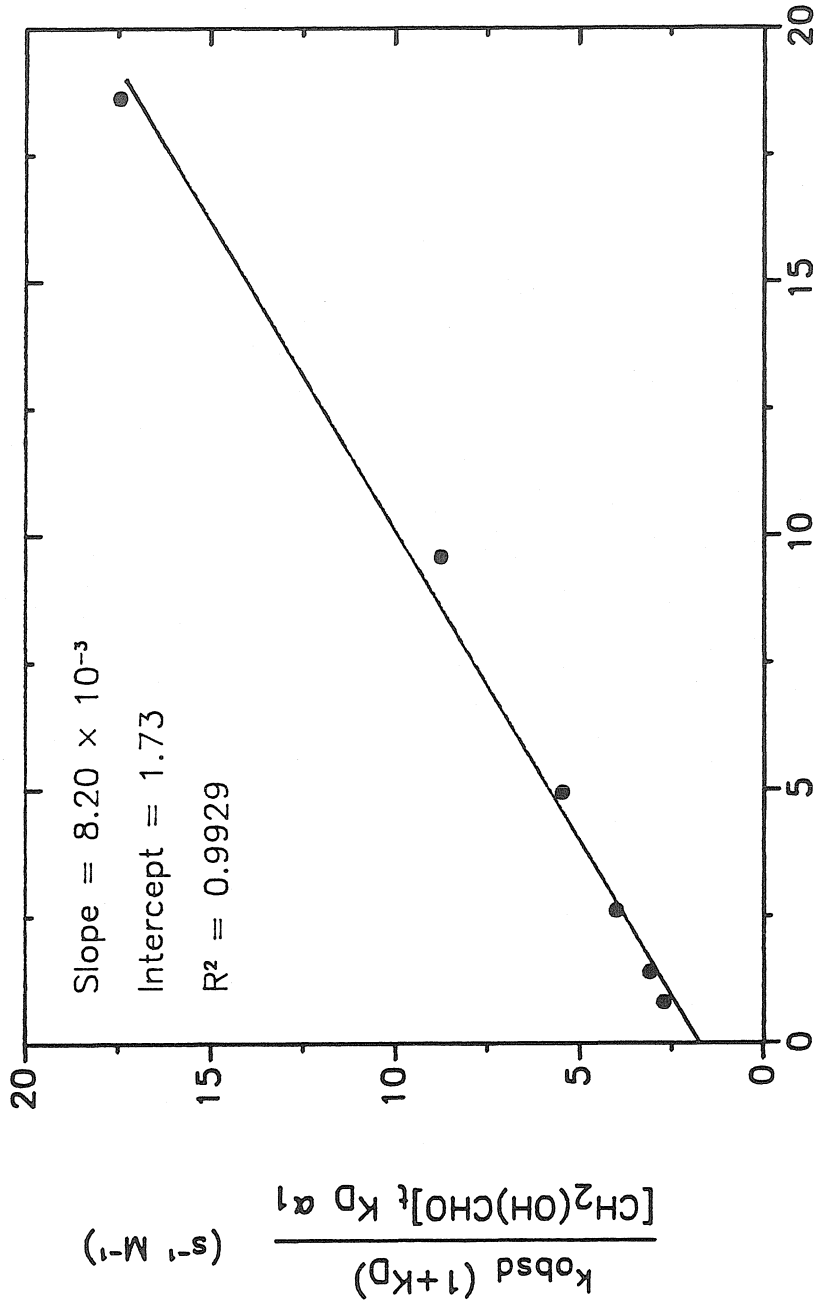
Slope = 8.20 × 10⁻³
Intercept = 1.73
R² = 0.9929
0
5
10
15
20
0
5
10
15
20
1/{H+} × 10⁻² (M⁻¹)
kobsd (1+KD) / [CH2(OH)CHO]t KD α1 (s⁻¹ M⁻¹)

Figure 3

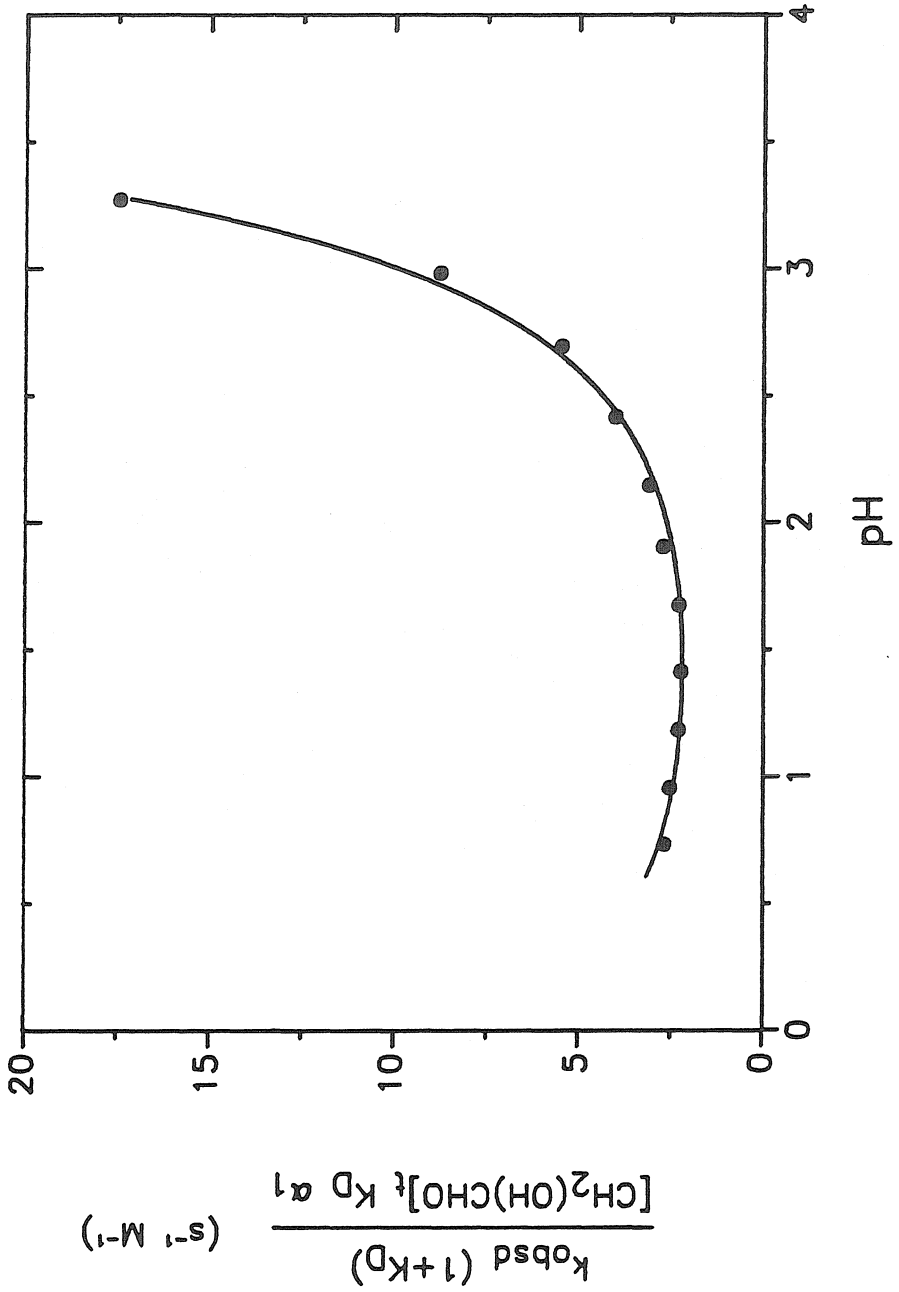

Figure 4

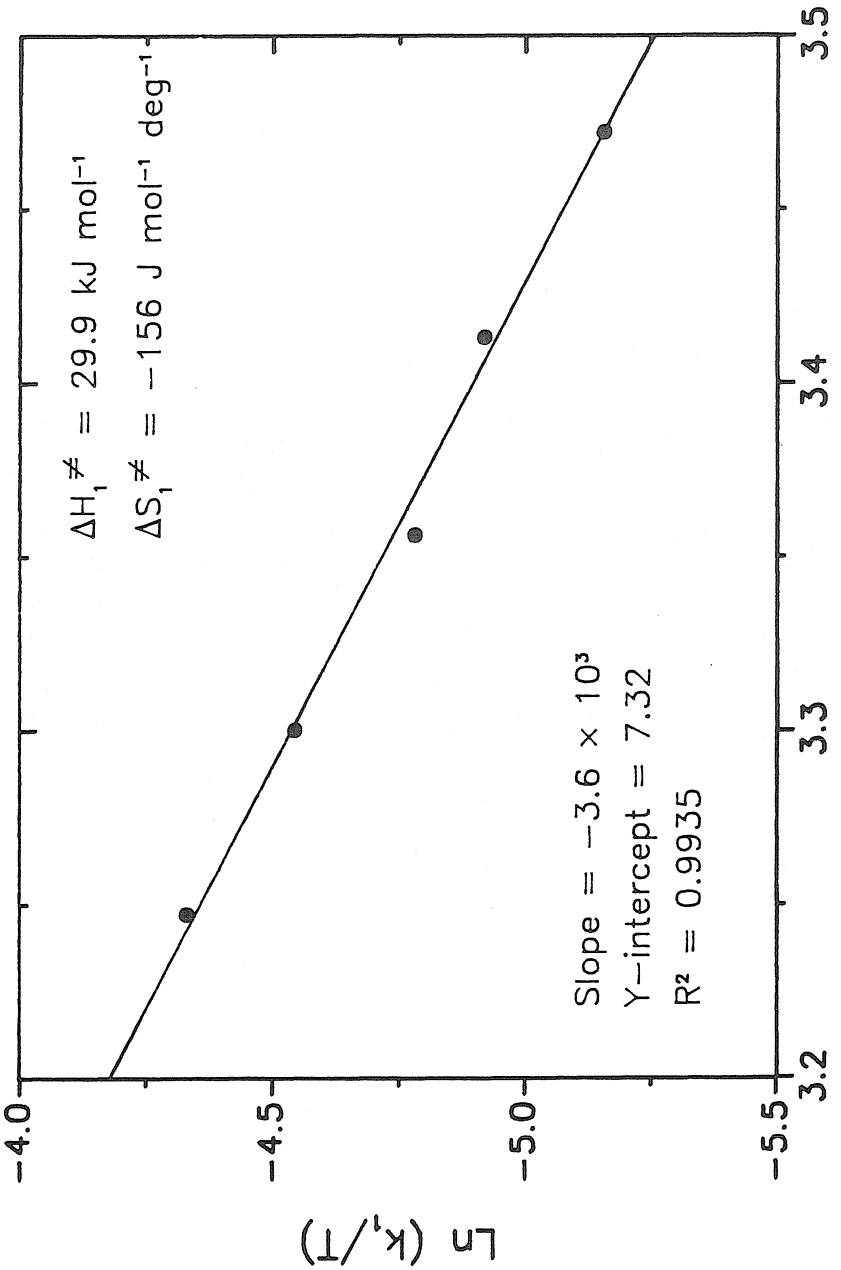
$\Delta H_1^{\neq}$ = 29.9 kJ mol^{-1}
$\Delta S_1^{\neq}$ = −156 J mol^{-1} deg^{-1}
Slope = −3.6 × 10^3
Y−intercept = 7.32
R^2 = 0.9935
Ln (k_1/T)
1/T × 10^3 (°K^{-1})
−4.0
−4.5
−5.0
−5.5
3.2
3.3
3.4
3.5

Figure 5a

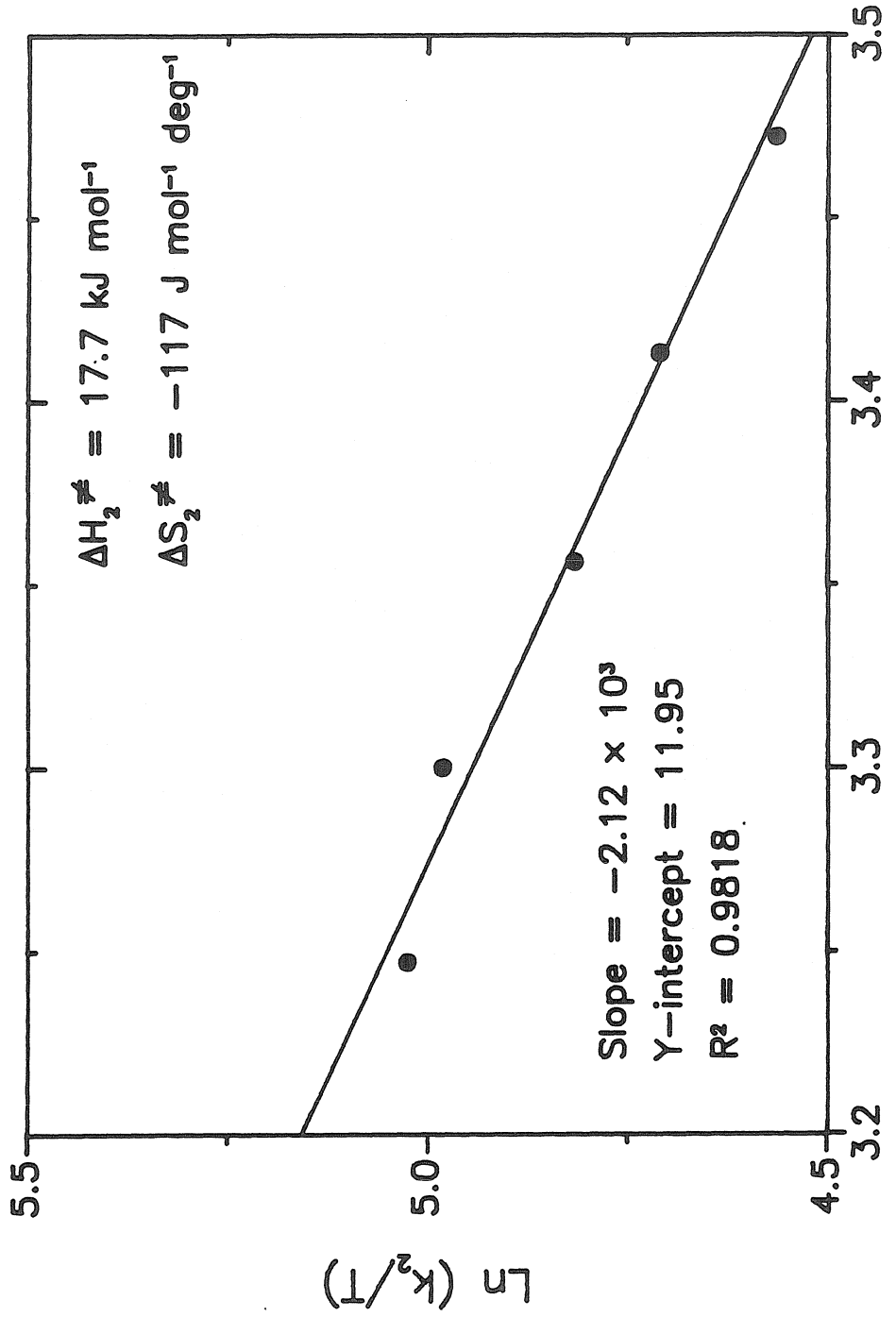
$\Delta H_2^{\neq}$ = 17.7 kJ mol^{-1}
$\Delta S_2^{\neq}$ = −117 J mol^{-1} deg^{-1}
Slope = −2.12 × 10^3
Y−intercept = 11.95
R^2 = 0.9818
ln (k_2/T)
1/T × 10^3 (°K^{-1})
5.5
5.0
4.5
3.2
3.3
3.4
3.5

Figure 5b

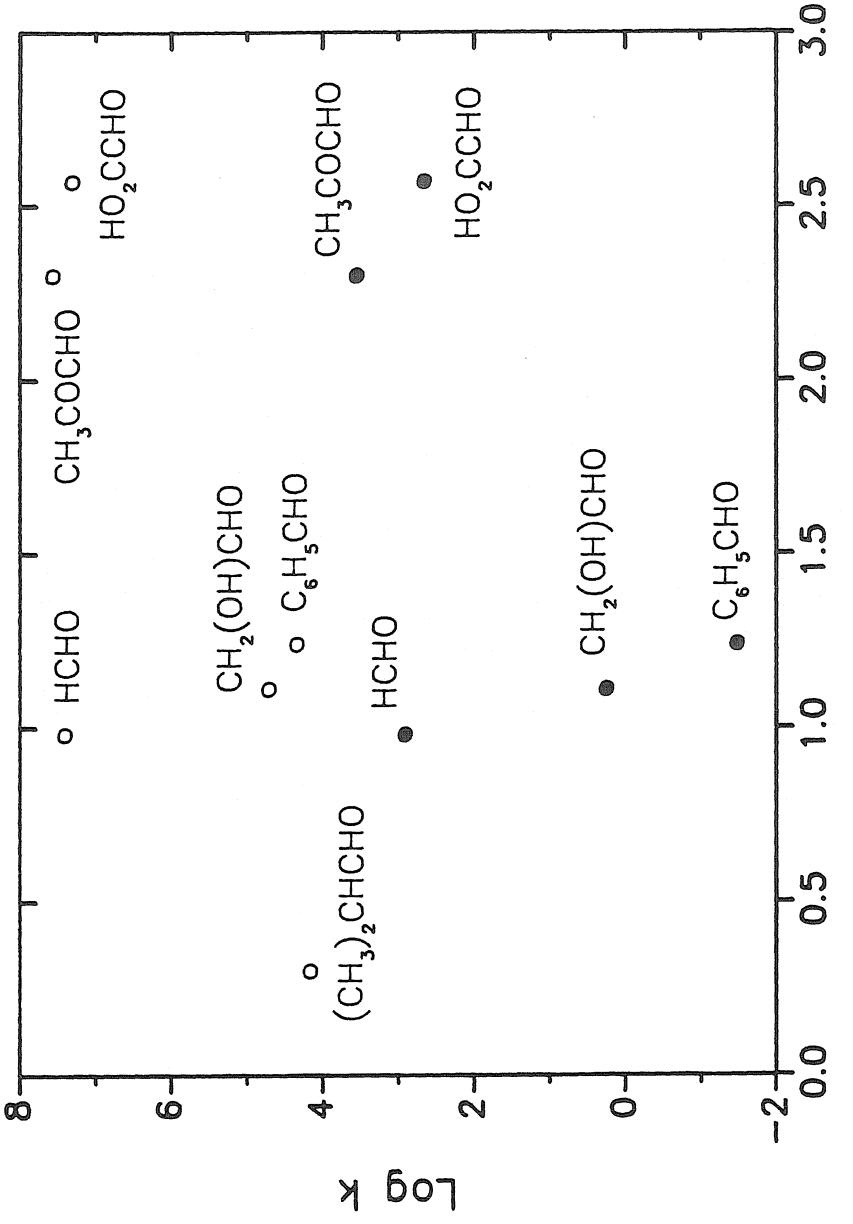
Log k
Σσ*
8
6
4
2
0
−2
0.0
0.5
1.0
1.5
2.0
2.5
3.0
HCHO
CH3COCHO
HO2CCHO
CH2(OH)CHO
C6H5CHO
(CH3)2CHCHO
CH3COCHO
HO2CCHO
HCHO
CH2(OH)CHO
C6H5CHO

Figure 6

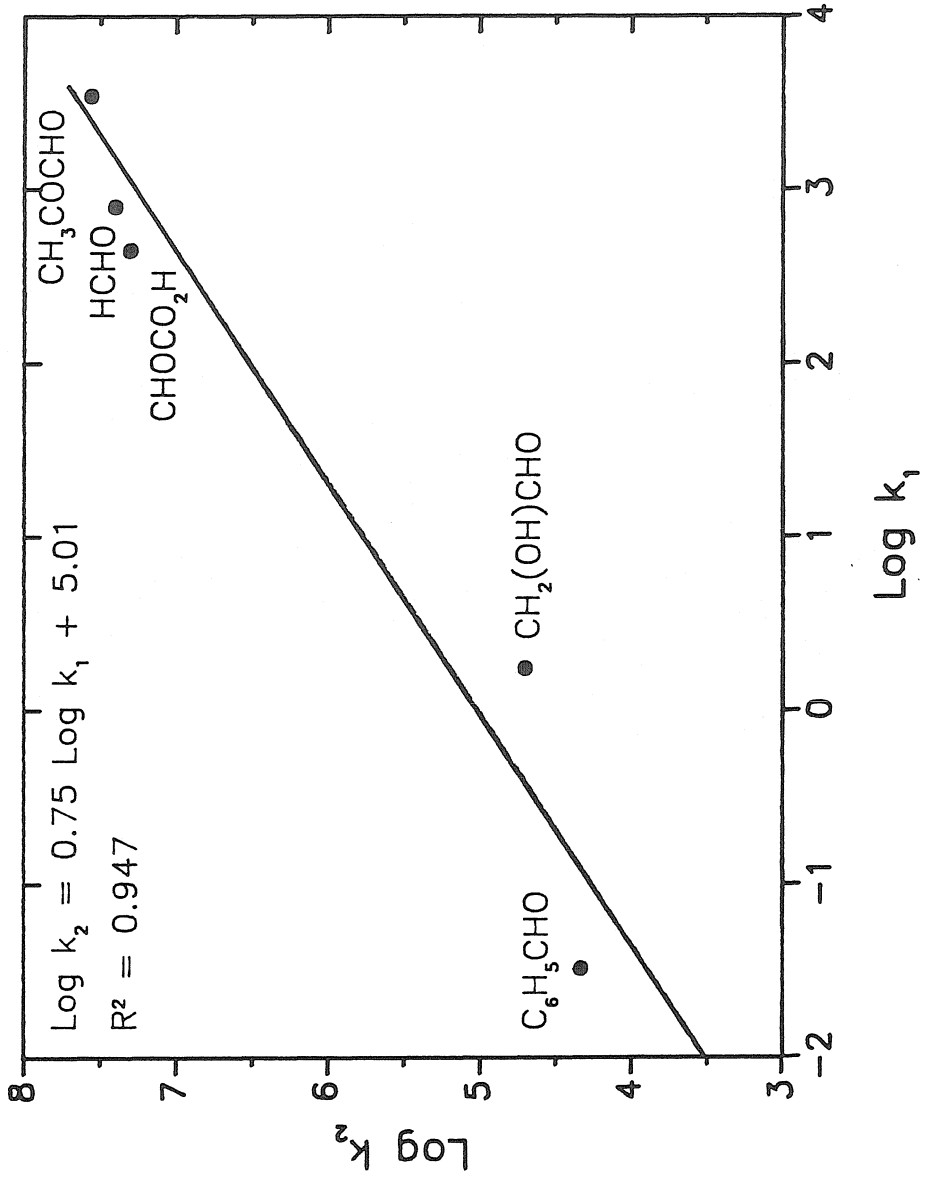
Log k_2 = 0.75 Log k_1 + 5.01
R^2 = 0.947
CH_3COCHO
HCHO
$CHOCO_2H$
$CH_2(OH)CHO$
C_6H_5CHO
Log k_2
Log k_1
8
7
6
5
4
3
-2
-1
0
1
2
3
4

Figure 7

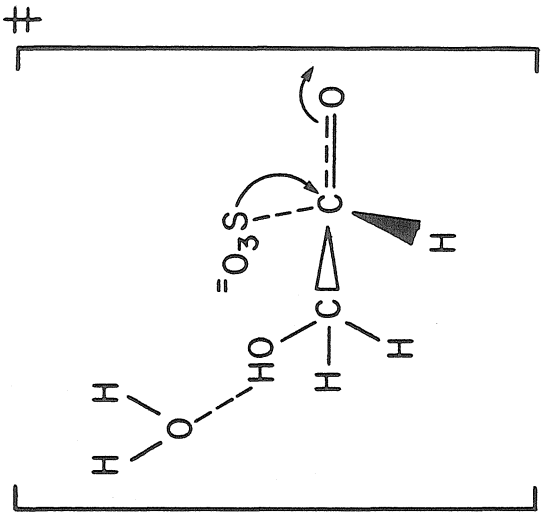

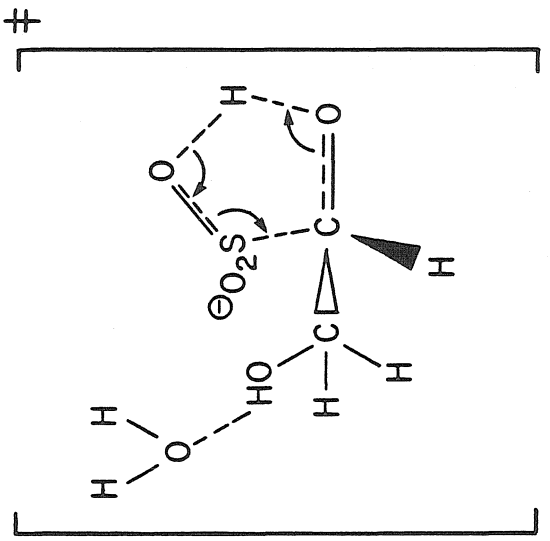

Figures 8a,b

CHAPTER 7

Recommendations for Future Research

Our experimental studies predict that other aldehydes besides formaldehyde may potentially affect the distribution of S(IV) in the atmosphere. Still, the answers to many remaining questions must await the results of additional research. A few of the most important research areas are outlined here.

Field Studies:

1. Characterization of the Gas–phase Aldehyde Content.

The abundance and sources of many of the aldehydes which we have identified as potential S(IV) reservoirs are not well known. This is undoubtedly due in part to analytical difficulties. A first step towards characterizing the ambient gas–phase carbonyl mixture, therefore, might be the development of improved analytical techniques. It is recommended that aldehydes such as glyoxal, methylglyoxal, hydroxyacetaldehyde, and glyoxylic acid, be high–priority targets in these field studies.

2. Characterization of the Hydroxyalkylsulfonate Content in Fog– and Cloudwater.

Verification efforts to determine the importance of the aldehyde–bisulfite addition compounds we examined are now needed. Already sensitive techniques for detecting free aqueous aldehyde concentrations of methylglyoxal and glyoxal in fogwater have been developed in this laboratory (Igawa *et al.*, 1988). These could be used in conjunction with total aldehyde and S(IV) analyses to infer indirectly the concentrations of bisulfite addition compounds. Very preliminary use of this approach in this laboratory suggests that methylglyoxal– and glyoxal–S(IV)

adducts are present in Los Angeles coastal fogwater. The development of specific analytical methods for hydroxyalkylsulfonates, similar to the ion chromatographic method developed by Munger *et al.* (1986) for HMS, would be even more desirable.

3. Studies of the Fates of Aldehyde–Bisulfite Addition Compounds.

Under acidic conditions (pH < 4), the dissociation rates of hydroxyalkyl–sulfonates are slow. As a fog droplet evaporates, and as ion concentrations and acidities subsequently increase, it is likely that the sulfonate salts which form during the fog will remain as part of the haze aerosol. In order to understand fully how fog and hydroxyalkylsulfonate formation affect the distribution of atmospheric S(IV) and aldehydes, it is necessary to determine what fraction ends up as aerosol. Collection and analysis of aerosol samples, particularly after fog events, to test for possible correlations between the S(IV) and aldehyde contents are therefore recommended.

Laboratory Studies:

1. Kinetics and Mechanism of Hydroxyalkylsulfonate Oxidation by OH Radicals.

Preliminary evidence obtained in this laboratory suggests that OH radicals readily attack hydroxymethanesulfonate (HMS). (An explosive reaction in a closed cell results upon the addition of Fe^{2+} to a solution of HMS and H_2O_2. It is hypothesized that OH radicals are first generated by a Fenton's reagent mechanism (Walling, 1975) and that the heat liberated by the subsequent reaction of OH with $CH(OH)SO_3^-$ is responsible for the explosion.) Actual rate constant data for

$$CH_2(OH)SO_3^- + OH \longrightarrow \qquad (1)$$

is not available; however, the rate constant for

$$CH_3SO_3^- + OH \longrightarrow \qquad (2)$$

has been determined as 1.3×10^9 $M^{-1}s^{-1}$ by Lind and Eriksen (1975). Models developed by Jacob (1986) suggest that the oxidation of HMS by OH contributes significantly to the oxidation of S(IV) in remote clouds during day–time hours, if the rate constant is similar to the methanesulfonic acid constant. Detailed studies of the mechanism and an identification of the oxidation products are needed.

2. Thermodynamics and Mechanisms of Aminoalkylsulfonate Formation.

In areas where SO_2, aldehydes and NH_3 are ubiquitous gas–phase pollutants, aminoalkylsulfonates may form. The formaldehyde–NH_3–bisulfite adduct, aminomethanesulfonate ($CH_2NH_2SO_3^-$, abbreviated as AMS here) is commercially available (as $CH_2NH_2SO_3H$, Aldrich), and we have found that it is easily recrystallized at room temperature. The reaction mechanism has not been established, but one possibility is as follows:

$$HCHO + NH_3 \rightleftharpoons CH_2(NH_2)OH \qquad (3)$$

$$CH_2(NH_2)OH \rightleftharpoons H_2O + CH_2{=}NH \qquad (4)$$

$$CH_2{=}NH + H^+ \rightleftharpoons CH_2{=}NH_2^+ \qquad (5)$$

$$SO_3^{2-} + CH_2{=}NH_2^+ \rightleftharpoons CH_2(NH_2)SO_3^- \qquad (6)$$

$$CH(NH_2)SO_3^- + H^+ \overset{K_b}{\rightleftharpoons} CH_2(NH_3^+)SO_3^- \,. \qquad (7)$$

LeHenaff (1963) proposed a much more complex mechanism; however, the supporting details are unclear.

Under most fogwater conditions, the zwitterion, $CH_2(NH_3^+)SO_3^-$, would be

the dominant aminomethanesulfonate species, since $-\log 1/K_b = 5.75$ (Albert and Sarjeant, 1984). Of the substituents, X = NH_3^+ and X = OH for the group, $CH_2(X)SO_3^-$, NH_3^+ would provide a more favorable inductive effect. (Their Taft parameters are $\sigma^*_{NH_3^+} = 3.76$ and $\sigma^*_{OH} = 1.34$.) Consequently, a larger stability constant for AMS,

$$K_{AMS} = \frac{[CH_2(NH_3^+)SO_3^-]}{[NH_4^+][HSO_3^-][HCHO]}, \qquad (8)$$

than for HMS is expected. In order for the concentrations of AMS and HMS to be comparable, however, K_{AMS} would have to be much larger than K_{HMS} because of the $[NH_4^+]$ term in the denominator of Eq. 8. To determine whether or not AMS is another important S(IV) reservoir, more study is recommended.

3. *Solubility Measurements of Hydroxyalkylsulfonate Salts.*

These measurements are needed to address the questions raised in item 3 of "Field Studies."

Toxicological Studies:

The historical coincidence of major world air pollution disasters and fog events has been recognized (Hoffmann, 1984). While the extent of the impact that $SO_{2(g)}$, $S(IV)_{(aq)}$, and $S(VI)_{(aq)}$ species have had on human health during these episodes is not known, exposure of sensitive individuals to SO_2 at levels > 250 ppb leads to increased rates of respiratory illness (Seinfeld, 1986). The common use of sulfite as a preservative in foods and beverages has also come under scrutiny because of its potential to impair respiration. Formaldehyde is another respiratory irritant and a potential carcinogen (National Research Council, 1981).

In terms of developing control strategies for SO_2 and carbonyl emissions, it will be important to know whether the formation of carbonyl–bisulfite addition compounds leads to an increase or reduction in health risks. Reducing the levels of SO_2 emissions, for example, may lead to a greater partitioning of aldehydes into the gas phase. Toxicity studies are needed to determine the form (gaseous, free aqueous, or adduct–bound) in which S(IV) and carbonyls present the greatest health hazard.

REFERENCES

Albert, A. and Serjeant, E.P. (1984) *The Determination of Ionization Constants*, 3rd ed.; Chapman and Hall: New York, p. 161.

Hoffmann, M.R. (1984) *Environ. Sci. Technol.* **18**, 61–64.

Igawa,M., Munger, J.W., and Hoffmann, M.R. (1988) *Anal. Chem.* (in review).

Jacob, D.J. (1986) *J. Geophys. Res.* **91**, 9807–9826.

LeHenaff, P. (1963) *Compt. Rend.* **256**(14), 3090–3092.

Lind, J. and Eriksen, T.E. (1975) *Radiochem. Radioanal. Lett.* **21**, 177–181.

Munger, J.W., Tiller, C., and Hoffmann, M.R. (1986) *Science* **231**, 247–249.

National Research Council (1981) *Formaldehyde and Other Aldehydes*; National Academy Press: Washington, D.C.

Perrin, D.D., Dempsey, B., and Serjeant, E.P. (1981) *pK_a Prediction for Organic Acids and Bases*; Chapman and Hall: London.

Seinfeld, J.H. (1986) *Atmospheric Chemistry and Physics of Air Pollution*; John Wiley & Sons: New York.

Walling, C. (1975) *Acc. Chem. Res.* **8**, 125–131.

APPENDIX A

On the Kinetics of Formaldehyde–S(IV) Adduct Formation in Slightly Acidic Solution

by

Terese M. Olson and Michael R. Hoffmann

Atmospheric Environment, 20, 2277–2278 (1986)

Atmospheric Environment Vol. 20, No. 11, pp. 2277–2278, 1986.
Printed in Great Britain.

0004–6981/86 $3.00 + 0.00
Pergamon Journals Ltd.

ON THE KINETICS OF FORMALDEHYDE–S(IV) ADDUCT FORMATION IN SLIGHTLY ACIDIC SOLUTION

T. M. Olson and M. R. Hoffmann
Environmental Engineering Science, M. W. Keck Laboratories 138078, California Institute of Technology, Pasadena, California 91125, U.S.A.

(*First received* 30 *December* 1985 *and in final form* 10 *March* 1986)

Abstract—Calculations are presented which demonstrate that the kinetics of dehydration of methylene glycol (hydrated formaldehyde) must be considered in determining the rate of hydroxymethanesulfonic acid formation in weakly acidic or neutral solution.

Key word index: Hydroxymethanesulfonic acid (HMSA), formation kinetics, methylene glycol, S(IV).

The kinetics of the reaction of formaldehyde with SO_2 to form hydroxymethanesulfonic acid (HMSA) in aqueous solution were recently studied by Boyce and Hoffmann (1984). Since the primary objective of this study was to apply the findings to the chemistry of acidic fog- and cloudwater, a low pH range (0–3.5) was used. We wish to emphasize, however, that extrapolation of this mechanism to higher pH without consideration of the kinetics of dehydration of methylene glycol may lead to erroneous predictions of the formation rate of the adduct.

In aqueous solution, formaldehyde is present primarily as the hydrate, $CH_2(OH)_2$. Over the weakly acidic to neutral pH range, the two possible rate determining steps for production of HMSA, therefore, are:

$$CH_2(OH)_2 \underset{k_{-d}}{\overset{k_d}{\rightleftharpoons}} HCHO + H_2O \quad (1)$$

$$SO_3^{2-} + HCHO \underset{k_{-1}}{\overset{k_1}{\rightleftharpoons}} CH_2(O^-)SO_3^- \quad (2)$$

where the dehydration of the hydrate can be catalyzed by H^+ or OH^-. Rapid protonation of $CH_2(O^-)SO_3^-$ follows reaction (2) to give HMSA. The notation, HCHO, is used to refer to the carbonyl form of formaldehyde. Bell and Evans (1966) studied the kinetics of reaction (1) and were in fact able to use sulfite as a scavenger over the pH range 7.5–8.5 in measuring the reaction velocity. They obtained the following rate expression for dehydration in the absence of general acids and bases:

$$v = (k_0 + k_H\{H^+\} + k_{OH}\{OH^-\})[CH_2(OH)_2] \quad (3)$$

where $k_0 = 5.1 \times 10^{-3}\,s^{-1}$, $k_H = 2.7\,M^{-1}\,s^{-1}$ and $k_{OH} = 1580\,M^{-1}\,s^{-1}$ at 25°C and $\mu = 0.2$ M. Equation (3) also describes the rate of HMSA formation if reaction (1) is sufficiently slower than reaction (2).

When the bimolecular addition of sulfite is rate determining and the system is far from equilibrium then the rate of HMSA production is given by:

$$v = k_1\alpha_2\left[\frac{K_d}{1+K_d}\right][S(IV)]_{free}[CH_2O]_{free} \quad (4)$$

where:

$$[S(IV)]_{free} = [H_2O{\cdot}SO_2] + [HSO_3^-] + [SO_3^{2-}] \quad (5)$$

$$[CH_2O]_{free} = [HCHO] + [CH_2(OH)_2] \sim [CH_2(OH)_2] \quad (6)$$

$$\alpha_2 = \frac{K_{a1}K_{a2}}{[H^+]^2 + K_{a1}[H^+] + K_{a1}K_{a2}} \quad (7)$$

$$K_d = \frac{[HCHO]}{[CH_2(OH)_2]}. \quad (8)$$

Boyce and Hoffmann (1984) have reported a value of $k_1 = 5.4 \times 10^6\,M^{-1}\,s^{-1}$ and a value of $K_d = 5.5$

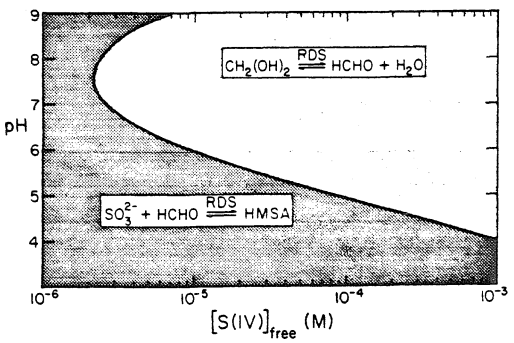

Fig. 1. Rate determining steps leading to the production of hydroxymethanesulfonate, HMSA, as a function of free [S(IV)] and pH. Boundary represents conditions at which the rate of dehydration of methylene glycol equals the rate of sulfite and HCHO addition. Calculations are based on $T = 25$°C and $\mu = 0.2$ M.

$\times 10^{-4}$ has been recommended by Bell (1966).

By equating Equations (3) and (4) and solving for pH at various values of [S(IV)], the boundary between the regions where dehydration and sulfite addition are rate-determining is obtained. Such a plot is shown in Fig. 1 for $T = 25°C$ and $\mu = 0.2$ M. Values used for the acid dissociation constants of sulfurous acid, K_{a1} and K_{a2}, were those determined by Deveez and Rumpf (1964) and Hayon *et al.* (1972), respectively and were corrected for temperature and ionic strength ($K_{a1} = 2.68 \times 10^{-2}$ M and $K_{a2} = 2.15 \times 10^{-7}$ M). As Fig. 1 demonstrates, dehydration of methylene glycol can become the rate limiting step in the formation of HMSA above pH 6 if the concentration of free S(IV) exceeds 10 μM and above pH 5 if [S(IV)] exceeds 100 μM.

REFERENCES

Bell R. P. (1966) The reversible hydration of carbonyl compounds. In *Advance in Physical and Organic Chemistry*, Vol. 4 (edited by Gold V.), pp. 1–29. Academic Press, New York.

Bell R. P. and Evans P. G. (1966) Kinetics of the dehydration of methylene glycol in aqueous solution. *Proc. R. Soc. Lond. Ser. A* **291**, 297–323.

Boyce S. and Hoffmann M. R. (1984) Kinetics and mechanism of the formation of hydroxymethanesulfonic acid at low pH. *J. phys. Chem.* **88**, 4740–46.

Deveez D. and Rumpf P. (1964) Spectrophotometric study of aqueous SO_2 in various acid buffers. *C. r. Acad. Sci. Paris* **258**, 6135–6138.

Hayon E., Treinin A. and Wilf J. (1972) Electronic spectra, photochemistry and autoxidation mechanism of the sulfite–bisulfite–pyrosulfite systems. The SO_2^-, SO_3^-, SO_4^- and SO_5^- radicals. *J. Am. Chem. Soc.* **94**, 47–57.

APPENDIX B

Stability Constant Calculations for the Pyruvate–Bisulfite Addition Compound

Apparent equilibrium (dissociation) constants for the pyruvic acid (CH_3COCO_2H) – bisulfite addition compound were reported as a function of pH by Burroughs and Sparks (1973). Converting their results to apparent *stability* constants, where

$$K_{app} = \frac{[\text{total bound S(IV)}]}{[\text{total free S(IV)}]\,[\text{total free carbonyl}]}, \tag{1}$$

the values in Table B.1 were obtained. The apparent formation constant is related to the intrinsic stability constant,

$$K_1 = \frac{[CH_3C(OH)(SO_3^-)CO_2H]}{[HSO_3^-]\,[CH_3COCO_2H]}, \tag{2}$$

by the expression:

$$K_{app} = K_1 \left(\frac{\alpha_1 \beta_1}{\phi_1}\right), \tag{3}$$

where

$$\alpha_1 = \frac{[HSO_3^-]}{[S(IV)]} = \frac{K_{a1}\{H^+\}}{\{H^+\}^2 + K_{a1}\{H^+\} + K_{a1}K_{a2}} \tag{4}$$

$$\beta_1 = \frac{[CH_3COCO_2H]}{[C_3H_4O_3]_t} = \frac{K_{d1}K_{d2}\{H^+\}}{K_{d2}(1+K_{d1})\{H^+\} + K_{a3}K_{d1}(1+K_{d2})} \tag{5}$$

$$\phi_1 = \frac{[CH_3C(OH)(SO_3^-)CO_2H]}{[CH_3C(OH)(SO_3^-)CO_2H] + [CH_3C(OH)(SO_3^-)CO_2^-]} \tag{6}$$

$$\approx \frac{\{H^+\}}{\{H^+\} + K_{a5}} \qquad (pH \ll 10)$$

$$[S(IV)] = [H_2O \cdot SO_2] + [HSO_3^-] + [SO_3^{2-}] \quad (7)$$

$$[C_3H_4O_3]_t = [CH_3COCO_2H] + [CH_3COCO_2^-] + [CH_3C(OH)_2CO_2H] + [CH_3C(OH)_2CO_2^-] \quad (8)$$

$$K_{a1} = \frac{[HSO_3^-]\{H^+\}}{[H_2O \cdot SO_2]} \quad (9)$$

$$K_{a2} = \frac{[SO_3^{2-}]\{H^+\}}{[HSO_3^-]} \quad (10)$$

$$K_{a3} = \frac{[CH_3COCO_2^-]\{H^+\}}{[CH_3COCO_2H]} \quad (11)$$

$$K_{a5} = \frac{[CH_3C(OH)(SO_3^-)CO_2^-]\{H^+\}}{[CH_3C(OH)(SO_3^-)CO_2H]} \quad (12)$$

$$K_{d1} = \frac{[CH_3COCO_2H]}{[CH_3C(OH)_2CO_2H]} \quad (13)$$

$$K_{d2} = \frac{[CH_3COCO_2^-]}{[CH_3C(OH)_2CO_2^-]}. \quad (14)$$

As in the case of glyoxylic acid, the pH dependence of K_{app} described by Eqs. 3,4,5, and 6, is quite complex. The data in Table B.1 reveal that the apparent stability constant is a maximum near pH 2.

An estimate of $K_1 = 4.56\ (\pm\ 0.17) \times 10^4\ M^{-1}$ was obtained by fitting Eq. 3 to Burroughs and Sparks' data with a Taylor's method (Draper and Smith, 1981) nonlinear least–squares regression routine. The thermodynamic constants in Table B.2 were held fixed in these calculations. Figure B.1 presents a comparison of the experimental data with the calculated K_{app} values resulting from our fit. Further discussion of the similarities between pyruvic– and glyoxylic acid–S(IV) adduct stabilities can be found in Chapter 5.

TABLE B.1 Apparent stability constants for the pyruvate–S(IV) addition compound at 20° C. (Data taken from Burroughs and Sparks, 1973).

pH	K_{app} (M^{-1})*
1.5	9.09×10^3
2.0	1.41×10^4
3.0	7.14×10^3
4.0	4.65×10^3
5.0	4.39×10^3
6.0	4.17×10^3

*K_{app} is defined in Eq. 1.

TABLE B.2 Thermodynamic Constants for Pyruvic and Sulfurous Acid.

Constant*	Value	Ref.
K_{a1}	1.99×10^{-2} M	*a*
K_{a2}	1.63×10^{-7} M	*b*
K_{a3}	6.61×10^{-3} M	*c*
K_{a5}	$\sim 5.0 \times 10^{-4}$ M	*d*
K_{d1}	1.62	*e*
K_{d2}	16.67	*e*

*Constants are defined in Eqs. 9–14.

Refs. (*a*) Deveze and Rumpf, (1964); (*b*) Hayon *et al.* (1972); (*c*) Becker (1964); (*d*) Estimated from corresponding value of K_{a3} for the glyoxylic acid – bisulfite adduct; (*e*) Pocker *et al.* (1969).

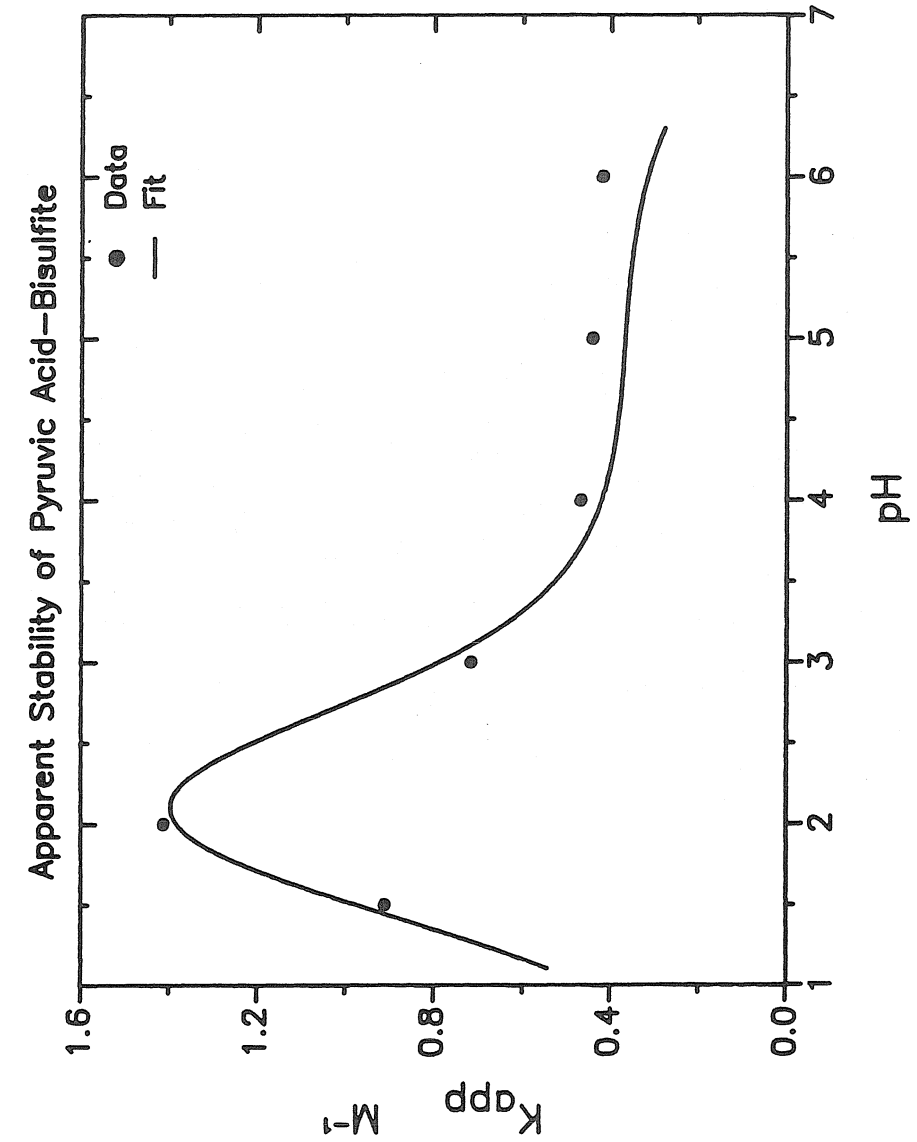

Figure B.1 Comparison of experimental and calculated values of the apparent stability constant for pyruvate–bisulfite addition compounds. K_{APP} is defined in Eq. 1. Experimental data were taken from Burroughs and Sparks (1973). The solid line is a nonlinear least–squares fit of Eq. 3 to their data.

REFERENCES

Becker, M. (1964) *Ber. Bunsenges. Physik. Chem.* **68**, 669–676.

Burroughs, L.F. and Sparks, A.H. (1973) *J. Sci. Fd. Agric.* **24**, 187–198.

Deveze, D. and Rumpf, P. (1964) *C.R. Acad. Sci. Paris*, **258**, 6135–6138.

Draper, N.R. and Smith, H. (1981) *Applied Regression Analysis*, 2nd ed.; John Wiley & Sons: New York; pp. 458–465.

Hayon, E., Treinin, A., and Wilf, J. (1972) *J. Am. Chem. Soc.* **94**, 47–57.

Pocker, Y., Meany, J.E., Nist, B.J., and Zadorojny, C. (1969) *J. Phys. Chem.* **73**, 2879–2882.